

**STUDY OF CONDUCTION MECHANISM IN  
PEO-PMMA POLYMER BLEND  
NANO-COMPOSITE ELECTROLYTES**

**THESIS**

SUBMITTED TO



**THE MAHARAJA SAYAJIRAO UNIVERSITY OF BARODA**

FOR THE AWARD OF THE DEGREE OF

**DOCTOR OF PHILOSOPHY**

IN

**PHYSICS**

*Submitted by*  
**Poonam Sharma**

*Under the supervision of*  
**Prof. D.K. Kanchan**

**SOLID STATE IONICS & GLASS RESEARCH LABORATORY**

Department of Physics, Faculty of Science  
The M.S. University of Baroda  
Vadodara - 390002

JULY-2013

## **DECLARATION**

I hereby declare that the thesis entitled “*Study of Conduction Mechanism in PEO-PMMA Polymer Blend Nano-Composite Electrolytes*” submitted for the award of “*Doctor of Philosophy*” to The M.S. University of Baroda, Vadodara, Gujarat, is original in its contents and has not formed the basis for the award of any Degree, Diploma, Associateship, Fellowship or other similar title of any other institution.

**POONAM SHARMA**

**Dr. Dinesh K. Kanchan**  
*Professor in Physics*  
email : d\_k\_kanchan@yahoo.com  
Ph : +91 9426765292



**PHYSICS DEPARTMENT**  
Faculty of Science  
**The M.S. University of Baroda**  
Vadodara - 390 002 (Guj.) INDIA  
Ph. : 91-265-2795339 (ext. 24)

---

## **CERTIFICATE**

This is to certify that Ms. Poonam Sharma, Research Scholar, has carried out the work of the thesis entitled *“Study of Conduction Mechanism in PEO-PMMA Polymer Blend Nano-Composite Electrolytes”* for the award of *“Doctor of Philosophy”* to The M.S. University of Baroda, Vadodara, Gujarat for the required period under the regulations in force. This thesis embodies a bonafide record of the work done by her under my guidance. The work is original in its contents and has not submitted the basis for the award of any Degree, Diploma or other similar title of any other institution.

**Prof. Dinesh. K. Kanchan**  
Research Supervisor  
&  
Director, Research and Consultancy Cell  
(MSU)

---

---

Dedicated to my family for believing in me

&

To the science community

---

---

## **ACNOWLEDGEMENTS**

It would not have been possible to write this Ph.D. thesis without the help and support of the people around me. I am indebted to all of them however over here I would like to mention. God has been really kind to me in providing strength and love to move forward in this endeavor which has been full of crests and troughs and He has made me tough to face all challenges.

The first person who has been the guiding force and pillar in this journey is Dr. Dinesh K. Kanchan who not only encouraged and guided me for pursuing my goal, but also worked with me as one team and incessantly pushed me to be focused on my target. His subject expertise helped me a great deal in overcoming challenges encountered in this research work. The words are not enough to thank him.

Thanks to Professor C.F. Desai, former HOD and coordinator DRS Phase III for providing all necessary laboratory facilities in the Department throughout this journey. Without all such support, this would not have been possible.

I would like to acknowledge the financial, academic and technical support of The M.S. University of Baroda and UGC, particularly in the award of a UGC-Research Fellowship in Sciences for Meritorious Students (UGC-RFSMS) that provided the necessary financial support for this research.

My thanks go to the entire faculty and staff in Department of Physics for financial support and assistance in my Ph.D. study. I am highly indebted to them for being there.

Very special thanks to my colleague, Manish Jayswal for helping me throughout my research work and providing insights. I am also thankful to my senior colleague Dr. Meenakshi Pant, my present colleagues Nirali Gondaliya, Chaitali Gavade, Prajakta Joge and Dharmesh Kothari for their love and friendly environment. They all were great encouragement to me.

Special thanks to my whole family for their encouragement and unselfish commitment to support me; right from enrollment in this Ph.D. program and reaching to the completion stage of this journey. Very special thanks to my father-in-law, Mr. S.C. Sharma for rendering support for my research work. His encouragement and help in writing the thesis was a great support for me.

I also would like to sincerely thank my mother-in-law, Mrs. Kamlesh Sharma, parents, Mr. & Mrs. R.P. Sharma and Bhabhi, Veena for their invaluable care, blessings and constant encouragement. Thanks to their generosity and love.

Finally, Thanks to my husband, Lalit for being there and strengthening my confidence and my loving son, Parth for being such a good kid for always cheering me up and his love provided me a great relief in the minor crisis of confidence. You are the reason for this journey.

**POONAM SHARMA**

## Preface

Solid electrolytes are materials that act as solid state ion conductors and conduct due to motion of ions. Solid electrolytes play an important role in several technological applications, such as electrochemical devices and fuel cells. There are various types of solid electrolytes; e.g., Framework crystalline electrolytes, glassy electrolytes, composite electrolytes and polymer electrolytes etc. Among these solid electrolytes, solid polymer electrolytes have advantages over other electrolytes. To demonstrate the objective of the present research work, a thesis is divided into six chapters and content of each chapters are as follows.

**Chapter-1** presents a comprehensive general background and introduction of solid polymer electrolytes. Different types of solid electrolytes are discussed in this chapter. Literature survey of effect of polymer blending, plasticization, incorporation of nano-fillers and ionic liquid is included. In **Chapter-2**, various theoretical models are discussed to explain conduction mechanism in solid polymer electrolytes. **Chapter-3** describes the preparation method and theories of characterization (experimental techniques). **Chapter-4** shows results and discussion of the characterization studies of prepared samples. In **Chapter-5**, frequency dependent impedance data has been used to calculate various physical parameters e.g.; impedance  $Z^*$ , dielectric  $\epsilon^*$  and modulus  $M^*$ . This chapter deals with results of conduction and relaxation measurements of polymer complexes at different temperatures. Variation of ionic conductivity with temperature showed a sudden jump near the melting temperature of PEO in polymer electrolytes. Effects of polymer blending, plasticizer and nanofiller concentration on conduction and relaxation mechanism are explained in this chapter. **Chapter-6** This chapter will summarize conclusion of investigations of prepared polymer electrolytes systems. The publications emerged out of present work are also included at the end of chapter 6.

Vadodara  
29<sup>th</sup> July, 2013

**POONAM SHARMA**

# CONTENTS

Page No.

<b>CHAPTER -1 Introduction</b>	<b>1- 34</b>
1.1 Introduction	2
1.2 Solid Electrolytes	2
1.2.1 General Characteristics of solid electrolytes	2
1.3 Classification of various Ion-Conducting Materials	3
1.3.1 Lithium ion conductors	4
1.3.2 Sodium ion conductors	4
1.3.3 Silver ion conductors	5
1.3.4 Copper ion conductors	5
1.3.5 Oxygen ion conductors	6
1.3.6 Fluorine ion conductors	6
1.3.7 Proton conductors	7
1.3.8 Magnesium ion conductors	7
1.4 Classification of Solid Electrolytes	8
1.4.1 Framework crystalline / polycrystalline solid electrolytes	8
1.4.2 Glassy / amorphous solid electrolytes	9
1.4.3 Composite solid electrolytes	9
1.4.4 Polymer electrolytes	10
1.5 Solid Polymer Electrolytes	11
1.5.1 Introduction to polymer electrolytes	11
1.5.2 Definition of Solid Polymer Electrolyte	14
1.5.3 Characteristics of polymer host	14
1.5.4 Characteristics of metal salts to favor complex formation	17
1.6 Classification of Polymer Electrolytes	17
1.6.1 Conventional polymer salt complexes or dry polymer electrolytes	17
1.6.2 Plasticized polymer-salt complexes	18
1.6.3 Rubbery polymer electrolytes	19
1.6.4 Gel polymer electrolytes	20
1.6.5 Composite polymer electrolytes	21
1.6.6 Plasticized-nano composite polymer electrolytes	21
1.7 Polymer blending	23
1.8 Applications of polymer electrolytes	25
1.9 Present work	26
References	32

<b>CHAPTER – 2 Theoretical details</b>	<b>35-76</b>
2.1 Introduction	36
2.2 Ionic Conductivity	36
2.2.1 Basic conditions for ionic conductivity	37
2.3 Ion transport mechanism	40
2.4 Empirical relationship for Temperature dependence of conductivity	42
2.4.1 Arrhenius Theory	43
2.4.2 VTF theory	44
2.4.3 WLF theory	44
2.5 Theoretical models of Conductivity	45
2.5.1. Free Volume Model	45
2.5.2 Configurational entropy model	48
2.5.3 Static bond percolation theory	48
2.5.4 Dynamic bond percolation model	49
2.5.5 Space charge models	50
2.5.6 Amorphous phase model	51
2.5.7 Effective medium theory	52
2.5.8 Rouse model	53
2.6 Plasticization theories	54
2.6.1 Lubricity theory	54
2.6.2 Gel theory	55
2.6.3 Free volume theory	56
2.7 Conductivity formalism	57
2.7.1 Complex Impedance Data Analysis	62
2.7.2 Dielectric properties of materials	64
2.7.3 Dielectric mechanisms	67
2.7.3.1 Orientation (dipolar) polarization	68
2.7.3.2 Electronic and atomic polarization	69
2.7.4 Modulus formalism	70
2.8 Frequency dependence of conductivity	72
2.8.1 Jonscher's Power law	73
2.8.2 Jump relaxation model	74
References	75
<b>CHAPTER – 3 Experimental details</b>	<b>76-111</b>
3.1 Introduction	77
3.2 Material and methods	77
3.2.1 Details of the materials used in the present investigation	77

3.3 Various polymer electrolyte systems	82
3.3.1 First Polymer Blend Electrolytes System (PPS system)	82
3.3.2 Second Polymer Blend Electrolytes System (PPSP system)	82
3.3.3 Third Polymer Blend Electrolytes System (PPSE system)	83
3.3.4 Fourth Polymer Blend Electrolytes System (PPSPA system)	83
3.3.5 Fifth Polymer Blend Electrolyte System (PPSEA system)	84
3.3.6 Sample preparation	84
3.4 Theoretical details of different characterization techniques	85
3.4.1 X-Ray Diffraction (XRD)	85
3.4.2 Scanning Electron Microscopy (SEM)	89
3.4.3 Differential Scanning Calorimetry (DSC)	92
3.4.4 Fourier Transform Infrared (FTIR) Spectroscopy	96
3.5 Complex Impedance Analysis	105
3.6. Transport number measurement	107
3.6.1 Wagner Polarization technique	108
3.6.2 EMF method	109
3.6.3 DC polarization technique	110
References	111
<b>CHAPTER – 4 Characterization results</b>	<b>112-147</b>
4.1 Introduction	113
4.2 XRD analysis	113
4.2 SEM studies	120
4.3 DSC Studies	127
4.4 FTIR Studies	134
4.5 Transference number	142
References	146
<b>CHAPTER – 5 Electrical properties</b>	<b>148-237</b>
5.1 Introduction	149
5.2 Complex impedance plot and conductivity	151
5.3 Frequency dependent conductivity	174
5.4 Dielectric studies	185
5.4 Modulus Analysis	206
5.5 Scaling	226
References	235
<b>CHAPTER – 6 Conclusions</b>	<b>238-243</b>
<b>List of Publications</b>	<b>244-246</b>

# **CHAPTER 1- Introduction**

---

This chapter includes a brief introduction of solid electrolytes and their types. A thorough discussion on various solid polymer electrolytes has been given.

---

## 1.1 Introduction

Electrolyte materials with high ionic conductivity of the order of  $10^{-4}$  S/cm found their immense use in diverse technological applications [1-5]. These materials could be in the form of solid or liquid states. Disadvantages in practical applications with liquid electrolytes are leakage, controlling due to flow of the liquids, low energy and power density, the electrolytic solution used tends to corrode the electrodes and limited operation temperature range etc. [6]. The devices using liquid electrolytes are too bulky to be transported or carried. These disadvantages are removed by solid form of electrolytes. Some of these solids, which are also good electronic conductors, are often referred to as '*mixed conductors*' while the term '*superionic conductor*' or '*fast ion conductor*' or '*solid electrolytes*' is used for good ionic conductors with negligible electronic conductivity. Mixed ion conductors find application in electrochemical devices as electrode materials. Super-ionic conductor or fast ion conductor. '*Superionic conductor (SIC)*' or '*fast ion conductor (FIC)*' or '*solid electrolytes (SE)*' terms are synonyms to each other. One of the most important uses of superionic conductors is, as electrolyte at ambient temperature in electrochemical applications [1-12].

## 1.2 Solid Electrolytes

Solid electrolytes are materials which have following characteristics [7]:

### 1.2.1 General Characteristics

- I. A large number of the ions of cation and/or anion should be mobile. This requires a large number of empty sites, either vacancies or accessible interstitial sites.
  - ⇒ Empty sites are needed for ions to move through the lattice.
- II. The empty and occupied sites should have similar potential energies with a low

activation energy barrier for jumping between neighboring sites.

⇒ High activation energy decreases carrier mobility, very stable sites (deep potential energy wells) lead to carrier localization.

III. The structure should have solid framework, preferably 3D, permeated by open channels.

⇒ The migrating ion lattice should be “molten”, so that a solid framework of the other ions is needed in order to prevent the entire material from melting.

IV. The framework ions (usually anions) should be highly polarizable.

⇒ Such ions can deform to stabilize transition state geometries of the migrating ion through covalent interactions.

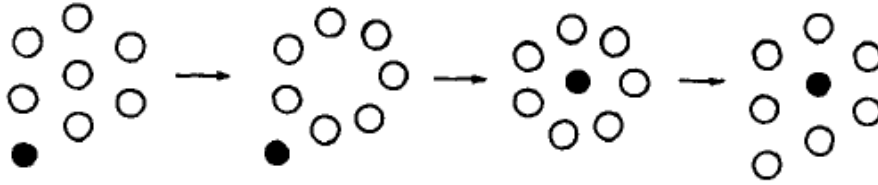


**Fig.1.1** Schematic view of transport of carrier particle. Dark circle is ion and white circle is segment.

### 1.3 Classification of various Ion-Conducting Materials

In mid 1960s, a very active research in the field of new materials as solid electrolytes has been pursued. Most of this research has been carried out on a “try it and see” concept because the structure of these materials was not known at that time [1]. Solid state ionics field has developed in after the work of  $\text{Ag}_3\text{SI}$  and  $\text{RbAg}_4\text{I}_5$  [13-15]. Later, Na- $\beta$ -alumina was successfully used in Na/S cell by Kummer and Weber [16]. The discovery of  $\beta$ - alumina, an excellent solid electrolyte with a fairly rigid framework structure, boosted searches for newer superionic conductors with skeleton structures [17].

Solid electrolytes can mainly be classified according to the nature of the ion conducting species as cation conductors ( $\text{Li}^+$ ,  $\text{Na}^+$ ,  $\text{Cu}^+$ ,  $\text{Ag}^+$ ,  $\text{H}^+$ ) and anion conductors ( $\text{F}^-$ ,  $\text{O}^{2-}$ ). Since then in the last nearly four and half decades, a large number of solids exhibiting fast ion transport involving variety of mobile species such as  $\text{H}^+$ ,  $\text{Ag}^+$ ,  $\text{Cu}^+$ ,  $\text{Li}^+$ ,  $\text{Na}^+$ ,  $\text{K}^+$ ,  $\text{Mg}^{2+}$ ,  $\text{O}^{2-}$ ,  $\text{F}^-$  etc. has been investigated extensively.

### 1.3.1 Lithium ion conductors

A large number of  $\text{Li}^+$  ion conducting solid electrolytes have been developed since past for high energy density batteries due to their light weight, ease of handling and high electrochemical potential [18-20]. This is due to small cationic size and high polarizing power of  $\text{Li}^+$  ions as compared to other ions. Many research groups have pursued a viable solid-state inorganic  $\text{Li}^+$  solid electrolyte since the 1970s for application in solid-state lithium batteries. Numerous lithium ion conducting systems such as  $\text{Li}_2\text{O}-\text{LiX}-\text{M}_x\text{O}_y$  ( $\text{X} = \text{I}, \text{Br}, \text{Cl}$ ;  $\text{M}_x\text{O}_y = \text{P}_2\text{O}_5, \text{B}_2\text{O}_3$ ),  $\text{Li}_2\text{S}-\text{GeS}_2$ ,  $\text{Li}-\text{Na}-\beta$ -alumina,  $\text{LiAlSiO}_4$  [21-25] etc. and polymer electrolytes:  $\text{PEO}-\text{LiCF}_3\text{SO}_3$ ,  $\text{PEO}-\text{LiBF}_6$ ,  $\text{PEO}-\text{LiClO}_4$ ,  $\text{PPO}-\text{NaCF}_3\text{SO}_3$  [26] etc. have also been reported to possess high ionic conductivity enabling these electrolytes for their practical application in solid state ionic devices.

### 1.3.2 Sodium ion conductors

Sodium ion conductors or  $\beta$ -Alumina family of compounds having the general formula  $\text{M}_2\text{O} \cdot n\text{X}_2\text{O}_3$ , where M is a monovalent cation ( $\text{M} = \text{Cu}^+, \text{Ag}^+, \text{Na}^+, \text{K}^+$ ), X is a trivalent cation ( $\text{X} = \text{Al}^{3+}, \text{Ga}^{3+}, \text{Fe}^{3+}$ ) and n can have values in the range of 5 to 11, are most important member of this family due to their two-dimensional ionic structure for which various kinds of solid electrolyte materials can be derived. Among these, sodium  $\beta$ -alumina exhibits an ionic conductivity of the order of  $10^{-2}$  S/cm at ambient temperature

and it is the well known sodium ion conductor [27]. A large number of sodium ion conducting systems analogous to the lithium ion conducting counterparts e.g.;  $\text{Na}_7\text{M}_3(\text{X}_2\text{O}_7)_4$  (M =Al, Ga, Cr, Fe and X- As),  $\text{Na}_2\text{O-NaCl-Na}_2\text{O-B}_2\text{O}_3$ ,  $\text{PEO-NaI-SiO}_2$ , ranging from composites [28, 29], polymer electrolytes [30] and glasses [31, 32] have been investigated for device applications.

### **1.3.3 Silver ion conductors**

Silver ion conductors are the most widely studied class of solid electrolytes with high ionic conductivity at ambient temperatures. Compounds such as  $\text{RbAg}_4\text{I}_5$ ,  $\text{Ag}_3\text{SI}$  and  $\text{Ag}_6\text{I}_4\text{WO}_4$  belong to polycrystalline category of high ionic conducting electrolytes.  $\alpha\text{-AgI}$  is the unique superionic conductor which undergoes a phase transition at  $147^\circ\text{C}$  and exhibiting exceptionally high ionic conductivity due to structural disorder originating in its crystallographic nature. Fast silver ion conduction has also been reported on glassy [32-34] as well as polymer electrolyte systems [34, 35].

### **1.3.4 Copper ion conductors**

Generally, the fast  $\text{Cu}^+$ -ion conducting materials are obtained by stabilizing the high conducting  $\alpha$ -phase of  $\text{CuI}$ , at ambient temperatures similar to silver ion conductors. The replacement of silver by copper is of both scientific and practical interest due to its low cost compared to silver. Copper ion conducting amorphous electrolytes, such as  $\text{CuI-Cu}_2\text{O-MoO}_3$  and  $\text{CuI-Cu}_2\text{O-P}_2\text{O}_5$  have also been reported to have high conductivity of the order of  $10^{-2}$  S/cm at ambient temperatures [36, 37]. However, there is a possibility of electronic conductivity in Cu- based glasses since copper has two oxidation states.

### **1.3.5 Oxygen ion conductors**

$\text{CeO}_2$ ,  $\text{ZrO}_2$ ,  $\text{ThO}_2$  and YSZ materials show oxide ion conduction in adopt cubic

fluorite structure between ambient and their respective melting temperatures. An enhancement in ionic conductivity of about two orders of magnitude is observed when these materials form solid solutions with aliovalent oxides of  $\text{Ca}^{2+}$ ,  $\text{Y}^{3+}$  and  $\text{Sr}^{3+}$  [38]. These oxides are distinctive in that they form solid solutions in an unusually wide composition range with alkaline earth or rare earth oxides such as  $\text{CaO}$  and  $\text{Y}_2\text{O}_3$ . Practical application of fast oxide ionic conductor as  $\text{La}_{1-x}\text{Sr}_x\text{Ga}_{1-y}\text{Mg}_y\text{O}^{3-}_{0.5(x+y)}$ , an oxide ion conductivity superior to yttria stabilized zirconia, in solid oxide fuel cells is reported. These materials can have good future in solid state ionic devices.

### **1.3.6 Fluorine ion conductors**

Fluoride ion is more mobile in the solid state than in the oxide one because of its monovalent nature [39] however the ionic radii of these two ions are almost same (1.4 Å). Fluorine ion being the smallest among the halogen series provides good anionic conduction. A moderate ionic conductivity has also been noted in materials like  $\text{CaF}_2$  and  $\text{SrF}_2$ . These materials possess fluorite structure which provides an open path for fast ionic conduction. However, high ionic conductivity has been realized by generating vacancies through doping aliovalent cation fluorides. The solid solution of  $\text{PbF}_2$  with  $\text{SnF}_2$  i.e.  $\text{PbSnF}_4$ , and  $\text{CaF}_2$  with rare earth fluorides such as  $\text{LaF}_3$  has exhibited conductivity of the order of  $10^{-3}$  S/cm at ambient temperature [40, 41]. These materials have also been introduced as electrode materials for rechargeable lithium batteries due to the high electronegativity value of fluorine and high free energy of formation [41].

### **1.3.7 Proton conductors**

Solid state proton conductors remained attractive for many technological innovations which include hydrogen and humidity sensors, membranes for water

electrolyzers and also for high-efficiency electrochemical energy conversion in fuel cells [42]. The proton is extremely small compared with the ionic radii of ordinary ions. Therefore,  $H^+$ -ions can conduct through a channel composed of non-structural or Zeolitic water as if it is in a solution phase. In these materials,  $H^+$ -ion does not move itself instead it would bind itself to a molecular unit in a crystal such as  $H_3O^+$ ,  $OH^-$ , or  $NH_4^+$  and transfer from one site to another by molecular rotation. Examples are sulfonated fluorocarbon NAFION, sulfonated polybenzimidazole (SPBI), and sulfonated polyether ether ketone (S-PEEK) [43] etc. Numerous proton conducting materials have been developed for fuel cell and sensor applications [44].

### **1.3.7 Magnesium ion conductors**

Since last decade magnesium ion conducting material and specifically gel polymer electrolytes are reported fairly in literature [45]. These polymer electrolytes have found their practical application in Mg-batteries and other electrochemical devices [45, 46]. The significant attention towards rechargeable magnesium battery system is due to important characteristics of the magnesium metal which are its high charge density, considerably negative electrode potential, high melting point ( $649^\circ\text{C}$ ), low cost, ease of handling, disposal and low toxicity [47]. PEO based polymer electrolyte with magnesium salts offer moderately high ionic conductivity ( $10^{-5}$  to  $10^{-4}$  S/cm) only at higher temperatures ( $80\text{--}100^\circ\text{C}$ ). These PEO based electrolytes are predominantly anionic conductors as the cationic ( $Mg^{2+}$ -ion) transport number is reported to be closed to zero which is due to the fact that the dissociation of the Mg-salt in PEO matrix is difficult (a strong electrostatic interaction between the  $Mg^{2+}$ -ion and the counteranion and another strong electrostatic interaction between the  $Mg^{2+}$ -ion and the ether oxygen of the PEO

chains. Such situation is responsible for the restricted mobility of  $Mg^{2+}$ -ions.

## 1.4 Classification of Solid Electrolytes

Depending on various preparation methods, physical properties, phases and microstructures etc. solid electrolytes have been grouped into following broad categories [28]:

### 1.4.1 Framework crystalline / polycrystalline solid electrolytes

These materials have ordered structures whereas other electrolytes possess disordered structure. These materials contain two sub-lattices: a rigid cage like skeleton within which a molten sub-lattice is enclosed facilitating liquid like movement of ions. These materials are of two types as soft and hard-framework crystalline materials as:

*Soft-framework crystalline materials:* The bonding is ionic. Free ions have high polarizability with low Debye temperatures and melting points in which the conduction is due to ion hopping or liquid-like diffusion. A sharp ionic order-disorder phase transition appears between the low and high conducting phases. Examples are AgI and CuI, etc.

*Hard-framework crystals:* The bonding is covalent. Free ions have low polarizability of mobile ions with high Debye temperatures and melting points. Conductivity is by hopping of mobile ions through the favorable sites. There is less sharp or absence of the order-disorder phase transition. They are usually oxides. Examples are  $Ag_5I_3SO_4$ , NASICON and  $Ag_7I_4PO_4$ , etc.

These materials are prepared by solid solutions reaction. Various models proposed to explain conduction in this class of solid electrolytes are Phenomenological models, Lattice gas models, Free-ion model, Jump-diffusion model, Jump-relaxation model, Coupling Model and Counter-ion model etc. [49-53].

### 1.4.2 Glassy / amorphous solid electrolytes

These materials have advantages over poly-crystalline materials e.g., high isotropic ionic conduction, absence of grain boundary conduction, wide range of compositional variability, ease of preparation into desirable shapes with the possibility to form thin films etc. [52]. These materials have three basic constituent compounds as the generalized compositional formula:  $MX : M_2O : A_xO_y$  where MX-dopant salt (AgI, PbI<sub>2</sub>, CdI<sub>2</sub> etc.), M<sub>2</sub>O- glass modifier (Ag<sub>2</sub>O, Cu<sub>2</sub>O etc.) and A<sub>x</sub>O<sub>y</sub>-glass former (B<sub>2</sub>O<sub>3</sub>, MoO<sub>3</sub>, P<sub>2</sub>O<sub>5</sub>, SiO<sub>2</sub>, As<sub>2</sub>O<sub>5</sub> etc.) [54, 55]. Preparation of these solid electrolytes is done by splat quenching method or ball-milling or liquid N<sub>2</sub> method. Some examples are AgI – Ag<sub>2</sub>SeO<sub>4</sub>, AgI - Ag<sub>2</sub>O - B<sub>2</sub>O<sub>3</sub>, AgI -Ag<sub>2</sub>O- V<sub>2</sub>O<sub>5</sub>, CdI<sub>2</sub>–Ag<sub>2</sub>O–V<sub>2</sub>O<sub>5</sub>–B<sub>2</sub>O<sub>3</sub> and PbI<sub>2</sub>–Ag<sub>2</sub>O–V<sub>2</sub>O<sub>5</sub>–B<sub>2</sub>O<sub>3</sub> [56-61]. Theories proposed to explain conduction processes in these materials are Anderson-Stuart model, Weak Electrolyte model, Random Site model, Cluster by-pass model, Ion-Association model [62-67] etc.

### 1.4.3 Composite solid electrolytes

This category of materials is two-phase mixtures with a moderately conducting ionic solid such as AgI, CuI etc. as I<sup>st</sup>- phase host salt and a II<sup>nd</sup> - phase material [28], which may be either an inert insulating compound such as Al<sub>2</sub>O<sub>3</sub>, SiO<sub>2</sub>, ZrO<sub>2</sub> etc. or another low conducting ionic solid such as AgBr, AgCl, KCl etc. Some examples are AgI-Al<sub>2</sub>O<sub>3</sub>, AgI-SiO<sub>2</sub> fumed, AgI-AgCl, AgI-AgCl-Al<sub>2</sub>O<sub>3</sub>, LiI-Al<sub>2</sub>O<sub>3</sub>, LiCl- Al<sub>2</sub>O<sub>3</sub> and Li<sub>2</sub>MnClO<sub>4</sub>- CeO<sub>2</sub> [68-70] etc. Model proposed to explain conduction in these materials are Space charge model, Adsorption-desorption model, Percolation model, Mobility enhancement model [71-74] etc.

### 1.4.4 Polymer electrolytes

Polymer electrolytes are formed by complexation of polar polymers like PEO with ionic salts having low lattice energy and bulky anions [75]. In these materials, both types of ions i.e.; cation and anion can be mobile [76]. These electrolytes possess many advantageous properties over other solid electrolyte systems including high mechanical integrity, mouldability, flexible thin film form ensuing intimate electrode-electrolyte contacts during the fabrication of all-solid-state electrochemical devices etc. These materials are mostly prepared by solution-cast method, electro-deposition method, sol-gel method or hot-press technique [77-80]. Examples of solid polymer electrolytes are PEO-AgNO<sub>3</sub>, PEO-LiCF<sub>3</sub>SO<sub>3</sub>, PEO-LiClO<sub>4</sub> and PPO-LiClO<sub>4</sub> [10, 77, 81-84] etc. Polymer electrolytes showed fast-ion conduction behavior only above glass transition temperature [76]. Below the glass transition temperature, the ionic conductivity is quite low as the chain motion in the polymer segments do not occur. Models proposed to explain conduction mechanism in these materials are free volume model and percolation model [73, 85] etc.

*Following are the concrete reasons to accept that solid polymer electrolytes are better than other solid electrolytes [28, 86] for practical applications in electrochemical devices at ambient temperature:*

- Ease of formation of thin films of larger area through which the internal resistance of the battery can be reduced and subsequently current density can be improved.
- The polymer electrolyte is fairly stable or compatible in contact with electrode (anode and cathode) systems.
- The polymer electrolyte is fairly stable under ambient conditions such as temperature, pressure, and atmosphere to facilitate production on mass scale.

Solid polymer electrolytes can be fabricated in any desired shape, have higher

mechanical strength, higher safety due the absence of flammable organic solvent and flexibility of design thereby permitting extreme miniaturization [28]. These materials have better mechanical properties for the construction of all practical solid-state electrochemical cells. A detailed description about polymer electrolytes has been given in next section.

## **1.5 Solid Polymer Electrolytes**

### **1.5.1 Introduction to polymer electrolytes**

Since the beginning of time, polymers have been around and played a major role day today in human life. Around 18<sup>th</sup> century, manmade polymers came into existence. The term polymer was coined by the Swedish chemist Jakos Berzilius in 1833. The very first polymer was vulcanised rubber which became a commercially successful polymer product in 1840. The process of vulcanisation was nothing but adding sulphur to the natural rubber to prevent the stickiness. In 1884, Hiliare de chardonnet started the first artificial fibre plant based on regenerated cellulose or viscose rayon as a substitute for silk; however it was a flammable product. In 1907, Leo Baekeland invented the first synthetic polymer [87] which was a thermosetting phenol-formaldehyde resin called BAKELITE. In 1920, German chemist Herman Staudinger [88, 89] proposed that the polymers are giant molecules formed by the permanent attachment of countless smaller molecules but it took almost a decade to get the wide acceptance of his work in the scientific community. This theory earned him a Noble prize in 1953.

*Polymers are macromolecules that are formed by linking together monomers in a chain through a chemical reaction known as polymerization [90].* Polymers consist of long chains, which are composed of simple structural units (mers) strung together.

During 20th century most polymers were used as electric insulators. However, since the pioneering work of Wright in 1973, the scientific community has focused on various polymers as potential hosts to develop new high ion conducting polymers for various electrochemical devices. P.V. Wright (a polymer chemist from Sheffield) first showed in 1973 [91, 92] that polyethylene oxide (PEO) can act as a host for sodium (Na) and potassium (K) salts, thus producing a solid electrical conductor polymer/salt complex. Thereafter, in 1978 a French chemist M. Armand [93] suggested that PEO-Lithium complexes could be deployed as solid electrolytes. A lithium salt could be dissolved in a solvating polymer matrix through direct interaction of the cation and electron pairs. The complex formed (as result of the favorable competition between the solvation energy and the lattice energy of the salt) becomes a good conductor at 60-80°C.

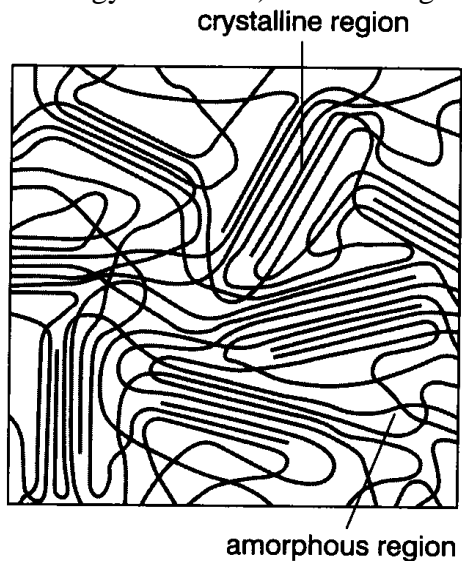


**Fig.1.2** *Crystalline and amorphous regions of a polymer.*

Later, Armand's suggestion aroused considerable interest at the Second International Meeting on Solid Electrolytes held at St. Andrews in Scotland. Experiments and detailed mechanistic studies clearly established in 1983 that ionic motion in salt-polymer complexes is not due to charges hopping from site to site rather it is a continuous

motion occurring in the amorphous regions (Fig.1.2) of the polymeric material [94]. The intrinsic phenomenon of a solid material exhibiting liquid- like conductivity without motion of the solvent itself was fascinating from a theoretical point of view and the applications to electrochemical devices sounded very promising at a time of emerging concerns with energy and pollution. A polymer electrolyte can be easily manufactured into shapes not available to liquid containing systems, and it is safer than liquid electrolytes. In 1980, PEO served as prototype material for investigating alternative models for ionic transport for developing the concept of the film cell for solid batteries. For more than three decades, a considerable work in the field of polymer electrolytes is carried out in  $\text{Li}^+$ ,  $\text{H}^+$ ,  $\text{Ag}^+$ ,  $\text{Na}^+$ ,  $\text{K}^+$ ,  $\text{Mg}^{2+}$ ,  $\text{F}^-$  and  $\text{O}^{2-}$  etc.[95] conducting polymer electrolytes. These polymeric materials have been investigated and have showed tremendous potential applicability as electrolytes in a variety of all-solid state electrochemical batteries, fuel cells and super-capacitors etc. The applicability of polymer electrolytes in electrochemical devices is being explored extensively by different workers. In addition to this, PEO, PMMA, PVA, PVC and PVdF etc. as polymer host are being used for polymer electrolytes [82].

### **1.5.2 Definition of Solid Polymer Electrolyte (SPE)**

*An SPE is defined as a solvent-free material where the ionically conducting pathway is generated by dissolving the low lattice energy metal salts in a high molecular weight polar polymer matrix with aprotic solvent as polymers are generally electrical insulators. Thus solid polymer electrolytes are complex systems. The fundamental of ionic conduction in the polymer electrolytes is the covalent bonding between the polymer backbones with the ionizing groups. Initially, the electron donor group in the polymer*

forms solvation to the cation component in dopant salt and then facilitates ion separation, leading to ionic hopping mechanism. Hence, it generates the ionic conductivity. In other words, the ionic conduction of SPE arises from rapid segmental motion of polymer matrix combined with strong Lewis–acid–base type interaction between cations and donor atom.

### 1.5.3 Characteristics of polymer host

*Polymer has to possess following characteristics to act as a successful polymer host for polymer electrolytes [12]:*

- A polymer repeat unit should have a donor group (an atom with at least one lone pair of electron) to form coordinate bond with cations.
- Low barriers to bond rotation so that segmental motion of the polymer chain can take place readily.
- A suitable distance between coordinating centers, because the formation of multiple intra polymer ion bonds appears to be important.

Numerous potential polymer hosts for solid polymer electrolyte have been explored [82]. These include both polyethers as well as nonpolyether groups [97]. Among the polyethers PEO, propylene oxide (PPO), PEO-PPO and PEO-PPO-PEO etc. have been successfully tried for reasonable conductivities. To design a polymer electrolyte, care must be taken that the branches of the polymer backbone should not add rigidity to the overall chain and the added branches should not have chemical constitutions that will reduce the glass transition temperature. Although a number of macromolecules satisfy the above criteria, but to date PEO is still an active candidate for widely studied host polymer due to its good complex formation with metal salts, low cost, easy manufacturing and availability. It is recognized to be the most facile material because of its low cost, no

toxicity, high chain flexibility, solubility in many solvents (easy processing), relatively high dielectric constant, high donor number, low glass transition temperature ( $T_g$ ) leading to high plasticity (good contact with electrodes), substantial viscosity of high molecular weight PEO melts allowing the material to withstand creeping at high temperatures, and many others. Another point of mention is that the polymer backbone also should be flexible to curl around the cation and the length of monomeric units must be such that the donor groups are neither too far from, nor too near to each other. This can be observed from the fact that although PEO (-CH<sub>2</sub>-CH<sub>2</sub>-O-) coordinates a number of cations, -CH<sub>2</sub>-O and -CH<sub>2</sub>-CH<sub>2</sub>-CH<sub>2</sub>-O- are not good host polymers. In other words, PEO has the right monomeric length for complexation. Addition or removal of another -CH<sub>2</sub>- group to or from the repeat unit will reduce the ability to complex many salts. Introduction of CH<sub>3</sub> group on carbon of PEO though helps formation of an amorphous polymer, forces the polymer to adopt a more open helical structure which is less favorable for complexing cations. However, from a practical standpoint the PEO was not itself an ideal electrolyte. Several manipulations were needed to prevent its crystallization and to extend the domain of existence of the elastomeric phase favorable to high ionic conductivity: plasticizing the matrix by addition of a low molecular weight polar molecule or forming block or comb copolymers.

Usually polymer electrolytes consist of long organic molecular chains and dissolved salts (Fig.1.3). When a charged polymer chain is cut into small pieces, it becomes an ionic liquid and by being frozen into glassy states it becomes an insulator glass or super-ionic conductor glass. Polymer electrolytes are usually composed of two main components, one is the polymerized network of organic monomer units examples

[82] are given in Table 1.1 along-with their glass transition values ( $T_g$ ). The counter anions are distributed in the open space between the polymer chains and also contribute to the ionic conductivity, which causes the electrode polarization in battery applications.

**Table 1.1** Typical host polymers for polymer electrolytes.

S. N.	Polymer	Abbreviation	Repeat unit	$T_g$ ( $^{\circ}\text{C}$ )
1.	Poly ethylene oxide	PEO	$-(\text{CH}_2-\text{CH}_2\text{O}-)_n-$	-60
2.	Poly vinylidene fluoride	PVdF	$-(\text{CHCF}_2-)_n-$	-40
3.	Poly propylene oxide	PPO	$-(\text{CH}(-\text{CH}_3)-\text{CH}_2\text{O}-)_n-$	-60
4.	Poly vinyl choride	PVC	$-(\text{CH}_2-\text{CHCl}-)_n-$	82
5.	Poly acrylonitrile	PAN	$-(\text{CH}_2-\text{CH}(-\text{CN}))_n-$	125
6.	Poly metha methacrylate	PMMA	$-(\text{CH}_2\text{C}(-\text{CH}_3(-\text{COOCH}_3)-)_n-$	108

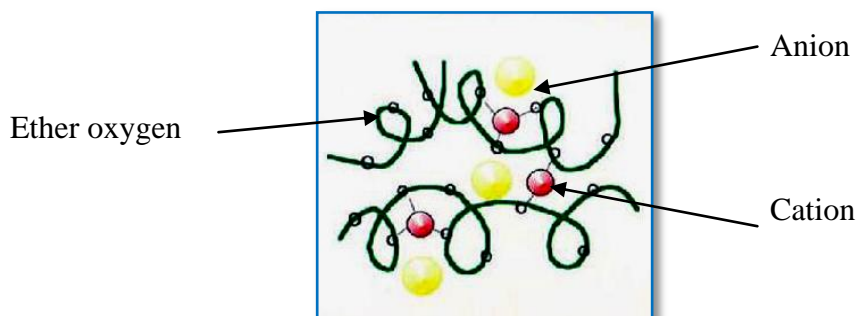


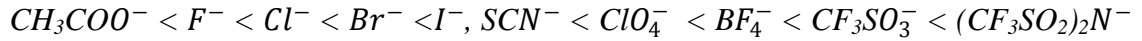
**Fig.1.3** Structure model of solid polymer electrolytes of polymer chains.

#### 1.5.4 Characteristics of metal salts to favor complex formation

A metal salt should favor following characteristics for polymer salt complex formation [12]:

- Low lattice energy or high solvation energy
- Smaller cationic radii and bigger anionic size
- The charge density of the anion should be low to reduce the number of ion-pairs with cation.

Among the most frequently used anions, the ionic conductivity for a given cation e.g.;  $\text{Na}^+$ ,  $\text{Li}^+$  ion etc. increases in the sequence given below:



The large 'soft' anions towards the right such as  $ClO_4^-$  or  $CF_3SO_3^-$  which have low ion-dipole stabilization energies, but relatively large energies of solvation due to mutual polarizability, are therefore likely to be the most suitable choice for polymer electrolytes. But different kinds of salts have been used for forming the salt-polymer complexes. Most common are the monovalent cations:  $Li^+$ ,  $Na^+$ ,  $K^+$ ,  $Cs^+$  and  $NH_4^+$ . Some divalent cations:  $Mg^{2+}$ ,  $Zn^{2+}$ ,  $Ni^{2+}$  and some trivalent cations like  $La^{3+}$ ,  $Nd^{3+}$  and  $Eu^{3+}$  have also been utilized [12].

## 1.6 Classification of Polymer Electrolytes

The polymer electrolytes can be further divided into following broad categories [26]:

### 1.6.1 Conventional polymer salt complexes or dry polymer electrolytes

These electrolytes were originally introduced two decades ago. These complexes are prepared by complexing/dissolving ionic salts e.g.;  $LiClO_4$ ,  $LiCF_3SO_3$ ,  $LiBF_4$  and  $NH_4I$  etc. into coordinating polar polymer hosts, namely, PEO and PPO etc (Table 1.2). The casting of the polymer films is done either by the usual solution cast method or by hot-press technique. The good dry solid polymeric electrolytes reported so far are based on high molecular weight polymers, e.g.; PEO and/or PPO complexed/ dissolved with different alkali metal salts. These polymers usually form stable dry complexes with a

**Table 1.2** Some polymer-salt complexes and their conductivity values. (Resource: Ref. [26])

<b>Polymer electrolytes</b>	<b>Ionic conductivity (S/cm)</b>
PEO- $NH_4I$	$10^{-5}$
PEO- $LiClO_4$	$10^{-7}$
PEO- $LiBF_4$	$10^{-6}$
PEO- $Cu(ClO_4)_2$	$10^{-5}$
PPO- $NaCF_3SO_3$	$10^{-5}$

relatively higher conductivity other than other solvating polymers. Examples are PEO-NH<sub>4</sub>I, PEO-LiClO<sub>4</sub>, PEO-LiBF<sub>4</sub>, PEO-Cu(ClO<sub>4</sub>)<sub>2</sub> and PPO-NaCF<sub>3</sub>SO<sub>3</sub> with an ionic conductivity of the order of 10<sup>-5</sup> to 10<sup>-7</sup> S/cm.

### 1.6.2 Plasticized polymer-salt complexes

These are prepared by adding plasticizers into solid polymer electrolytes. The magnitude of ambient conductivity gets substantially enhanced by this, but plasticization can result in deterioration in the mechanical integrity of the film as well as increased corrosive reactivity of polymer electrolyte towards the metal electrode. Examples of plasticized polymer-salt complexes are PEO-LiClO<sub>4</sub>-EC, PAN-EC-PC- LiCF<sub>3</sub>SO<sub>3</sub>, PMMA-EC/PC- LiClO<sub>4</sub> and PEO-PEG- LiCF<sub>3</sub>SO<sub>3</sub>etc.

Plasticizers are low molecular weight non-volatile substances when added to a polymer improve its flexibility and processibility. Plasticizer molecules are relatively smaller in size compared to polymer molecules and hence they can easily penetrate into the polymer matrix and establish polar attractive forces between themselves and the chain segments. These attractive forces reduce the cohesive forces between the polymer chains and increase the segmental mobility, thereby reducing the glass transition temperature ( $T_g$ ) value of the polymer [82]. It provides conduction channels and their high dielectric constant values are responsible for the enhancement in conductivity values by the way of associating the polymer salts [98]. Plasticizer is generally a low volatile liquid. High salt-solvating power, sufficient mobility of ionic conduction and reduction in crystalline nature of the polymer matrix are the main features of the plasticizer.

The increase in concentration of plasticizer causes the transition from the glassy

state to rubbery region at progressively lower temperature. In addition, it can occur over a wide range of temperatures rather than unplasticized polymer. Besides, it improves the flexibility of polymer chains in the polymer matrix. M.H. Buraidah *et.al.* [99] suggest that the polymer and plasticizer do not interact chemically with one another but interaction between salt and plasticizer exists. The donor atom of the plasticizer may be placed in between coordinating sites in the polymer and present a network of sites for the ions to reside. The ion is able to hop from one coordinating site to another via donor atom sites contributed by the plasticizer. The hops will therefore require a low activation energy and the conduction of ions resembles the conduction of polarons in polaronic conductors. However, upon addition of plasticizer, some limitations are obtained such as low flash point, slow evaporation, decreases in thermal, electrical and electrochemical stabilities. Low performances, for instance, small working voltage range, narrow electrochemical window, high vapor pressure and poor interfacial stability with lithium electrodes are the disadvantages of plasticized–gel polymer electrolytes.

### **1.6.3 Rubbery polymer electrolytes**

These polymer electrolytes were discovered by Angell and coworkers [100] in 1993 in which lithium salts were mixed in small quantities of PEO and PPO polymers. These polymer electrolytes are prepared by dissolving small amount of higher molecular weight polymer in relatively larger amount of salt. Above mentioned polymer electrolytes have polymer content in large amount and are referred to as salt-in-polymer systems while due to larger salt content, these polymer electrolytes are referred to as polymer-in-salt systems. The glass transition temperature ( $T_g$ ) of these electrolytes is usually low enough to maintain rubbery state. The ambient conductivity of these electrolytes is quite

high but due to crystallization of salt at lower temperatures prevents their practical applications. Examples are  $\text{AlCl}_3\text{-LiBr-LiClO}_4\text{-PPO}$ ,  $\text{PLMA-b-POEM}$  and  $\text{PEO - [LiAlCl}_4\text{-LiN(CF}_3\text{SO}_2)_2\text{-LiC(CF}_3\text{SO}_2)_2]$  etc. [100, 101].

#### **1.6.4 Gel polymer electrolytes**

These electrolytes present the latest development in the field of electrolytes. Gel electrolytes are usually obtained by incorporating large amount of organic liquid solvent or liquid plasticizer i.e.; ionic liquid in into the polymer matrix capable of forming stable gel with a polymer host structure [26]. Polymer gel electrolytes combine the ionic conductivity of liquid polymer electrolytes with the attractive mechanical and processing advantages of polymer. These materials also offer high ambient conductivities but suffer from similar disadvantages as mentioned for the plasticized polymer electrolytes. Examples are  $\text{P(VdF-HFP)-(PC-DEC)-LiClO}_4$ , {where  $\text{P(VdF-HFP)}$ -Poly(vinylidene fluoride-co-hexafluoropropylene) and DEC-diethyl carbonate},  $\text{P(VdF-HFP)-NaTf-EMITf}$  {where EMITf- 1-ethyl 3-methyl imidazolium trifluoro methanesulfonate and NaTf -sodium triflate } and  $\text{PVdF-HFP- Mg(Tf)}_2\text{-EMITf}$  etc. [102-104].

These polymer electrolytes have drawn considerable interest of researchers due to its many attractive properties such as excellent thermal, chemical and electrochemical stabilities. It is able to dissolve a wide range of organic, inorganic and organo-metallic compounds. It retains liquid form in a wide temperature range and does not coordinate with metal complexes, enzymes and different organic substrates. It is also a promising item for electrochemical potential window, wider decomposition temperature range, non-toxicity and non-volatility as well as non-flammability. Other intrinsic features are excellent safety performance, and, relatively high ionic conductivity due to high ion

content. The low viscosity of ionic liquid improves the ionic mobility among the polymer matrix. Doping of ionic liquid produces gel-like polymer electrolyte, perhaps sticky gel polymer electrolyte. Sticky gel polymer electrolyte has advantage in electrochemical devices designing by providing a good contact between electrolyte and electrode. Ionic liquid is a versatile molten salt and is primarily used as an additive in gel polymer electrolytes. Such gel polymer electrolytes are applied onto electrochemical devices such as dye-sensitized solar cells, electrical super-capacitors, actuators, light-emitting electrochemical cells and lithium batteries.

### **1.6.5 Composite polymer electrolytes**

These polymer electrolytes are formed by dispersing inorganic inert micro/ nano-sized fillers in conventional solid polymer electrolytes. These electrolytes offer enhanced electrode/electrolyte compatibility as well as safety especially in lithium polymer batteries [26]. Dispersion of nano/micro fillers like zeolites, ionites, solid superacid sulfated-zirconia as well as insulating ceramic materials such as  $\text{Al}_2\text{O}_3$ ,  $\text{SiO}_2$  and  $\text{TiO}_2$  in polymer electrolytes also improves their physical, morphological, electrochemical and mechanical properties [105]. Generally, it has been observed that the particle size and the physical nature of the dispersoid particles also play a significant role. Hence, dispersal of nano-sized filler particles has been found to be more effective in the composite polymer electrolyte systems, especially in terms of improvements in the properties. Examples are PEO- $\text{LiClO}_4$ - $\text{SiO}_2$  and PEO- $\text{LiClO}_4$ - $\text{Al}_2\text{O}_3$  [106, 107] etc.

### **1.6.6 Plasticized-nano composite polymer electrolytes**

These polymer electrolytes are formed by dispersing inorganic inert micro/ nano-sized fillers in plasticized polymer electrolytes. Examples are PEO- $\text{AgCF}_3\text{SO}_3$ -PEG- $\text{SiO}_2$  and PMMA- $\text{LiN}(\text{CF}_3\text{SO}_2)_2$ -EC-PC- $\text{SiO}_2$  [108, 109] etc. The main purpose of dispersion of nano-filler is

to enhance processability and improve electrical properties as well as mechanical strength (modulus, tension or tear strength) of polymer films. The improvement in the mechanical properties has been explained on the premise that the filler particles act as a supporting matrix for the conductive polymer. The enhancement in electrical conductivity due to the addition of inert filler particles has been generally explained in terms of the disruption of crystallization in the polymer host matrix [110]. The fillers are divided into two types i.e.; inorganic and organic. The examples of inorganic fillers include fly ash, calcium carbonate, mica, clay, titania ( $\text{TiO}_2$ ), fumed silica ( $\text{SiO}_2$ ) and alumina ( $\text{Al}_2\text{O}_3$ ), whereas the graphite fiber and aromatic polyamide are the examples of organic fillers. Several intrinsic advantages are possessed by inorganic filler. Dispersion of inorganic fillers also improves the ionic conductivity in a polymer electrolyte. The enhancement of ionic conductivity with dispersion of filler is mainly due to the decrease in the crystalline phase of the polymer electrolyte.

In PEO based polymer electrolytes, the addition of a ceramic filler considerably diminishes the crystallization kinetics of PEO in the polymer electrolytes, giving rise to a

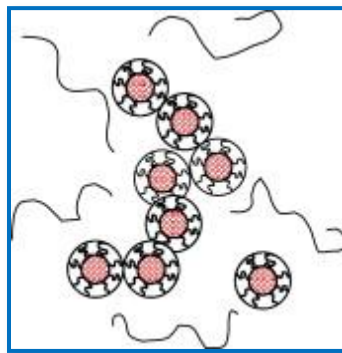


**Fig.1.4** Dispersion of nano-filler in polymer electrolytes.

larger fraction of amorphous material which usually exhibits higher ionic mobility than the crystalline counterparts. The addition of ceramic particles leads to formation of highly

conductive pathways in the amorphous interfacial regime (Fig.1.4) and thus to enhanced conductivities. Above a certain concentration of filler material, these paths collapse and conductivity drops again. The electrostatic interactions between the cations, anions (and the polymer chains) on the one hand, and, the surface of the ceramic particle on the other may be viewed as Lewis acid Lewis base interactions, and may intervene with the electrostatic interactions between the cationic and anionic species and assist the ion transport by the creation of new hopping sites for cations. However, it remains ambiguous whether such an interaction presents a general feature for polymer electrolyte composites.

## **1.7 Polymer blending**

Besides many polymers that were developed in past which had their unique properties and applications, during the period of 1940-1960s, the polymer industry and academia have realized the requirement of new polymers. But the cost of bringing a new polymer to market and its commercial production seemed unviable. The polymer industry and academia both focused on developing a polymer material of novel and valuable properties. Therefore, it was suggested to develop new techniques for the modification of already existing polymers which would be economically viable. A new polymers modification process, based on a simple mechanical mixture of two polymers first appeared when Thomas Hancock (founder of British rubber industry) developed one mixture of natural rubber with Gutta-percha. This process generated a brand new polymer class called polymer blend.

Polymers which can produce better polymer electrolytes are generally semi-crystalline at room temperature and those are amorphous, do not possess criteria for

polymer electrolyte i.e., they should have properties like high molecular weight, low glass transition temperature, low cohesive energy density and high flexibility.

In this way, polymer blends became key components of current polymer research and technology. Mixing of two or more polymers at their matrix level is termed as polymer blends [82]. It is a physical mixture of two or more polymers which are not linked by covalent bond. When two or more polymers are completely miscible down to the segmental level, they form a single homogeneous phase. Their properties are generally proportional to the ratio of the polymers in the blend, and the polymer blend is called homogeneous blends. Polymer blend provides a new desirable polymeric material for a variety of applications. It has many advantages such as simple to prepare, easier to control of physical properties by compositional changes and possession of better properties compared to individual polymer component. Commercially, it can be used in industries as it enhances the processability of high temperature or heat-sensitive thermoplastic to improve the impact resistance. It also reduces the cost of an expensive engineering thermoplastic. The properties of polymer blends depend on the physical and chemical properties of the participating polymers, and, on the state of the phase, whether it is in homogenous or heterogeneous phase. If two different polymers are able to be dissolved successfully in a common solvent, this polymer blends or intermixing of the dissolved polymers will occur due to the fast establishment of the thermodynamic equilibrium. Polymer blending is one of the effective methods to reduce the crystalline content and to enhance the amorphous content. Polymer blends often exhibit properties that are superior to the individual component polymers.

In recent years, polymer blends have drawn considerable interest in most rapidly

growing areas in polymer material science. Other objectives of blending are to dilute polymers through addition of low cost commodity polymers and to recycle industrial plastic waste. Application of polymer blends in numerous fields such as adhesion, colloidal stability, and design of composite and biocompatible materials requires fundamental understanding of the structure, phase state and composition of blends in the vicinity of interacting surfaces. As polymeric materials are rarely used in their pure form, and, are usually filled with additives that improve their processability and properties, including creating some new ones. For these purposes, particulate disperse fillers and fibrous fillers are widely used. Polymer blends may be considered as composite materials. These can be considered as heterogeneous systems with developed phase boundaries between constituent components or phases. At the polymer–polymer interface, interphase layers are formed whose structure and properties depend on the thermodynamic interactions between two components or phases. Due to thermodynamic and kinetic reasons, polymer blends are usually characterized by two-phase structure arising as a result of thermodynamic immiscibility of initial components. The processes that occur during their formation lead to development of a complex structure because of incomplete phase separation. Though extensive research has been carried out, very few polymer blend electrolytes have been found to show significant comprehensive properties which can fulfill the practical requirements.

## **1.8 Applications of polymer electrolytes**

Polymers with dissolved ionic salts have a relatively high ionic conductivity and therefore have a potential application as solid electrolytes. The solid state ion conducting polymers are used as electrolytes in different electrochemical devices such as [26, 111]

- Electrochemical Batteries
- Electrochemical sensors
- Fuel cells
- Super capacitors
- Memory devices
- High-vacuum electrochemistry
- Electro chromic display devices
- Thermoelectric generators and
- Electrochemical switching

## **1.9 Present work**

Solid polymer electrolytes are being studied over decades due to their commercial applications such as supercapacitors, high energy-density batteries and electrochromic devices etc. In this context, PEO based polymer electrolytes are the most intensively studied electrolytes and it may be seen that continuous research is being concentrated on PEO based polymer electrolytes due to following characteristics of PEO:

- Presence of sequential polar groups with large sufficient electron donor power
- Low hindrance to bond rotations
- A suitable distance between coordinating centers to form multiple intra-polymer ion bonds
- Ability to dissolve high concentrations of variety of salts etc.

Despite these virtues, PEO based polymer electrolytes possess poor conductivity at ambient temperature in practical applications. These electrolytes attain useful ionic

conductivity only at temperatures above their transition temperature i.e., melting temperature which leads to certain problems such as leakage and loss of electrode-electrolyte contact, as encountered in devices based on liquid electrolytes. Many groups have attempted over past three decades to enhance the electrochemical properties of PEO based polymer electrolytes by various methods such as polymer blending and plasticization etc; as already discussed in previous sections which is generally carried out by trial and error [8-10, 12]. Each of these modified systems has its own strength and weakness.

Polymer blending provides a strategic route to improve the performance of the electrolyte over each individual polymer. Blending of PEO with PVC, PMMA, PVA etc. is available in literature. Out of many polymer blends reported so far, PEO-PMMA polymer blend is one of the most suitable, and, of particular interest due to various reasons. Some of these reasons are listed below:

1. PMMA inhibits the crystallization of PEO,
2. the components are available commercially in a large range of molecular weights with narrow distributions,
3. PEO and PMMA are miscible,
4. a large difference in the glass transition temperature ( $T_g$ ) values of both polymers and
5. dilution of PEO with PMMA causes a depression of the spherulite growth rate of PEO.

PEO-PMMA blends are reported to be a class of unique blend [112], exhibiting significant dynamic heterogeneity. Dynamic heterogeneity is a phenomenon in which each component retains much of its own dynamic characteristics in the blend rather than

conform to a mean blend behavior. This is due to large difference in the dynamics of the pure components. In this blend system, it had been postulated that the PEO retains its high mobility almost regardless of its surroundings due to the fact that its ether oxygen has no side groups. The dynamics of the PEO chains are much faster than those of the PMMA chains despite the fact that the blend is miscible. The segmental dynamics of PEO are 12 orders of magnitude greater than PMMA dynamics at the blend  $T_g$  [113]. In addition, the dynamics of the PEO chains were nearly independent of composition for PEO concentrations of 0.5-30%. The observation of widely spaced chain dynamics indicates that the PMMA acts glassy on the time scale for motion of the PEO chains. The implications of these highly different dynamics may be very much important in crystallization processes. The relatively slow motion of the PMMA chains may hinder the PEO from reaching a growing crystal and affect the observed morphology. Experimental variables such as the molecular weight, crystallization temperature, and PMMA tacticity have been studied. Parizel *et. al.* [114] have discussed NMR and DSC studies on PEO-PMMA blends and Jedi *et. al.* [115] reported enhancement in ionic conductivity of Li-based PMMA polymer system when blended with PEO. Effect of solvent in PEO-PMMA polymer blend system has been studied by Radhakrishnan *et. al.* [116] whereas Sakai *et. al.* [117] described the dynamics of PEO in blends with PMMA using neutron scattering. The rate of crystallization was shown to decrease with increasing PMMA content.

Although PEO being a semi-crystalline polymer, PEO based polymer electrolyte systems show good conductivity of the order of  $10^{-4}$  S/cm [45]. Rather poor conductivities of plain salt-polymer mixtures resulting from large crystalline fraction of

PEO and its complexes induced extended studies on related materials with reduced crystallinity and increased ionic conductivities. On the other hand, PMMA is an x-ray amorphous polymer and predominantly insulating one only with electronic transport. Polymer electrolytes based on PMMA show conductivity of the range of  $10^{-6}$  to  $10^{-7}$  S/cm [118] which is quite low compared to that of PEO based systems. The miscibility of these two polymers is quite good. It is observed that the amount of PEO has been kept below 30% in most of the work on PEO-PMMA polymer blends.

Studies on interaction of alkali metal-ion salts such as lithium salts (e.g., LiSCN, LiI,  $\text{LiCF}_3\text{SO}_3$ ,  $\text{LiClO}_4$ ), sodium salts (e.g., NaI,  $\text{NaClO}_4$ ,  $\text{NaPF}_6$ ,  $\text{NaNO}_3$ , NaSCN,  $\text{NaCF}_3\text{SO}_3$  etc.), magnesium salts (e.g.,  $\text{Mg}(\text{CF}_3\text{SO}_3)_2$ ,  $\text{Mg}(\text{ClO}_4)_2$ , MgO,  $\text{MgCl}_2$ ) and silver salt ( $\text{AgI}$ ,  $\text{AgClO}_4$ ,  $\text{AgCF}_3\text{SO}_3$ ) with polymer are seen in literature. Among the metal-ions conducting salts, transition metal ion conducting salt i.e.; silver salt {silver nitrate ( $\text{AgNO}_3$ )} is selected for the present study. Apart from the scientific interest, silver salts have several advantages over that of other salts. Silver salts are non-toxic i.e., environment friendly, non-inflammable and have good coordination between polar groups. In past, many researchers have already conducted studies on different silver salts. Generally, it is found that a higher salt concentration in polymer systems make the ion aggregates which results in decrease in conduction process. Hence, silver salt at lower concentration was selected for present study.

Out of various optimization techniques to improve the electrical properties of polymer electrolytes, plasticization is a conventional method. Addition of plasticizers decreases the glass transition temperature which helps in easy movement of polymer chains. Plasticizers are small organic molecules which embed themselves between the

polymer chains and increase the spacing and free volume by dissociating ion aggregates. . However, the effect of plasticizer on electrical properties of polymer depends upon viscosity, dielectric constant, polymer plasticizer interaction and ion plasticizer coordination. Plasticization effects using polyethylene glycol (PEG) and ethylene carbonate (EC) were taken in the present work where the former one has lower value of dielectric constant than polymer while latter has higher value.

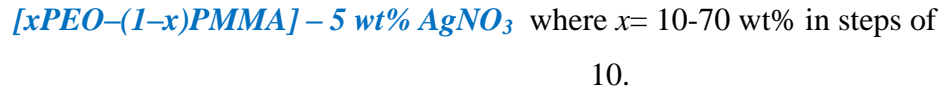
Generally, the addition of plasticizer alone would yield polymer electrolytes with enhanced properties but gives rise to loss of mechanical stability. To pursue this line of work, incorporation of nano-fillers such as  $\text{Al}_2\text{O}_3$ ,  $\text{SiO}_2$ ,  $\text{TiO}_2$  etc. to polymer electrolytes or plasticized polymer electrolytes has been undertaken by many workers to prepare mechanically stable thin films. The addition of nano-fillers basically improves the resistance to crystallization and the stability of the electrode-electrolyte interface. Thus it is expected that the combined effect of plasticizer and nano-filler to polymer electrolytes would be of great importance. Limited work on combined effect is available in literature.

For the present study, a systematic study on PEO-PMMA polymer blend nano-composite electrolytes is undertaken. In this study, the improvement in the conductivity of polymer electrolytes has been observed step by step. This is done through conductivity studies with the support of characterization studies upon blending effect, then plasticization effect using two different plasticizers and at last combined effect of plasticizer and nano-fillers. The optimum concentration of sample from each step is identified and brought to the next step. For this, first the ratio of PEO to PMMA was optimized to find the effect of blending and then plasticization of optimized ratio of polymer blend with different plasticizers is carried out. Finally, incorporation of nano-

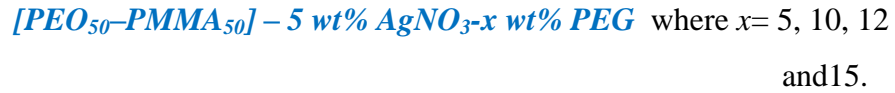
fillers in plasticized polymer blend electrolytes was taken. After the preparation of samples, the silver ion conduction by means of electrical and relaxation properties in polymer blend nano-composite electrolytes is carried out.

For the present work, series of silver ion conducting polymer electrolyte systems is prepared. Polyethylene oxide (PEO) and polymethyl methacrylate (PMMA) are taken as host polymers with silver nitrate ( $\text{AgNO}_3$ ) as dopant metal salt. The amount of salt is kept as low as 5wt% in all systems. A systematic description of research work is given below:

1. First system (PPS-system): In this system, polymer blend electrolytes were prepared according to:



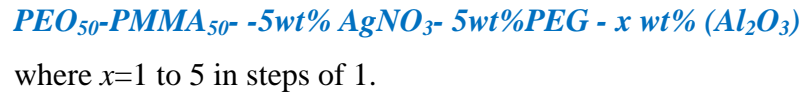
2. Second system (PPSP-system):



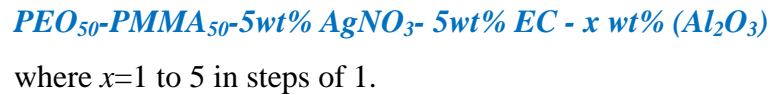
3. Third system (PPSE-system):



4. Fourth system (PPSP-system):



5. Fifth system (PPSEA-system):



These systems will be known as PPS, PPSP, PPSE, PPSPA and PPSEA in forthcoming chapters.

## References:

1. A.R. West, *Solid State Chemistry and its applications*, John Wiley & Sons Pt. Ltd., Singapore 2003.
2. W. H. Meyer, *Adv. Mater.* 10(1998) 439–448.
3. M. Armand, J.M. Tarascon, *Nature* 2008, 451, 652–657.
4. M. B. Armand, *Ann. Rev. Mater. Sci.* 16 (1986) 1986.
5. J. W. Fergus, *J. Power Sources* 195 (2010) 4554–4569.
6. M.Z.A. Munshi (ed.), *Handbook of Solid State Batteries and Capacitors*, World Scientific Pub. Co. Inc, 1995.
7. F.M. Gray, *Polymer electrolytes*. Springer Verlag, 1997.
8. S.A. Hashmi, A. Chandra, S. Chandra, in: B.V.R.Chowdari, et. al (Ed.), (1992) *Solid State Ionics: Materials and Applications*, World Scientific, Singapore, p. 567.
9. R. G.Linford, *Applications of Electroactive Polymers*, B. Scrosati (ed.), Chapman and Hall, London 1993.
10. J.R. MacCallum, C.A. Vincent (Eds.), *Polymer Electrolyte Reviews*, Elsevier, Amsterdam (1987).
11. D.Kunze, *Fast Ion Transport in Solids*, W. V. Gool (ed.), North Holland, Amsterdam, (1973).
12. F.M. Gray, *Solid Polymer Electrolytes: Fundamental and Technological Applications*, VCH Publishers, New York, 1991.
13. B. Reuter, K. Hardel, *Naturwissenschaften* 48 (1961)161.
14. B. B. Owens, G. R Argue, *Science* 157 (1967)308.
15. J. N. Bradley, P. D. Green, *Trans. Farad. Soc.* 63(1967)424.
16. J. T. Kummer, N. Weber, *U.S. patent* 3 458 356 (1968)
17. P. P. Kumar, S. Yashonath, *J. Chem. Sci.* 118(2006)135–154.
18. B.K. Money, *Ph.D. thesis*, Submitted to IIT Madras, 2010.
19. P. Knauth, *Solid State Ionics* 180(2009) 911–916.
20. G. Nazri, G. Pistoia (Eds), *Lithium batteries-Science and Technology*, Kluwer Academic Publishers, London, 2004.
21. J.P. Malugani, G. Robert, *Solid State Ionics* 1 (1980) 519.
22. R. Mercier, J.P. Malugani, B. Fahys, G. Robert, *Solid State Ionics* 5(1981) 663–666.
23. J.L. Souquet, A. Kone, M. Ribes, *J. Non-Cryst. Solids* 38-39(1980) 307.
24. W. L. Roth, G. C. Farrington, *Science* 196(1977) 1332.
25. I.D. Raistrick, C. Ho, R. A. Huggins, *Mater. Res. Bull.* 11(1976) 953.
26. R. C. Agrawal and G. P. Pandey *J. Phys. D: Appl. Phys.* 41(2008) 223001.
27. Y. Yao, J.T. Kummer, *J. Inorg. Nucl. Chem.* 29(1967) 2453-2475.
28. R. C. Agrawal, R. K. Gupta, *J. Mater. Sci.* 34(1999) 1131 – 1162.
29. P.S. Anantha, K. Hariharan, *J. Phys. Chem. Solids* 64(2003) 1131-1137.
30. Y.Chatani, S. Okamura, *Polymer* 28(1987) 1815-1820.
31. C.C. Hunter, M.D. Ingram *Solid State Ionics* 14(1984) 31-40.
32. S. Chandra, *Superionic Solids:Principles and Applications*, North Holland, Amsterdam, 1981.
33. K.P. Padmasree, D.K. Kanchan, *J. Non-Cryst. Solids* 352(2006) 3841-3848.
34. H. Eliasson, I. Albinsson, B.E. Mellander, *Electrochim. Acta* 43(1998) 1459-1463.
35. S.A. Suthanthiraraj, R. Kumar, B.J. Paul, *International J. Nanosci.* 10(2011) 241-246.
36. N. Machida, M. Chusho, T. Minami, *J. Non-Cryst. Solids* 101(1988) 70-74.
37. M. Sureshini, K. Hariharan, *J. Mater. Sci. Lett.* 9(1990) 544-546.
38. C. Singhal, K. Kendall, *High temperature Solid oxide fuel cells: fundamental, design and applications*, Elsevier Advanced Technology, U.K. 2003.
39. P.J. Gellings, H. J. M. Bouwmeester, *The CRC Handbook of Solid State Electrochemistry*, CRC Press, Inc. 1997.

40. J.M.Reau, C. Lucat, J. Portier, P. Hagenmuller, L. Cot, S. Vilminot, *Mater. Res. Bull.* 13(1978) 877-882.
41. L. Patro, K. Hariharan, *Solid State Ionics* 239 (2013) 41–49.
42. P. Knauth, M. L. D. Vona, *Solid State Proton Conductors: Properties and Applications in Fuel Cells*, John Wiley & Sons Ltd. 2012.
43. J. W. Phair . S. P. S. Badwal, *Ionics* 12 (2006) 103–115.
44. E. K. Cho, J.S. Park, S.S. Sekhon, G.G. Park, T.H. Yang, W.Y. Lee, C.S. Kim, S.B. Park, *J. Electrochem. Soc.* 156(2009) B197-202.
45. G.P. Pandey, Y. Kumar, S.A. Hashmi, *Solid State Ionics* 190 (2011) 93–98.
46. G.G. Kumar, N. Munichandraiah, *J. Power Sources* 102 (2001) 46.
47. E. Sheha, M.K. El-Mansy, *J. Power Sources* 185(2008) 1509-1513.
48. P. G. Bruce, *Solid state Electrochemistry*, Cambridge University Press, 1995.
49. B. A. Huberman, *Phys. Rev. B* 32(1974) 1000-1002.
50. D. H. Rothman, S. Zaleski, *Reviews Modern Physics* 66(1994) 1417-1481.
51. K. Funke, *Prog. Solid State Chem.* 22 (1993) 11.
52. K. Funke, *Rad. Effects & Defects in solids* 119-121 (1991) 463-468.
53. B.A.Huberman, P.N.Sen, *Phys. Rev. Lett.* 33(1974) 1379.
54. S. Geller, in *Superionic Conductors*, G.D. Mahan, W.L. Roth (eds.), Springer-Verlag US, 1976, pp.171-182.
55. M.C.R. Shastry, K. J. Rao, *Proc. Indian Acad. Sci. (Chem. Sci.)*102 (1990) 541-553.
56. G. Licheri, A. Musinu, G. Paschina, G. Piccaluga, G. Pinna, A. Magistris, *J. Chem. Phys.* 85(1986) 500-506.
57. K.P. Padmasree, D.K. Kanchan, A.R. Kulkarni, *Solid State Ionics* 177 (2006)475-482.
58. M. S. Jayswal, D.K. Kanchan, P. Sharma, M. Pant, *Solid State Ionics* 186(2011)7-13.
59. J.P. Malugani, G. Robert, *Mater. Res. Bull.* 14 (1979) 1075.
60. T. Minami, N. Machida, in *Solid state Ionics*, M. Balkanski, T. Takahashi, H. L. Tuller (eds.) Elsevier Science 1992.
61. J. Kawamura in : *Recent Advance in Fast Ion Conducting Materials and Devices*, B.V.R. Chowdari, Q.G Liu, L.Q. Chen (eds.), World Scientific, Singapore (1990) 47.
62. O. L. Anderson, D. A. Stuart, *J. Am. Ceram. Soc.* 37 (1954)573.
63. D. Ravaine, J.L. Souquet, *Phys. Chem. Glasses* 18 (1977) 27
64. D. Ravaine, J.L. Souquet, *Phys. Chem. Glasses* 19 (1978) 115.
65. A.M. Glass, K. Nassau, *J.Appl. Phys.* 51 (1980) 375.
66. T. Minami, Y. Ikeda, M. Tanaka, *Solid State Ionics* 9-10(1982) 577.
67. M.D.Ingram, M.A. Mackenzic, W. Muller, M. Torge, *Solid State Ionics* 28-30 (1988) 677.
68. M. Nagai, T. Nishino, *Solid State Ionics* 117 (1999) 317-321.
69. U. Lauer, J. Maier, *Solid State Ionics* 51 (1992) 209-213.
70. M. Nagai, T. Nishino, *J Amer. Cer. Soc.* 76 (1993) 1057-1060.
71. T. Jow, J. B. Jr Wagner, *J. Electrochem. Soc.* 126 (1979) 1963.
72. J. Maier, *Phys.Status Solidi (b)* 123 (1984) K89-K91.
73. A. Bunde, W. Dieterich, E. Roman, *Phys. Rev. Lett.* 55 (1985) 5.
74. K. M. Shaju, S. Chandra, *J. Mater. Sci.* 30 (1995) 3457.
75. J.K. Kim, S.H. Kim, *Solid State Ionics* 124(1999) 91-99.
76. J. Kawamura, R.Asayama, N. Kuwata, O. Kamishima, in *Physics of Solid State Ionics* , T. Sakuma, H.Takahashi (eds.) 2006, pp.193-246.
77. A. Karmakar, A. Ghosh, *Phys. Rev. E* 84(2011)051802.
78. G.P. Pandey, S.A.Hashmi, R. C. Agrawal, *Solid state Ionics* 179(2008) 543-549.
79. S. D. Thompson, L.R. Jordan, M. Forsyth, *Electrochim. Acta* 46 (2001)1657–1663.
80. R. C. Agrawal, Y. K. Mahipal, *Int. J. Electrochem. Sci.* 6 (2011) 867 – 881.

81. S. Chandra, S.A. Hashmi, M. Saleem, R.C. Agrawal, *Solid State Ionics* 67(1993) 1.
82. J.Y. Song, Y.Y. Wang, C.C. Wan, *J. Power Sources* 77(1999) 183-197.
83. P.W.M. Jacobs, L.W. Lorimer, A. Russer, M. Wasiucionek, *J. Power Sources* 26(1989) 503.
84. M. Vogel, T.Torbrugge, *J. Chem. Phys.* 125(2006) 054905.
85. T. Miyamoto, K. Shibayama, *J. Appl. Phys.* 44(1973) 5372.
86. M.B. Armand, *Annual Rev. Mater. Sci.* 16(1986) 245-261.
87. L.H. Sperling, Chapter 5, *ACS Symposium Series* 1080(2011) pp.69-82.
88. American Chemical Society International Historic Chemical Landmarks. Foundations of Polymer Science: Hermann Staudinger and Macromolecules.  
<http://portal.acs.org/portal/PublicWebSite/education/whatischemistry/>
89. C. E. Carraher Jr., *Giant molecules*, John Wiley & Sons, 2003
90. V.R. Gowariker, N.V. Viswanathan, J. Sreedhar, *Polymer Science*, New Age International Ltd., New Delhi, 1986.
91. P.V. Wright, *British Poly. J.* 7 (1975), 319
92. D.E. Fenton, J. M. Parker, P. V. Wright, *Polymer* 14(1973) 589.
93. M. B. Armand, J.M. Chabagno, M.J. Duclot, Book of abstracts, *2nd International conference on Solid Electrolytes*, St. Andrews, Scotland, 20-22 Sept. 1978.
94. C. Berthier, W. Gorecki, M. Minier, M.B. Armand, J.M. Chabagno, P. Rigand, *Solid State Ionics* 11 (1983) 91.
95. S. Chandra, S.B. Rai, P.K. Singh, K. Kumar, A. Chandra, *J. Phys. D: Appl. Phys.* 39(2006) 3680-3683.
96. F.M. Gray, *Solid Polymer Electrolytes: Fundamental and Technological Applications*, Wiley, 1991
97. P. Bahadur, N V Sastry, *Principles of Polymer Science*, 2nd Edition, Narosa Publishing House Ltd.2009.
98. M. Kumar, S.S. Sekhon, *Ionics* 8(2002) 223-233.
99. M.H. Buraidah, L.P. Teo, S.R. Majid, A.K. Arof, *Physica B* 404(2009)1373–1379.
100. C. A. Angell, C. Liu, E. Sanchez, *Nature* 362 (1993) 137 – 139.
101. L. Feng, H. Cui, *J. Power Sources* 63 (1996) 145-148.
102. D. Saikia, A. Kumar, *Electrochim. Acta* 49 (2004) 2581–2589
103. D. Kumar, S.A. Hashmi, *Solid State Ionics* 181 (2010) 416–423
104. G.P. Pandey, S.A. Hashmi, *J. Power Sources* 187 (2009) 627–634
105. F. Croce, G.B. Appetecchi, L. Persi, B. Scrosati, *Nature* 394(1998) 456.
106. C. Capiglia, P. Mustarelli, E. Quartarone, C. Tomassi, A. Magistris, *Solid State Ionics* 118 (1999) 73.
107. S. K. F. Shirey, J.K. Maranas, *J. Phys. Chem. C* 114 (2010) 9196–9206.
108. N. Gondaliya, D.K. Kanchan, P. Sharma, M. S. Jayswal, *Polymer Composites* 33(2012) 2195-2200.
109. S. Ramesh, G. P. Ang, *Ionics* 16(2010) 465–473.
110. A. K. Thakur, S.A. Hashmi, *Solid State Ionics* 181(2010) 1270-1278.
111. B. Smitha, S. Sridhar, A.A. Khan, *J. Membrane Sci.* 259(2005) 10-26.
112. I. Zeroni, S. Ozair, T. P. Lodge, *Macromolecules* 41(2005)5033-5041.
113. K.L. Ngai, *Relaxation and diffusion in complex systems*, Springer, New York, 2011
114. N. Parizel, F. Laupretre, L. Monnerie, *Polymer* 38(1997) 3719-3725.
115. K. Jeddi, N.T. Qazvini, S.H. Jafari, H.A. Khonakdar, *J. Poly. Sci. B: Poly. Phys.* 48(2010)2065-2071.
116. S. Radhakrishnan, P.D. Venkatachalapathy, *Polymer* 37(1996) 3749-3752.
117. V.G. Sakai, J.K. Maranas, I. Peral, J.R.D. Copley, *Macromolecules* 41 (2008)3701-3710.
118. N. Shukla, A.K. Thakur, *Ionics* 15(2009) 357-367.

## **CHAPTER 2-Theoretical details**

---

This chapter deals with the ion conduction mechanism and various theories related to conduction mechanism in polymer electrolytes. Different formalisms of impedance spectroscopy have been discussed to probe the ion dynamics process.

---

## **2.1 Introduction**

Electrical conduction mechanism in polymer electrolytes is a challenging task to decipher. In addition to that, ion conduction process in these materials is even more challenging job. Polymer electrolytes can be simply pictured as ionic solutions in an essentially immobile solvent. Ionic conductivity is the main aspect to be concerned in the solid polymer electrolytes. The mechanism of ionic transport in polymer electrolytes is novel and quite distinct from the processes occurring in liquid solutions, molten salts or crystalline solid electrolytes.

## **2.2 Ionic Conductivity**

Conductivity is the ability of a material to conduct electric current. Ionic transport in liquid and solid is a consequence of the random migration of ions stimulated by thermal energy as long as the applied electric field is small enough. Ionic conductivity is defined as ionic transportation under the influence of an external electric field. It is the movement of an ion from one site to another through defects in the crystal lattice of a solid. In solids, ions typically occupy the fixed positions in the crystal lattice and do not move. However, the ions rarely have enough thermal energy to escape from their lattice sites although they vibrate continuously. Ionic conduction occurs if the ions are able to escape and move into their adjacent available (energy) sites. There are two possible mechanisms for the movement of ions through a lattice viz., vacancy mechanism and interstitial mechanism [1]. These mechanisms are sketched in Fig.2.1. Vacancy mechanism is created by the hopping of an ion from its normal position on the lattice to an adjacent equivalent but empty site. While in an interstitial mechanism, ion jumps or hops to an adjacent equivalent sites. Hence it can be said that the minimum requirement

of ionic conduction is either the presence of some vacant sites or there are some ions in the interstitial sites which can hop into the adjacent vacant interstitial sites.

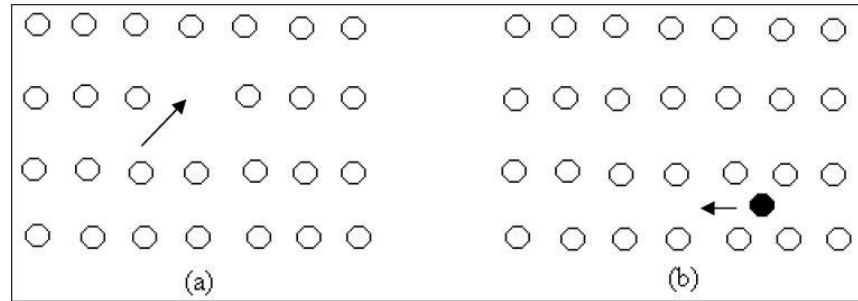


**Fig. 2.1** Schematic representation of ionic motion by (a) a vacancy mechanism and (b) an interstitial mechanism.

### 2.2.1 Basic conditions for ionic conductivity [2]

- A large number of the ions of one species should be mobile.
- A large number of empty sites should be available for the ionic conduction.
- The empty and occupied sites should have similar potential energies (equivalent sites) with a low activation barrier (also known as activation energy) for jumping between the neighboring sites. It is useless to have a large number of available vacant sites if either the mobile ions cannot get into these or if these are too small.
- The structure should have a framework, preferably three-dimensional, permeated by open channels through which mobile ions may migrate.
- The anion framework should be highly polarizable.

The magnitude of the ionic conductivity is generally affected by the degree of crystallinity, salt concentration and temperature in polymer electrolytes [3]. The ionic conduction is generated only if the crystal defects are involved. The deterioration of the crystalline portion in the polymer electrolytes will initiate the formation of amorphous phase. Amorphous phase is a physical state of a polymer where the molecules are in disordered arrangement, whereas the crystalline phase refers to the situation where polymer molecules chains are in oriented or aligned arrangement. Since the amorphous

regions are composed of disordered arrangement, thus the molecules within the polymeric chains are not packed tightly in their lattice sites. Therefore, it leads to higher flexibility of the polymeric segments and increases the mobility of charge carriers. These disordered regions create more empty spaces or voids for ionic hopping which in turn raise the ionic conductivity of polymer electrolytes. In principle, at low salt concentration, the ionic conductivity is strongly controlled by number of charge carriers and the mobility of ions is relatively unaffected. However, at high salt concentration, the ionic conductivity is strongly dependent on the mobility of ions and the ionic conduction pathway. The ionic transportation is closely correlated to the relaxation modes of the polymer. This can be observed through the increase in  $T_g$  of polymer system as the salt content is increased. In this phenomenon, the segmental mobility is significantly reduced as it increases the intra and inter coordination bonds within the polymer chains. Since polymer electrolytes fall apart into charged poly-ions and oppositely charged counter-ions, thus all the charges attached to the polymer matrix would repel each other. At low salt concentration, the random coils in the polymer chain expand tremendously due to the repulsion effect of the like charges on the polymer chain. The expansion allows these charges to be as far apart as possible. When the polymer matrix stretches out, it takes up more spaces. Therefore, the availability of vacant sites for ionic conduction is enormously decreased.

Solid polymer electrolytes differ from conventional glassy ion conductors in that the glass transition temperature ( $T_g$ ) of the former is, in general, below room temperature whereas that of the conventional glasses is way above room temperature [4]. Thus, polymer electrolytes are, in general, in rubbery state whereas the conventional glass

conductors are in “glassy” state, at room temperature. Hopping of the mobile ions between different fixed vacant sites in a frozen disordered structure gives rise to the conductivity in glassy ionic conductors. However, the situation is somewhat different than simple ion hopping in polymer electrolytes, as they are in rubbery state at room temperature and the hopping sites are not fixed in a dynamically evolving disordered structure. From the viewpoint of an individual hopper, this means that if the local environment at any given time does not permit a hop, that environment will evolve such that, after a certain average waiting time the hop will no longer be prohibited.

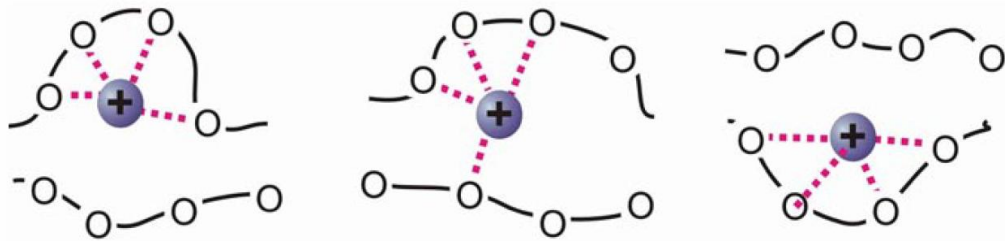


**Fig. 2.2** *Cation migration in solid polymer electrolyte (association with the segmental mobility of the polymer chains)* (Resource: Ref. [5])

In these so called polymer electrolytes, long range ionic diffusion leading to ionic conductivity only occurs in the presence of local segmental motions of the polymer host (Fig. 2.2) [5, 6]. The ionic conductivity in polymer electrolytes is very much coupled to the segmental motion of the host polymer i.e. more the segmental mobility, higher is the ionic conductivity. Different ionic conduction mechanisms were proposed by many workers [6-10] to explain ionic motion in polymer electrolytes. The ionic transport nature i.e.; ionic mobility and charge carrier concentration in these materials is quite complex and depends on many variables such as degree of hydration, impurity ions from the polymerization process, ion pairing, inhomogeneties in the sample and conduction due to both types of the mobile ions (cation and anion). Several empirical relations and

theories/models are developed/proposed to explain the ion conduction mechanism in different polymer electrolyte systems. Some of these theories/models are discussed below in brief:

### 2.3 Ion transport mechanism

Since the discovery of ionic conductivity in alkali metal salt complexes of polyethylene oxide (PEO) by Wright in 1973 [11], a great deal of effort has been focused on the study of ion transport mechanisms and on the development of materials for technological applications [12-19]. The movement of ions in polymer electrolytes is mediated by the local motion of the polymer chain segments above glass transition temperature,  $T_g$ . The liquid-like motion of polymer segments above  $T_g$  causes the local environment at any one point in the polymer sample to change with time. This has a strong influence on the charge transport in polymer electrolytes.

The basic equation of conductivity of conducting materials with all different charge carriers as [12]:

$$\sigma = \sum_i q_i n_i \mu_i \quad \dots(2.1)$$

where  $\sigma$  is the specific ionic conductivity, i.e.; the charge transport across a unit cross-sectional area per second per unit electric field applied,  $n$  and  $q$  are the number of each kind of carrier and its charges respectively. All these variables ( $\sigma$ ,  $n$ ,  $q$ ) depend on the material environment.

Earlier in studies of PEO salt complexes, it was suggested that cations reside inside the single or double helices of polyether chains [13, 14], and cation hopping through the helices was thought to be the mechanism for ion transport. The anions were supposed to be almost immobile and take position outside the helices. Later, it was

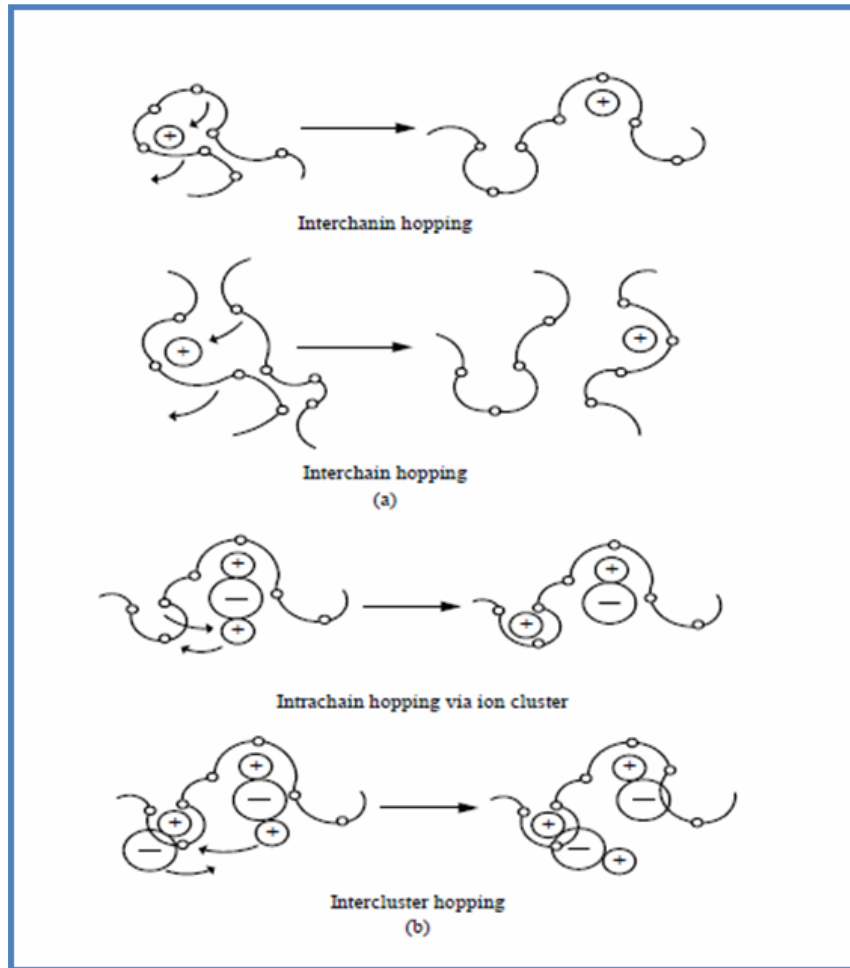


**Fig. 2.3** Representation of cation motions in a polymer electrolyte (a) assisted by polymer chain motion only; and (b) taking account of ionic cluster contributions. (Resource: Ref. [15])

suggested [13, 16] that a helical structure with small ions lying inside the helix of PEO-salt complex and cation mostly reside inside the helical PEO crystal regions i.e.; the cations are complexed in locally helical regions. The local segmental motions of the polymer chains assist the cationic and anionic transport through the bulk [17]. A hopping mechanism with only cations moving down channels within PEO helical crystalline assuming no anion motion was proposed [13]. However, this model cannot explain the ion motion in amorphous regions. Later on, Gray [14] suggested another picture of the ion movement associated with the polymer segmental motions via making and breaking

of the co-ordination bonds between cations and polymers, resulting in more free volume for ion diffusion under the electric field. Considering the ion-ion interaction and different ionic species in polymer electrolyte, he suggested two types of ionic motions, i.e.; ionic motion is either assisted by the polymer chain motion or it is from ionic cluster to ionic cluster with polymer chains acting as anchor points (Fig.2.3). He suggested that the mechanism depends, to a large extent, on the concentration of salts in polymer electrolytes.

## **2.4 Empirical relationship for Temperature dependence of conductivity**

A number of empirical relationships have been developed to explain the ion transport phenomena, particularly the temperature dependent conductivity of the polymer electrolytes [18-21]. In polymer electrolytes, the crystalline phase exhibits Arrhenius conductivity, whereas the amorphous phase exhibits the VTF conductivity [4]. Thus, polymer electrolytes may be considered as a two component system. At temperatures far below the melting point, the fraction of the crystalline phase is dominant and the overall conductivity behavior of polymer electrolytes is dominated by Arrhenius behavior. When the temperature is raised, the fraction of the amorphous phase regions increases such that at a certain temperature,  $T_c$ ; the fraction of the amorphous phase is large enough to create a continuous connection between the amorphous cubes. At this juncture, the electrical conductivity changes from Arrhenius-like to VTF-like behavior. This temperature  $T_c$  is called critical temperature or a percolation temperature. At temperatures above the melting point, all parts of polymer electrolytes are amorphous and the conductivity is absolutely VTF-like. Some of temperature dependent ion- conducting theories are

discussed below:

### 2.4.1 Arrhenius Theory

This gives a basic relationship which describes the linear relationship of  $\ln \sigma$  with  $1000/T$ . This theory was developed in 1889, by the Swedish chemist Svante Arrhenius [20]. It was found to be applicable for liquids and solids electrolytes later. In solids, the ions hop from one vacant site to another by overcoming the energy barrier i.e., activation energy  $E_a$  that exists between these [22]. On application of an electric field  $E$ , the potential energies in the direction of the field and that opposite to it get altered. Then the ions start hopping along the direction of field giving rise to an ion current density  $j$  (assuming only one direction) and one ion conducting species:

$$\vec{j} = (na^2e^2\nu\vec{E})/kT = \sigma\vec{E} \quad \dots(2.2)$$

where  $k$  is the Boltzmann constant,  $n$  is the number of defects per unit volume [23] ( $n \propto \exp(-G/2kT)$   $G$  is the Gibbs free energy for the creation of defects),  $a$  is the inter-ionic distance,  $e$  is the charge of the ion and  $\sigma$  is the ionic conductivity and  $\nu$  is the jump frequency or the probability of jumping from one site to another, in the absence of any external electric field and is given by:

$$\nu = \nu_0 \exp(-\Delta G/kT) \quad \dots(2.3)$$

where  $\nu_0$  is the attempt frequency and  $\Delta G = \Delta H - T\Delta S$ ,  $\Delta H$  and  $\Delta S$  are the enthalpy and entropy of diffusion respectively.  $\Delta G$  is the energy of migration and it is the difference between the free energy of the ion at the normal lattice point and that atop the barrier. Finally we have the form as:

$$\sigma = \frac{A}{T} \exp\left(-\frac{E_a}{kT}\right) \quad \dots(2.4)$$

where  $A = ba^2e^2k$  is the pre exponential factor ( $b$  is the constant of proportionality) and  $E_a = \Delta G + G/2$  is the activation energy for migration and creation of defects. This is the Arrhenius equation [24, 25]. This equation implies that  $\ln(\sigma T)$  vs.  $1/T$  fits a straight line (a linear relationship) and the slope gives the activation energy.

#### 2.4.2 VTF theory

The non-Arrhenius behavior of the temperature dependence of the ionic conductivity measured from polymer electrolytes is the hallmark of ionic motion being coupled with the host matrix. The temperature dependence of the conductivity exhibits an apparent activation energy that increases as temperature decreases. This behavior is most commonly described by the empirical Vogel–Tammann–Fulcher (VTF) equation, which was first developed to describe the viscosity of supercooled liquids [21, 26-29].

According to *Vogel-Tammann-Fulcher* (VTF) [30], the migration of metal ions depends mainly on the segmental motion of polymer chain in the amorphous region and the temperature of the conductivity of polymer films follows the relationship:

$$\sigma(T) = \frac{A}{\sqrt{T}} \exp\left(\frac{-E}{k(T-T_0)}\right) \quad \dots(2.5)$$

where  $T_0$  is the glass transition temperature;  $A$  is a pre-exponential factor, which is determined by the transport coefficient and proportional to the number of carrier ions,  $E$  is activation energy and  $k_B$  is Boltzmann constant.

#### 2.4.3 WLF theory

The *Williams, Landel and Ferry* (WLF) approach is a general extension of VTF treatment to characterize relaxation processes in amorphous materials. The ionic conductivity of some polymer electrolytes was found to obey WLF equation [31, 32].

This equation is given as:

$$\log(a_T) = \log \frac{\sigma(T)}{\sigma(T_g)} = \frac{C_1(T-T_g)}{C_2+(T-T_g)} \quad \dots(2.6)$$

where  $\sigma(T)$  and  $\sigma(T_g)$  are the ionic conductivity at  $T$  and  $T_g$  respectively,  $C_1$  and  $C_2$  are constant. WLF equation incorporates the relaxation processes of polymers into the relationship using the shift factor  $a_T$ . Values of shift factor  $a_T$  are obtained by horizontal shift  $\log(a_T)$  of creep compliance data plotted vs. frequency in double logarithm scale so that a data set obtained experimentally at temperature  $T$  superposes with the data set at temperature  $T_g$ . A minimum of three values of  $a_T$  are needed to obtain  $C_1$ ,  $C_2$ , and typically more than three are used. The shift factor is the ratio of any mechanical relaxation process at a given temperature to its value at some reference temperature. WLF equation implies that a decrease in  $T_g$  could lead to an increase in the ionic conductivity. Conductivity of Li-ion conducting boron polymer electrolytes [32] and PEO-alkali metal salts [33] polymer electrolytes have been explained using WLF equation.

Although the WLF equation provides useful information on the temperature dependence of the ionic conductivity in polymer electrolytes; but the above proposed transport mechanism is under debated. In contrast to the general belief that ionic conductivity occurs only in amorphous polymers above  $T_g$ , Gadjourova *et. al.* [34] in 2001, have shown that ionic conductivity in certain crystalline polymer electrolytes e.g.; PEO<sub>6</sub>-LiSbF<sub>6</sub> polymer electrolytes is more as compared to their amorphous counterparts over a range of corresponding temperatures.

## **2.5 Theoretical models of Conductivity**

### **2.5.1. Free Volume Model**

In polymeric materials, a small amount of unfilled volume is associated with the

end of a polymer chain. This volume is called the *free volume* and may be schematically represented in the Fig. 2.4. For a given mass of polymer, the amount of free volume will depend on the number of chain ends, hence the number of chains which in turn depends on the degree of polymerization.

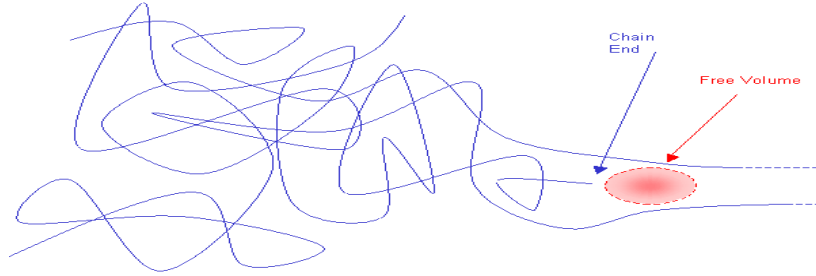


**Fig. 2.4** Schematic representation of creation of free volume in polymers.

This macroscopic approach has been successfully able to address the temperature and pressure dependence of ionic conductivity in polymer electrolytes. The free volume theory was developed by Cohen and Turnbull [35, 36] and is equally applicable to other amorphous systems like; glasses and super-cooled melts. The basic assumption of the free volume theory is that the diffusion of ions is not activated process but rather a result of redistribution of free volume within the material. The molecules are considered as hard spheres confined to their cages. Once a hole (free volume) is opened, the molecule moves in it with a thermal velocity  $u$ . Using this, it can be shown that the diffusion coefficient is given by:

$$D = ga^*u \exp \left[ \frac{-\gamma v^*}{\alpha v_M (T - T_0)} \right] \quad \dots(2.7)$$

where  $\gamma$  is a geometric factor,  $a^*$  is roughly molecular diameter,  $\gamma v^*$  is molecular volume,  $v_M$  is mean molecular volume of the species whose motions create free volume,  $\alpha$  is the difference in thermal expansion coefficient between liquid and glass over the same range

and  $T_0$  is the temperature at which the free volume disappears (close to the equilibrium glass transition temperature). More specifically, the above equation is derived by maximizing the number of ways of distributing the free volume, without any consideration of whether all such distributions are in fact reasonably accessible. It is this question of accessibility (or, alternatively, of the rate of free volume motion or interchange) which limits the validity of VTF in situations involving ionic transport in polymeric electrolytes.

Using the Nernst-Einstein equation [37]  $\sigma = nq^2D/kT$  where  $n$  and  $q$  are the number and the charge of the conducting species respectively, with the assumption that  $u \sim T^{1/2}$  the equation can be transformed to:

$$\sigma = \sigma_0 \exp\left[\frac{-E}{k(T-T_0)}\right] \quad \dots(2.8)$$

which is identical to the empirical VTF equation which has been fitted to the thermal dependence of many polymer electrolytes exceedingly well. Though this equation is used to fit a large number of experimental results, one may note that it has been derived considering the motion of the polymer host alone. However, the picture of free volume is intuitively attractive, and can be well used to derive the VTF equation, there are some significant disadvantages associated with its use. The free volume model does not include any dynamics or kinetics; in particular, the free volume is assumed to move instantaneously with no constraints and no effects of ion-ion correlation or ion-polymer complexation are included. At last, saying straight forward towards the experimental findings, there are some discrepancies such as a maximum in conductivity as the ion concentration is varied that cannot be explained using VTF conductivity curves always [38]. Therefore in cases where the ionic motions are high or ion pair formation is large,

this equation may not be able to describe the results. Also, it does not account for the variation due to change in the percentage of amorphous regions in a semi-crystalline polymer.

### 2.5.2 Configurational Entropy model

Another approach as configurational entropy model was proposed by Adam and Gibbs [39] in 1965 where two parameters (the number of lattice site and number of distorted bonds) are introduced into the free volume theory. The mass transportation mechanism in this model is assumed to be a group cooperative rearrangement of the chain. The probability  $W$ , of a mass- transporting rearrangement in the polymer electrolytes can be expressed as:

$$w = A \exp(-\Delta \mu S_c^* / kTS_c) \quad \dots(2.9)$$

where  $A$  is a coefficient,  $S_c^*$  is the minimum configuration entropy required for rearrangement,  $S_c$  is the configurational entropy at temperature  $T$ , and  $\Delta$  is the free energy barrier per mole which impedes the rearrangement. Bruce [3] suggested that both VTF and WLF equation can be derived from the configurational entropy model.

### 2.5.3 Static Bond Percolation theory

The static bond percolation model [40], basically deals with the ionic motion in the electrolytes of rigid framework. This model explains various properties of polymer electrolytes which are useful in understanding transport processes. It is based on the concept that for any fixed polymer configuration, motion of ions is described by a percolation process (i.e., hopping) with the hopping rates between any two sites can be chosen as finite or zero depending upon whether these sites are mutually accessible (open bond/available) or not (close bond/unavailable) [41]. In this model, some sites are defined

at which the mobile carriers (ions/electrons etc.) reside and their motions can be expressed as:

$$P_i = \Sigma \{P_j W_{ji} - P_i W_{ij}\} \quad \dots(2.10)$$

where  $P_i = P_i(t)$  is the probability of finding the mobile carrier at site  $i$  at time  $t$  and  $W_{ji} = W_{ij}$  is the hopping rate at which carrier jumps from  $j$  to  $i$  site and vice-versa. The links between the localized sites for mobile carriers are called bonds. In the standard percolation model, the jumps are either permitted or not permitted. Thus, this model involves the motion of a carrier on a given lattice whose bonds are randomly available with certain availability. The static bond percolation theory successfully explained the well known experimentally observed property that the crystalline phase has no conductivity and amorphous phase is responsible for ionic conduction in polymer electrolytes.

#### **2.5.4 Dynamic Bond Percolation model**

*Druger, Nitzan and Ratner* proposed the dynamic bond percolation theory [41] in 1983 which describes diffusion of small particles (ions, electrons) in a medium which in addition to being statistically disordered is also undergoing dynamic rearrangement processes on a shorter time scale compared to the observation time. The dynamic percolation model deals with situations in which the structure is not only statically but also dynamically disordered [42]. In other words, this model is natural extension of the static bond percolation model, which describes transport in systems in which hops between sites are either forbidden or allowed with specific fixed probabilities to systems in which the host structure is evolving. This model is the only microscopic model developed so far that takes into account the actual situation in the polymer electrolytes i.e. ionic motion combining the ionic transitional motion/hopping and dynamic

segmental (chain) motion of the polymer host above the glass transition temperature ( $T > T_g$ ). Actually, dynamic static bond model, an extension of static bond percolation model, deals with the hopping/diffusion of small particles through a dynamically disordered medium. It is based on the idea that the lattice in polymer electrolytes is no longer static but undergoes rearrangements that re-assign the open and closed bonds. Physically, these rearrangements correspond to orientational motions of the host polymer lattice. In case of polymer electrolytes, the motion of polymer segments (chains) is expected above  $T_g$  value. So, for  $T > T_g$ , various stable sites with ion will move with respect to one another and thereby changing the complexation of open or close bonds. Such a dynamic motion of the polymeric host is then modeled by allowing the hopping probabilities to readjust or renew their values on a time scale corresponding to polymer motion.

### **2.5.5 Space Charge Model**

This model discussed the physical approaches to explain conductivity enhancement in some 2-phase composite electrolyte systems and was referred to as the space charge model [43]. One of the approaches suggested by Bhattacharya and Maier [44] was based on non-aqueous liquid electrolytes. In case of liquid systems, a composite can be formed but only with high inorganic particle content. These materials are described as a viscous grain ensemble wetted by the liquid or ‘soggy sand’ - like system [45]. A synergetic effect due to interfacial interactions is observed yielding about one order of magnitude increase of the conductivity value. The ‘soggy sand’ systems show some similarities with the properties of solid composite polymeric electrolytes. In both cases, a covalent organic matrix can produce a ground state for the charge carriers present

in the form of undissociated salt particles. Thus, the conductivity effect would consist of absorption of one of the pair's constituents, resulting in a break-up of the ion pair and generating a mobile counter ion. In all these types, a percolation type of behavior is observed, which is essential for the enhancement of the conductivity.

### 2.5.6 Amorphous phase model

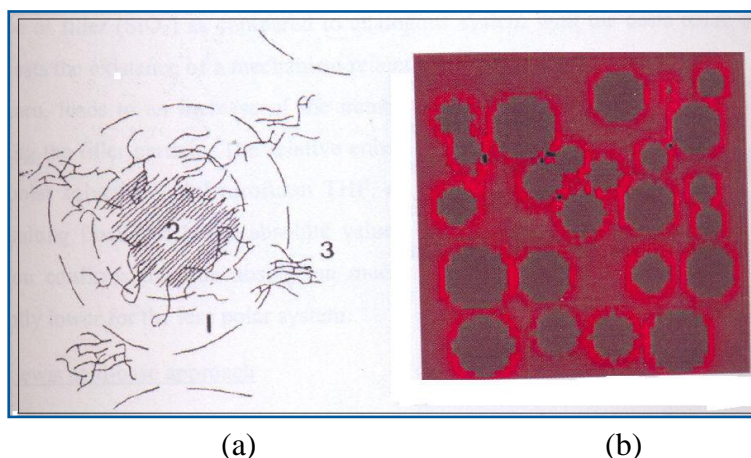


**Fig. 2.5** (a) Schematic drawing of morphology of composite polyether non-conductive-filler electrolytes: (1) highly conductive interface layers coating the surfaces of grains, (2) dispersed insulating grains, (3) polymer ionic conductor matrix; (b) Formation of conducting pathways (Resource: Ref. [46]).

In a variety of composite polymer electrolytes, based on high molecular weight PEO matrix, a decrease in the degree of crystallinity has been identified, which is related to an increase in the ionic conductivity as measured in these systems as compared to undispersed PEO-salt complexes. On the basis of the results obtained, an 'amorphous phase' model was developed, which explained the increase in the conductivity in composite polymer electrolytes [47]. In the crystalline PEO-salt complex systems, filler particles (e.g.  $\alpha$ - $\text{Al}_2\text{O}_3$ ) act as nucleation centers and probably attached to PEO segments (Fig. 2.5). Since, there are a large number of such nucleation centers, crystallization process becomes faster due to higher nucleation rate and, in consequence, a bigger level of disorder, typically, like the liquid state, is frozen during solidification of the polymeric

matrix as observed in the cooling process or solvent evaporation.

### 2.5.7 Effective Medium Theory

This theory was proposed by C.W. Nan, in 1994, to treat coupled electromechanical behavior in composite media [48]. It has been successfully applied to describe electrical properties of various heterogeneous systems including polymer electrolytes. It can also explain very well, the effect of insulating fillers and consequent enhancement in the conductivity in composite solid electrolytes. The conductivity enhancement is attributed to high defect concentration on the surface of the filler grains due to the formation of ‘space – charge’ layers.

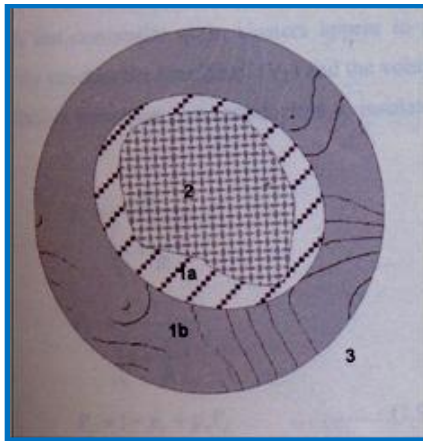


**Fig. 2.6** A schematic diagram showing a single grain dispersed in the polymer electrolyte matrix (Resource: Ref. [45]).

Like amorphous phase model, effective medium theory approach for composite polymer electrolytes also assumed that there are three phases present in the composite polymer electrolyte as shown in Fig. 2.6. Each phase has different electrical property. Phase (1a) represents part of the amorphous shell formed on the grain surface in which the influence of stiffening over imposes the amorphization. Phase (1b) is the highly conductive (due to the amorphization) interface layer coating on the surface of the grain. Phase (2) is the dispersed insulating grain dispersed in the matrix of polymer ion

conductor. In phase (3), the composite grain units are dispersed throughout the polymer electrolyte host matrix and the highly conducting interface layer coating on the surface of grains overlap or touch each other resulting into high conducting pathways. However, the extent of conductivity enhancement in composite polymer electrolytes depends on the conductivity of interface layers, dispersoid particle distribution and their size. A higher conductivity enhancement is expected at relatively smaller volume fraction with smaller particle size.

### **2.5.8 Rouse Model**

Rouse model describes the Langevin dynamics of random networks applied to the dynamics of polymer electrolytes [49]. In this model, it is assumed that ions form temporary cross-links between oxygen atoms of the polymer backbone which results in slow down of structural relaxations. Also, this relaxation becomes more stretched. By calculating the mean square displacement of the ions and applying the Nernst –Einstein relation, the concentration dependence of the conductivity can be calculated. It shows that after an increase with ion concentration, the conductivity reaches a plateau and eventually starts to decrease. At short time-scales, the ions are attached to the polymer host and therefore, the area these ions can move in is limited. After a while, due to structural relaxations of the polymer host, cross-links break and new ones are formed. This enables the ion to diffuse through the entire system, leading to ionic conductivity.

However, most of these models can be successfully applied only in amorphous and single-phase systems, and they cannot give satisfactory explanation of the ion transport behavior in complicated multi-phase systems such as composite polymer electrolytes.

## 2.3 Plasticization theories

Apart from these ion transport theories in polymer electrolytes, there are theories that describe the effects of plasticizer in polymer electrolytes. Plasticizers or dispersants are additives that increase the plasticity or fluidity of the material to which they are added. Organic plasticizers are used to increase the flexibility of the host polymer chains. Low molecule weight polyglycols are some of the more common plasticizers [50]. However, plasticized systems generally display poor mechanical stability, which greatly limits their technological applications and hence should be used with caution.

Plasticization theories are given below in brief:

### 2.6.1 Lubricity theory

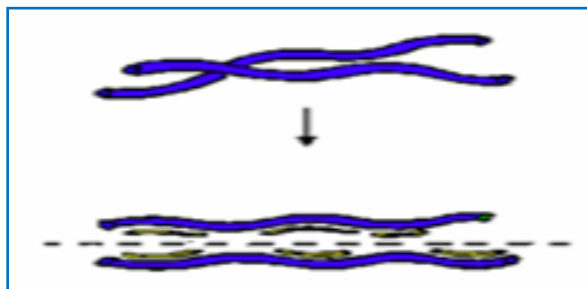


**Fig. 2.7** *Plasticizer polymer response based on Lubricity theory.*

The lubricity theory was developed by Kilpatrick [51], Clark [52], and Houwink [53]. This theory states that plasticizer acts as a lubricant between polymer molecules. In other words, the function of plasticizer is to reduce the intermolecular friction between the polymer chain molecules. The plasticizer acts by lubricating the movement of the molecules and reducing their internal resistance to sliding (Fig. 2.7). This theory assumes that the polymer macromolecules have very weak bonds away from their cross-linked sites.

## 2.6.2 Gel theory

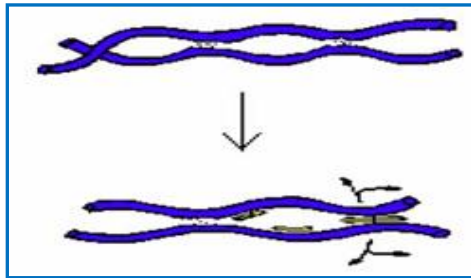


**Fig. 2.8** *Gel Theory of Plasticizers.*

Gel theory of plasticization was developed by Aiken and others [54, 55]. This theory is an extension of Lubricant theory. It proposes that plasticizer molecules break up the polymer-polymer interaction by getting in between the chains and “obscuring” these interaction sites from the polymer molecules. This theory considers that the polymers formed by a tridimensional honeycomb structure maintained by loose attachments between the polymer molecules along their chains. There are solvation-desolvation and aggregation-deaggregation equilibria between the polymer and the plasticizer molecules. The rigidity in polymers occurs primarily due to the resistance of their tridimensional structures rather than to the internal frictions, as the lubricant theory states.

Gel theory of plasticization starts with a model of polymer molecules in a three-dimensional structure. The stiffness of the polymer results from a gel of weak attachments at intervals along the polymer chains. The points of gel are close together, thus, permitting little movement gel sites must be the result of Vander Waals forces, hydrogen bonding or crystalline structure. The gel sites can interact with plasticizer, thus, separating a gel site of the adjacent polymer chains (Fig. 2.8). The plasticizer by its presence separates the polymer chains allowing the polymer molecules to move more freely.

### 2.6.3 Free volume theory

The free volume theory of plasticization sought to explain the reduction in polymer glass transition temperature upon the addition of plasticizer. It had been observed that the specific volume of polymers decrease linearly with decreasing temperatures until the  $T_g$  was reached (Fig. 2.9). After that, the specific volume decreased more slowly. It was assumed that the increased specific volume above the glass transition temperature was attributable to “free volume”, space between molecules. Today, free

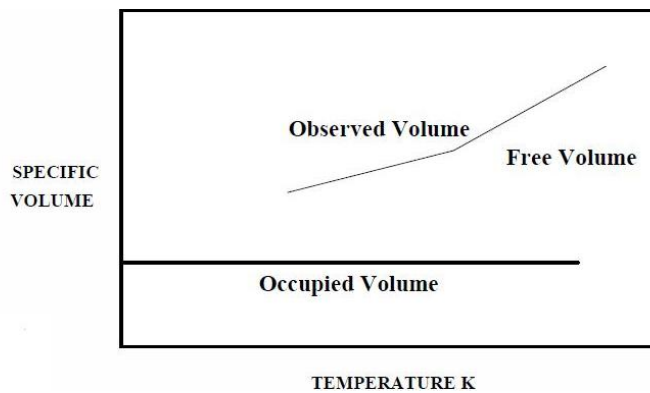


**Fig. 2.9** *Free Volume Theory of Plasticization.*

volume is typically defined as the difference in specific volume at some temperature of interest and some reference temperature, usually absolute zero. Practically, it is difficult to determine that what volume of the plastic would be at absolute zero; theoretically it is difficult to determine what the volume of a plastic would be at absolute zero, so that figure is an approximation. Free volume in the polymer could come from several sources, motion of polymer end groups, motion of polymer side groups, and internal polymer motions. Below their glass transition temperature, polymers show limited motions of these types. When plasticizer is added to the polymer, motions in the plasticizer molecule, like motions in the polymer, create free volume [55, 56].

## 2.7 Conductivity formalism

*Complex impedance spectroscopy: a tool for electrical characterization* [57].

Complex impedance spectroscopy (CIS) is the most elegant and powerful technique for electrical characterization of solids, in general, and electrochemical devices including electrodes as well as electrolytes, in particular. Impedance spectroscopy is a general term that subsumes the small-signal measurement of the linear electrical response of a material of interest (including electrode effects) and the subsequent analysis of the response to yield useful information about the physicochemical properties of the system [57-59]. This can span more than 17 decades on the frequency scale, ranging from a fraction of a mHz up to about 100 THz. It provides a time-resolved view of the dynamics of the mobile ions in materials with disordered structures, acting as a “microscope in time”. It thus has the potential to elucidate the development from an individual ionic displacement or hop to macroscopic transport of mass and charge, *i.e.*, from less than a picosecond up to minutes and hours [60].

This technique is often used to obtain bulk conductivity, but additional information related to the motion of charged particles could also be obtained. It even resolves the elementary hopping processes of mobile charges. The advances in the technique followed by mathematical formulation and data analyses using equivalent electrical models are obtained [61]. The experimental set-ups required to cover the entire frequency range are sketched in Fig. 2.10.

Impedance spectroscopy is a powerful two-probe technique for electrical characterization of the electrochemical systems including electrodes as well as electrolytes, in particular. It provides the information on electrical properties of materials

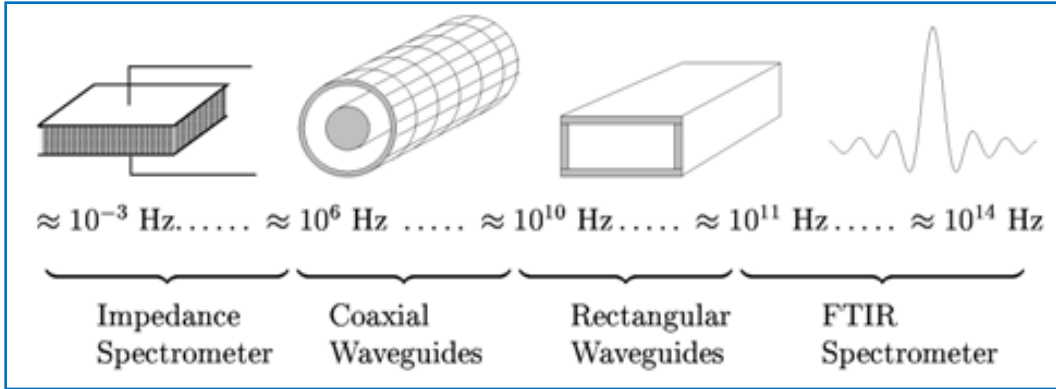


**Fig. 2.10** Schematic overview of techniques for the measurement of frequency-dependent conductivities (Resource: Ref [60]).

and their interface with electronically conducting electrodes. The advances in the technique followed by mathematical formulation and data analyses using electrical equivalent models are reviewed. In this approach, a small amplitude sinusoidal current excitation is applied to the system under the steady-state and measure the voltage response as a function of frequencies. Impedance analysis of ionic solids identifies elementary process such as, the bulk resistance, ionic transport, grain boundary conduction and the electrode-electrolyte interface processes in the measured frequency domain. It is a non-destructive technique and also can provide the dynamic properties to understand the microscopic nature of the ionic materials [61]. It may be used to investigate the dynamics of bound or mobile charge in the bulk or interfacial regions of any kind of solid or liquid material: ionic, semiconducting, mixed electronic-ionic and even insulators (dielectrics). The value of AC impedance spectroscopy derives from the effectiveness of the technique in isolating migration steps in a multistep process because each migration step has ideally a unique time constant associated with it which can be separated in the frequency domain. In recent years, impedance spectroscopy has found widespread applications in the field of characterization of materials. This technique is

routinely used in the characterization of coatings, batteries, fuel cells etc.

The impedance spectroscopy is based on studies made on the measurement of cell impedance over a range of temperatures and frequencies and analyzing them in complex impedance plane [62]. This is particularly characterized by the measurement and analysis of  $Z^*$  (complex impedance) and plotting of this function in the complex plane, known as Nyquist diagrams. In 1960, Sluyter *et. al.* [63] have extensively used impedance spectroscopy technique to study the polarization phenomenon of aqueous electrochemical cells. Thereafter, it has been widely used as one of the most powerful tool to analyze electrochemical processes in the field of aqueous electrochemistry [64, 65]. In 1969, Bauerle [66] was the first to apply this technique to study the basic polarization process in the cell of yttria stabilized zirconia (YSZ). Since then, this technique has been in use for characterizing a wide range of electrolyte and electrode materials, which include polymers, oxides, glasses, polycrystalline composites and ionic liquids etc.

Impedance spectroscopy has become a basic and ideal technique to characterize the solid electrolyte material [57] where the frequency dependent impedance data give the information about the bulk conductivity and the overall transport process of the solid electrolytes. When the impedance frequency data is obtained then it is desirable to do three things namely; **I**- represent graphically the real part,  $Z'$  as a parametric function of frequency of the complex impedance plane along the abscissa and imaginary part,  $Z''$ , along the ordinate, **II**- analyze the data to obtain gross and possibly even microscopic parameters and **III**- convert it into different presentation viz. complex dielectric constant and modulus etc. following appropriate Mathematics.

In impedance measurements, a sine wave is used because sinusoidal signal

applied to a line system; the input and output have the same form, so the magnitude of the response is directly proportional to the electrical stimulus. The applied AC voltage and the resulting current across a cell have the form

$$V = V_{max} \sin (\omega t) \quad \dots(2.11)$$

$$I = I_{max} \sin (\omega t + \phi) \quad \dots(2.12)$$

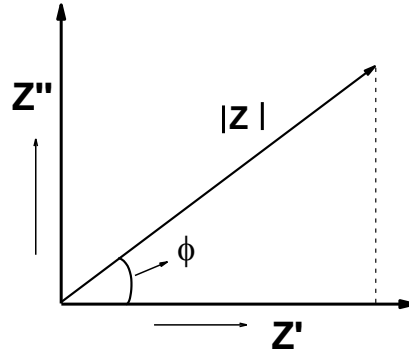


**Fig. 2.11** Impedance plot in complex plane.

where  $\phi$  is the phase angle and  $\omega=2\pi f$ ,  $f$  is the frequency of measurement. The phase angle  $\phi$  corresponds to the phase difference between the applied voltage and current. Thus, the magnitude of impedance is given by  $|Z| = V_{max}/I_{max}$ . The impedance is composed of a frequency independent resistive term  $R$  and a capacitive term  $1/j\omega C$ , where  $j = \sqrt{-1}$ . The absolute value  $|Z|$  and the phase angle  $\phi$  are related to real and imaginary parts of the impedance ( $Z'$  and  $Z''$ ) as follows:

$$Z' = |Z| \cos \phi \quad \dots(2.13)$$

$$Z'' = |Z| \sin \phi \quad \dots(2.14)$$

The projection of real and imaginary parts of impedance on the x and y axis is known as complex impedance plane (Fig.2.11) which is an implicit function of frequency. The complex impedance,  $Z^*$  can be written as

$$Z^* = Z' - jZ'' \quad \dots(2.15)$$

where  $Z'$  is the real part and  $Z''$  the imaginary part of  $Z^*$ .

The complex impedance  $Z^*(\omega)$  has both magnitude  $|Z|$  and phase angle  $\phi$  and can be expressed in both polar as well as Cartesian forms. In Polar form, complex impedance  $Z(\omega)$  may be written as

$$Z^*(\omega) = |Z| \exp(-j\omega), \quad \dots(2.16)$$

where phase angle ( $\phi$ ) is expressed as  $\phi = \tan^{-1}\left(\frac{Z''}{Z'}\right)$ , magnitude  $|Z| = [(Z')^2 + (Z'')^2]^{1/2}$  and  $\exp(-j\phi) = \cos(\phi) - j \sin(\phi)$ .

### 2.7.1 Complex Impedance Data Analysis

Typically ac impedance experiments are carried out over a wide range of frequencies and the interpretation of the resulting spectra is aided by analogy to equivalent circuits are not unique, and indeed there exists an infinite set of circuits that can represent a physically

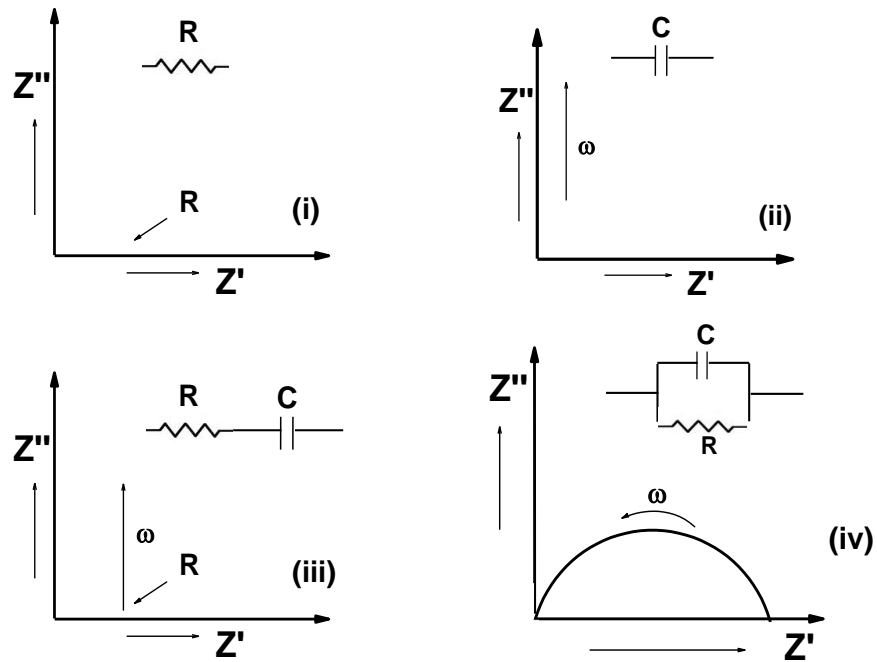


**Fig. 2.12** Complex Impedance plots for some elementary R, C and RC circuits.

plausible circuit containing a minimal number of components. Ionic conductivity can be visualized as a series process involving consecutive hops of an ion over potential energy barriers along the direction of the electric field. This can be modeled as a parallel RC

circuit and the admittance of the circuit is given by

$$Y^* = (Z^*)^{-1} = R^{-1} + j \omega C \quad \dots(2.17)$$

or 
$$\frac{1}{Z^*} = \frac{1}{R} + j\omega C \quad \dots(2.18)$$

so that 
$$Z^* = \frac{R}{(1 + j\omega CR)} \quad \dots(2.19)$$

Simplifying the above expression by using complex conjugate, gives

$$Z^* = \frac{R(1 + j\omega CR)}{1 + (\omega CR)^2} \quad \dots(2.20)$$

so that 
$$Z' = \frac{R}{1 + (\omega CR)^2} \quad \dots(2.21)$$

and 
$$Z'' = \frac{\omega CR^2}{1 + (\omega CR)^2} \quad \dots(2.22)$$

when  $\omega=0$ ,  $Z'=R$  and  $Z''=0$  and when  $\omega=\infty$ ,  $Z'=0$  and  $Z''=0$ . Between these extreme values it can be seen that  $Z'$  and  $Z''$  comply with the following Eq.

$$\frac{R^2}{4} = \left( Z' - \frac{R}{2} \right)^2 + Z''^2 \quad \dots(2.23)$$

This is an equation of a circle with radius  $R/2$  and centre at  $(R/2,0)$  as shown in Fig.2.12 (iv). It represents the response of a resistor  $R$  in parallel with capacitor  $C$  which will be a perfect semicircle intersecting the real axis at  $(R, 0)$ .

In Cartesian form, impedance can be written as:

$$Z^*(\omega) = |Z| [\cos(\phi) - j \sin(\phi)] = Z' - jZ'' \quad \dots(2.24)$$

The data is computed and displayed in the complex plane in the form of real and imaginary component as an implicit function of frequency and is called the *complex impedance plot*. Some complex impedance plots corresponding to  $R$ ,  $C$  and  $RC$  circuit network, which form the basis for the conductivity measurements in the electrochemical

cells, are shown in the Fig.2.13. The relaxation time  $\tau_0=1/\omega_0=RC$  is given by the inverse of frequency  $\omega_0$  at the top of the semicircle in ideal case (Fig. 2.13 (i)). A wide range of materials so reported [67] have shown a depressed semicircle in the impedance spectrum (Fig. 2.13 (ii)) indicating distributed elements of the equivalent circuit [61].

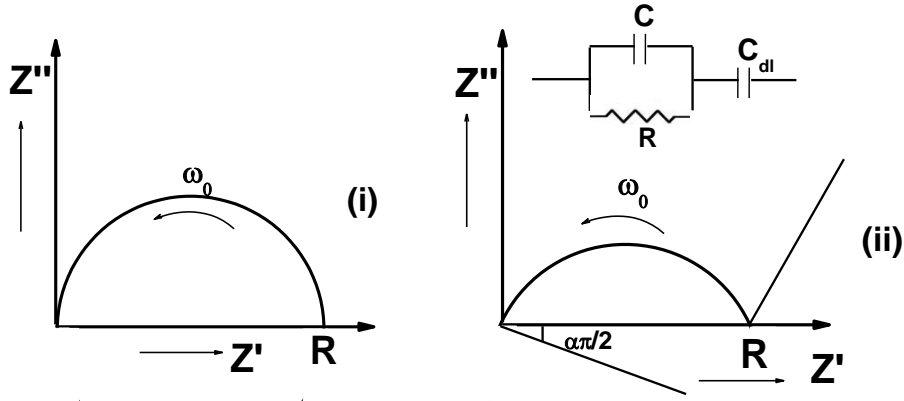


**Fig. 2.13** Geometric response for an (i) ideal circuit (ii) distributed elements.

There are several other measured or derived quantities related to impedance which often play important roles in Impedance Spectroscopy. The two other quantities complex dielectric constant or dielectric permittivity ( $\epsilon^*$ ) and the modulus function ( $M^*$ ) are usually defined as [67-71]

$$\epsilon^* = 1/M^* = 1/(j\omega C_0 Z^*) = \epsilon' - j\epsilon'' \quad \dots(2.25)$$

$$M^* = j\omega C_0 Z^* = M' + jM'' \quad \dots(2.26)$$

In these expressions  $C_0 = \epsilon_0 \left( \frac{A}{t} \right)$  is the capacitance of the empty measuring cell of electrode area  $A$  and thickness  $t$ . The quantity  $\epsilon_0$  is the dielectric permittivity of free space,  $8.854 \times 10^{-12}$  F/m.

## 2.7.2 Dielectric properties of materials

It is important to note that permittivity and permeability are not constant. They can change with frequency, temperature, orientation, mixture, pressure, and molecular

structure of the material [68, 71].

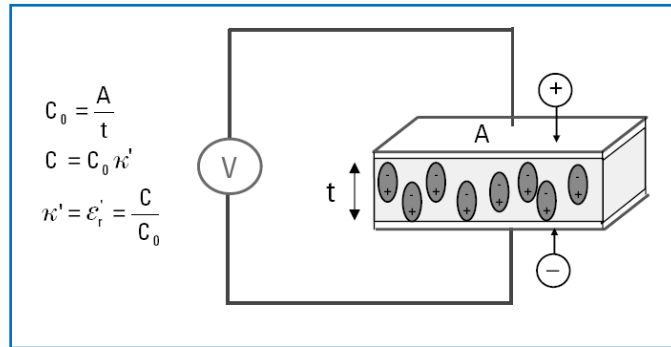


**Fig. 2.14** *Parallel plate capacitor, DC case.*

A material is termed as “dielectric” if it has the ability to store energy when an external electric field is applied. If a DC voltage source is placed across a parallel plate capacitor, more charge is stored when a dielectric material is between the plates than if no material (a vacuum) is between the plates. The dielectric material increases the storage capacity of the capacitor by neutralizing charges at the electrodes, which ordinarily would contribute to the external field. The capacitance with the dielectric material is related to dielectric constant. If a DC voltage source  $V$  is placed across a parallel plate capacitor (Fig. 2.14), more charge is stored when a dielectric material is between the plates than if no material (a vacuum) is between the plates.

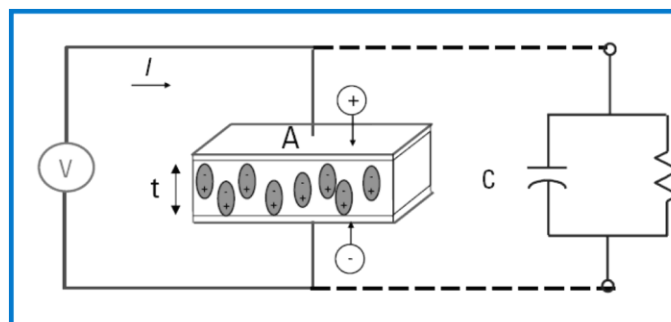


**Fig. 2.15** *Parallel plate capacitor, AC case*

In Fig.2.14,  $C$  and  $C_0$  are capacitance values with and without dielectric,  $k'$  is the real dielectric constant or permittivity, and  $A$  and  $t$  are the area of the capacitor plates and

the distance between them, respectively. The dielectric material increases the storage capacity of the capacitor by neutralizing charges at the electrodes, which ordinarily would contribute to the external field. The capacitance of the dielectric material is related to the dielectric constant as indicated in equation in Fig. 2.14.

If an AC sinusoidal voltage source  $V$  is placed across the same capacitor (Fig.2.15), the resulting current will be made up of a charging current  $I_c$  and a loss current  $I_l$ . The losses in the material can be represented as a conductance (G) in parallel with a capacitor (C) The complex dielectric constant  $k$  consists of a real part  $k'$  which represents the storage and an imaginary part  $k''$  which represents the loss. The following notations are used for the complex dielectric constant interchangeably  $k = k^* = \epsilon^*$ .

From the point of view of electromagnetic theory, the definition of electric displacement (electric flux density)  $D_f$  is:  $D_f = \epsilon E$  where  $\epsilon = \epsilon^* = \epsilon_0 \epsilon_r$  is the absolute permittivity,  $\epsilon_r$  is the relative permittivity,  $\epsilon_0 \approx 8.864 \times 10^{-14}$  F/cm is the free space permittivity and  $E$  is the electric field. Dielectric permittivity describes the interaction of a material with an electric field  $E$  and is a complex quantity i.e.,  $\epsilon^* = \epsilon' - j \epsilon''$ . Here, the real part of permittivity ( $\epsilon'$ ) is a measure of how much energy from an external electric field is stored in the material. The imaginary part of permittivity ( $\epsilon''$ ) is called the loss factor and is a measure of how dissipative or lossy a material is to an external electric field.  $\epsilon''$  is always greater than zero and is usually much smaller than  $\epsilon'$ . The loss factor includes the effects of both dielectric loss and conductivity.

When complex permittivity is drawn as a simple vector diagram (Fig.2.16), the real and imaginary components are  $90^\circ$  out of phase. The vector sum forms an angle  $\delta$  with the real axis ( $\epsilon'$ ). The relative “loss” of a material is the ratio of the energy lost to the

energy stored. The loss tangent or  $\tan \delta$  is defined as the ratio of the imaginary part of the dielectric constant to the real part [72].  $D$  denotes dissipation factor and  $Q$  is quality factor. The loss tangent  $\tan \delta$  is called  $\tan \delta$ , loss tangent or dissipation factor. Sometimes the term “quality factor or Q-factor” is used with respect to an electronic microwave material, which is the reciprocal of the loss tangent. For very low loss materials, since  $\tan \delta \approx \delta$ , the loss tangent can be expressed in angle units, milliradians or microradians.

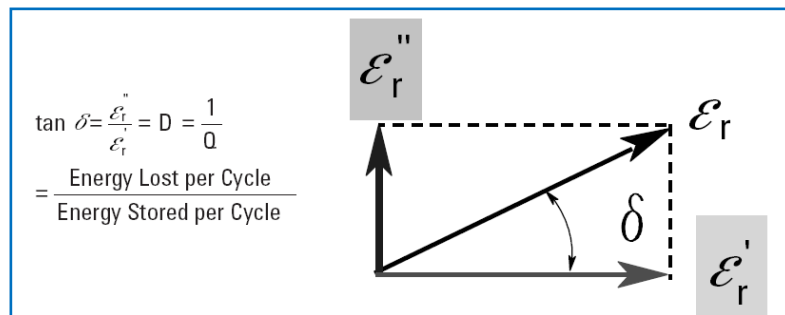


**Fig. 2.16** Loss tangent Vector diagram

### 2.7.3 Dielectric mechanisms

A material may have several dielectric mechanisms or polarization effects that contribute to its overall permittivity (Fig.2.17). A dielectric material has an arrangement of electric charge carriers that can be displaced by an electric field. The charges become polarized to compensate for the electric field such that the positive and negative charges move in opposite directions. At microscopic level, several dielectric mechanisms can contribute to the overall dielectric behavior of the sample. Dipole orientation and ionic conduction interact strongly at microwave frequencies. Water molecules, for example, are permanent dipoles, which rotate to follow an alternating electric field. These mechanisms are quite lossy which explains why food heats in a microwave oven. Atomic and electronic mechanisms are relatively weak and usually constant over the microwave

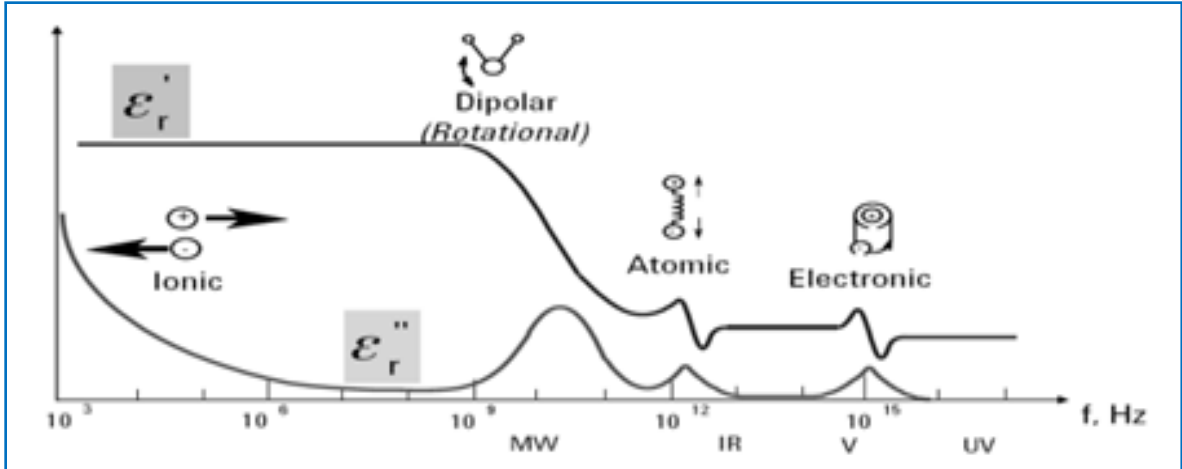


**Fig. 2.17** Frequency response of dielectric mechanisms

region. Each dielectric mechanism has a characteristic “cutoff frequency.” As frequency increases, the slow mechanisms drop out in turn, leaving the faster ones to contribute to  $\epsilon'$ . The loss factor,  $\epsilon''$  will correspondingly peak at each critical frequency. The magnitude and “cutoff frequency” of each mechanism is unique for different materials. Water has a strong dipolar effect at low frequencies – but its dielectric constant rolls off dramatically around 22 GHz. Teflon, on the other hand, has no dipolar mechanisms and its permittivity is remarkably constant well into the millimeter-wave region. A resonant effect is usually associated with electronic or atomic polarization. A relaxation effect is usually associated with orientation polarization.

### 2.7.3.1 Orientational (dipolar) polarization

A molecule is formed when atoms combine to share one or more of their electrons. This rearrangement of electrons may cause an imbalance in charge distribution, creating a permanent dipole moment. These moments are oriented in a random manner in the absence of an electric field so that no net polarization exists. The electric field  $E$  will exercise torque  $T$  on the electric dipole, and the dipole will rotate to align with the electric field causing orientation polarization to occur (Fig. 2.18). If the field changes the

direction, the torque will also change. The friction accompanying the orientation of the dipole will contribute to the dielectric losses. The dipole rotation causes a variation in both  $\epsilon'$  and  $\epsilon''$  at the relaxation frequency which usually occurs in the microwave region. As mentioned, water is an example of a substance that exhibits a strong orientation polarization.

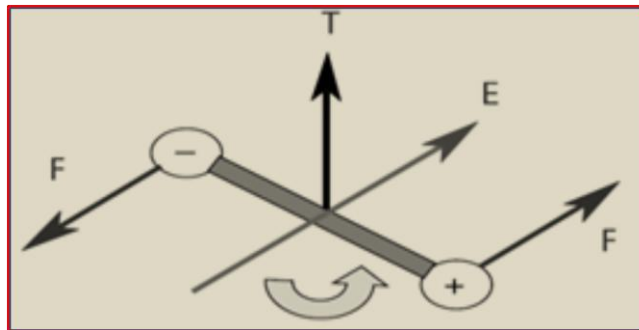


**Fig. 2.18** *Dipole rotation in electric field.*

### 2.7.3.2 Electronic and atomic polarization

Electronic polarization occurs in neutral atoms when an electric field displaces the nucleus with respect to the electrons that surround it. Atomic polarization occurs when adjacent positive and negative ions “stretch” under an applied electric field. For many dry solids, these are the dominant polarization mechanisms at microwave frequencies, although the actual resonance occurs at a much higher frequency. In the infrared and visible light regions the inertia of the orbiting electrons must be taken into account. Atoms can be modeled as oscillators with a damping effect similar to a mechanical spring and mass system. The amplitude of the oscillations will be small for any frequency other than the resonant frequency. Far below resonance, the electronic and atomic mechanisms contribute only a small constant amount to  $\epsilon'$  and are almost lossless. The resonant frequency is identified by a resonant response in  $\epsilon'$  and a peak of maximum absorption in

$\varepsilon''$ . Above the resonance, the contribution from these mechanisms disappears.

### 2.7.3 Modulus formalism

The dispersion behavior of the conductivity in the frequency domain is more conveniently interpreted in terms of conductivity relaxation time,  $\tau$ , using the electrical modulus,  $M^* = 1/\varepsilon^*$  representation [69]. Complex electric modulus  $M^*$  formalism is used very frequently when the relaxation behavior is presumed to be due to the motion of ions or electrons. Although, originally conceived as a formalism to separate space-charge effects from the bulk conductivity, the  $M^*$  representation is now widely used to analyze ionic conductivities by associating a conductivity relaxation time ( $\tau$ ) with the ionic process [69]. The use of modulus formalism in presenting frequency dependent dielectric or conductivity data has the advantage of eliminating any spurious effects due to contacts or interfaces (Maxwell-Wagner effects) [73].

Maxwell-Wagner polarization may be viewed as charge build up between two parallel RC elements in series [74]. Thus in principle, the single loss peak observed in  $\varepsilon''$  should correspond to two peaks in  $M''$ . For the Maxwell-Wagner effect the effective resistance of the suspending medium is infinite, so that only a single peak in  $M''$  reflecting the RC loss in the sphere should be observed. However, their position and intensities reflect the relaxation of the sphere itself, whereas the dielectric loss also reflects the permittivity of the surrounding medium [69].

According to Macedo *et. al.* [69], the electric modulus was defined as the electric analog of the dynamical mechanical modulus and was related to the complex permittivity

$\varepsilon^*(\omega)$  by

$$M^*(\omega) = \left( \frac{1}{\varepsilon^*(\omega)} \right)$$

$$= M'(\omega) + jM''(\omega) \quad \dots(2.27)$$

$$= M_\infty \left[ 1 - \int_0^\infty \exp(-j\omega t) \left( -\frac{d\phi(t)}{dt} \right) dt \right] \quad \dots(2.28)$$

where  $M'$  and  $M''$  are the real and imaginary parts of the complex modulus  $M^*$  and  $M_\infty = 1/\epsilon_\infty$  is the inverse of high frequency dielectric constant  $\epsilon_\infty$ . The function  $\phi(t)$  gives the time evolution of the electric field within the material and  $\omega = 2\pi f$  is the angular frequency.

Analysis of electrical relaxation in terms of complex permittivity  $\epsilon^*(\omega)$  gives relaxational parameters, characteristics of the decay of the displacement vector  $\vec{D}$ , under the constraint of constant electric field,  $\vec{E}$ . It has been suggested [75] that for electrical relaxation in dielectrics containing a substantial concentration of mobile charges, it is generally more fruitful to focus attention on the decay of electric field  $\vec{E}$  at constant  $\vec{D}$  (displacement vector). If surface charges of an opposite sign are instantaneously placed on opposite faces of an ionic conductor at time zero and then maintained at a constant value, an electric field will arise inside the material which with time will decay to zero due to migration of the mobile ions. The expression for the decay of electric field in time domain can be written as

$$\vec{E}(t) = \vec{E}(0)\phi(t) \quad \dots(2.29)$$

where  $\vec{E}(0)$  denotes the electric field at time  $t=0$  and  $\phi(t)$  is a macroscopic decay function of the general form

$$\phi(t) = \int_0^\infty g(\tau_\sigma) \exp\left[-(t/\tau_\sigma)^\beta\right] d\tau_\sigma \quad \dots(2.30)$$

$$\text{Thus, } \vec{E}(t) = \vec{E}(0) \int_0^\infty g(\tau_\sigma) \exp\left[-(t/\tau_\sigma)^\beta\right] d\tau_\sigma \quad \dots(2.31)$$

where  $\tau_\sigma$  is conductivity relaxation time, and  $g(\tau_\sigma)$  is a normalized density function for relaxation times. Thus, using Eqs. 2.28 and 2.30, it becomes

$$M^*(\omega) = M_\infty \int_0^\infty g(\tau_\sigma) \left[ \frac{j\omega\tau_\sigma}{1 + j\omega\tau_\sigma} \right] d\tau_\sigma \quad \dots(2.32)$$

In glassy materials, the decay function  $\phi(t)$  is found to exhibit non exponential (i.e., if there is a distribution of relaxation times and  $g(\tau_\sigma)$  is not a delta function) nature. The decay of the electric field due to the migration of mobile ions will then give rise to a non zero frequency dispersion ( $\epsilon_0 - \epsilon_\infty$ ) in the dielectric constant  $\epsilon'$ . In time domain, a good description for the decay function is the so called *stretched exponential* introduced by *Kohlraush-Williams-Watts* (KWW) [76, 77] and is given as

$$\phi(t) = \exp \left[ - \left( \frac{t}{\tau_\sigma} \right)^\beta \right] ; \quad 0 < \beta < 1 \quad \dots(2.33)$$

where  $\tau_\sigma$  and  $\beta$  are the parameters of stretched exponential function and are respectively the conductivity relaxation time and the Kohlrausch exponent [78]. The smaller is the value of  $\beta$ , the larger is the deviation of the relaxation with respect to a Debye type relaxation. The  $\beta$  parameter has been interpreted either as representatives of a distribution of relaxation times [79] or as characteristic of cooperative motions between charge carriers.

## 2.8 Frequency dependence of conductivity

In general, electrical characterization of the materials can be done by dc and ac measurement technique. Though the dc measurement technique is straight forward, it cannot be implemented for ionic or mixed electronic-ionic systems because on application of dc field, the ionic material gets polarized. Due to which the ionic

conductivity gradually ceases, giving only electronic conductivity. To overcome the above problem, ac technique is preferred over dc technique. Frequency dependent conductivity behavior of ionically conducting solid electrolytes has been the focus of a large number of studies [4, 61, 73, 78] although very limited understanding of this multifaceted problem has been achieved so far.

### 2.8.1 Jonscher's Power law

There are large numbers of theories, to explain the dispersion behavior of solid polymer electrolytes, among them universal model for ac transport seems to have been successful. The frequency dependence of conductivity is a sum of dc conductivity due to the movement of free charges and polarization conductivity due to the movement of bound charges. With decreasing frequency, the conductivity  $\sigma(\omega, T)$  decreases and approaches the direct current conductivity  $\sigma_{dc}$ . The low conductivity value at low frequencies is related to the accumulation of ions due to the slow periodic reversal of the electric field. In the high frequency region, the power law nature  $\sigma(\omega) \propto \omega^n$  is observed and the conductivity sharply increases with frequency. This universal behavior in conductivity is given by Jonscher [80] which describe the dispersion behavior observed in ac conductivity. The variation of conductivity with frequency may be expressed to the well known power law of ac behavior which indicates a non-random process where in the ion motion is correlated [80, 81] given by the following empirical relation;

$$\sigma(\omega) = \sigma_{dc} + A\omega^n \quad \dots(2.34)$$

where  $\sigma(\omega)$  is the conductivity at a particular frequency,  $\sigma_{dc}$  is the dc conductivity at zero frequency,  $A$  is a constant and  $n$  is the frequency exponent lies in the range of  $0 < n < 1$ . The above expression is known as the *power law of ac behavior*. Because the power

law of ac behavior is observed in wide range of materials, Jonscher called it “*Universal Behavior*” [81]. The eq. 2.34 is accepted universally for considering the sample conductivity, hopping charges, frequency dependence of conductivity etc. The frequency exponent  $n$  was calculated from the slope of the plot  $\log(\sigma' - \sigma_{dc})$  versus  $\log \omega$ , which is a straight line. If exponent  $n$  values lie in the range 0.6-0.9 then it is said that the correlation motion is sub-diffusive and indicates a preference on the part of ions that have hopped away to return to the site from where they started. The exponent,  $n$  is a measure of degree of interaction with the environment. Jonscher [81] had shown that a non zero  $n$  in the dispersive region of conductivity is due to the energy stored in the short range collective motion of ions. A higher  $n$  implies that large energy is stored in such collective motions.

### **2.8.2 Jump relaxation model**

In *jump relaxation model*, Funke [82] has proposed that the dc plateau and the power law region should be considered as a single entity. Both these regions together represent ‘*successful*’ and ‘*unsuccessful*’ hopping of the mobile ions. According to this model, at very low frequencies ( $\omega \rightarrow 0$ ), an ion can jump from one site to its neighboring vacant site successfully contributing to dc conductivity. At high frequency, the probability for the ion to go back again to its initial site increases due to the short time periods available. This high probability for the correlated forward backward hopping at high frequencies together with the relaxation of the dynamic cage potential is responsible for the high frequency dispersion. This theory is generally applicable in glassy electrolytes.

## References:

1. R. W. Cahn, P. Haasen, *Physical Metallurgy*, North-Holland Physics, 1996.
2. A.R. West, *Solid state chemistry and its applications*, John Wiley & Sons, Singapore, 1984.
3. P. G. Bruce, C. A. Vincent, *J. Chem. Soc., Faraday Trans.*, 89 (1993) 3187-3203.
4. N.K. Karan, D.K. Pradhan, R. Thomas, B. Natesan, R.S. Katiyar, *Solid State Ionics* 179 (2008) 689–696.
5. P. Judeinstein, D. Reichert, E. R. deAzevedo, T.J. Bonagamba, *Acta Chim. Slov.* 52 (2005) 349-360.
6. M. C. Lonergan, A. Nitzan, M. A. Ratner, D. F. Shriver, *J. Chem. Phys.* 103 (1995) 3253- 3261.
7. C A Angell, *First International Symposium on Polymer Electrolytes*, St. Andrews Scotland, 1987
8. M.A. Ratner, D.F. Shriver, *Chemical Reviews* 88(1988) 109-124.
9. M.A. Ratner, A. Nitzan, *Faraday Discuss. Chem. Soc.* 88(1989) 19-42.
10. C. A. Vincent, *Electrochimica Acta* 40(1995) 2035-2040.
11. D.E. Fenton, J. M. Parker, P. V. Wright, *Polymer* 14(1973) 589.
12. R.C. Agrawal, R.K. Gupta, *J. Mater. Sci.* 34(1999)1131-1162.
13. M. B. Armand, J. M. Chabagno, M. J. Duclot, in *Fast Ion Transport in Solids*, P. Vashishta, J. N. Mundy, G. K. Shenoy (eds.), North-Holland, New York, 1979.
14. P.G. Bruce, C.A. Vincent, *J. Chem. Soc. Faraday Trans.* 89(1993) 3187-2303.
15. F. M. Gray, *Polymer Electrolytes*, The Royal Society of Chemistry, Cambridge Ltd., UK (1997).
16. B. L. Papke, M.A. Ratner, D.F. Shriver, *J. Electrochem. Soc.* 129(1982) 1694.
17. C. Berthier, W. Gorecki, M. Minier, M.B. Armand, J. M. Chabagno, P. Rigand, *Solid State Ionics* 11 (1983) 91.
18. P.G. Bruce, F. Krok, C.A. Vincent, *Solid State Ionics* 27 (1988) 81-88.
19. P.G. Bruce, F.M. Gray, J. Shi, C.A. Vincent, *Philosophical Magazine A* 64 (1991) 1091-1099.
20. E. T. Crawford, *Arrhenius: From Ionic Theory to the Greenhouse Effect*, Science History Publications, USA, 1996.
21. D. Baril, C. Michot, M. Armand, *Solid State Ionics* 94 (1997) 35-47.
22. P.P. Kumar, S. Yashonath, *J. Chem. Sci.* 118(2006) 135-154.
23. A. G. Guy, *Introduction to Materials Science*. McGraw Hill Book Co., New York, 1971.
24. P. Colomban (ed.), *Proton Conductors: Solids, membranes and gels - materials and devices*, Cambridge University Press, 1992.
25. S.K. Upadhyay, *Chemical Kinetics and reaction dynamics*, Springer 2006.
26. H. Vogel, *Phys. Z.* 22 (1921) 645.
27. G. Tammann, W. Hesse, *Z. Anorg. Allg. Chem.* 156 (1926) 245.
28. G.S. Fulcher, *J. Am. Ceram. Soc.* 8(1925) 339.
29. S.J. Pas, M. D. Ingram, K.Funke, A.J. Hill, *Electrochim. Acta* 50 (2005) 3955–3962
30. T. Uma, T. Mahalingam, U. Stimming, *Mater. Chem. Phys.* 85(2004)131.
31. M.L. Williams, R.F. Landel, J.D. Ferry, *J. Am. Chem. Soc.* 77(1955) 3701.
32. S.I. Tabata, T. Hirakimoto, H. Tokuda, Md. A.B.H. Susan, M. Watanabe, *J. Phys. Chem. B* 108(2004) 19518-19526
33. M. Watanabe, in *International Symposium on Polymer Electrolytes*, C.A. Angell (ed.) 1987.
34. Z. Gadjourova, Y.G. Andreev, D.P.Tunstall, P.G. Bruce, *Nature* 412 (2001) 520.
35. M.H. Cohen, D. Turnbull, *J. Chemical Phys.* 31(1959) 1164-1173.
36. D. Turnbull, M.H. Cohen, *J. Chemical Phys.* 34(1961)120-131.
37. R.J.D. Tilley, *Understanding solids: The science of materials*, John Wiley & Sons, Ltd. 2004.
38. N.A. Stolwijk, M. Wiencierz, C. Heddier, J. Koster, *J. Phys. Chem. B* 116(2012) 3065-3074.
39. G. Adam, J.H. Gibbs, *J. Chem. Phys.* 43(1965) 139.
40. R. Zallen, *The Physics of Amorphous Solids*, Wiley, New York, 1983.

41. S.D. Druger, A. Nitzan, M.A. Ratner, *J. Chem. Phys.* 79(1983)3133-3142.
42. A. Nitzan, M.A. Ratner, *J. Phys. Chem.* 98(1994)1765-1775.
43. P. Knauth, *J. Electroceramics* 5 (2000)111-125.
44. A.J. Bhattacharya, J. Maier, *Adv. Mater.* 16(2004) 811-814.
45. Y.K. Mahipal, *Ph.D. Thesis*, Submitted to Pt. Ravi Shankar University, Raipur, 2011.
46. J. Przulski, W. Wieczorek, *Solid State Ionics* 53-56 (1992)1071-1076.
47. W. Wieczorek, Z. Florjanczyk, J.R. Stevens, *Electrochim. Acta* 40(1995) 2251-2258.
48. C.W. Nan, *J. Appl. Phys.* 76(1994) 1155-1163.
49. P.E. Rouse, *J. Chem. Phys.* 21(1953)1272.
50. J.Y. Song, Y.Y. Wang, C.C. Wan, *J. Power Sources* 77(1999) 183-197.
51. A. J. Kilpatrick, *J. Appl. Phys.* 11(1940) 255.
52. F. W. Clark, *Chem. Ind.* 60(1941) 225.
53. R. Houwink, *Proc. XI Cong. Pure Appl. Chem.*, London, 1947, p. 575–583.
54. W. Aiken, T. Alfrey, A. Janssen, H. Mark, *J. Polym. Sci.* 2(1947) 178–198.
55. D. F. Cadogan, C. J. Howick, *Plasticizers in Kirk-Othmer Encyclopedia of Chemical Technology*, John Wiley and Sons, New York (1996).
56. A. Marcilla, M. Beltran, *Mechanisms of Plasticizer Action in Handbook of Plasticizers*, G. Wypych, (ed.), Chem. Tec. Publishing, Toronto, (2004) 107–120.
57. J.R. Macdonald, *Impedance Spectroscopy Emphasizing Solid Materials and Systems*, Wiley, New York, 1987.
58. J.R. Macdonald, *Annals Biomed. Engg.* 20(1992) 289-305.
59. E. Barsoukov, J.R. Macdonald, *Impedance Spectroscopy: Theory, experiment, and applications*, Wiley, New York, 2005.
60. K. Funke, R.D. Banhatti, *Diffusion Fundamentals* 12(2010)1-2.
61. A.K. Jonscher, *J. Mater. Sci.* 13 (1978)553-562.
62. U. Retter, H. Lohse *Chapter II.5, Electrochemical Impedance Spectroscopy*, F. Scholz (ed.), *Electroanalytical Methods*, 2nd ed., Springer-Verlag Berlin Heidelberg 2010.
63. J. H. Sluyters, *Rec. Trav. Chim.* 79 (1960) 1092–1100.
64. W.A. Badawy, N.H. Hilal, M.El-Rabiee, H. Nady, *Electrochim. Acta* 55(2010) 1880-1887.
65. X.Z. Yuan, C. Song, H. Wang, J. Zhang, *Electrochemical Impedance Spectroscopy in PEM Fuel Cells*, Springer-Verlag London Ltd. 2010.
66. J.E. Bauerle, *J. Phys. Chem. Solids* 30(1969) 2657.
67. A.K. Jonscher, *Dielectric relaxation in Solids*, Chelsea Dielectric Press, London, 1983.
68. M.S. Venkatesh, G.S.V. Raghavan, *Canadian Biosystems Engineering* 47 (2005)7.15-7.30.
69. P.B. Macedo, C.T. Moynihan, R. Bose, *Phys. Chem. Solids* 13(1972) 171-179.
70. M. Wubbenhorst, J. V. Turnhout, *J. Non-Cryst. Solids* 305 (2002) 40–49.
71. R.H. Cole, *Annual Rev. Physical Chem.* 11(1960) 149-168.
72. G. Makaya, *Phys. Lett.* 75A (1980) 513-515.
73. I.M. Hodge, M.D. Ingram, A.R. West, *J. Electroanal. Chem.* 58(1975)429.
74. J. R. Macdonald, *J. Electroanal. Chem.* 223(1987) 25-50.
75. D. L. Sidebottom, B. Roling, K. Funke, *Phys. Rev. B* 63(2000) 024301-1.
76. R. Kohlraush, *Ann. Phys. (Leipzig)* 12(1847)393.
77. G. Williams, D.C.Watts, *Trans. Faraday Soc.* 66(1970)80.
78. N. Baskaran, *J. Appl. Phys.* 92(2002) 825-833.
79. C.T. Moynihan, L.P. Boesch, N.L. Laberge, *Phys. Chem. Glasses* 14(1973) 122-125.
80. A. K. Jonscher, *Nature* 267 (1973) 673.
81. A.K. Jonscher, *J Phys. D: Appl. Phys.* 32 (1999) R57-R70.
82. K. Funke, *Progr. Solid State Chem.* 22 (1993) 111-195.

## **Chapter 3- Experimental details**

---

In this chapter, description of materials used, preparation of samples and different characterization techniques employed to the prepared samples are discussed in detail.

---

### 3.1 Introduction

This chapter describes the sample preparation method and theories of characterization (experimental techniques). The experimental techniques includes *X-ray diffraction (XRD)*, *Differential Scanning Calorimetry (DSC)*, *Fourier transform infra red spectroscopy (FT-IR)*, *Scanning electron microscope (SEM)* and *Wagner's polarization technique*.

### 3.2 Materials and methods

#### 3.2.1 Details of the materials used in the present investigation

##### I. Poly (ethylene oxide) (PEO) polymer

Structure  $\rightarrow$  - (CH<sub>2</sub> - CH<sub>2</sub> - O)-<sub>n</sub> (Fig.3.1), Molecular weight (M.W) = 3 x 10<sup>5</sup>, Glass transition temperature = -60° C, Melting temperature = 66° C, Alfa- Aesar, U.S.A

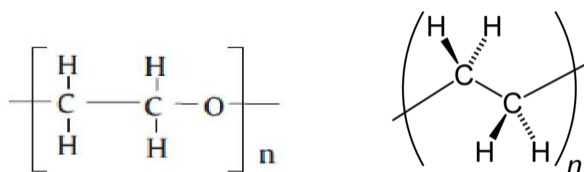


**Fig. 3.1** Structure of Polyethylene

Poly ethylene oxide (PEO) is a white powder with no special smell. It is a semi crystalline material with about 70-85% crystallinity and amorphous elastomeric phase at room temperature [1-3]. Due to partial crystallinity in the structure the problem arises both at micro and macroscopical level. Microscopically, it is due to arrangement at atomic level but arrangement of crystalline and amorphous phases in the polymer and/or polymer-salt complex is termed as macroscopically level. The form of the polycrystalline phase is often dendritic or spherulitic crystalline structure with well separated amorphous boundary [2]. The gross morphological structure of PEO-salt complexes may play an

important role in determining the ion transport properties of the material [4]. PEO is a linear polymer and the regularity of the unit is  $-(\text{CH}_2\text{-CH}_2\text{-O})-$ . The melting point,  $T_m$  of the crystalline phase is  $65^\circ\text{C}$  and the glass transition temperature,  $T_g$  of the amorphous phase is  $-60^\circ\text{C}$ . In PEO polymer, ether oxygens have sufficient electron donor power to form the coordinate bonds with cations. These electrons also facilitate the multiple intra polymer-ion bonding with low potential barrier for rotation of atoms in the polymer main chains. This makes the high flexibility as well as the good segmental motion of polymer chains in the PEO polymer.

## II. Poly (methyl methacrylate) (PMMA) polymer

Structure  $\rightarrow$   $-(\text{C}_4\text{H}_8\text{O}_2)_n-$ , (Fig.3.2) Molecular weight (M.W) =  $3.5 \times 10^5$ , Glass transition temperature =  $108^\circ\text{C}$ , Melting temperature =  $170^\circ\text{C}$ , Alfa- Aesar, U.S.A

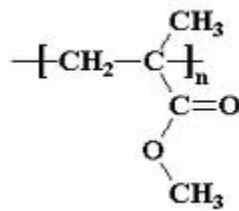


Fig. 3.2 Structure of pure PMMA.

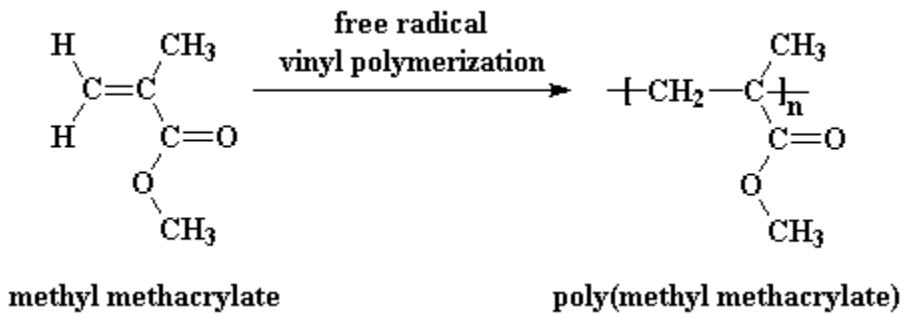


Fig. 3.3 Polymerization of monomer methyl methacrylate.

Poly (methyl methacrylate) (PMMA) is a hard and transparent polymer with good resistance to the effects of light and weathering [5]. It is a synthetic amorphous polymer of methyl methacrylate. The common name for PMMA is acrylic glass because it is a

member of a family of polymers called acrylates. It is a hard thermoplastic with high light transparency and more impact resistant than glass. It has a polar functional group in its polymer chain that exhibits a high affinity for lithium ions and plasticizing solvents. PMMA was polymerized from the monomer methyl methacrylate (Fig.3.3) by free radical initiators such as peroxides and azo compounds via free radical vinyl polymerization. The rigid PMMA is produced due to the substitution of the methyl and methacrylate groups on every carbon of the main carbon backbone chain, providing the steric effects.

### **III. Poly(ethylene) glycol (PEG)**

Structure  $\rightarrow$   $[H(-O-CH_2-CH_2-)_n-OH]$  (Fig. 3.4) , Molecular weight (M.W.)  $\rightarrow$  4000, Glass transition temperature  $\rightarrow$   $-60^\circ C$  , Melting temperature  $\rightarrow$   $55^\circ C$  , Loba Media

Polyethylene glycols (PEGs) are prepared by polymerization of ethylene oxide and are commercially available over a wide range of molecular weights from 300 g/mol to 10,000,000 g/mol. PEG is also known as the low molecular weight waxy or soft solid PEO which has the end product of the polymerization of ethylene oxide (oxyalkylation) in the presence of Lewis acid or base catalysts. PEG is similar to PEO i.e., semicrystalline and water-soluble polymers that are commercially available in a wide range of molecular weights depending on the number of monomers. While PEG and PEO with different molecular weights find use in different applications and have different physical properties (e.g., viscosity) due to chain length effects, their chemical properties are nearly identical. Polyethylene glycol is produced by the interaction of ethylene oxide with water, ethylene glycol, or ethylene glycol oligomers [6]. The reaction is catalyzed by acidic or basic catalysts. The polymer chains can adopt either a helical or

extended structure depending upon the electrostatic interaction of the oxygen units with either ions or charged surfaces. Lower molecular weight ( $M_w < 1000$ ) PEGs are viscous and colorless liquids, while PEGs with the molecular weight of 800 to 2000 is pasty or flaky materials with a low melting range, while above a molecular weight of 3000, PEGs are available in solid form with the melting point to an upper limit of about 65°C.

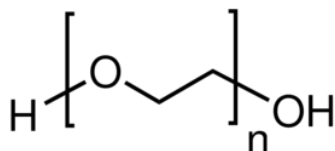


**Fig. 3.4** Chemical structure of Polyethylene glycol (PEG).

#### **IV. Ethylene Carbonate (EC)**

Structure  $\rightarrow \text{C}_3\text{H}_4\text{O}_3$ , Molecular Weight  $\rightarrow 88.06$ , Melting temperature  $\rightarrow 35^\circ - 40^\circ\text{C}$ , Aldrich chemical

Ethylene carbonate is an ester of ethylene glycol and carbonic acid (Fig.3.5). At room temperature (25°C) ethylene carbonate is a transparent crystalline solid, practically odorless and colorless, and somewhat soluble in water. In the liquid state (m.p. 34- 37°C) it is a colorless odorless liquid. Ethylene carbonate is used as a polar solvent and it can be used as a high permittivity component of electrolytes in lithium batteries. Ethylene carbonate is also used as plasticizer and as a precursor to vinylene carbonate which is used in polymers and in organic synthesis.

The effect of plasticizer on the polymer electrolyte strongly relies on the specific nature of the plasticizer, including the dielectric constant, polymer-plasticizer interaction and ion-plasticizer coordination. The choice of choosing ethylene carbonate (EC) instead of propylene carbonate (PC) and dimethyl carbonate (DMC) is because it has superior properties when compared to other organic solvents, including a high dielectric constant

(89.1) [7], a high donor number (16.4) and also a high boiling temperature (248°C).

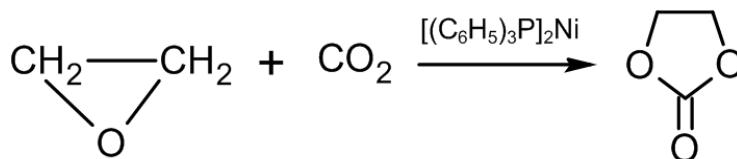


**Fig. 3.5** Production of ethylene carbonate (EC).

### V. Silver Nitrate (AgNO<sub>3</sub>)

Molecular Weight → 169.87 g mol<sup>-1</sup>, Melting temperature → 212 °C,

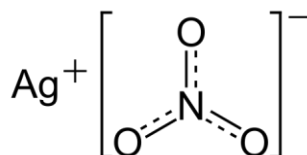


**Fig. 3.6** Structure of Silver Nitrate (AgNO<sub>3</sub>).

### VI. Common Solvent: Acetonitrile

Acetonitrile is a polar aprotic solvent. It is used for the synthesis of polymer electrolytes by solution cast technique. It has a high static permittivity (36.6 at 30 °C) which promotes the dissociation of alkali metal salt in the solution.

### VII. Nano-filler Aluminum Oxide Al<sub>2</sub>O<sub>3</sub>

Molecular Weight → 101.96 g/mol, Melting temperature → 35°-40°C, Sigma-Aldrich chemical, Particle size → < 50nm

Aluminum Oxide, Al<sub>2</sub>O<sub>3</sub>, commonly referred to as alumina, is the most cost effective and widely used material in the family of material science. Aluminum oxide possesses strong ionic interatomic bonding giving rise to its desirable material characteristics. It can exist in several crystalline phases which all revert to the most stable hexagonal alpha phase at elevated temperatures. The composition of the ceramic body can be changed to enhance particular desirable material characteristics.

### 3.3 Various polymer electrolyte systems

Commercially available chemicals of PEO, PMMA, AgNO<sub>3</sub>, PEG, EC and nano-filler Al<sub>2</sub>O<sub>3</sub> were employed as starting materials and were used as-received. Acetonitrile (MERCK) was used as common solvent for blend polymer films. The inorganic dopant salt silver nitrate (AgNO<sub>3</sub>) was used as metal salt. All materials were used without further purification. All the polymer blend electrolytes were prepared by solution casting technique as described below.

#### 3.3.1 First Polymer Blend Electrolytes System (PPS system)

First polymer blend electrolytes system was employed to figure out the most compatible ratio of PEO to PMMA. Solid polymer electrolytes were formed in this system. The compositions prepared were  $[xPEO-(1-x)PMMA]$  where  $x= 10-70$  wt% in steps of 10 with fixed amount of silver nitrate (AgNO<sub>3</sub>) salt. The compositions of various polymer blends and their designations are tabulated in table below (Table 3.1).

**Table 3.1** Designations of first polymer blend electrolytes system.

S.N.	Designations	PEO (wt %)	PMMA (wt %)	AgNO <sub>3</sub> (wt%)
1	PPS-10	10	90	5
2	PPS-20	20	80	5
3	PPS-30	30	70	5
4	PPS-40	40	60	5
5	PPS-50	50	50	5
6	PPS-60	60	40	5
7	PPS-70	70	30	5

#### 3.3.2 Second Polymer Blend Electrolytes System (PPSP system)

From first system, 50 wt% of PEO and 50 wt% of PMMA was achieved the highest ionic conductivity (Chapter 5). In PPSP-system, the effect of addition of plasticizer, poly ethylene glycol (PEG) in highest conducting polymer electrolyte obtained from PPS-system is studied. Thus, the amount of AgNO<sub>3</sub> is kept constant as 5

wt% in this system. The amount of PEG plasticizer added into the polymer blends was ranged from 5 wt% to 15 wt%. The weight fractions of polymer blends electrolytes and their designations are shown in Table 3.2.

**Table 3.2** Designations of second polymer blend electrolytes system.

S.N.	Designations	PEO (wt %)	PMMA (wt %)	AgNO <sub>3</sub> (wt%)	PEG (wt%)
1	PPSP -5	50	50	5	5
2	PPSP -10	50	50	5	10
3	PPSP -12	50	50	5	12
4	PPSP -15	50	50	5	15

### 3.3.3 Third Polymer Blend Electrolytes System (PPSE system)

In this (third) system, the PEG plasticizer has been replaced by ethylene carbonate (EC) plasticizer to study the effect of EC concentration in PEO-PMMA polymer blend which has a higher dielectric constant than that of polymer hosts. The PEO-PMMA blend ratio was kept same as 50-50 wt% with 5 wt% of AgNO<sub>3</sub> salt. In this system, the amount of EC was varied from 5 to 15 wt%.

**Table 3.3** Designations of third polymer blend electrolytes system.

S.N.	Designations	PEO (wt %)	PMMA (wt %)	AgNO <sub>3</sub> (wt%)	EC (wt%)
1	PPSE-5	50	50	5	5
2	PPSE -7	50	50	5	7
3	PPSE -10	50	50	5	10
4	PPSE -12	50	50	5	12
5	PPSE -15	50	50	5	15

### 3.3.4 Fourth Polymer Blend Electrolytes System (PPSPA system)

In this system, the effect of addition of nano-filler Al<sub>2</sub>O<sub>3</sub> is studied. For this, nano-fillers were dispersed in PEG containing plasticized polymer film with optimum conductivity (obtained from conductivity results of third polymer blend electrolyte system) in the lower concentration range. The range of nano-filler is studied at 1,2,3,4 and 5 wt%. The concentration of PEO-PMMA was kept 50 wt%.. PEG and silver salt are

also kept constant as 5 wt% each. As PEG-5 wt% was found to show the maximum ionic conductivity (Chapter 5). Table 3.3 shows the variation of the compositions of polymer blend electrolytes and their designations.

**Table 3.4** Designations of fourth polymer blend electrolytes system.

S.N.	Designations	PEO (wt %)	PMMA (wt %)	AgNO <sub>3</sub> (wt%)	PEG (wt%)	Al <sub>2</sub> O <sub>3</sub> (wt%)
1	PPSPA -1	50	50	5	5	1
2	PPSPA-2	50	50	5	5	2
3	PPSPA-3	50	50	5	5	3
4	PPSPA-4	50	50	5	5	4
5	PPSPA-5	50	50	5	5	5

### 3.3.5 Fifth Polymer Blend Electrolyte System (PPSEA system)

In the fifth system, the effect of nano-filler Al<sub>2</sub>O<sub>3</sub> in EC containing polymer film (optimized from conductivity results of PPSE system) is studied. The PEO-PMMA blend ratio was kept same as 50:50 with 5 wt% of AgNO<sub>3</sub> salt. The amount of EC was also kept constant as 5wt%. Nano-filler Al<sub>2</sub>O<sub>3</sub> concentration was varied from 1 to 5 wt% (Table 3.5).

**Table 3.5** Designations of fifth polymer blend electrolytes system.

S.N.	Designations	PEO (wt %)	PMMA (wt %)	AgNO <sub>3</sub> (wt%)	EC (wt%)	Al <sub>2</sub> O <sub>3</sub> (wt%)
1	PPSEA-1	50	50	5	5	1
2	PPSEA -2	50	50	5	5	2
3	PPSEA -3	50	50	5	5	3
4	PPSEA -4	50	50	5	5	4
5	PPSEA -5	50	50	5	5	5

### 3.3.6 Sample preparation

Sample preparation is carried out by solution cast technique [8, 9]. In this technique, there is a competition between solvent and polymer to interact with the ions. There are five polymer blend electrolyte systems prepared in the present work. The quantity of materials added is expressed as weight percentage (wt%). Appropriate

amounts of materials are dissolved in common solvent acetonitrile. PEO and PMMA are separately dissolved in acetonitrile separately and stirred by using a magnetic stirrer. The stirring of PMMA solution is carried out at 323K for 24 h to dissolve PMMA in acetonitrile. PEO and AgNO<sub>3</sub> are mixed and stirred for 4-5 h at room temperature. Both the solutions are mixed along with the desired amount of plasticizer (PEG or EC) and nano-filler (Al<sub>2</sub>O<sub>3</sub>). The obtained mixture was again stirred at room temperature for another 10 h for homogenous mixing. Finally, the solution was poured into a Teflon Petri dish and left to evaporate the solvent slowly at ambient temperature. The resulting films are kept in an oven at 313K for 2 days to ensure the removal of the solvent traces. The dried films are peeled off from the Petri-dish and then were stored in dark desiccators to prevent them any contamination from moisture and/or light.

### **3.4 Theoretical details of different characterization techniques**

Different experimental techniques have been used to characterize the prepared polymer films which are discussed briefly in the sub-sections below:

#### **3.4.1 X-Ray Diffraction (XRD)**

X-ray diffraction (XRD) technique is used to determine the atomic arrangements (i.e., crystal structure) of the material because the inter-planar spacing (d-spacing) of the diffracting planes is of the order of X-ray wavelength [10]. For a crystal of given d-spacing and wavelength  $\lambda$ , the various orders of diffraction peaks,  $n$  of reflection occurs only at the precise values of angle,  $\theta$  which satisfies the Bragg condition

$$n\lambda = 2d \sin \theta \quad \dots(3.1)$$

The accurate determination of inter-planar spacing, lattice parameters etc. provides an important basis for understanding the various physical properties of materials.

X-rays are relatively short-wavelength, high-energy beams of electromagnetic radiation. When an X-ray beam is viewed as a wave, one can think of it as a sinusoidal oscillation of electric field and magnetic field changing with time right angle to each other. Another description of X-rays is as particles of energy called photons. All electromagnetic radiation is characterized either by its wave character using its wavelength  $\lambda$  or its frequency  $\nu$  or by means of its photon energy  $E$ . The energy of an X-ray photon is  $E = \frac{hc}{\lambda}$ . Insertion of the appropriate values for the fundamental constants gives  $E = 12.398/\lambda$ , where  $E$  is in keV and  $\lambda$  in angstroms. As an example the  $\text{CuK}\alpha_1, \text{K}\alpha_2$  doublet has energy of about 8.05 keV, corresponding to a wavelength of  $12.398/8.05 = 1.5402 \text{ \AA}$ . The X-ray region lies between 0.1 and  $100 \text{ \AA}$  ( $1 \text{ \AA} = 10^{-10} \text{ m}$ ), being bounded by the  $\gamma$ -ray region to the short-wavelength side and the vacuum ultraviolet region to the long-wavelength side.

X-rays are produced from bombarding a metallic target with electrons [11]. The electrons, accelerated by an electrical field, are suddenly slowed down when they come into contact with the target and lose some of their energy which is dispersed in the form of radiation, a process called braking radiation. The resulting X-rays do not have a specific wavelength, the emission spectrum is continuous and its intensity increases with the electron acceleration voltage (Fig. 3.7(a)). The electron bombardment generates a second type of emission. The electrons transmit their energy to the atoms of the target and cause electronic transitions meaning that the atoms reach an excited state. They return to a more stable energy level through a series of electronic transitions and the emission of X photons with non-random energies  $E = h\nu$ , equivalent to the energy gaps between the different electron shells of the atom. Therefore, this radiation is comprised of

several wavelengths, but the emission spectrum is totally discontinuous. Fig. 3.7(b) shows an illustration of this type of emission. The emission spectrum still includes a contribution from the braking radiation which causes the continuous background emission.

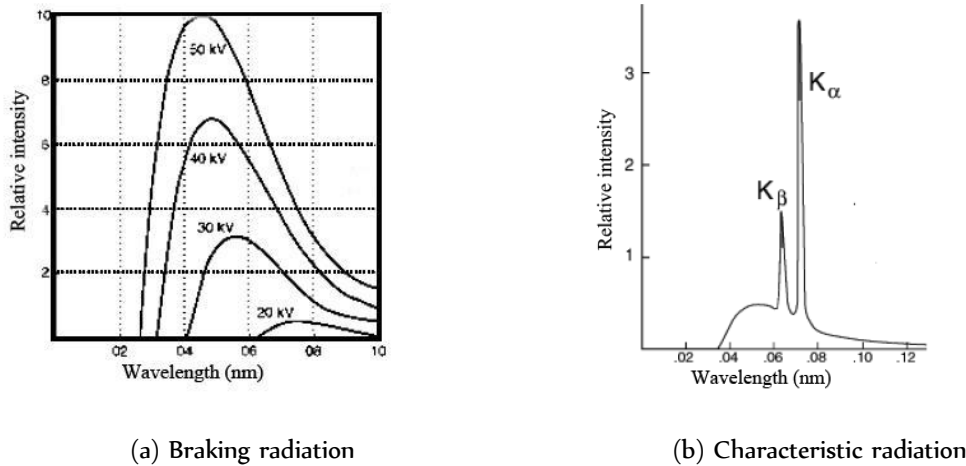


**Fig. 3.7** Emission spectrum of a molybdenum anode bombarded with an electron beam.

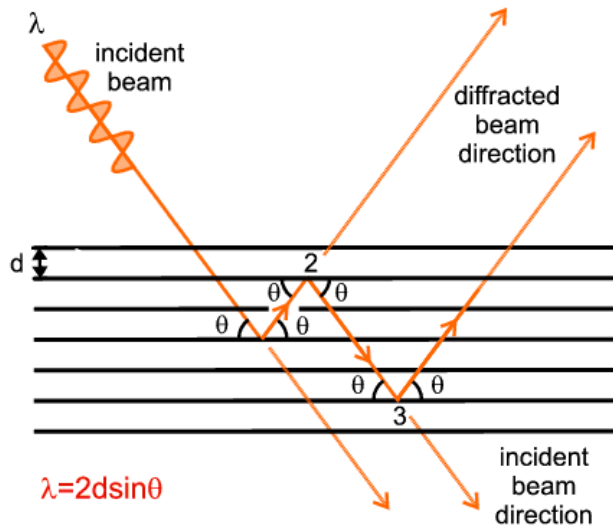


**Fig.3.8** Schematic representation of diffraction X-rays by crystal.

XRD is based on the constructive interference of monochromatic x-rays from a crystalline sample. These x-rays are generated by a cathode ray tube, filtered to produce monochromatic radiation, collimated to concentrate and directed toward the sample. The

interaction of the incident rays with the sample produces constructive interference (and a diffracted ray) when conditions satisfy Bragg's law (Fig.3.8) ( $n\lambda=2d \sin \theta$ ) [10]. This law relates the wavelength of electromagnetic radiation to the diffraction angle and the lattice spacing in a crystalline sample. These diffracted x-rays are then detected, processed and counted by scanning the sample through a range of  $2\theta$  angles. All possible diffraction directions of the lattice should be attained due to the random orientation of the powdered material. Diffraction occurs as waves interact with a regular structure whose repeat distance is about the same as wavelength. Diffracted waves from different atoms can interfere with each other and the resultant intensity distribution is strongly modulated by this interaction [12]. In crystals, the diffracted waves will consist of sharp interference maxima (peaks) with the same symmetry as in the distribution of atoms while for amorphous sample; diffraction pattern shows few diffused halos instead of sharp peaks.



**Fig. 3.9** *Image of XRD instrument.*

*Instrument:* For structural characterization of the prepared samples, the XRD patterns of all samples have been recorded at room temperature using X-ray powder diffractometer (Bruker X-ray diffractometer, Model D8) (Fig.3.9) with Cu  $K_{\alpha}$  radiation ( $\lambda = 1.5405 \text{ \AA}$ ) in a wide  $2\theta$  (Bragg angle) range ( $0^{\circ} \leq 2\theta \leq 60^{\circ}$ ) at a scanning rate of  $2^{\circ}/\text{min}$ .

### 3.4.2 Scanning Electron Microscopy (SEM)

In the characterization of solid-state compounds, scanning electron microscopy (SEM) is widely used to investigate their structure, morphology and crystallite size, to examine the surface defects of crystal, and to determine the distribution of elements (EDAX) [13]. In this technique (Figs.3.10 ((a)-(b)) and Fig.3.11), an electron beam is produced by heating the tungsten filament and then focused by magnetic fields in a high vacuum. The vacuum prevents the interaction of the beam with any extraneous particles in the atmosphere. The electrons from this finely focused beam are scanned across the surface of a sample in a series of lines and frames called a raster. At any given moment, the specimen is then bombarded with electrons over a very small area. These electrons may be elastically reflected by the surface of the sample with no loss of energy (backscattered electrons), they may be absorbed and emitted secondary electrons of low energy, they may be absorbed and give rise to the emission of visible light, and they may give rise to electric currents within the specimen. All these effects can be detected and hence given a map of the surface topography of samples. Some of the sample may need to be coated with gold or graphite to stop charge building up on the surface of the

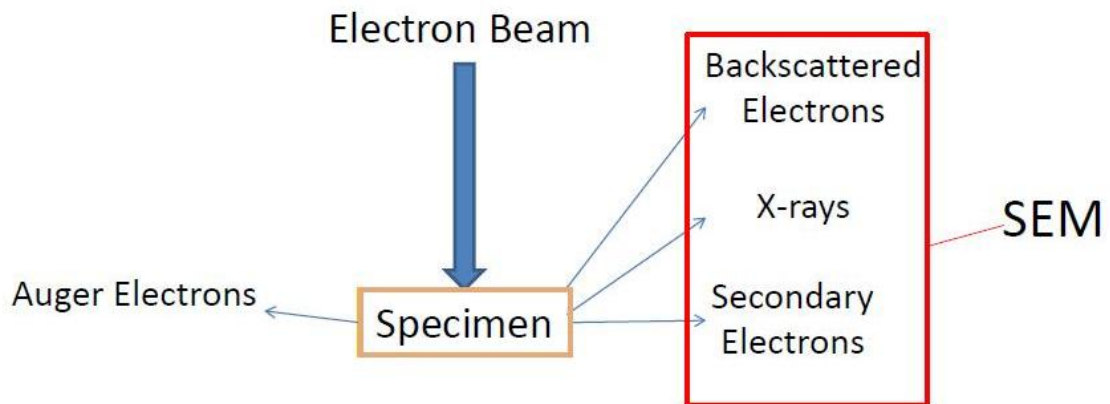


**Fig. 3.10(a)** Principle of SEM.

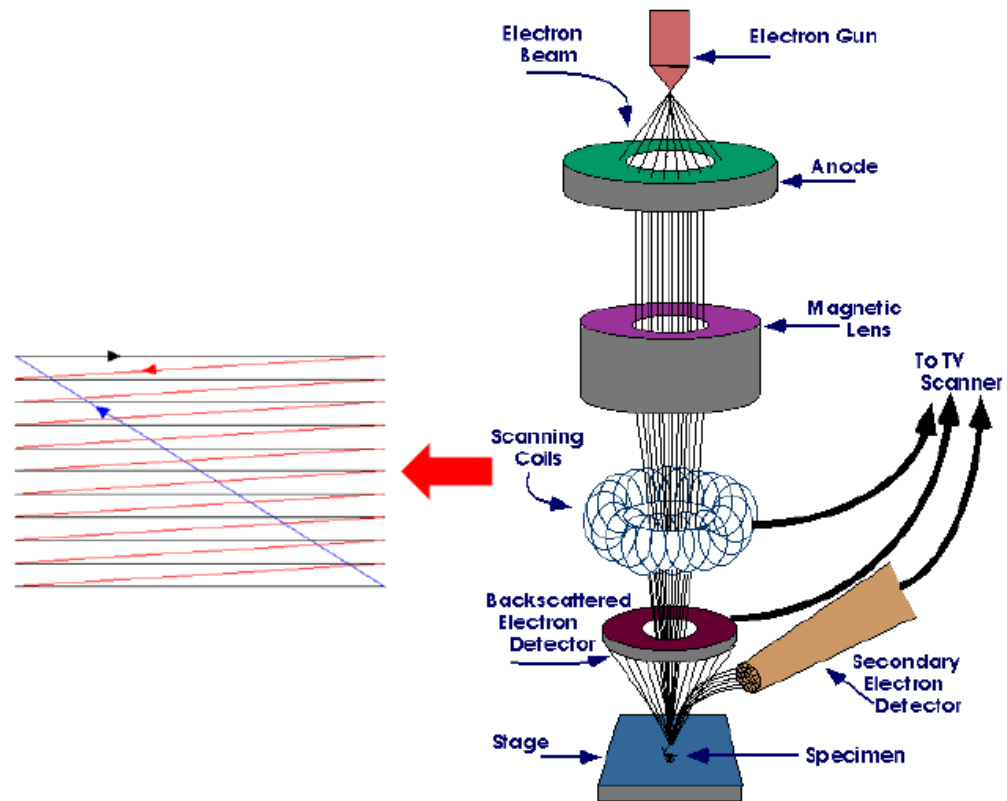


Fig. 3.10(b) Principle of SEM instrument.

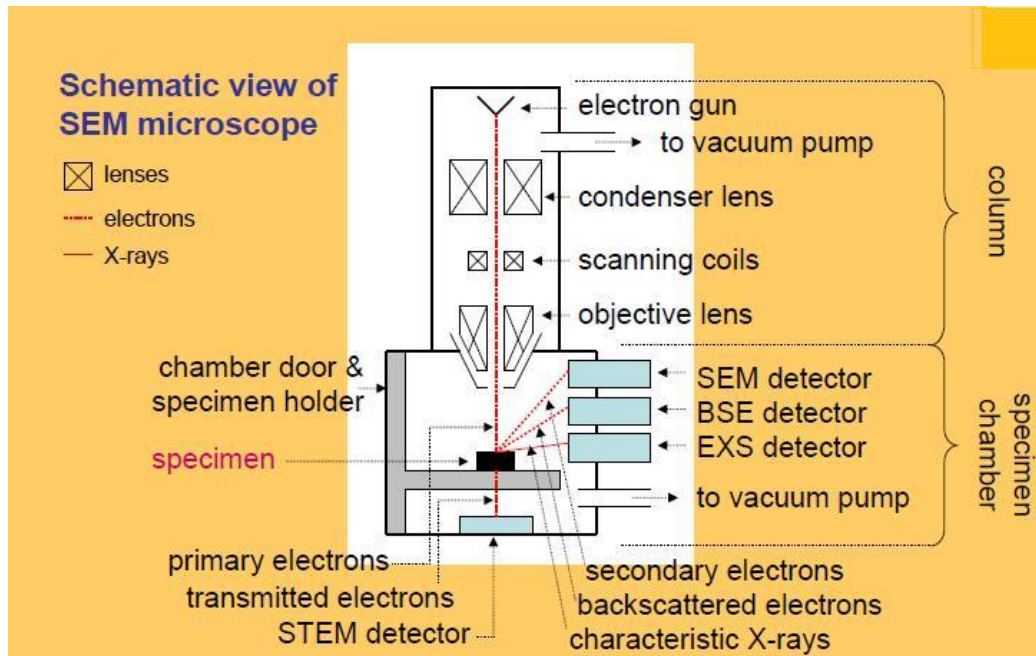


Fig. 3.11 Simplified schematic view of SEM microscope.

specimen. For backscattered electrons, the atomic number of the elements in the sample is used to determine the contrast in the produced image. The image will show the distribution of different chemical phases in the sample. The resolution in the image is not as good as for secondary electrons because of the emission of these electrons from a depth in the sample. Among all the means, the low-energy secondary electron technique is the most common method. The primary electrons enter a surface of the specimen with energy of 0.5–30keV and generate many low-energy secondary electrons. The intensity of these secondary electrons is mainly governed by the surface topography of the sample. The image of the sample can thus be constructed by measuring secondary electron intensity as a function of the position of the scanning primary electron beam. High spatial resolution can be obtained because the primary electron beam can be focused to a very small spot.



**Fig. 3.12** Image of SEM microscope.



**Fig. 3.13** Image of the gold/palladium source coating unit for SEM studies.

*Instrument:* The surface morphology/micro structural studies of the prepared polymer film samples is studied by using a computer-controlled Scanning Electron Microscope (JOEL JSM-6380LV) (Fig.3.12) at 20kV with 100  $\mu\text{m}$  resolution and 1000 magnification. The polymer films were gold coated under vacuum by electron beam gold

palladium source (80% Au, 20% Pd) by JEOL coater (Model JFC-1600) (Fig.3.13) to make them conducting and mounted onto circular aluminum stubs with double side sticky tapes.

### **3.4.3 Differential Scanning Calorimetry (DSC)**

Thermal analysis techniques like thermo gravimetric analysis (TGA), differential thermal analysis (DTA), differential scanning calorimetry (DSC) and dynamic mechanical thermal analysis (DMTA) etc. are a group of methods which are used to determine the physical and chemical properties of materials as a function of temperature or time [14, 15]. In each method, the sample is subjected to a controlled temperature programme, which may involve heating or cooling or holding the temperature constant. Le Chatelier [16] was the father of thermal analysis.

DSC is widely used to characterize the thermo-physical properties of polymers. DSC is a thermo-analytical technique in which the difference in the amount of heat required to increase the temperature of the sample and reference are measured as a function of temperature. Basically DSC measures the amount of heat released by a sample as the temperature increased or decreased at a controlled uniform rate [17]. The reference is either an empty pan or a pan with inert material, such as anhydrous alumina. In DSC, the individual heaters are provided to the sample and reference. Both the sample and reference are maintained at nearly the same temperature throughout the experiment. Generally, the temperature program for a DSC analysis is designed such that the sample holder temperature increases linearly as a function of time. The reference sample should have a well defined heat capacity over the range of temperatures to be scanned. The basic principle is that when the sample undergoes a physical transformation such as phase

transitions, more (or less) heat will need to flow to it than the reference to maintain both at the same temperature. Whether more or less, heat must flow to the sample depends on whether the process is exothermic or endothermic. For example, as a solid sample melts to a liquid it will require more heat flowing to the sample to increase its temperature at the same rate as the reference. This is due to the absorption of heat by the sample as it undergoes the endothermic phase transition from solid to liquid. Likewise, as the sample undergoes exothermic processes (such as crystallization) less heat is required to raise the sample temperature. By observing the difference in heat flow between the sample and reference, differential scanning calorimeters are able to measure the amount of heat absorbed or released during such transitions [18].

Fig. 3.14 shows the cross sectional diagram of DSC cell. In the cell, a metallic disc (made of constantan alloy) is the primary means of heat transfer to and from the sample and the reference. The sample contained in a metal pan and the reference (an empty pan) sit on raised platforms formed in the constantan disc. As heat transferred through the disc, the differential heat flowing to the sample and reference is measured by thermocouples formed by the junction of the disc and chromel wafers which cover the underside of the platforms. These thermocouples are connected in series and measure the differential heat flow using the thermal equivalent of ohms written as:

$$\frac{dQ}{dt} = \frac{\Delta T}{R_D} \quad \dots(3.2)$$

where  $\frac{dQ}{dt}$  is heat flow,  $\Delta T$  is the temperature difference between reference and sample

$R_D$  is the thermal resistance of the disc.

The result of a DSC experiment is a curve of heat flux versus temperature as

observed in Fig.3.15. In the DSC plot, exothermic peak is due to the evolution of heat from the sample which raises the temperature temporarily above that of the reference material; whereas, endothermic peak is just due to the reverse type of process.

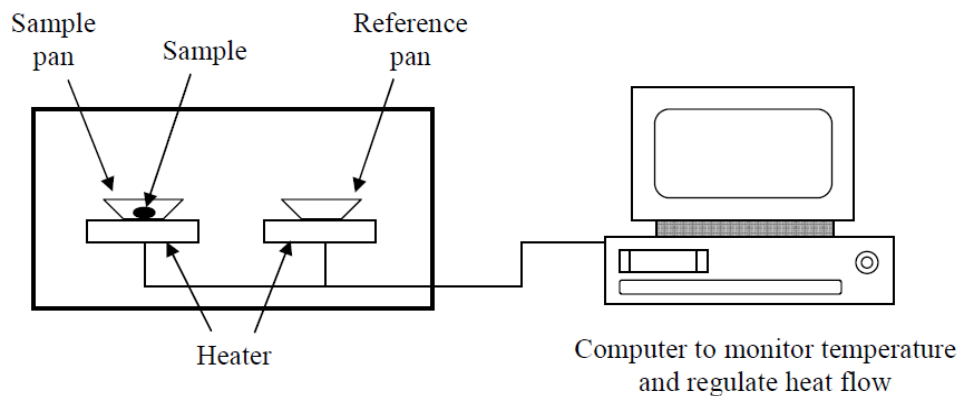


**Fig. 3.14** Schematic representation of the DSC unit.

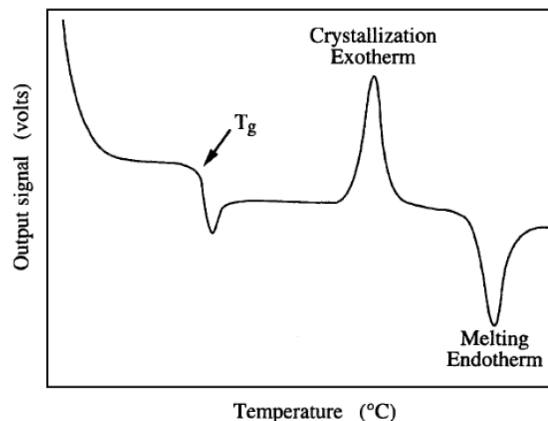


**Fig. 3.15** A schematic DSC curve.

The basic principle of DSC depends on the *amount of heat needed to flow in to maintain the samples and reference at the same temperature when the sample undergoes some physical transformation* such as phase transition. The amount of less or more heat through the sample depends on whether the process is exothermic or endothermic. Glass transition temperature  $T_g$  is a vital characteristic of the amorphous behavior of a polymer during the transition from solid to liquid (or melt) state [19]. The kinetic energy of the molecules increases if an amorphous polymer is heated. As the polymer retains in the

glass-like properties, the mobility of molecules are still restricted even there is a presence of short-range vibrations and rotations. As the temperature is further increased or the polymer matrix is further melted, its glass-like structure will be converted into rubbery state which is soft and elastomeric. This characteristic temperature is known as  $T_g$ . At this transition, it is accompanied by more long range molecular motion and thus the degree of rotational freedom increases. As a result, there is more segmental movement among the atoms of the chains. Thus, the space between the atoms will be increased and then results in the increase of the specific volume.

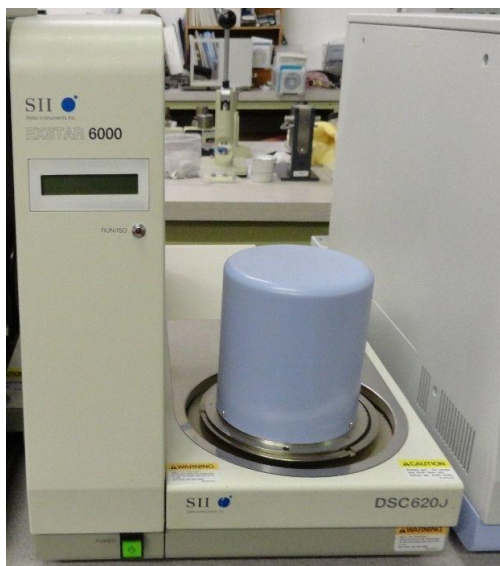


**Fig. 3.16** *Image of DSC equipment.*

Above  $T_g$ , the molecules start to gain the freedom in motion and after reaching a particular stage where they have enough freedom of motion, they will arrange themselves continuously into a crystalline form. At this stage, heat is given out from the system and it is known as crystallization temperature. This result and exothermic peak in DSC thermogram as can be seen from Fig.3.15. As the polymer is further heated, it loses its elastomeric behavior and results in an endothermic dip in DSC thermogram. At this stage, the crystalline melting temperature ( $T_m$ ) is reached. In short, DSC plays an

important role to determine the glass transition temperature ( $T_g$ ) and crystalline melting point ( $T_m$ ).

The main application of DSC is in detection of transitions like melts, glass transitions, phase changes, and curing. These transitions involve energy changes or heat capacity changes that can be detected by DSC with great sensitivity.

*Instrument:* In the present work, the thermal analysis employed, is DSC using model SII EXSTAR-6000 DSC differential scanning calorimeter (from SII SEIKO (Fig.3.16)).

#### **3.4.4 Fourier Transform Infrared (FTIR) Spectroscopy**

FTIR Spectroscopy is a fundamental technique for chemical identification of a functional group, which provides a useful information regarding structure of molecules [21]. It involves the twisting, bending, rotating and vibrational motions of atoms in a molecule. Upon interacting with IR radiation, portions of the incident radiation are absorbed at particular wavelengths. The multiplicity of vibrations occurring simultaneously produces a highly complex absorption spectrum, which is uniquely characteristic of the functional groups comprising the molecule and of the overall configuration of the atoms as well.

Changes in vibrational and rotational states of the molecules result in absorption in the infrared region. The absorption frequency depends on the vibrational frequency of the molecules, whereas the absorption intensity depends on how effectively the infrared photon energy can be transferred to the molecule and this depends on the change in the dipole moment that occurs as a result of molecular vibration moment and known as “*IR active molecule*”. Thus, all those compounds which are IR active can be analyzed by their characteristic infrared absorption.

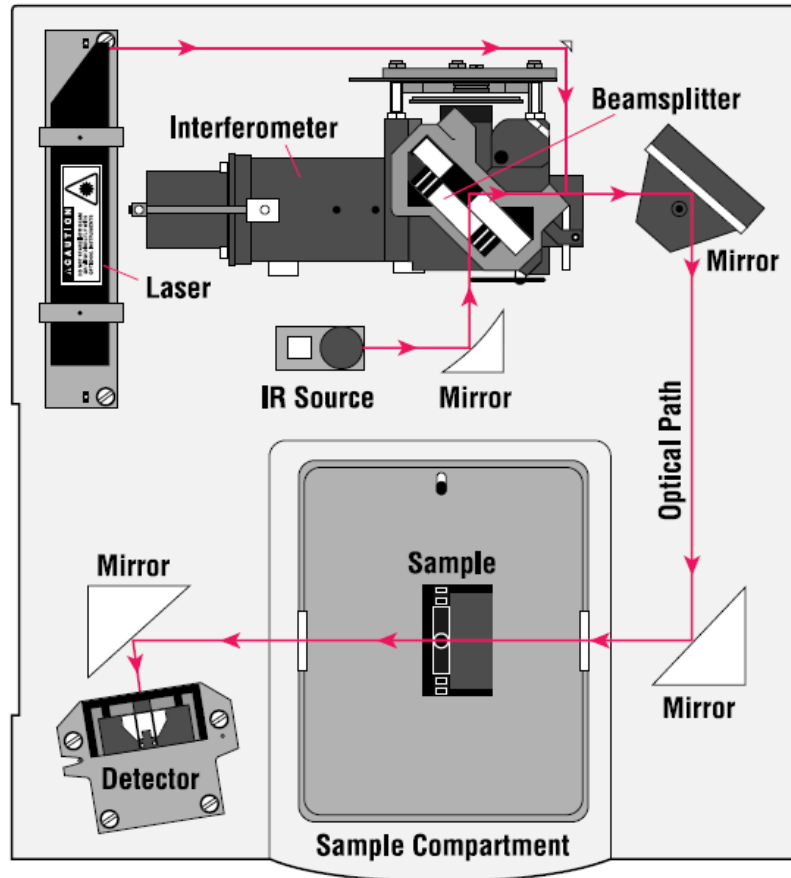


**Fig. 3.17** Block diagram of a typical Fourier Transform Infrared Spectrometer.

The block diagram of a typical FTIR-spectrometer is shown in Fig.3.17. In this, the source of radiation e.g.; heated wire, generates infrared radiation over the entire mid-infrared range [19]. The radiation then enters the Interferometer which consists of a beam splitter, a fixed mirror and a moveable mirror. The beam splitter has the property of transmitting approximately half the radiation falling on it, the remaining half being reflected. The reflected beam passes to the fixed mirror and the transmitted beam passes to a movable mirror. Each of these two mirrors reflects the beam back towards the beam splitter. Here again, half of the radiation is reflected and the other half is transmitted. The radiation reaching the detector thus comprises of beams which can combine

constructively or destructively. Their recombination depends on the path difference between the upper arm and the right arm of the interferometer as the position of the moving mirror is changed. A cosine wave is detected at the detector when the moving mirror is gradually moved along the beam direction when the source is emitting a single frequency. When a broad band source is used, the interference pattern becomes the sum of all the frequencies present. This interferogram consists of a strong signal at the point where the path difference is zero, gradually falling away rapidly on either side. A single beam spectrum is obtained when the interferogram is treated by a mathematical process of Fourier transformation. Normally, interferometers operate by first recording the background and then rationing it against the spectrum that is obtained when the sample is inserted in the beam between the interferometer and detector.

IR radiation is passed through the sample. Some of the infrared radiation is absorbed by the sample and some of it is passed through (transmitted). The resulting spectrum represents the molecular absorption and transmission, creating a molecular fingerprint of the sample. Like a fingerprint, no two unique molecular structures produce the same infrared spectrum. This makes infrared spectroscopy useful for several types of analysis.

A natural vibrational mode within a molecule will absorb IR radiation, if the following conditions are fulfilled:

- 1) Those molecules will absorb IR radiation in which the natural frequency of vibration of the molecule is the same as the frequency of the incident radiation. The IR radiation, that is absorbed, causes the molecule to vibrate at increased amplitude (Resonance).
- 2) Those molecules can absorb IR radiation in which absorption produces some changes

in the electric dipole of the molecules. Such molecules are known as IR active materials.

The dipole moment is determined by the positions of the centers of gravity of the positive and negative electrical charges. When a molecule having electric dipole is kept in the electric field, it exerts a force on the electric charges in the molecules, which gives rise to decrease or increase of a separation. Change in the electric field of IR radiation causes a change in polarity periodically. It means that the spacing between the charged atoms of the molecule also changes periodically and vibration of these charged atoms causes the absorption of IR radiation. In symmetrical stretching vibration, the centers of gravity of the charges coincide in every vibrational position, no dipole moment is created and the absorption characteristic of this mode is not observed in IR. Such vibrations are said to be IR inactive. However, in asymmetrical stretching vibration, a dipole moment is produced and the vibration is IR active and is observed in IR spectrum.

The position of atoms in a molecule is not fixed; they are subjected to a number of different vibrations and rotations. Two atoms are joined by a covalent bond which may undergo stretching vibrations. The atoms can undergo a variety of stretching and bending vibrations. Energy of a vibration depends on (1) the mass of the atom present in the molecule, (2) strength of the bond and (3) the arrangement of various atoms in the molecule. The position of IR band is described in terms of wavelength  $\lambda$  (usually measured in microns,  $\mu$ ) or wave number,  $\bar{\nu}$ . Both these units are related to each other by the relation

$$\bar{\nu}(\text{in } cm^{-1}) = \frac{10^4}{\lambda} (\text{in } \mu) \quad \dots(3.3)$$

The positions of absorption bands, as determined from the mechanical theory of harmonic oscillators, are given by

$$\bar{\nu} \text{ (in } cm^{-1}\text{)} = \frac{1}{2\pi c} \sqrt{\frac{k(m_1 + m_2)}{m_1 m_2}} \quad \dots(3.4)$$

where  $m_1$  and  $m_2$  are the masses of two adjacent atoms in a molecule and  $k$  is the restoring force per unit displacement and can be expressed as

$$k = aN \left( \frac{\chi_1 \chi_2}{d^2} \right)^{3/4} + b \quad \dots(3.5)$$

where  $N$  is the band order (i.e., effective number of covalent or ionic bands),  $\chi_1$  and  $\chi_2$  are the electro negativities of the atoms,  $d$  is the internuclear distance in angstroms and  $a(=1.67)$  and  $b(=0.30)$  are constants. From the above relations, it is clear that the bond length can be a good guide to the direction of a shift of band resulting from a change in chemical group- the greater the length, the lower the frequency. *Bending modes usually produce lower frequency absorption bands than fundamental stretching modes.*

### Stretching vibrations:

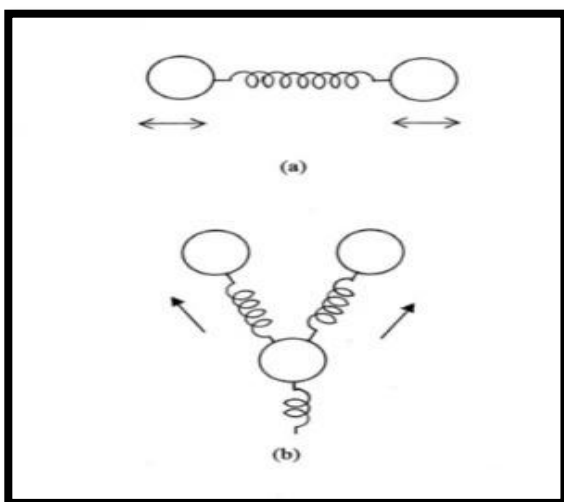


**Fig. 3.18** *Symmetric stretching vibrations:*  
(a) diatomic molecule (b) triatomic molecule.

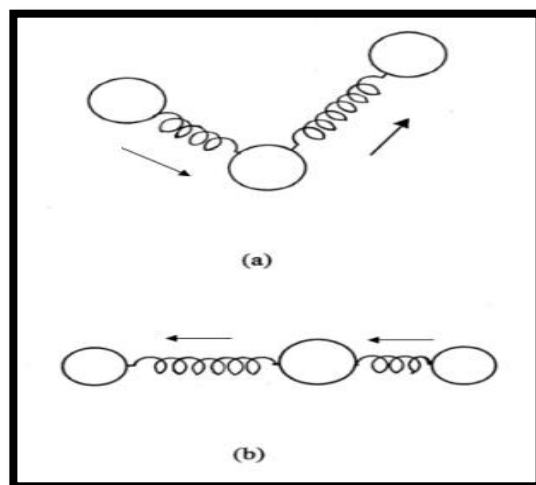


**Fig. 3.19** *Asymmetric Stretching Vibrations:*  
(a) and (b) triatomic molecule.

It arises due to stretching and contracting of bond without producing any change in the bond angles, which are of two types namely, symmetric and asymmetric stretching. If the movement of atoms with respect to a particular atom in a molecule is in the same direction, it is called symmetrical stretching vibrations as shown in Fig. 3.18. If one atom approaches the central atom whereas the other approaches away from it in a triatomic system, it gives unequal movement of the outer atom with respect to central one, as shown in Fig. 3.19. Because of this, the change in electric dipole takes place. Therefore, asymmetric stretching gives it vibrational frequency at higher wave number than for symmetric system.

### **Bending vibrations**

It gives rise to deformation of bond angle but there is no change in bond lengths. In diatomic molecules, most of the bond angles are found to be in two categories i.e.; linear or  $180^\circ$  bond angle and bond angle in a neighborhood of  $120^\circ$  to  $110^\circ$ .

In triatomic molecules, the two atoms are the same and are bound to the middle atom by two equal bonds with two different frequencies symmetric or asymmetric.

$$\nu_{sym} (cm^{-1}) \approx \left( \frac{1}{2\pi c} \right) \left[ k \left\{ \frac{1}{m_{end}} + \frac{(1 + \cos \alpha)}{m_{mid}} \right\} \right]^{1/2} \dots(3.6)$$

where  $\alpha$  is a bond angle,  $\nu$  is a frequency in  $cm^{-1}$ ,  $k$  is the force constant in dyne/cm,  $m_{end}$  and  $m_{mid}$  are the masses of one end and middle atom respectively. The above Eqn. 3.5 and 3.6 can also be written as.

$$\nu_{asym} (cm^{-1}) \approx \left( \frac{1}{2\pi c} \right) \left[ k \left\{ \frac{1}{m_{end}} + \frac{(1 - \cos \alpha)}{m_{mid}} \right\} \right]^{1/2} \dots(3.7)$$

$$\nu_{sym} (cm^{-1}) \approx \left( \frac{1}{2\pi c} \right) \left[ k \left\{ \frac{1}{M_{end}} + \frac{(1 + \cos \alpha)}{M_{mid}} \right\} \right]^{1/2} \quad \dots(3.8)$$

$$\nu_{asym} (cm^{-1}) \approx \left( \frac{1}{2\pi c} \right) \left[ k \left\{ \frac{1}{M_{end}} + \frac{(1 - \cos \alpha)}{M_{mid}} \right\} \right]^{1/2} \quad \dots(3.9)$$

where  $M_{end}$  and  $M_{mid}$  are the atomic weights of end atom and middle atoms.

Bending vibrations are classified into four types i.e.; scissoring (Fig. 3.20 (a)), rocking (Fig.3.20 (b)), wagging (Fig.3.21.(a)) and twisting (Fig.3.21(b)) bending. In scissoring bending vibrations of the bonds, the two atoms approach each other in the same plane as shown in Fig. 3.20 (a).

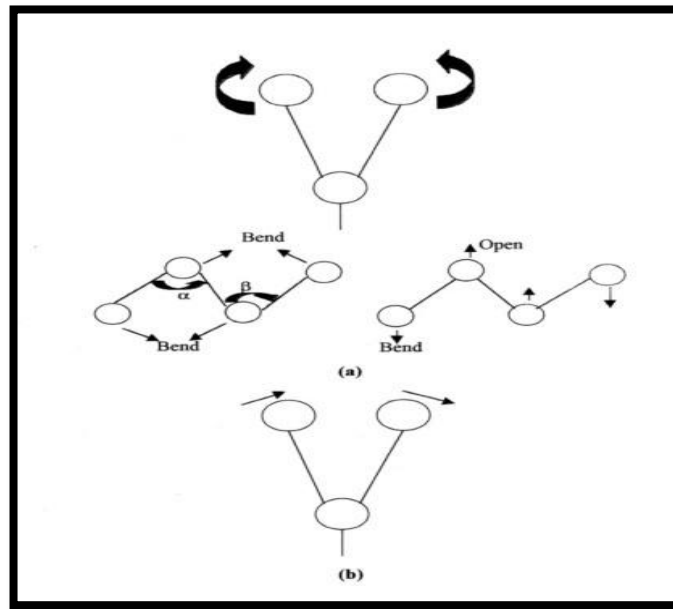


**Fig. 3.20** (a) Scissoring bending (in plane bending with lower frequency of vibration)  
(b) Rocking bending (in plane bending with lower frequency of vibration).

In rocking bending of bond vibration, the movements of atoms occur in the same direction and also in the same plane as shown in Fig.3.20(b). Wagging bending of bond vibrations is due to the two atoms move up and down below the plane with respect to the central atom as shown in Fig.3.21(a). In twisting bending vibrations, one of the atoms

moves up the plane and the other moves down the plane with respect to the central atom as shown in Fig.3.21(b). Here (+ve) and (-ve) sign represents motion above and below the plane of the paper respectively. The energy required to stretch a spring is more than that needed to bend it so the stretching absorption of the bond will appear at higher frequencies than the bending absorption of a bond. Thus IR spectroscopy is widely used for molecular structural studies of various materials.

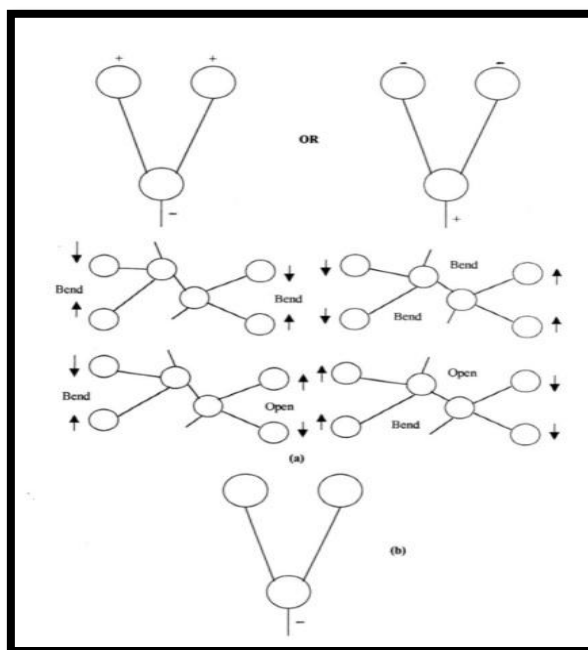


**Fig. 3.21** (a) *Wagging bending (out of plane having high frequency of vibration).*  
 (b) *Twisting bending (out of plane bending with high frequency of vibration).*

Fourier transform infrared spectroscopy is preferred over dispersive or filter methods of infrared spectral analysis for the following reasons:

➤ **Multiplex Advantage:**

An interferometer in an FT-IR instrument does not separate energy into individual frequencies for measurement of the infrared spectrum. Each point in the interferogram contains information from each wavelength of light being measured whereas; every wavelength across the spectrum is measured individually in a dispersive spectrometer.

This is a slow process, and typically only one measurement scan of the sample is made in a dispersive instrument. The multiplex advantage results in faster data collection of an FT-IR spectrum.

➤ **Precision Advantage:**

Accuracy and precision in infrared spectra are much higher when collected on an FT-IR due to maintaining of internal precision and accuracy of the wavelength positions by laser which controls the velocity of the moving mirror and to time the collection of data points.

➤ **Throughput Advantage:**

There are less reflection losses in FT-IR spectrometer than in a dispersive spectrometer. This means that the signal-to-noise ratio of an infrared spectrum measured on an FT-IR is higher hence, the sensitivity of small peaks will be greater, and details i.e., high-resolution in a spectrum will be clearer and more distinguishable in the FT-IR spectrum than the dispersive spectrum of the same sample.

*Instrument:* FTIR spectra of prepared polymer electrolyte system are carried out using FT-IR 4100 JASCO model (Fig.3.22).



**Fig. 3.22** *Image of FTIR instrument.*

### 3.5 Complex Impedance Analysis

Complex impedance analysis is a powerful technique to characterize the electrical properties of the solid electrolytes [20]. The complex impedance measurement were carried out using a computer-interfaced impedance analyzer (Impedance Gain/Phase Analyzer, Solartron 1260) in the frequency range of 100 Hz to 1MHz at a.c. signal of 100 mV at 303-373K temperatures (Fig.3.23). The polymer electrolyte film is sandwiched between two stainless silver block electrodes used as cell for the electrical measurement.



**Fig.3.23** Image of setup of impedance measurement (Impedance analyzer interfaced with computer).

The complex impedance spectrum data is used to evaluate the conductivity and other related electrical properties e.g.; ac conductivity, dielectric permittivity and modulus. The real,  $Z'$  and imaginary,  $Z''$  parts of complex impedance  $Z^*$  are directly measured from the instrument. The impedance plot of prepared polymer electrolyte films is obtained by plotting the real,  $Z'$  on x-axis and imaginary,  $Z''$  on y-axis, parts of complex impedance  $Z^*$ . The bulk resistance,  $R_b$  was determined by extrapolating the

complex impedance plot curve to intercept at the real axis ( $Z'$ -axis). The obtained impedance plots can be fitted using “Zview2 program” (developed by Solartron Analytical). Then the ionic conductivity can be calculated from bulk resistance with the dimension of polymer electrolyte sample using the formula given below:

$$\text{Ionic conductivity } \sigma = \left(\frac{t}{A}\right) * \left(\frac{1}{R_b}\right)$$

The complex conductivity can be given as,

$$\begin{aligned} \sigma^*(\omega) &= \frac{t}{A} \left( \frac{Z^*(\omega)}{Z'^2 + Z''^2} \right) \\ &= \sigma'(\omega) + \sigma''(\omega) \quad \dots (3.10) \end{aligned}$$

where,  $\omega$ ,  $t$  and  $A$  are the angular frequency, thickness and cross sectional area of the sample, respectively. The real part,  $\sigma'$ , of  $\sigma^*$  is called the AC conductivity.

The complex dielectric function  $\epsilon^*$  is given as [21]

$$\epsilon^*(\omega) = j\omega C_0 Z^* = \epsilon'(\omega) - i \epsilon''(\omega) \quad \dots (3.11)$$

where,  $C_0$  is the vacuum capacitance and is expressed as  $C_0 = \epsilon_0 \frac{A}{t}$ ,  $\epsilon_0$  is the permittivity of free space (constant). The real part of complex dielectric function is called the dielectric constant,  $\epsilon'$  and the imaginary part,  $\epsilon''$  is considered to be the loss occurring due to conduction process.

The modulus formalism is used to analyze the relaxation processes in solids [22],

The complex modulus function can be given as,

$$M^*(\omega) = 1/\epsilon^*(\omega) = j\omega C_0 Z^* = M' + i M'' \quad \dots (3.12)$$

The complex dielectric analysis provides information about the electrode polarization while the modulus formalism gives the conductivity relaxation effects as these effects

become prominent in modulus formalism due to suppression of electrode-electrolyte interface polarization effects [23].

### **3.6. Transference number measurement**

Solid polymer electrolytes are solutions of salts in polymers, both of cation and anion have a chance to move [24]. It is of great importance to clarify the ionic transport number in terms of the understanding of the ion-conduction mechanism and of their practical applications. The ionic transference number has been measured in certain kinds of the polymer electrolytes using various methods including Wagner's polarization technique, PEFM-NMR measurements, EMF measurements, potentiostatic polarization, Tubandt method and DC polarization technique [25-30]. The data obtained are somewhat distributed. The transference number measurement of solid materials signifies the contribution of ionic conductivity to the total conductivity. Therefore, it is one of the key factors to be considered while choosing the system as an electrolyte (in super ionic system) or to be used as a cathode material (in mixed conducting system) for battery application. Normally, the transference number measurement can be carried out through different methods namely, Tubandt's method [30], Hebb-Wagner's polarization method [25] and electrochemical (EMF) method [27]. The electronic contribution to the total conductivity can be obtained from Wagner polarization technique, whereas the other techniques brief about ionic nature of the conducting species.

*The transference number of a moving charged particle is defined as the ratio of the conductivity due to itself and the total conductivity.*

There are many methods to ensure the transference number, few of these described below in brief:

### 3.6.1 Wagner Polarization technique

The Wagner's polarization method, which is generally used to determine ionic and electronic transference numbers, is schematically shown in Fig.4.2. In this technique, the sample is placed between two electrode one blocking and the other non-blocking for the mobile ionic species. The sample was polarized under dc bias of constant voltage. Current versus time is monitored for a fixed applied dc potential. The initial current is the total current ( $i_T$ ), due to the ions ( $i_i$ ) and electrons ( $i_e$ ). As the polarization builds up the  $i_i$  is blocked and the final current is only the electronic current. The initial total current decreases with time due to the depletion of ionic species in the samples and becomes constant in the fully depleted situation. At this stage, the residual current is only electronic current.

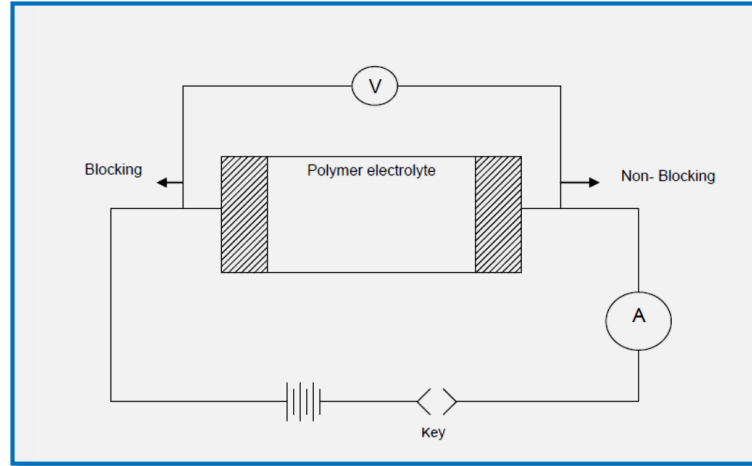


**Fig. 3.24** Experimental arrangement of Wagner's polarization method for determining transference number.

The electronic transference number  $t_e$  and the ionic transference number  $t_i$  respectively are given by

$$t_e = \frac{\sigma_e}{\sigma_T} = \frac{i_e}{i_T} \quad \dots(3.13)$$

and 
$$t_i = 1 - t_e \quad \dots(3.14)$$

where  $\sigma_e$  and  $\sigma_T$  are the electronic conductivity and total conductivity respectively while  $i_e$  is the electronic current and  $i_T$  is the total current.

### 3.6.2 EMF method

Transference number can also be measured by EMF method [33]. In this method the ionic conductor is placed between a pair of electrodes of different chemical potentials  $\mu_1$  and  $\mu_2$ . The potential difference (emf) developed across the electrodes is given by [34]:

$$E_{obs} = \frac{-1}{|Z|F} \int_{\mu_1}^{\mu_2} t_i d\mu = \frac{t_i(\mu_1 - \mu_2)}{|Z|F} = \frac{t_i \Delta G}{F|Z|} \quad \dots(3.15)$$

where  $t_i$  is the ionic transport number,  $\mu_1$  and  $\mu_2$  are chemical potential of the electrodes,  $\Delta G$  is the change in free energy involved for a given pair of electrodes,  $|Z|$  is the valence of mobile ion and F is the Faraday's constant. For an ideal electrolyte with  $t_i = 1$ , the emf generated is given by

$$E_{theo} = \Delta G / F|Z| \quad \dots(3.16)$$

From the above relations,  $E_{obs} = t_i E_{theo}$ . Thus the transport number of the mobile ion can be calculated from the ratio of observed emf ( $E_{obs}$ ) to the theoretical value of emf ( $E_{theo}$ ) for a given pair of electrodes.

### 3.6.3 DC polarization technique

This method was proposed by Evans *et.al.* [27]. According to this technique, Na-Hg | polymer electrolyte film | Na-Hg cells are polarized by applying a voltage

$\Delta V=20\text{mV}$  for 2h. The initial and final currents are subsequently recorded. Further, as a part of this method, the cells are subjected to ac impedance measurements prior to and after the polarization, and the values of the electrode-electrolyte contact resistances are estimated from the impedance plots. The ionic transference number values are calculated using the expression:

$$t_{Na} = \frac{I_s(\Delta V - R_0 I_0)}{I_0(\Delta V - R_s I_s)}$$

where  $I_0$  and  $I_s$  are the initial and final current;  $R_0$  and  $R_s$  are the cell resistance before and after polarization.

Out of these different methods for obtaining the transference number, in the present investigation, Wagner's polarization technique is used. Keithley model 6514 electrometer was employed for the accurate measurements of current as a function of time.

## References:

1. L.A. Belfiore, *Physical Properties of macromolecules*, John Wiley & Sons, 2010.
2. R.A.V. Raff, A.S. Ahmad, *Northwest Sci.* 44(1970)184-205.
3. D.L. Dorest, *Characterization of solid Polymers*, S.J. Spells (ed.), Chapman & Hall, UK, 1994.
4. J.Y. Kim, S.H. Kim, *Solid State Ionics* 24(1999)91-99.
5. P. Bahadur, N V Sastry, *Principles of Polymer Science*, Narosa Publishing House Pvt. Ltd. 2009.
6. Z.Z. Yang, Q.W. Song, L.N. He, *Capture and utilization of carbon dioxide with Polyethylene glycol*, Springer Heidelberg, New York, 2012.
7. S. Ramesh, O.P. Ling, *Polym. Chem.* 702(2010) 702-707.
8. R.C. Agrawal, G. P. Pandey, *J. Phys. D: Appl. Phys.* 41 (2008)223001.
9. A.M. Stephan, *Euro. Poly. J.* 42 (2006) 21-42.
10. R. Guinebretiere, *X-ray Diffraction by Polycrystalline Materials*, ISTE Ltd., Great Britain, 2007.
11. B.D. Cullity, *Elements of X-ray Diffraction*, Addison-Wesley Publishing Company, Inc. Massachusetts, 1956.
12. J. Goldstein, *Scanning electron microscopy and x-ray microanalysis*, Kluwer Academic/Plenum Publishers, 2003.
13. V.V. Tsukruk, S. Singamaneni, *Scanning Probe Microscopy of Soft Matter*, Wiley-VCH, 2012.
14. M.P. Sepe, *Thermal analysis of Polymers*, Rapra Rev. Reports 11(1997).
15. L. Reimer, *Scanning electron microscopy : physics of image formation and microanalysis*, Springer, 1998.
16. H.L. Chatelier, *Bull. Soc., Franc. Mineral* 10(1987) 203.
17. M.E. Brown, *Introduction to thermal analysis*, Kluwer Academic Publishers, 2001.
18. B.C. Smith, *Fundamentals of Fourier Transform Infrared Spectroscopy*, CRC Press, Taylor & Francis Group, 2011
19. M. Joffre, A. Bonvalet, A. Migus, J.L. Martin, *Optics Lett.* 21(1996)964-966.
20. E. Barsoukov, J.R. Macdonald, *Impedance Spectroscopy: Theory, experiment, and applications*, Wiley, New York, 2005.
21. A.K. Jonscher, *Dielectric relaxation in Solids*, Chalsea Dielectric press, London, 1983.
22. P.B. Macedo, C.T. Moynihan, R. Bose, *Phys. Chem. Glass.* 13 (1972)171-179.
23. A. Bhide, K. Hariharan, *Euro. Poly. J.* 43(2007) 4253-4270.
24. R.C. Agrawal, R.K. Gupta, *J. Mater. Sci.* 24(1999)1131-1162.
25. J.B. Wagner and C. Wagner, *J. Chem. Phys.* 26 (1957) 1957.
26. Y. Saito, H. Yamamoto, O. Nakamura, H. Kageyama, H. Ishikawa, T. Miyoshi, M. Matsuoka, *J. Power Sources* 81-82(1999)772-776.
27. J.W. Evans, C.A. Vincent, P.G. Bruce, *Polymer* 28(1987) 2324-2328.
28. R.A. Robinson, R.H. Stokes, *Electrolyte Solutions*, Dover Publications, New York, 2003.
29. J.H. Kennedy, *J. Electrochem. Soc.* 124 (1977) 865.
30. C. Tubandt, *Z. Anorg. Allg. Chem.* 110 (1920) 234.
31. K. Kiukkola, C. Wagner, *J. Electro chem. Soc.* 104 (1957) 308.
32. M. Watanabe S. Nagano, K. Sanui, N. Ogata, *Solid State Ionics* 28-30 (1988) 911-917.
33. T. Ishihara, T. Akbay, H. Furutani, Y. Takita, *Solid State Ionics* 113-115 (1998) 585-591.
34. A. Basili, P.R. Mussini, T. Mussini, S. Rondinini, B. Sala, A. Vertova, *J. Chem. Eng. Data* 44 (1999)1002.

## **Chapter 4- Characterization results**

---

In this chapter, the characterization results of prepared different samples have been presented and discussed.

---

## **4.1 Introduction**

This chapter deals with the characterization results carried out for the prepared polymer blends, plasticized and polymer nano-composites. Characterization results are helpful in correlating the electrical and transport analysis with an understanding in the changes in structural, morphological and thermal properties.

## **4.2 XRD analysis**

Polymers are the materials consisting of covalently bonded chain structures formed by repetition of similar units, in which the chains are of sufficient length to confer on the material additional properties that are not possible by the individual units alone. There is a possibility within the solid polymer, for the chains to align themselves in a systematic manner by folding themselves or by the formation of single or multiple helices, for at least part of their length. These regions will possess long-range order and therefore are crystalline in nature [1]. X-ray diffraction (XRD) analysis is very useful in determining the solid-state structural information of semi-crystalline polymers, which includes thermoplastics, thermoplastic elastomers and liquid crystalline polymers [2]. XRD is also used to measure the nature of polymer and the extent of crystallinity present in the polymer sample. XRD pattern of polymer contain both sharp as well as defused peaks. Sharp peaks correspond to crystalline orderly regions and defused peaks/halos correspond to amorphous regions. XRD studies imply the higher degree of amorphous nature of the polymer electrolytes by the reduction in the intensity of characteristic peaks. XRD is one of the most powerful techniques for qualitative and quantitative analysis of crystalline compounds. The information obtained includes types and nature of present crystalline phases, structural make-up of phases, degree of crystallinity, amount of

of amorphous content, micro strain & size and orientation of crystallites.

The plasticization, salt dissolution and dispersion of nano-filler in PEO-PMMA and even blending of polymers are essential to characterize. For this, XRD patterns of prepared polymer electrolyte films along with pure PEO and PMMA are recorded to correlate the structure of polymer complexes. Fig.4.1 represents the XRD pattern of pure PMMA which exhibits a broad hump at  $\sim 14^\circ$  indicating amorphous nature of the film.

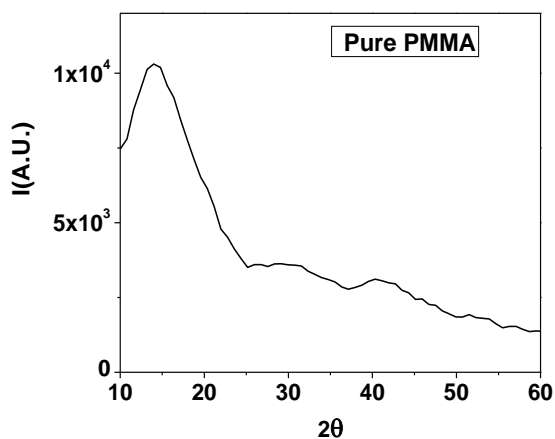


**Fig. 4.1** XRD pattern of pure PMMA.

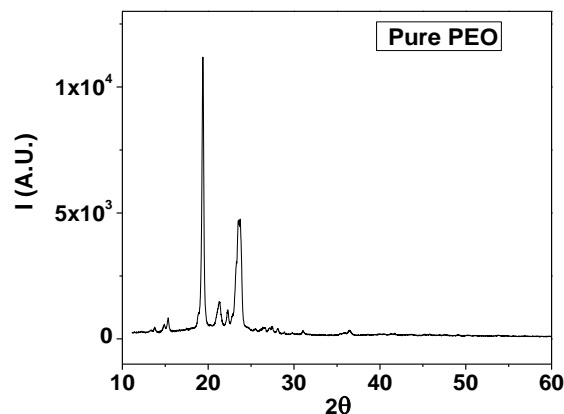


**Fig.4.2** XRD pattern of pure PEO.

The diffractogram of pure PEO (Fig. 4.2) shows the presence of crystalline phase with characteristic diffraction peaks in the range of  $2\theta = 15^\circ - 30^\circ$  [3, 4] ( $19.3^\circ$  and  $23.7^\circ$ ). Such a crystalline nature of PEO originates due to the orderings of the poly ether side chains.

XRD patterns of the samples, having different PEO concentration with respect to PMMA at fixed concentration of  $\text{AgNO}_3$  salt as 5 wt%, are depicted in the Fig. 4.3. The observed background halo below  $17^\circ$  in XRD patterns is due to amorphous PMMA, while main X-ray peaks corresponding to PEO [3] show the presence of semi-crystalline phase of due to PEO in all samples. In the polymer film containing 10wt% of PEO, the X-ray peaks correspond to pure PEO, just start emerging with big halo in background showing the dominance of amorphous phase due to PMMA structure. As the concentration of

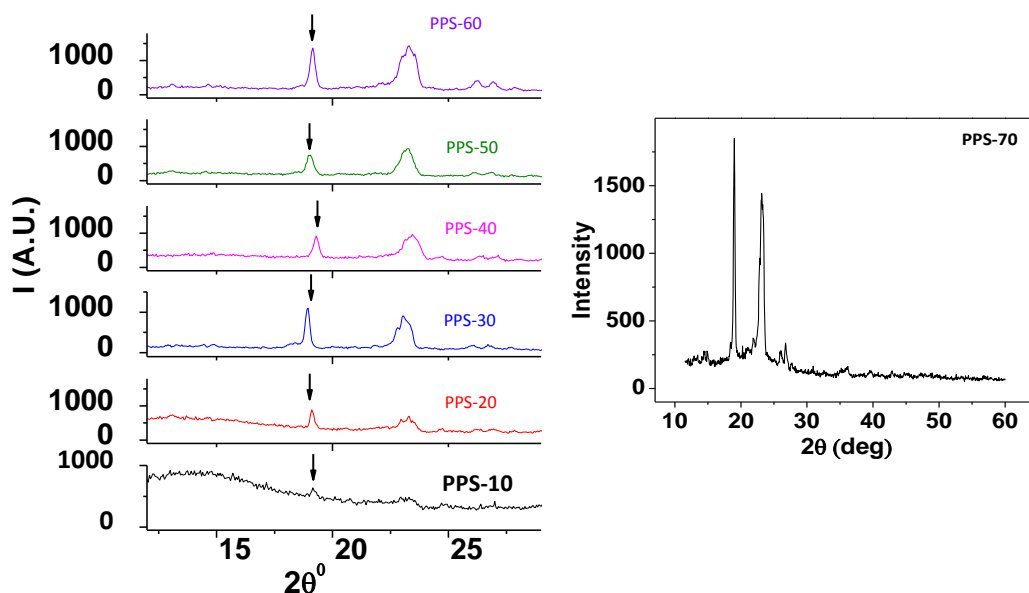


**Fig.4.3** XRD patterns of PPS- polymer blended samples.

PEO is increased, the background halo gets diminished and the main peaks of pure PEO with low intensity start emerging along with broadened peak at  $23.7^\circ$ . Further addition of PEO shows a shift in the XRD peak to  $18^\circ$ . All X-ray spectra depict a slight shift as well as change in intensity of peaks of PEO. No sample shows any X-ray peak of the salt ( $\text{AgNO}_3$ ) with the variation of PEO in all blend electrolyte samples. Rajendran et. al. [5] reported the absence of X-ray peaks of salt due to predominance of amorphous nature in PVA-PMMA polymer blend electrolyte system. The gradual suppression of halo due to PMMA and appearance of X-ray peaks of PEO clearly ascribes that both PEO and PMMA make a good blend complexation and salt also mixes uniformly between the polymer chains.

The optimized ratio of 50:50 for PEO and PMMA has been ascertained on the basis of good ionic conductivity (discussed in Chapter 5). However, the low ionic conductivity of polymer electrolytes at ambient temperature limits their applications. Therefore, to study the effect of the low molecular weight plasticizers on the polymer

electrolyte system, plasticization is carried out with varying amount of *Poly Ethylene Glycol* (PEG) (PPSP System) and *Ethylene Carbonate* (EC) from 5wt% to 15wt% (PPSE System) in the (PEO:PMMA)-5wt%  $AgNO_3$  electrolyte system each as a separate system.

Plasticization is the conventional way to reduce the crystallinity of polymers [6-8] and increases the amorphous phase content of the polymer electrolytes but at the same time, it promotes deterioration of the electrolyte's mechanical properties. The diffraction patterns show variation in intensity as well as broadening for polymer complex.

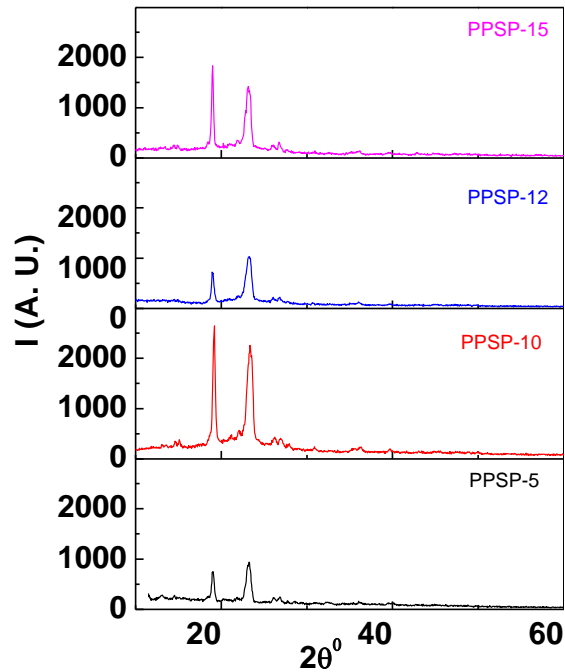


**Fig.4.4** XRD spectra of PPSP-system at room temperature.

In these polymer films, plasticized with PEG (PPSP); the presence of prominent crystalline peaks of PEO at  $19^\circ$  and  $23^\circ$  for PEG = 5 and 12 wt% show the lower intensity while for 10 and 15 wt% the X-ray peak intensity is higher (Fig.4.4). It is well known that PEG plasticizer does not show its own X-ray peaks as it possesses the same molecular structure as PEO. With the increase in PEG concentration, X-ray peak at  $23^\circ$

does not change but variation in intensity of the X-ray peak at  $19^\circ$  for PEG 5 and 12 wt% is observed. XRD spectra of PPSP-system clearly indicate that the PPSP-5 polymer film shows the lowest crystallinity than other polymer films with PEG 12, 10 and 15 wt% respectively. Dilution of crystalline phase with the increase in plasticizer [8] can be noticed wherein the sharp peaks in the XRD pattern become intense. It is quite obvious from Fig.4.4 that the intensity of the crystalline peaks consistently increases.

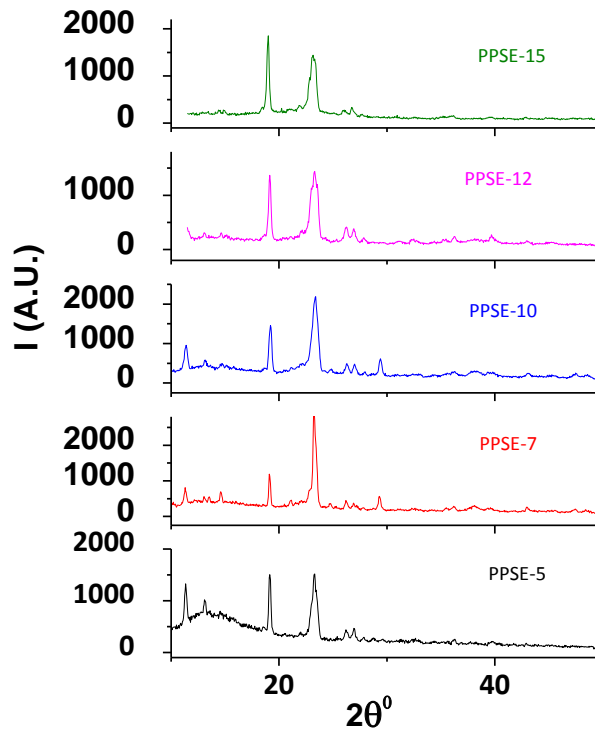


**Fig.4.5** XRD spectra of PPSE system at room temperature.

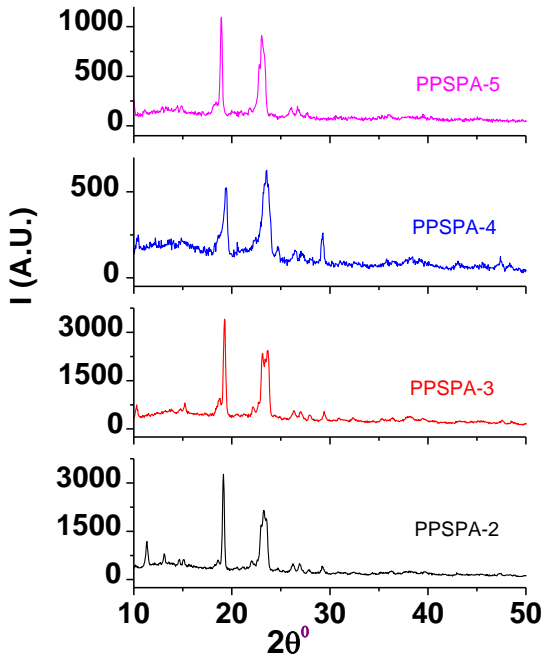
In third system (PPSE-system) EC has been added in the place of PEG in the PEO-PMMA-AgNO<sub>3</sub> polymer electrolyte system. Fig.4.5 depicts the XRD patterns of PPSE-system at ambient temperature. This system shows PEO peaks at  $19^\circ$  and  $23^\circ$  along with two new peaks at  $11^\circ$  and  $13^\circ$  in PPSE-5, PPSE-7 and PPSE-10. No individual peaks of either AgNO<sub>3</sub> [9] or the plasticizer is observed. At lower amount of EC two new peaks at  $11^\circ$  and  $13^\circ$  are observed which are, however, not seen in PEG system. With the

increase in EC concentration, the relative intensity of X-ray peak at  $19^\circ$  continues to decrease up to 12 wt% of EC, whereas for the sample with 15wt% EC, intensity of this x-ray peak increases, while peaks at  $11^\circ$  and  $13^\circ$  disappear. Another feature of the X-ray spectra is that the peak at  $23^\circ$  gradually broadens with the addition of EC in all electrolyte films. Reduction in intensity, broadening and /or disappearance of any X-ray peak is attributed to decrease of crystalline phase [10, 12] of polymer complexes.

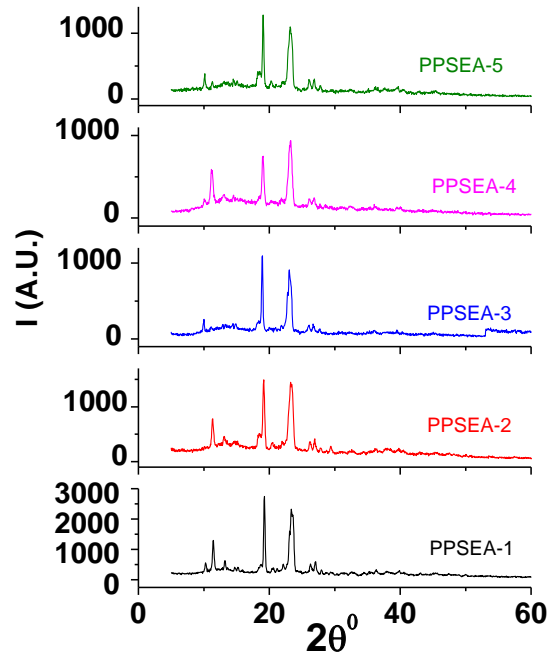
Both ionic conductivity and mechanical stability of the electrolytes are considerably and simultaneously enhanced when the inorganic fillers are added to form the composite electrolytes. The inert fillers due to their large surface area prevent the local chain reorganization with the result of a high degree of disorder characteristic of the amorphous phase [8]. Therefore, finally, the effect of varying concentration of nano-filler has been undertaken in an optimized PEO-PMMA polymer blend with 5 wt%  $\text{AgNO}_3$  and an optimized amount of PEG and EC plasticizer concentration for which the highest conductivity is found.

For this, the variation of inorganic nano filler  $\text{Al}_2\text{O}_3$  in an optimized PEG (PPSP) and EC based plasticized systems (PPSE) is carried out and shown in Figs. 4.6 and 4.7. XRD spectra in Fig. 4.6 for PPSP- $\text{Al}_2\text{O}_3$  system show sharp peak at  $19^\circ$  but the peak at  $23^\circ$  is broadened with reduced intensity as compared to that obtained in pure PEO possessing semi-crystalline matrix. The lowest intensities of X-ray diffraction peaks for 4 wt% of nano-filler (PPSPA-4) are observed and also a new peak at around  $29^\circ$  emerges only at 4 wt %. With further addition of  $\text{Al}_2\text{O}_3$  i.e.; PPSPA-5, the broadening of diffraction peaks along-with the slight shifting and increase in the intensity in X-ray spectra indicate a reduction in the degree of disorder i.e. amorphousness of the system.

Incorporation of nano sized  $\text{Al}_2\text{O}_3$  into PPSP also exhibits an increase in conductivity compared to those without nano-filler systems (Chapter 5).



**Fig.4.6** XRD patterns of PPSPA polymer electrolytes.



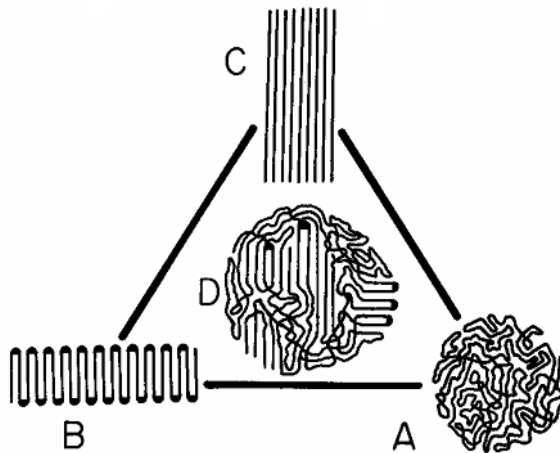
**Fig.4.7** XRD patterns of PPSEA polymer electrolytes with varying  $\text{Al}_2\text{O}_3$  concentration.

Fig. 4.7 shows XRD spectra of PPSEA system with varying  $\text{Al}_2\text{O}_3$  concentration. In this system, apart from the x-ray peaks at  $19^\circ$  and  $23^\circ$ , peaks at  $11^\circ$  and  $13^\circ$  are also observed with increasing filler concentration. Gradual reduction in the peak intensity of diffraction peaks with nano-filler concentration up to 4 wt % of nano-filler (PPSEA-4) in the EC-plasticized polymer electrolyte film is observed. The shifting and broadening in XRD peaks up to 4 wt% of nano-filler concentration is an indicative of an enhancement in the degree of disorder. The obtained change in XRD patterns in polymer films clearly confirms that the inert filler,  $\text{Al}_2\text{O}_3$  due to its large surface area facilitates the high degree of disorder, characteristic of the amorphous phase and prevents the local chain

reorganization [13].

## 4.2 SEM studies

Morphological observation is an important element, not only the external inspection of polymer films, where exterior appearance is considered to be extremely important, but also in product design and defect analysis [13]. Various types of microscope viz.; scanning electron microscopes (SEM), transmission electron microscopes (TEM), scanning tunneling microscopes (STM) and laser microanalysis (LM) [13-17] are used to observe samples ranging in size from tens of centimeters to as small as several nanometers. SEM analyzes the surface morphology of materials [17]. It also measures and evaluates surface pitting, failure analysis, characterization of dust, deposits, contaminants, particles, filter residues, and other applications.



**Fig.4.8** *Semicrystalline polymer (D)*

Semi-crystalline polymers exhibit number of morphologies. The most frequent are polymer spherulites [18]. SEM imaging is used to investigate the surface morphology of prepared plasticized polymer films. SEM images of various samples of PPS-system are shown in Figs. 4.9 ((a)-(g)).

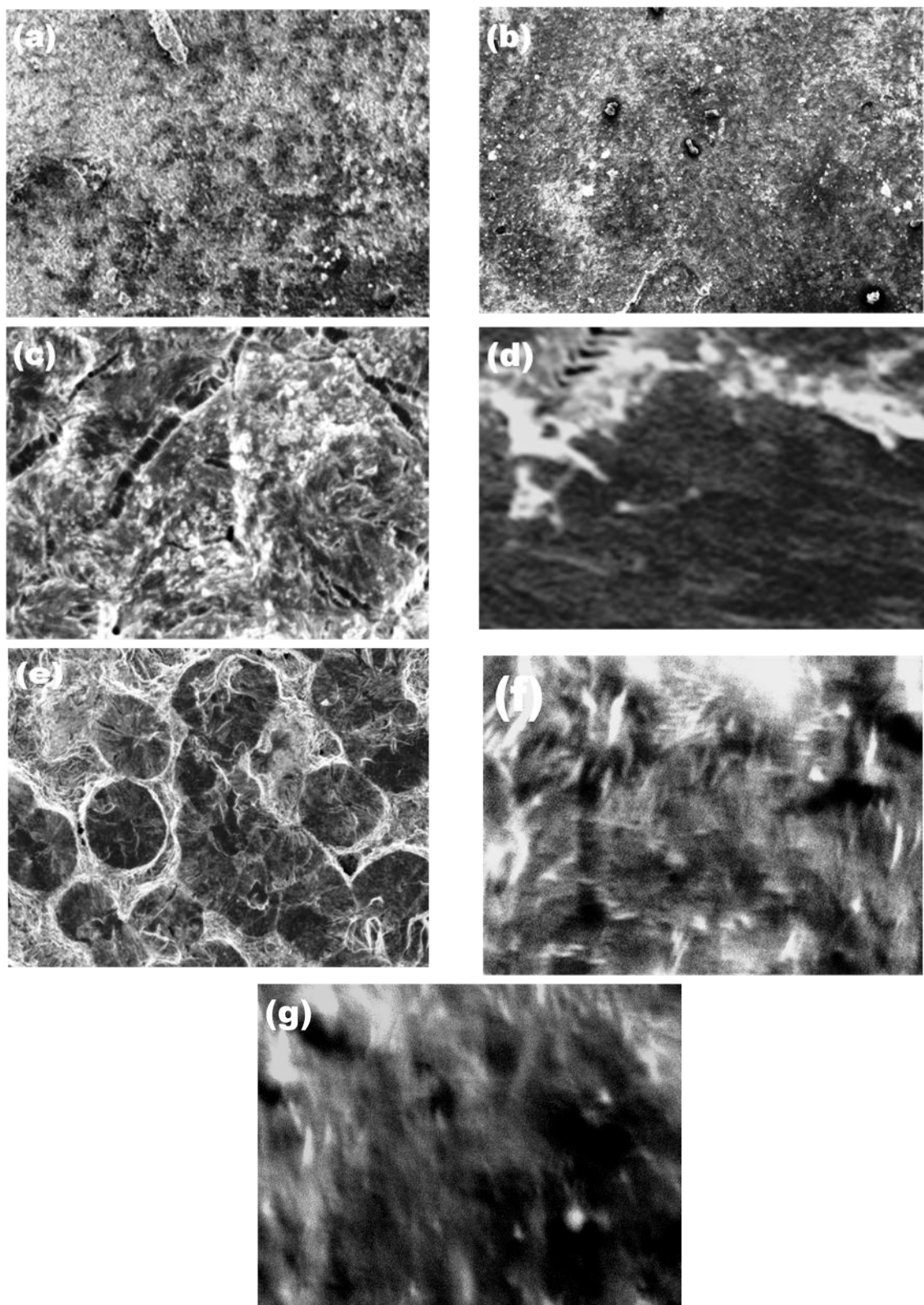


**Fig. 4.9** SEM images of PPS-system a) PPS-10, b) PPS-20, c) PPS-30, d) PPS-40, e) PPS-50, f) PPS-60 and g) PPS-70.

It is observed from figures that only 30 and 50 wt% of PEO containing samples show the spherulitic structure with “eye like” morphology near the spherulite centre. The spherulite structure starts to appear in the polymer film with PEO-30wt% and larger in size in the polymer film with 50 wt% PEO. Other samples do not show any such spherulitic structure.

Figs. 4.10 ((a)-(d)) show the SEM micrographs of the plasticized polymer complexes with different PEG concentrations (PPSP-system). The micrographs show that the roughness of the sample increases with the addition of the plasticizer PEG content which is an indication of the loss of mechanical strength of the polymer blend electrolyte film.

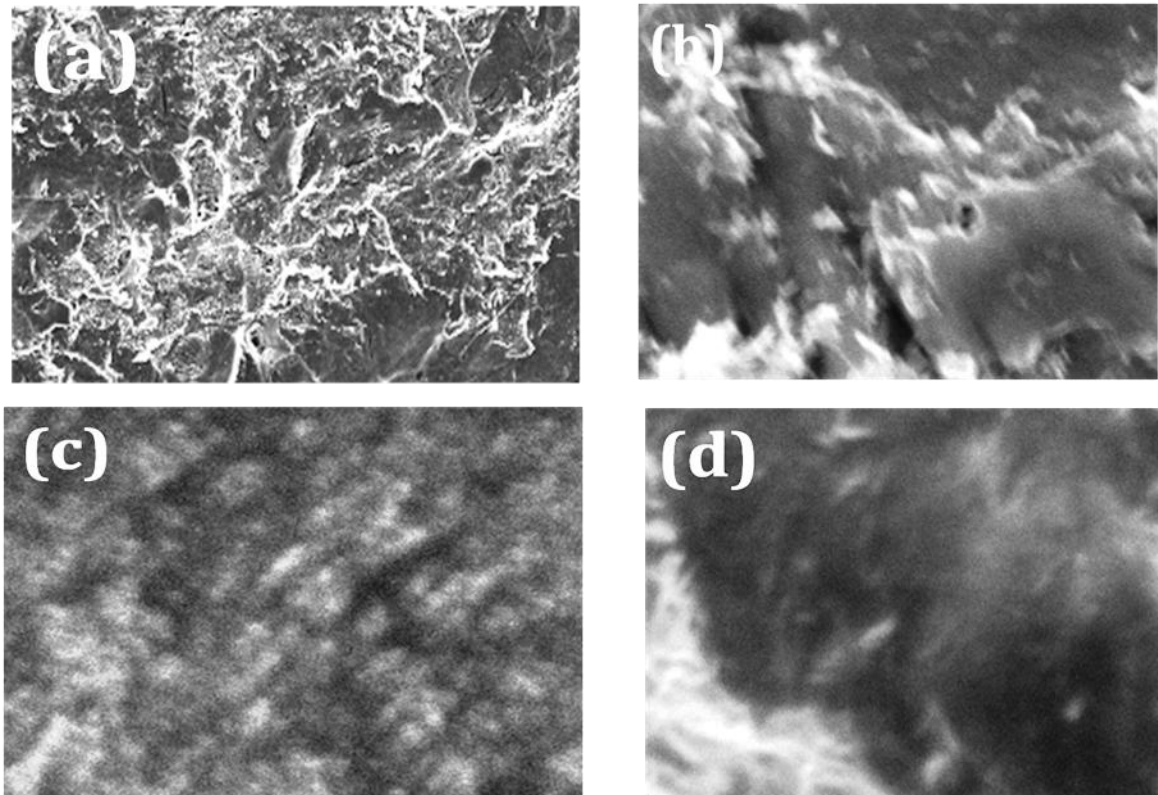


**Fig. 4.10** SEM images of PPSP-system a) PPSP-5, b) PPSP-10, c) PPSP-12 and d) PPSP-15.

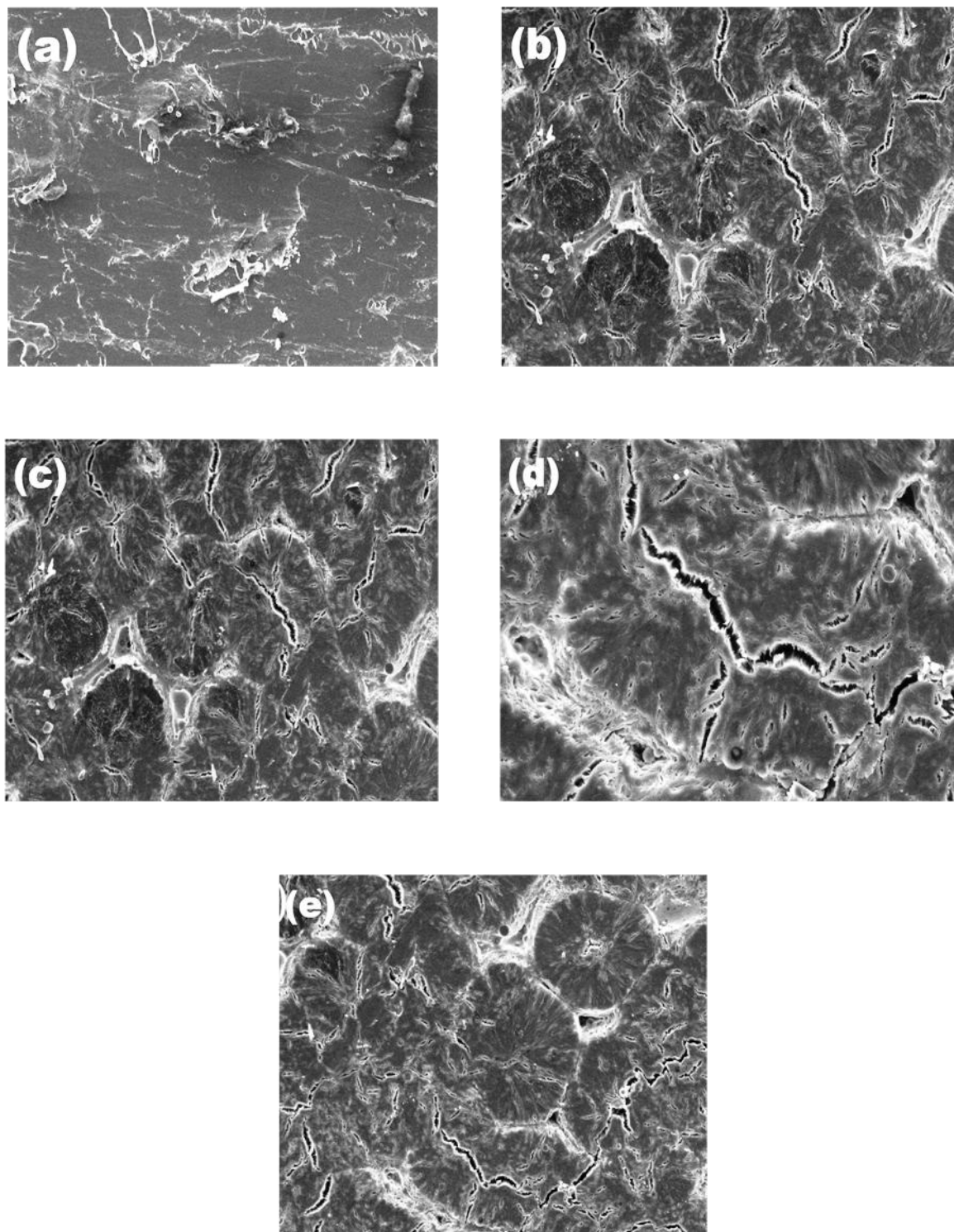


**Fig. 4.11** SEM images of PPSE-system a) PPSE-5, b) PPSE-7, c) PPSE-10, d) PPSE-12 and e) PPSE-15.

However, a substantial change in the morphological features is observed in SEM analysis (Figs.4.11 ((a)-(e)). Fig. 4.11(a) shows smooth areas in SEM micrograph of the EC-5wt% polymer blend. Spherulitic texture of the composite starts appearing after further addition of EC. The boundary between the spherulites is an indicative of the existence of amorphous phase. For the sample with EC-10wt%, with the decrease in the size, the spherulites become distinctive which in turn increase the boundary regions. The polymer blend films exhibit a good distribution and presence of amorphous and crystalline regions inside the polymer complex.

SEM micrographs of the plasticized polymer system with nano-fillers (PPSPA and PPSEA) are shown in Figs.4.12 and 4.13. Figs. 4.12 ((a)-(e)) show the SEM images of PPSPA samples (polymer system with PEG plasticizer). Figures indicate that the increase in nano-filler concentration affects substantially in morphology of prepared films. At lower concentrations of nano-filler a smooth surface morphology with homogenous dispersed nanofiller is observed while a clear aggregation of nano-fillers can be seen in the polymer film with higher amount of  $Al_2O_3$  (Fig.4.12(e)). The observed smooth surface may closely be related to the reduction in crystallinity of polymer film with nano-filler concentration which leads to an increase in the amorphous content.

Similar observations are made in PPSEA-system (polymer nano-composites plasticized with EC). Increment in uniformity, smoothness and homogeneity in surface is observed up to PPSEA-4 polymer film (Fig.4.13 ((a)-(e))) while above this concentration of nano-filler aggregation is noticeable.

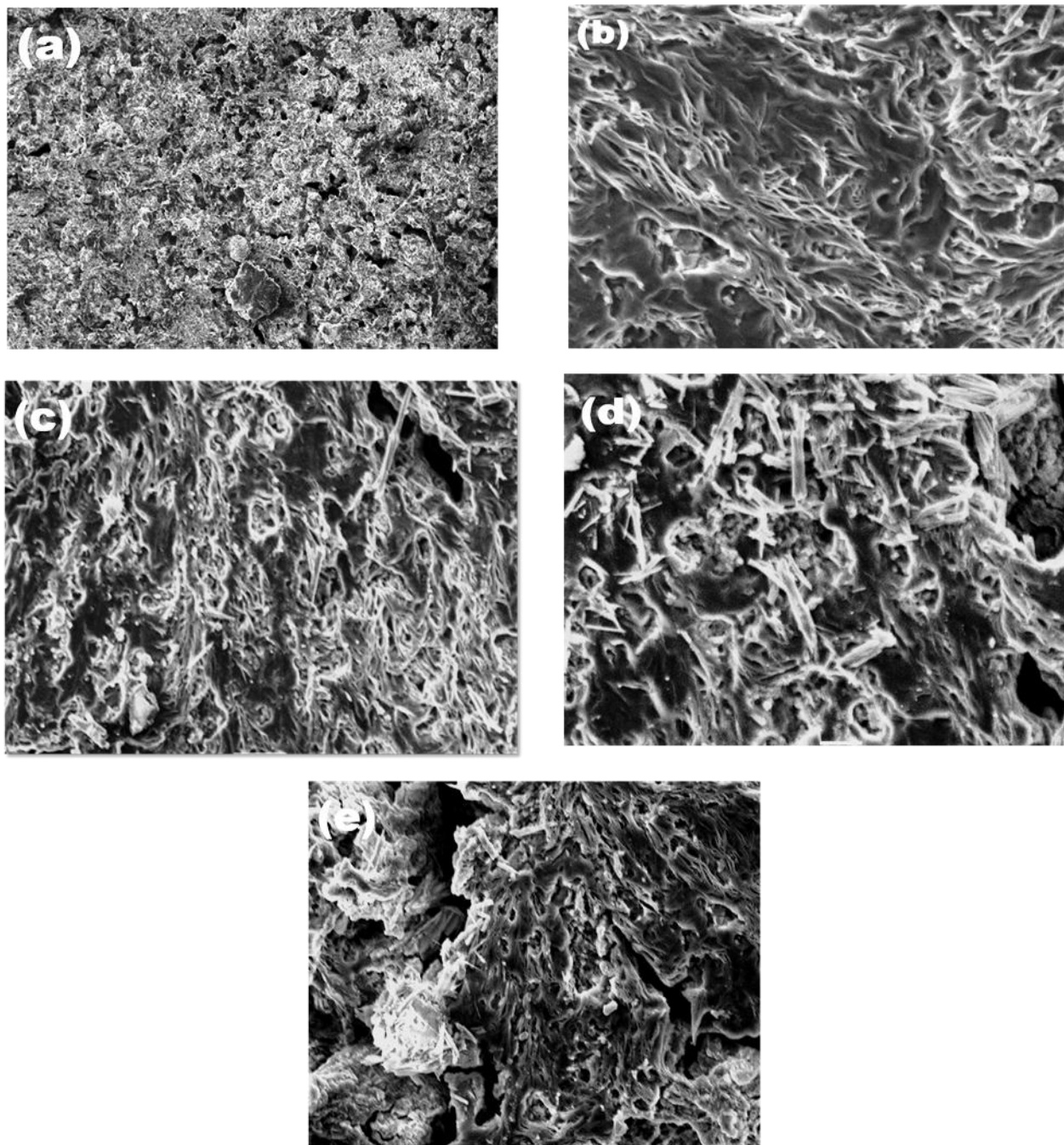


**Fig. 4.12** SEM images of polymer films of PPSPA-system a) PPSPA-1, b) PPSPA-2, c) PPSPA-3, d) PPSPA-4 and e) PPSPA-5.

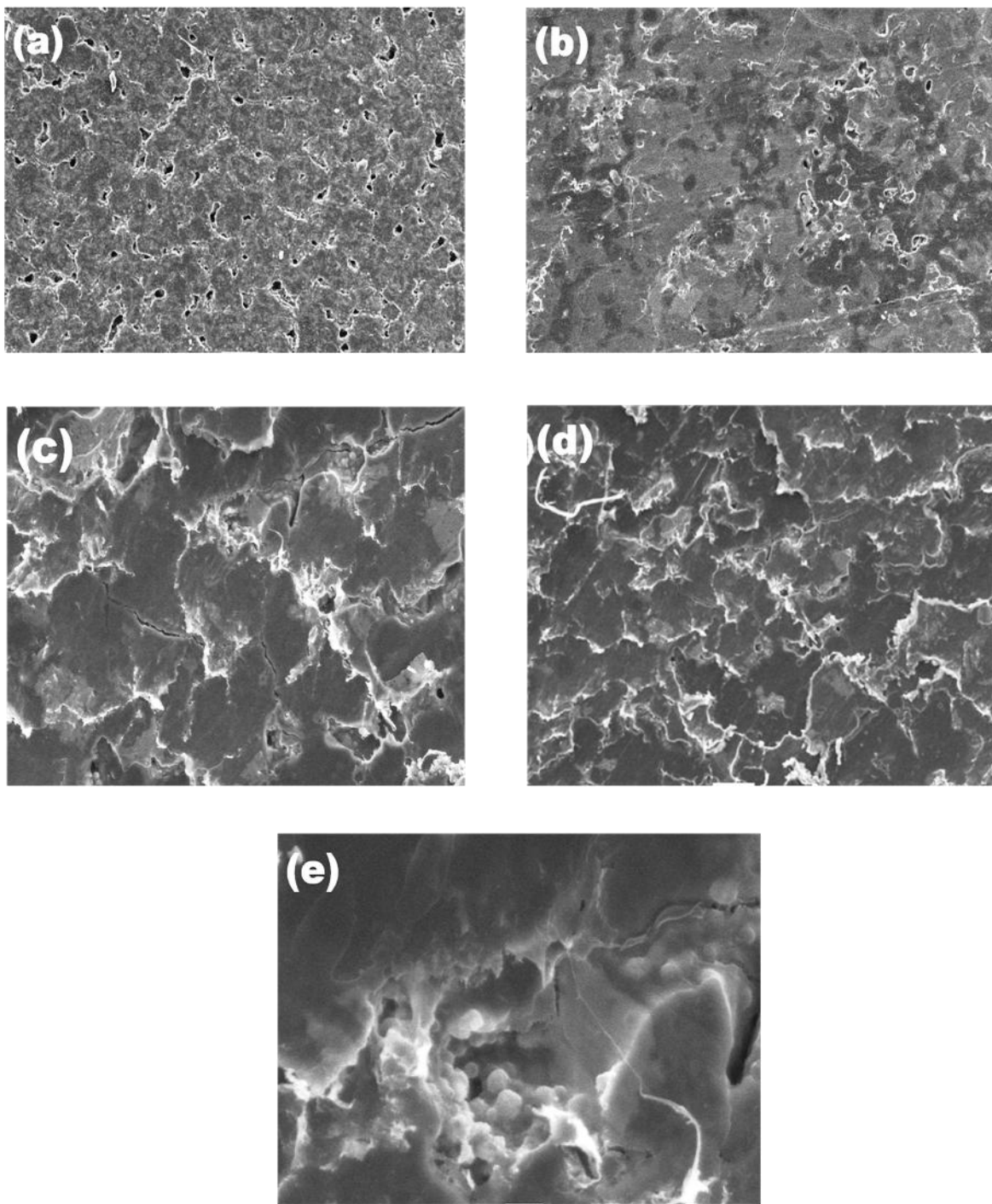


**Fig. 4.13** SEM images of polymer films of PPSEA-system a) PPSEA-1, b) PPSEA-2, c) PPSEA-3, d) PPSEA-4 and e) PPSEA-5.

### 4.3 DSC Studies

Differential scanning calorimetry (DSC) is an important technique used for characterizing solid materials and to determine their melting, crystallization, and mesomorphic transition temperatures, and the corresponding change in enthalpy, entropy with glass transition and other effects that show either changes in heat capacity or latent heat [19]. The advantage of DSC compared with other calorimetric techniques lies in the broad dynamic range regarding heating and cooling rates, including isothermal and temperature-modulated operations. DSC measures the temperatures and heat flows associated with transitions in materials as a function of time and temperature in a controlled atmosphere [20]. These measurements provide quantitative and qualitative information about physical and chemical changes that involve endothermic or exothermic processes, or changes in heat capacity.

*A differential calorimeter measures the heat of a sample relative to a reference [20]. It does all of the above discussed and heats the sample with a linear temperature ramp. Endothermic heat flows into the sample and exothermic heat flows out of the sample.*

Important properties of polymers, such as the glass transition, the melting temperature and crystallization are frequently used for characterization. Each polymer can be identified by peak temperature and enthalpy, as well as the initial crystallinity can be determined from the peak area of the corresponding thermal transition. The glass transition of a material marks the temperature below which amorphous materials behave as a glassy solid and above which the same materials behave as if they are liquids or in a rubbery state. Below the glass transition temperature, the polymer exists in a hard, rigid, brittle, glassy state in which the molecules are held together tightly by intermolecular

forces and the motion of the polymer molecules is restricted to molecular vibrations. As the polymer is heated the molecules acquire thermal energy. At the *glass transition temperature*,  $T_g$ , the molecules have enough energy to partially overcome the intermolecular forces, and they have more freedom of movement. The amorphous region now becomes rubbery, and the polymer becomes soft and flexible.

The glass transition is the reversible change of the amorphous region of a polymer from, or/ to, a viscous or rubbery condition to, or/from, a hard and relatively brittle one. The glass transition temperature is a temperature taken to represent the temperature range over which the glass transition takes place. Glass transition is affected by heating rate, crystalline content, heating and cooling history of the sample, copolymers aging, side chains, molecular weight, polymer backbone, plasticizer hydrogen bonding and filler. The endothermic transition upon heating from a crystalline solid to the liquid state is known as melting of solid [21]. This process is also called fusion. The melt is another term for the polymer liquid phase. DSC thermal analysis is available for a wide range of samples, such as polymers, elastomers and plastics, serving a wide range of industries.

DSC technique is employed to study the thermal behavior of polymer blends. The pure PEO is known to be a semi-crystalline (with small amorphosity) polymer. Fig.4.13 gives the characteristic endothermic peak at 340K which is attributed to the melting temperature ( $T_m$ ) of the crystalline PEO phase [22, 23]. The melting depression of a crystalline polymer in a binary blend consisting of other amorphous polymer arises from two sources namely; the dilution effect in the amorphous phase and morphological change of the crystalline component due to the presence of the other component in the blend [25]. The dilution effect will lower the chemical potential of PEO at the melt of the

blend than that in the pure state to cause the depression of the melting temperature and morphological changes depend on the interfacial energy between the crystal and the amorphous phases and also on the composition and crystallization rate of the blend [24].

To study the effect of blending on thermal properties DSC thermograms of various compositions of PEO in PEO-PMMA-AgNO<sub>3</sub> system (PPS-system) are recorded. These DSC thermograms are shown in Fig. 4.14(a). All polymer blends have the same behavior i.e.; sharp endothermic peak. Nishi *et. al.* [25] concluded that presence of melting depression in blended system is an indication of miscibility and compatibility. The observed endothermic peaks are assigned to the transition from semi-crystalline phase to amorphous phase i.e., melting temperature ( $T_m$ ) of PEO in polymer complexes. The intensity of endothermic peak is observed to be amplifying with PEO concentration. In present system, a reduction in  $T_m$  values than  $T_m$  value of pure PEO is observed. This may be ascribed to the interactions between Ag<sup>+</sup>-ion and PEO chains which strongly resist the possibility of crystalline organization of PEO chains to form the amorphous state. It is observed that the melting temperature,  $T_m$  of all polymer complexes is observed around 335K. These values are in good agreement with the values of  $T_m$  of PEO reported by Parizel *et. al.* [26] in PEO-PMMA polymer blends. In the present case,  $T_m$  values do not follow any systematic order in the different blend compositions of PEO in PPS-system (Fig. 4.15(b)), however the polymer film with PEO-50 wt% i.e; PPS-50 shows the lowest  $T_m$  value.

After studying the blending effect, plasticization effect using different plasticizers on thermal properties in optimized blended ratio of PEO and PMMA (on the basis of conductivity results discussed in Chapter 5) is carried out. For this, plasticization using

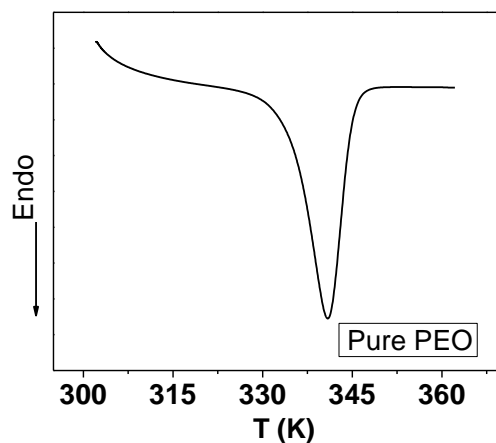


Fig.4.14 DSC thermogram of pure PEO polymer.

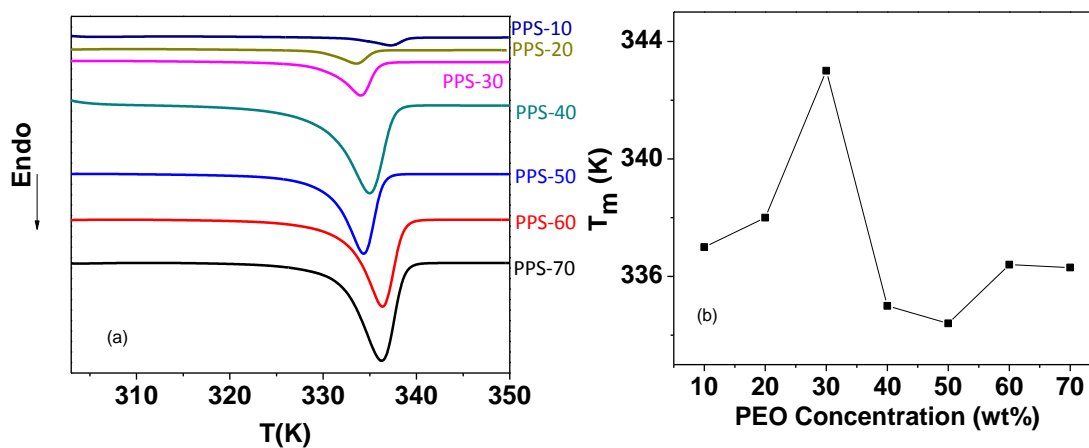


Fig.4.15 (a) DSC traces and (b) variation of  $T_m$  value with PEO concentration in PPS-system.

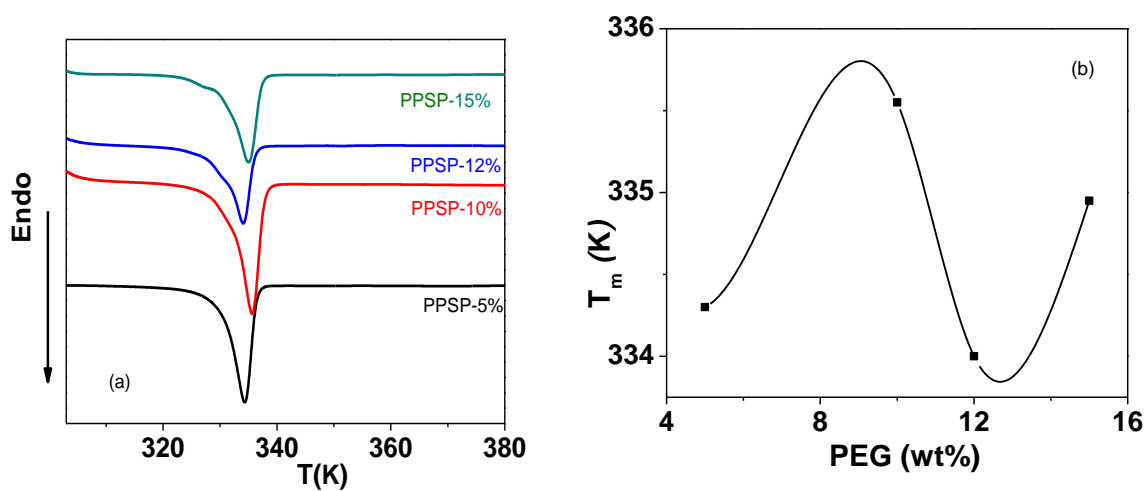
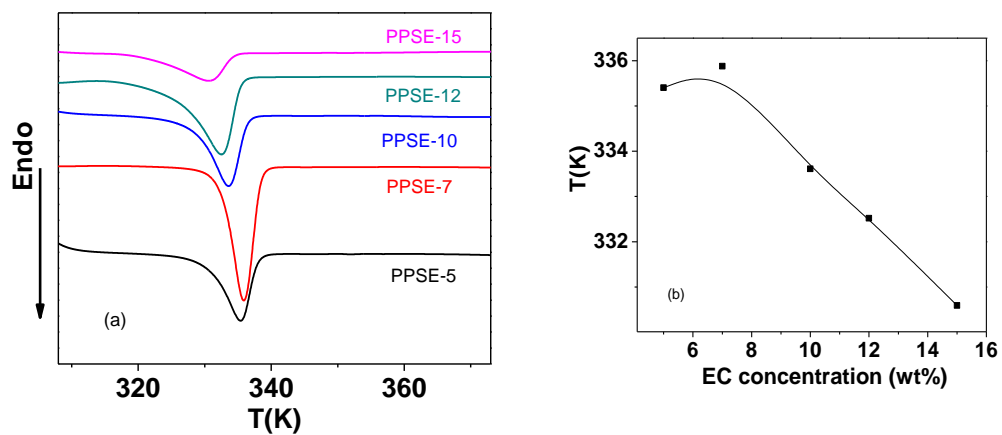


Fig. 4.16 (a) DSC thermograms and (b) variation of  $T_m$  values of PPSP system with PEG concentrations.

PEG and EC plasticizer has been done and the systems are named as PPSP and PPSE systems respectively. Fig.4.16 (a) shows the DSC thermograms of polymer films plasticized with various concentrations of PEG. These plasticized polymer electrolytes also show sharp endothermic peak near the melting temperature of PEO as found in PEO-blended system (PPS-system). These DSC curves clearly indicate that the variation in plasticizer concentration in PPSP-system affects the melting transition temperature ( $T_m$ ). Although  $T_m$  values were observed to be non-linear with PEG concentration (Fig.4.16 (b)), the shift in  $T_m$  values of polymer films as well as compared to pure PEO [27] corroborates the good compatibility and miscibility of PMMA and PEO in plasticized polymer electrolytes.

DSC traces of next plasticized polymer blended system (PPSE-system), wherein PEG plasticizer is replaced by EC, are recorded and depicted in Fig. 4.17(a). DSC traces of polymer blends plasticized with EC show a sharp endothermic peak which is expected. These endothermic peaks are assigned to melting temperature, ( $T_m$ ) of PEO (transition from semi-crystalline phase to amorphous phase). In this system, the steepness of melting



**Fig. 4.17** (a) DSC thermograms and (b) variation of  $T_m$  values of PPSE system with different EC concentrations.

peak increases as the concentration of EC increases from 5wt% to 7wt% while in EC-12wt% and 15 wt% peak broadening is observed. The increase in EC concentration possibly reduces the internal viscosity of the polymer films, in other words, it interrupts polymer-polymer interaction by occupying the inter and intra chain free volume which in turn, reduces the crystalline fraction of the polymer system, leading to an enhancement in the flexibility of the polymer chains [28]. This observed variation in  $T_m$  values (Fig. 4.17(b)) suggests the complexation of EC with increase in amorphous phase in the host polymer blend.

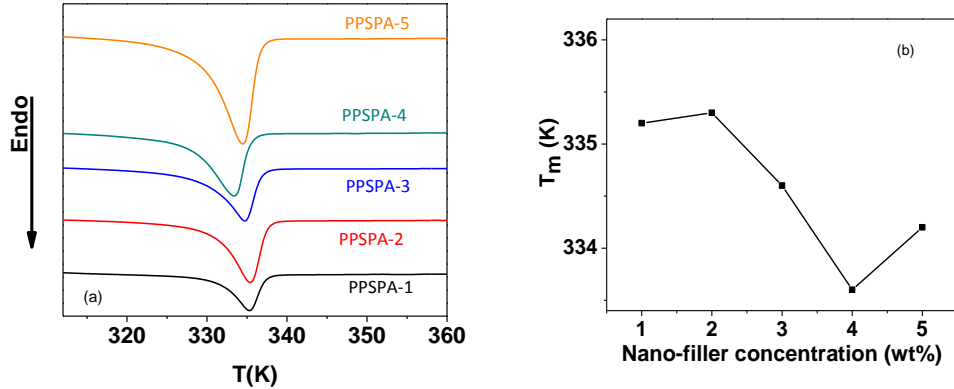


**Fig. 4.18** (a) DSC thermograms and (b) variation of  $T_m$  values of PPSPA system with different nano-fillers concentrations.

Next to plasticization, the effect of nano-filler  $\text{Al}_2\text{O}_3$  at lower concentrations in both plasticized systems is studied. DSC thermograms of fourth system i.e.; polymer nano-composites (PEG based polymer electrolyte film with optimized ratio of PEO and PMMA i.e.; PPSP-5 with different nano-filler concentration) are shown in Fig.4.18(a). DSC traces show sharp endothermic peak which is discussed above and well reported in PEO-based systems. The sharpness of endothermic peak represents the transition from semi-crystalline to amorphous phase i.e., melting temperature ( $T_m$ ) of PEO in polymer nano-composite. With increase in nano-filler concentration, the melting or semi

crystalline-amorphous phase transition temperature shifts towards the lower temperature side upto Al<sub>2</sub>O<sub>3</sub>-4wt% and further increment of Al<sub>2</sub>O<sub>3</sub> concentration gives the melting temperature to the higher temperature side. The lowering in  $T_m$  values with nano-filler concentration upto Al<sub>2</sub>O<sub>3</sub>-4wt% (Fig. 4.18(b)) indicates weakening of intermolecular interactions due to the interaction of nano-filler with polymer matrix resulting in increased amorphousity. At Al<sub>2</sub>O<sub>3</sub>-5wt%, the rise in  $T_m$  value is a signature of the increment in crystallinity or a decrease in amorphousity [28].

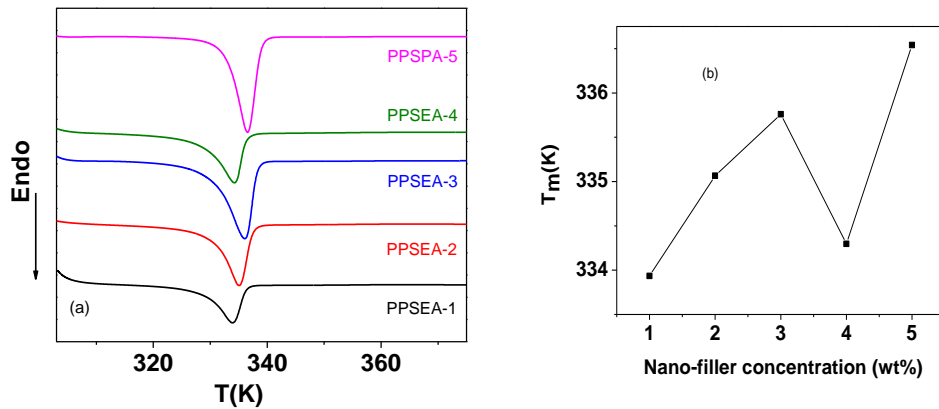


**Fig. 4.19** (a) DSC thermograms and (b) variation of  $T_m$  values of PPSEA system with different nano-filler concentrations.

DSC thermograms of fifth system (polymer nano-composites plasticized with EC, PPSEA-system) are shown in Fig. 4.19(a). This system also shows sharp endothermic peak similar to other systems as well as reported by many researchers for PEO based systems [3, 23, 28]. This represents the transition from semi-crystalline to amorphous phase of PEO in polymer nano-composite. With increase in nano-filler concentration, the melting temperature is also observed to increase with a reverse behavior at Al<sub>2</sub>O<sub>3</sub>-4wt% (Fig.4.19(b)) and further increment of Al<sub>2</sub>O<sub>3</sub> concentration shifts the melting temperature to the higher temperature side similar to observed in PEG based system. In addition, the melting endotherm is found to broaden with increase of nano-filler content. The decrease

in the melting temperature and the broadening of the melting endotherms are clear indications of decrease in the degree of crystallinity and dominant presence of amorphous phase.

#### 4.4 FTIR Studies

FTIR spectroscopy is a powerful tool to investigate the structural details of materials. This study was carried out to analyze the molecular interactions in the polymer blend. If two polymers are miscible in polymer blend then each individual polymer cannot be recognized in the FTIR spectra terms [35]. The chemical interactions may result in band shifts and broadening. Infrared spectroscopy measures the vibrational energy levels in the region of different molecules. The FTIR spectra of materials vary according to their compositions and show the occurrence of the complexation and interaction between the various constituents. The FTIR spectra of pure PEO, PMMA in  $500\text{-}4000\text{cm}^{-1}$  wave number range are given in Figs.4.20 & 4.21 respectively.

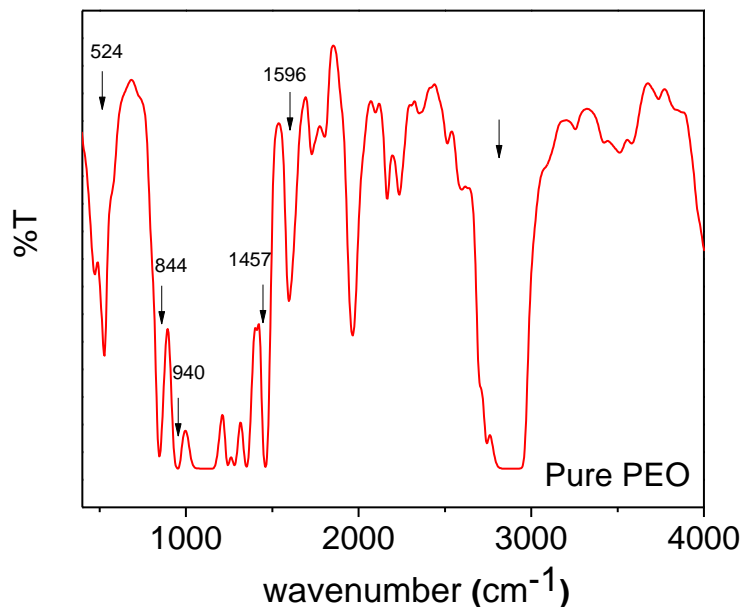


**Fig.4.20** FTIR spectra of pure PEO.

The vibrational assignments of pure PEO, PMMA are fairly reported in literature [3, 5, 23, 28, 31-38]. In pure PEO, the C-O-C bending mode at  $524\text{ cm}^{-1}$ ,  $\text{CH}_2$  rocking mode at  $844$  and  $940\text{ cm}^{-1}$  are observed. Also, weak bands in the region of  $1220\text{-}1360\text{ cm}^{-1}$  represent  $\text{CH}_2$  twisting and wagging modes of pure PEO while an intense band at  $1457$  and  $1596\text{ cm}^{-1}$  are due to  $\text{CH}_2$  scissoring mode and C=C stretching, respectively of pure PEO is observed. The broad band observed in the wavenumber range  $2700\text{-}2950\text{ cm}^{-1}$  (Fig. 4.20) in pure PEO is attributed to the symmetric and asymmetric C-H stretching modes of  $\text{CH}_2$  group [36].

In pure PMMA (Fig. 4.21), the frequency  $750\text{ cm}^{-1}$  corresponds to  $\text{CH}_2$  rocking with skeleton stretching,  $842\text{ cm}^{-1}$  is assigned to C-H rocking vibrations, the band at  $986\text{ cm}^{-1}$  is attributed to the symmetrical stretching of the C-O bond in the C-O-C linkage of PMMA. The peaks at  $1137$ ,  $1275$ ,  $1433$  and  $1721\text{ cm}^{-1}$  are assigned to C-O, asymmetric  $\text{CH}_2$  transformation,  $-\text{OCH}_3$  deformation and C=O stretching vibrations respectively. The sharp intense band at  $1721\text{ cm}^{-1}$  is assigned to C=O stretching vibration of ether oxygen of PMMA. The FTIR-spectra of pure silver nitrate ( $\text{AgNO}_3$ ) salt (Fig. 4.22) depicts an intense absorption band at  $1384\text{ cm}^{-1}$  which is characteristic of the  $\text{NO}_3^-$  ion in the free form. This vibration band is due to the displacement caused by change in the electronic environment of the anion as a result of the separation of its counterpart  $\text{Ag}^+$  [39, 40]. The vibration band at  $825\text{ cm}^{-1}$  is assigned to O-N stretching of nitrate group.

IR spectra of pure plasticizers i.e.; PEG and EC are also recorded and represented in Figs. 4.23 and 4.24, respectively. IR spectrum of PEG shows the important peaks at  $840$ ,  $1110$ ,  $1461$ ,  $2884$  and  $3432\text{ cm}^{-1}$ . The peak at  $840\text{ cm}^{-1}$  is assigned to  $\text{CH}_2$  rocking vibration. The absorption bands at  $1110$ ,  $1461$ ,  $2884\text{ cm}^{-1}$  and  $3432\text{ cm}^{-1}$  are due to C-O-

C linkage, CH bending and stretching and OH stretching vibrations, respectively [31, 41, 42]. While EC spectrum shows the main characteristic bands at  $713\text{ cm}^{-1}$  (ring bending),  $775\text{ cm}^{-1}$  ( $\text{CH}_2$  rocking),  $890\text{ cm}^{-1}$  and  $1076\text{ cm}^{-1}$  (ring breathing),  $1168\text{ cm}^{-1}$  (C-O-C symmetric),  $1392\text{ cm}^{-1}$  ( $\text{CH}_2$  wagging),  $1481$  ( $\text{CH}_2$  bending) and  $1808\text{ cm}^{-1}$  (C=O stretching) [43-45].

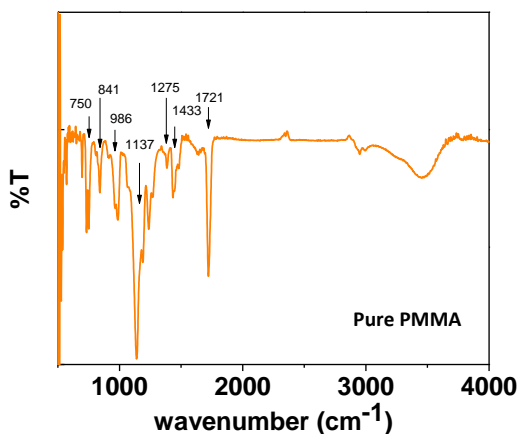


**Fig. 4.21** FTIR spectra of pure PMMA.

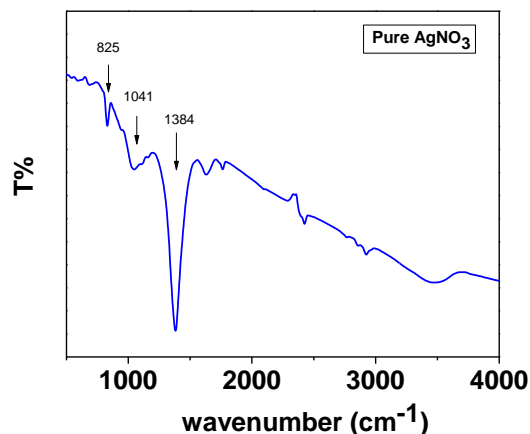


**Fig. 4.22** FTIR spectra of pure AgNO<sub>3</sub>.

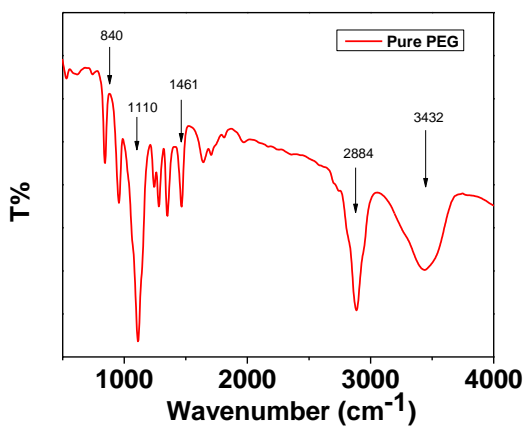


**Fig.4.23** FTIR spectra of pure PEG.

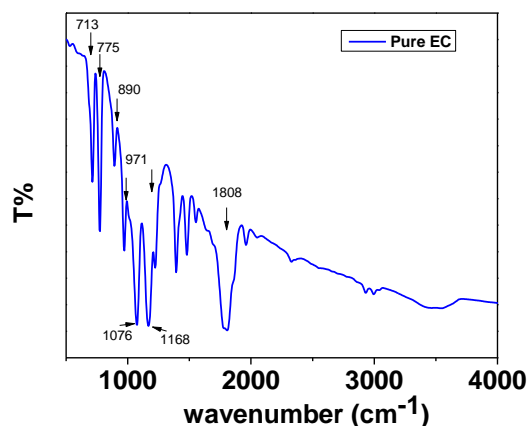


**Fig.4.24** FTIR spectra of pure EC.

To study the complexation of silver salt in host polymer blends along with the level of interaction among various constituents of polymer blend electrolytes, FTIR spectra

of prepared polymer electrolytes are recorded. FTIR spectra may be an evidence for interactions among polymers, salt and plasticizer. The effect of blending is analyzed

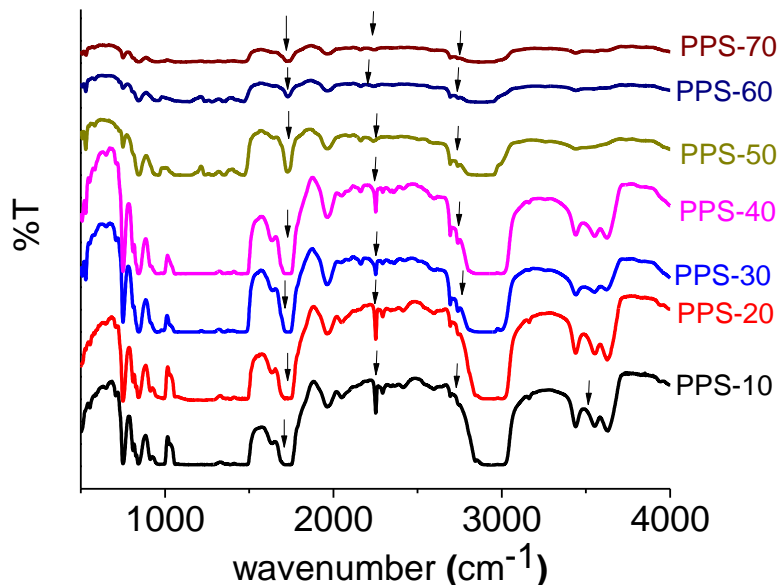


**Fig. 4.25** FTIR spectra of PPS system at room temperature.

firstly for PPS-system and their IR spectra are recorded at room temperature. It is observed from figure that the C-O-C bending mode of PEO at  $524\text{ cm}^{-1}$  is absent in 10 and 20% of PEO blend samples. This bending mode is observed to reappear after 30% PEO with a less intensity as well as with a shift towards lower wave numbers with increasing PEO ratio. In polymer blends, shifting of  $750\text{ cm}^{-1}$  vibration band (rocking vibration of  $\text{CH}_2$  group of PMMA) towards lower wave numbers, splitting of  $844\text{ cm}^{-1}$  peak which disappears at 50% of PEO ratio and broadening of  $948\text{ cm}^{-1}$  peak ( $\text{CH}_2$  rocking mode of PEO) are observed. The peaks at  $1461$ ,  $1596$  and  $2159\text{ cm}^{-1}$  of pure PEO are absent in polymer blends. A small kink at  $1024\text{ cm}^{-1}$  and an intense peak at  $2251\text{ cm}^{-1}$  are observed in blend samples however,  $2251\text{ cm}^{-1}$  peak disappears after 50% of PEO. The intense peak at  $1724\text{ cm}^{-1}$  due to asymmetric stretching vibration of C=O (ester carbonyl) group of pure PMMA is observed to broaden in polymer blends. In addition to

this, the characteristic peaks of pure  $\text{AgNO}_3$  [46] are absolutely absent in plasticized polymer blends which confirm good complexation of the salt with the host polymers. Hence, it can be concluded that the increased or decreased manner of shifting of frequency from pure polymers shows an interaction of the polymers with salt in plasticized polymer electrolytes.

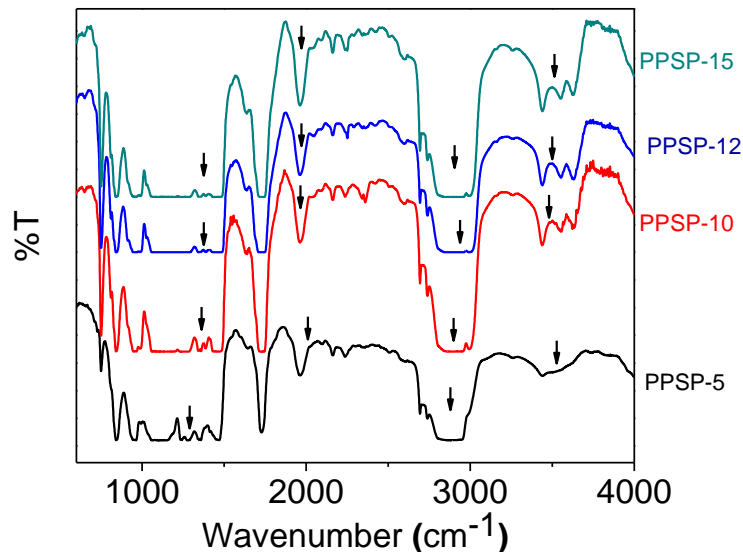


**Fig. 4.26** FTIR spectra of PPSP system at ambient temperature.

After investigating the effect of blending on FTIR spectra, plasticizer effect using two plasticizers PEG and EC has been carried out. Fig. 4.26 shows the FTIR spectra of the polymer electrolyte system plasticized with PEG i.e.; PPSP-system. In this system, the rocking, wagging and twisting modes of  $\text{CH}_2$  at 749, 842 and 991  $\text{cm}^{-1}$  respectively of pure PEO shift to lower frequencies. The peak at 1963  $\text{cm}^{-1}$  is assigned to asymmetric stretching vibration of PEO [32] remains at the same position. Ramesh *et. al.* [47, 48] reported the characteristic peak of pure PMMA, due to ester carbonyl ( $\text{C}=\text{O}$ ) stretching mode, to be at 1721  $\text{cm}^{-1}$ ; it was found at 1725  $\text{cm}^{-1}$  in PPSP-5 polymer film and broadens in rest of the samples. The other vibrational bands were found at similar positions in all of the plasticized polymer electrolytes. In addition to this, a closer

inspection of IR spectra shows increase in the intensity of various bands with increasing the PEG concentration, however PPSP-12 and PPSP-15 polymer films show less intensity than that of PPSP-10 sample. Similar to PPS-system, the characteristic peaks of  $\text{AgNO}_3$  are absent in this system also and confirms the complexation of salt with the host polymer matrix. From FTIR analysis an interaction between polymers, plasticizer and salt is confirmed in plasticized polymer electrolytes. However, the increased intensity of vibration bands in IR spectra studies indicates increase in crystalline nature in the PPSP-10 polymer electrolyte film.

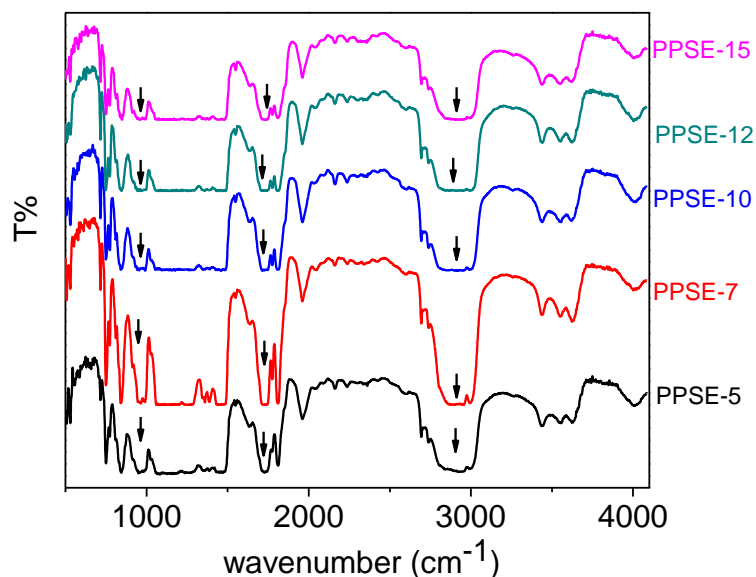


**Fig. 4.27** FTIR spectra of PPSE-system at room temperature.

Next to PEG based system, attempts have been made to study the change in various vibrational energy level when plasticization is carried out using EC plasticizer. Fig. 4.27 depicts the FTIR Spectra of PPSE-system. In this system, the broadening of characteristic peak of  $\text{AgNO}_3$  indicates complexation of salt with polymer blend. In the prepared polymer films, the stretching frequency at  $1721\text{ cm}^{-1}$  corresponding to  $\text{C}=\text{O}$  of pure PMMA gets broadened and shifts to  $1709\text{-}1746\text{ cm}^{-1}$  which indicate the complex

formation [40]. The triplet peak of C-O-C stretching of PEO is absent and CH<sub>2</sub> rocking vibration of pure PEO is observed to shift to 839 cm<sup>-1</sup>. Stretching vibration of methoxy group and wagging mode of CH<sub>2</sub> of pure PMMA and PEO respectively, are absent in polymer complexes. In addition to this, some small new peaks appear at 1964 cm<sup>-1</sup> and in the 2690-3630 cm<sup>-1</sup> frequency range. Also, the bending mode of EC at 903cm<sup>-1</sup> [49] shifts to 912cm<sup>-1</sup> in polymer complexes indicating interaction of salt and EC. In FTIR spectra, the disappearance and change in position of PEO and PMMA vibrational bands along with some new peaks confirm the complexation among various constituents of PEO-PMMA polymer electrolytes.

After studying the plasticization effect, addition of nano-fillers (Al<sub>2</sub>O<sub>3</sub>) at lower concentration in both plasticized (PEG and EC) polymer blends has been done. FTIR spectra of polymer nano-composites (plasticized with PEG) i.e.; PPSPA-system is shown in Fig.4.28. In this system (polymer nano-composites), it has been observed that the stretching frequency at 1721 cm<sup>-1</sup> corresponding to C=O of pure PMMA is broadened and shifted to 1729 cm<sup>-1</sup> along with some new peaks in the complexes. The observed shift in the carbonyl stretching frequencies of the complexes confirms the complex formation. Stretching vibration and wagging mode of CH<sub>2</sub> of pure PMMA and PEO respectively, are not observed in polymer complex. No IR features of AgNO<sub>3</sub> are seen in any of the samples which signify the good complexation of salt in the polymer nano-composites. IR bands in the wave number range 600-1500 cm<sup>-1</sup> are observed to be feeble and the intensities of the various bands between 600-1500 cm<sup>-1</sup>, at 1727, 1968 cm<sup>-1</sup>, between 2819-3000 cm<sup>-1</sup> and 3393-3617 cm<sup>-1</sup> start decreasing and the peaks get broadened with nano-filler concentration up to Al<sub>2</sub>O<sub>3</sub>-4wt% i.e., PPSPA-4 polymer electrolyte film.

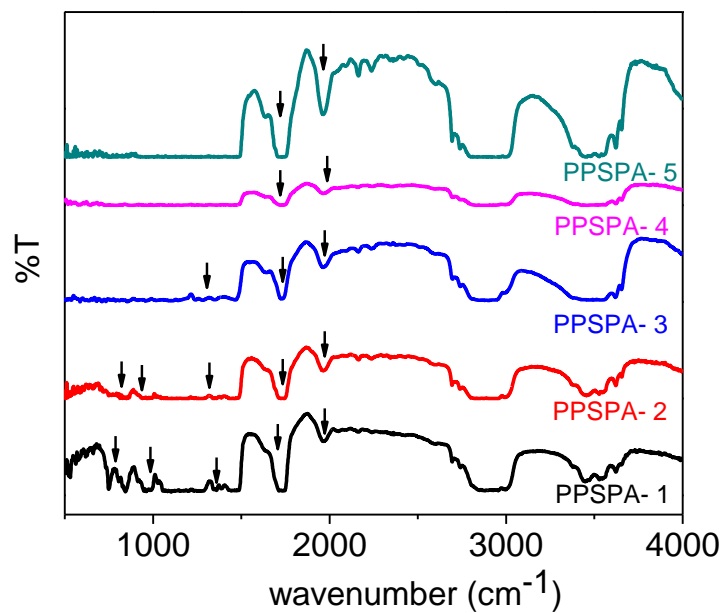


**Fig. 4.28** FTIR spectra of PPSPA-system at room temperature.

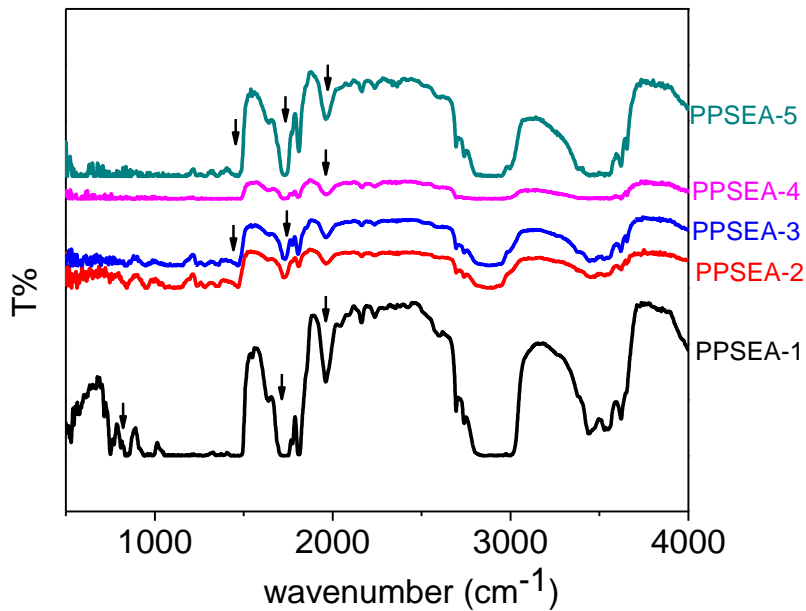


**Fig. 4.29** FTIR spectra of PPSEA-system at room temperature.

Further addition of nano-filler concentration results in reappearance of more intensified IR bands. Such features or variations are indicative of increased amorphousity till 4 wt% of nano filler and subsequently, the process retards and level of amorphousity decreases in the polymer blend system with further addition of nano particles.

Similar features are observed in IR spectra of PPSEA-system (Fig.4.29). However, in this system a significant decrease in the intensity of IR bands is found with increase in nano-filler concentration. An IR spectrum of polymer film with Al<sub>2</sub>O<sub>3</sub>-4 wt% (PPSEA-4) is observed to be least intense while reappearance of more peaks at Al<sub>2</sub>O<sub>3</sub>-5 wt% is also the main feature of this system. The reduction in crystallinity upon the addition of filler is attributed to small particles of filler, which changes the chain reorganization and facilitates for higher ionic conduction [8].

#### **4.5 Transference number**

Generally, the transport of electrical charge conduction in solid electrolytes occurs through migration of ions. In these materials, the total conductivity is primarily due to the conduction of ionic species with very small electronic contribution. The contribution of ionic conductivity to the total conductivity due to possible ionic conducting species can be calculated using transference number. *Transference number is defined as the ratio of the ionic conductivity to the total conductivity attributed due to the possible conducting species.* For an ideal electrolyte, the transference number for ionic species should approach nearly unity with negligible zero electronic contribution and therefore, transference number is one of the key factors to select the electrolyte for a device application [50].

The conductivity in an electrolyte material is expressed by the transference number which denotes the fraction of current carried by anions, cations or electrons in the material in terms of the total conductivity ( $\sigma_T$ ). The transference number of any charge particle/ion may be defined as the ratio of the conductivity due to it to the total conductivity. The total conductivity can be written as the sum of ionic and electronic/hole

conductivity:  $\sigma_T = \sigma_e/h + \sigma_i$

In this way, the ionic transference number can be written as:  $t_i = \frac{\sigma_i}{\sigma_T}$

and the electronic transference number as :  $t_e = \frac{\sigma_e}{\sigma_T}$

In the present study, the transference number of the prepared polymer films is measured by Wagner's polarization technique. In this method, the electronic contribution to the total conductivity can be obtained. In this technique, the which current was monitored as a function of time current was monitored as a function of time on application of fixed dc potential 500mV across the cell Ag || polymer electrolyte || Ag. The initial current is the total current ( $i_T$ ) which is due to the ions ( $i_i$ ) and the electrons ( $i_e$ ) i.e.,  $i_T = i_e + i_i$ . As polarization builds up the  $i_i$  is blocked and the final current is only the electronic current.

Therefore, the electronic transference number  $t_e = \frac{\sigma_e}{\sigma_T} = \frac{i_e}{i_T}$

and the ionic transference number  $t_i = \frac{\sigma_i}{\sigma_T} = \frac{i_T - i_e}{i_T}$

are used to determine the ionic transference number. Table 4.1 depicts the ionic transport number for prepared systems. It is observed from the table that in PPS-system, the ionic transference numbers are in the range of 0.75-0.91. Transference number shows the maximum values for PPS-30 and PPS-50 polymer films. S. Chandra *et. al.* [51] also found the ionic transport number in PEO-AgNO<sub>3</sub> polymer electrolyte ~ 0.91.

In PPSP- series,  $t_i$  values varies from 0.92-0.78. The polymer film plasticized with PEG-5 wt% shows the highest ionic transference number. With the increase in PEG

concentration, the ionic transport number values are observed to decrease. The variation in ionic transference number is in good agreement with conductivity behavior (Chapter 5-Fig.5.15) in PPSP-system.

Next to PPSP-system, in PPSE system, PEG plasticizer is replaced by ethylene carbonate (EC), in order to find the effect of plasticization using a plasticizer with a higher dielectric constant than host polymer blend. In this system, the ionic transport number initially decreases with increasing plasticizer content and starts increasing at EC-12wt% (Table 4.1). It is suggested by Bruce and Vincent [52] that in EC containing polymer system, at low EC concentration, stabilization of ion pairs takes place and viscosity decreases at higher EC concentration. This may be the reason for the observed variation in ionic transport number with increasing EC concentration.

The effect of addition of nano-filler in polymer blend electrolytes plasticized with PEG and EC is studied. In polymer nano-composites containing PEG plasticizer, the ionic transference number varies from 0.68 to 0.94. The observed increase in  $t_i$  with nano-filler concentration upto an optimum concentration is observed. The reason for decrease in ionic transport number after highest value may be due dilution effect on increasing plasticizer concentration. Similarly,  $t_i$  in EC containing polymer nano-composites also shows increasing trend with nano-filler concentration upto an optimum concentration i.e.; Al<sub>2</sub>O<sub>3</sub>-4wt%.

Analysis of ionic transference number data (Table 4.1) implies that all the investigated polymer electrolyte samples possess low electronic charge transport. Therefore, it can be concluded that charge transport in the polymer electrolyte is predominantly due to ionic species with negligible electronic contribution.

**Table 4.1.** Ionic transference number values for PPS, PPSP, PPSE, PPSPA and PPSEA systems.

<b>Sample name</b>	$t_i$	$t_e$
<i>PPS-system</i>		
PPS-10	0.75	0.25
PPS-20	0.79	0.21
PPS-30	0.89	0.11
PPS-40	0.82	0.18
<b>PPS-50</b>	<b>0.91</b>	<b>0.07</b>
PPS-60	0.85	0.15
PPS-70	0.87	0.13
<i>PPSP-system</i>		
<b>PPSP-5</b>	<b>0.92</b>	<b>0.08</b>
PPSP-10	0.72	0.28
PPSP-12	0.74	0.26
PPSP-15	0.78	0.22
<i>PPSE-system</i>		
PPSE-5	0.91	0.09
PPSE-7	0.88	0.12
PPSE-10	0.89	0.11
PPSE-12	0.90	0.10
<b>PPSE-15</b>	<b>0.93</b>	<b>0.07</b>
<i>PPSPA-system</i>		
PPSPA-1	0.68	0.32
PPSPA-2	0.84	0.16
PPSPA-3	0.90	0.10
<b>PPSPA-4</b>	<b>0.94</b>	<b>0.06</b>
PPSPA-5	0.78	0.22
<i>PPSEA-system</i>		
PPSEA-1	0.81	0.19
PPSEA-2	0.94	0.06
PPSEA-3	0.95	0.05
<b>PPSEA-4</b>	<b>0.98</b>	<b>0.02</b>
PPSEA-5	0.82	0.18

## References:

1. R. G. Linford, *Applications of Electroactive Polymers*, B. Scrosati (ed.), Chapman & Hall, Suffolk, 1993.
2. N. S. Murthy, *Rigaku J.* 21(2004) 15–24.
3. S. K Chaurasia, R.K. Singh, S. Chandra, *Solid State Ionics* 183(2011) 32- 39.
4. B.K. Money, K. Hariharan, *Appl. Phys. A*, 88(2007) 647-652.
5. S. Rajendran, V.S. Bama, M.R. Prabhu, *Ionics*, 16(2010)27-32
6. G. Wypych, *Handbook of plasticizers*, ChemTec. Publishing, 2004.
7. N. Platzer, in *Plasticization and Plasticizer Processes*, R.F. Gould (ed.), *Advances in Chemistry*, ACS, Washington, DC, 1965.
8. M. R. Johan, L. B. Fen, *Ionics* 16 (2010) 335-338.
9. S.S. Rao, K. V. S. Rao, Md. Shareefuddin, U. V.S. Rao, S. Chandra, *Solid State Ionics* 67 (1994) 331-334.
10. M. Forsyth, *Solid State Ionics* 99(1997)257.
11. M. R. Johan, L.M. Ting, *Int. J. Electrochem. Sci.* 6(2011)4737-4738.
12. F. H. Chung, D.K. Smith, *Industrial Applications of X-ray Diffraction*, F. Smith, Marcel Dekker Inc., USA, 2000.
13. M. Ulaganathan, R. Nithya, S. Rajendran, *Scanning Electron Microscopy*, V. Kazmiruk (ed.), InTech, 2012.
14. D.B. Williams, C.B. Carter, *Transmission Electron Microscopy*, Springer, 2009.
15. C.F.D. Chidsey, D.N. Loiacono, T. Sleator, S. Nakahara, *Surface Sci.* 200(1988) 45-66.
16. F. Leis, W. Sdorra, J.B. Ko, K. Niemax, *Microchim. Acta* 98(1989)185-199.
17. K. Merrett, R. M. Cornelius, W. G. Mcclung, L. D. Unsworth, H. Sheardown, *J. Biomater. Sci. Polymer Edn.* 13(2002)593–621.
18. J.H. Magill, *J. mater. Sci.* 36(2001) 3143-3164.
19. M.E. Brown, *Introduction to thermal analysis*, Kluwer Academic Publishers, 2001.
20. G.W.H. Hohne, W.F. Hemminger, H.J. Flammersheim, *Differential scanning Calorimetry*, Springer-VCH, 2003.
21. C.W. Liew, Y. S. Ong, J.Y. Lim, C.S. Lim, K.H. Teoh, S. Ramesh, *Int. J. Electrochem. Sci.*, 8 (2013) 7779 - 7794.
22. P.K. Singh, K.W. Kim, R K Nagarale, H.W. Rhee, *J. Phys. D: Appl. Phys.* 42(2009)125101
23. Y. Kumar, S.A. Hashmi, G.P. Pandey, *Solid State Ionics* 201(2011) 73-80.
24. Y. T. Shieh, G.L.Liu, K. C. Hwang, C.C. Chen, *Polymer* 46(2005) 10945-10951.
25. T. Nishi, T.T. Wang, *Macromolecules* 25(1975) 909.
26. N. Parizel, F. Laupretre, L. Monnerie, *Polymer* 38(1997)3719-3725.
27. M. Maitra, K.C. Verma, M. Sinha, R. Kumar, T.R. Middy, S. Tarafdar, P. Sen, S.K. Bandyopadhyay, U. De, *Nucl. Instr. Methods Phys. Res. B* 244 (2006) 239–242.
28. M.R. Johan, O.H. Shy, S. Ibrahim, S.M.M. Yassin, T.Y. Hui, *Solid State Ionics* 196(2011)41-47.
29. L. Yua, K. Dean, L. Li, *Prog. Polym. Sci.* 31 (2006) 576–602.
30. M. M. Coleman, P.C. Painter, *Appl. Spect. Rev.* 20(1984) 255-346.
31. D. Snavely, J. Dubsky, *J. Poly. Sci. A* 34(1996) 2575-2579.
32. Z. Osman, N. M. Ansor, K.W. Chew, N. Kamarulzaman, *Ionics* 11 (2005) 431.
33. S. Ramesh, L.C. Wen, *Ionics* 16 (2010) 255.
34. N. Shukla, A.K.Thakur, *Ionics* 15 (2009) 357.
35. M. Sundar, S. Selladurai, *Ionics* 12 (2006) 281.
36. V.M. Mohan, V. Raja, A.K. Sharma, V.V.R.N. Rao, *Ionics* 12(2006)219-226.
37. S. Ramesh, T.F. Yuen, C.J. Shen, *Spectrochem. Acta A* 69(2008) 670-675.
38. S.A.M. Noor, A. Ahmad, I.A. Talib, M.Y.A. Rahman, *Ionics* 16(2010)161-170.

39. M.A.A. Mendez, E.S.M. Martinez, L.O. Arroyo, G.C. Portillo, E.S. Espindola, *J. Nanopart. Res.* 13(2011)2525–2532.
40. J. W. Cho, J. H. So, *Mater. Lett.* 60(2006)2653–2656.
41. M. Rozenberg, A. Loewenschuss, Y. Marcus, *Spectrochim. Acta A* 54 (1998) 1819–1826.
42. T. Kumar, *Analyst* 15(1990)1597.
43. T. Winie, A.K. Arof, *Spectrochim Acta A* 63 (2006) 677–684.
44. T. Matsushita, K. Dokko, K. Kanamura, *J. Power Sources* 146 (2005) 360–364.
45. Y. Akita, M. Segawa, H. Munakata, K. Kanamura, *J. Power Sources* 239 (2013) 175-180.
46. G. Hirankumar, S. Selvasekarapandian, M.S. Bhuvneswari, R. Baskaran, M. Vijaykumar, *J. Solid State Electrochem.* 10(2006) 193-197.
47. S. Ramesh, K.N. Bing, *J. Mater. Engg. Perform.* 21(2012) 89–94.
48. S. Ramesh, G.P. Ang, *Ionics* 16(2010) 465–473.
49. S. Kalyanasundraram, A. Gopalan, N. Muniyandi, N.G. Renganathan, Y. Saito, H. Kataoka, A.M. Stephan, R.N. Elizabeth, *Ionics* 7(2001) 44-52.
50. R.C. Agrawal, R.K. Gupta, *J. Mater. Sci.* 34 (1999) 1131 – 1162.
51. S. Chandra, S.A.Hashmi, M.Saleem, R.C. Agrawal, *Solid State Ionics* 67 (1993) 1-7.
52. P G Bruce, C. A. Vincent, *J. Chem. Soc. Faraday Trans.* 89 (1993) 3187.

## **Chapter 5-Electrical properties**

---

This chapter deals with the different formalism obtained from impedance spectroscopy data viz., impedance, bulk conductivity, AC conductivity, dielectric, relaxation and modulus of samples at different temperatures.

---

## 5.1 Introduction

The impedance spectroscopic technique is employed to understand ion conduction mechanism. When we apply a DC bias to a sample, polarization at the electrodes, due to the failure of the mobile ions to traverse the electrolyte/electrode interface, is observed because ionic current drops to zero. This problem can be solved by using AC techniques, alternately, called as Impedance spectroscopy [1-7]. In AC impedance measurements, a small sinusoidal potential perturbation is applied to the sample [1], the response to the applied perturbation is, generally, different in phase and amplitude from the applied signal. Measurement of the phase difference and the impedance allows analysis of the electrode process relating to contributions from diffusion, kinetics, double layer capacitance and coupled homogeneous reactions, etc. The plot between real and imaginary part of impedance is called the Nyquist plot or the complex impedance plot [5]. It should be noticed that in the Nyquist plot of impedance spectroscopy data, each point corresponds to the impedance at one specific frequency; low frequency data are on the right-hand side, while those of higher frequencies are on the left-hand side of the plot.

Frequency dependence conductivity and dielectric studies are useful techniques to obtain the detailed information of ionic conduction mechanism in solid electrolytes [6]. Using dielectric relaxation study, the dynamic and relaxation behavior of the electric dipoles in the polymer matrix can be understood by studying the electrode polarization effect in the polymer electrolytes [8-10]. Conductivity relaxation refers to the time that is required to build up the charge carriers at the electrode electrolyte interface before the electric field changes its direction [8]. The resulting in a net cumulative moment will give

rise to a relaxation. The buildup of the charge carriers are known as polarization [9-12]. The polarization disappears when the voltage is removed [12].

Dielectric and modulus formalisms have their own advantage at particular circumstances. Among these principal quantities ( $Z^*(\omega)$  &  $\varepsilon^*(\omega)$ ) have a long history while the modulus  $M^*(\omega)$ , was introduced relatively recently [13] and it seems to be useful in analysis of the electric response of the materials where the parasite capacitance effects, such as the electrode polarization, double layer formation etc. are occurring [14]. Relaxation processes occurring inside the ionic materials can be visualized and distinguished by impedance, electric modulus and dielectric permittivity. Variation of AC conductivity with temperature as well as compositions is presented and discussed. Dielectric and modulus studies were carried out and discussed to understand the relaxation phenomenon. The modulus study is used to discuss the distribution of relaxation times. The real,  $Z'$  and imaginary,  $Z''$  parts of complex impedance  $Z^*$  are directly measured from the instrument. The increase in ionic conductivity with temperature is due to ions receiving more thermal energy and because the number of defects in solids increases with temperature.

Ionic conductivity measures the ability of a charged particle (an ion) to move through the crystalline / amorphous structure of a material. Compounds and elements able to accept the movement of an ion through their structure are called electrolytes.

In the present study, electrical properties of prepared samples were carried out at different temperatures using the impedance spectroscopy in the frequency range of 10Hz to 1MHz. Complex impedance data can be drawn directly from the instrument.

## 5.2 Complex impedance plot and conductivity

The following given systems of polymer electrolytes were prepared to study the conduction mechanism in these polymer blend films using the method described in Chapter III:

**Series I:**  $(PEO)_x-(PMMA)_{100-x} - 5 \text{ wt}\% AgNO_3$  [PPS]

where  $x$  is varied from 10-70 wt% in steps of 10.

**Series II:**  $PPS \text{ system} + x \text{ wt}\% PEG$  [PPSP]

where  $x$  is varied from 5-15 wt%.

**Series III:**  $PPS \text{ System} + x \text{ wt}\% EC$  [PPSE]

where  $x = 5, 7, 10, 12, 15$ .

**Series IV:**  $PPSP \text{ System} + x \text{ wt}\% \text{ nano-filler } Al_2O_3$  [PPSPA]

where  $x$  is varied from 1-5 wt% in steps of 1.

**Series V:**  $PPSE \text{ System} + x \text{ wt}\% \text{ nano-filler } Al_2O_3$  [PPSEA]

where  $x$  is varied from 1-5 wt% in steps of 1.

To understand the effect of blending of semi-crystalline polymer PEO with amorphous and rigid polymer PMMA, the complex impedance data at different frequencies and temperatures is recorded. The impedance plots for different concentrations of PEO in PPS electrolyte films are obtained at different temperatures. Figs. 5.1 to 5.5 show the complex impedance plots for PPS-10, PPS-20, PPS-30, PPS-40 and PPS-70 samples. The impedance plots which show the semicircles for the PPS system at all temperatures indicate that the sample is partially resistive and capacitive in nature. The obtained impedance plots were fitted using *Zview2 program*. The intercept of

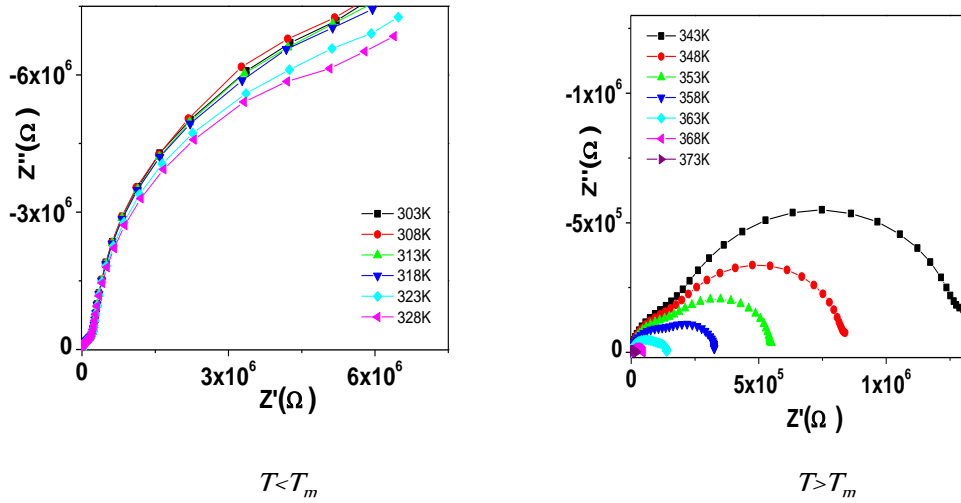


Fig. 5.1 Plot of  $Z'$  vs.  $Z''$  for PPS-10 polymer film at different temperatures.

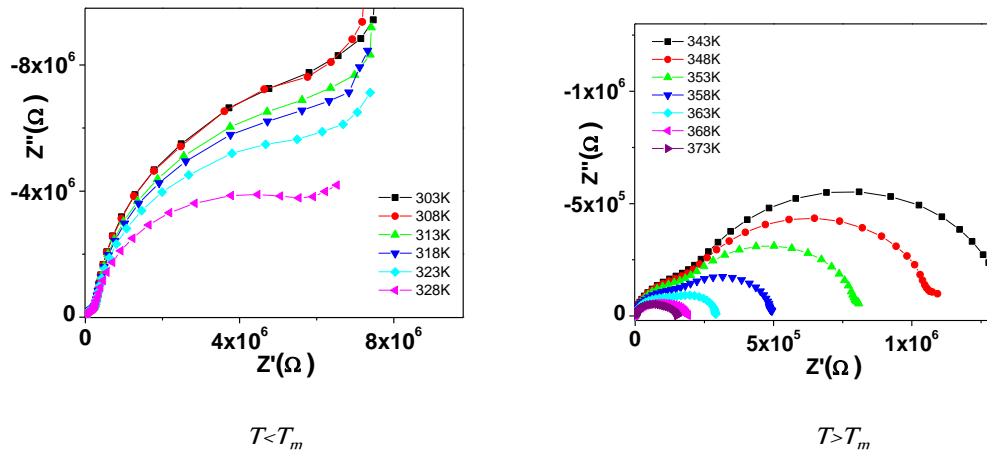


Fig. 5.2 Plot of  $Z'$  vs.  $Z''$  for PPS-20 sample at different temperatures.

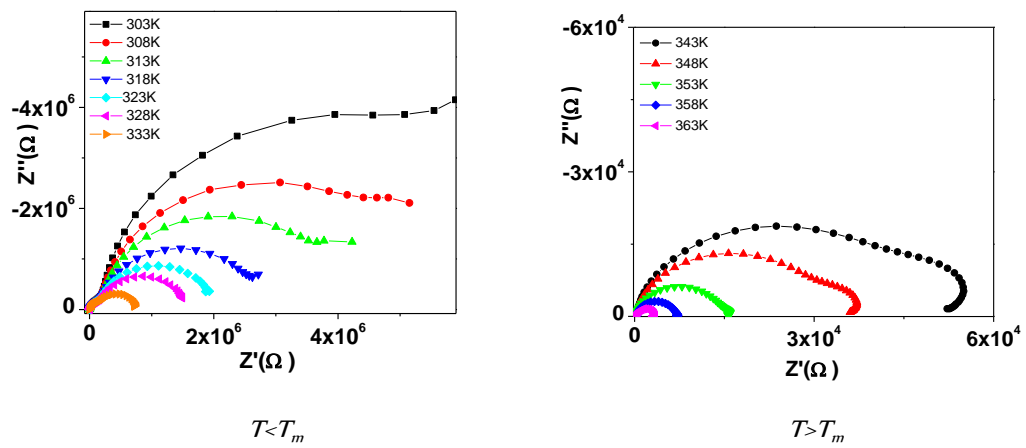


Fig. 5.3 Plot of  $Z'$  vs.  $Z''$  for PPS-30 sample at different temperatures.

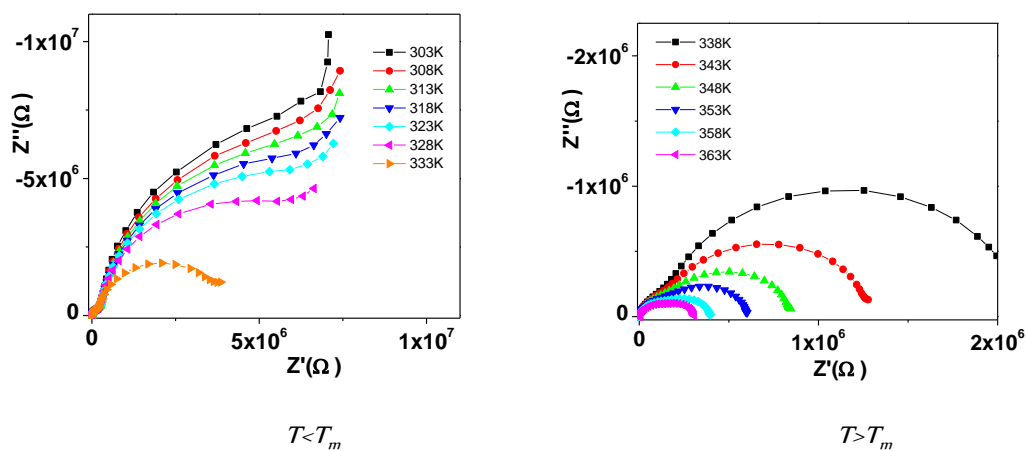


Fig. 5.4 Plot of  $Z'$  vs.  $Z''$  for PPS-40 sample at different temperatures.

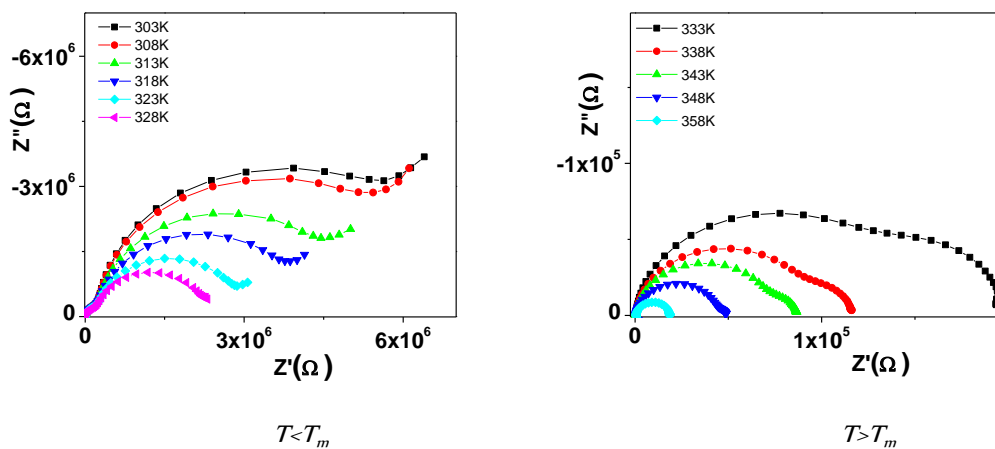


Fig. 5.5 Plot of  $Z'$  vs.  $Z''$  for PPS-70 sample at different temperatures.

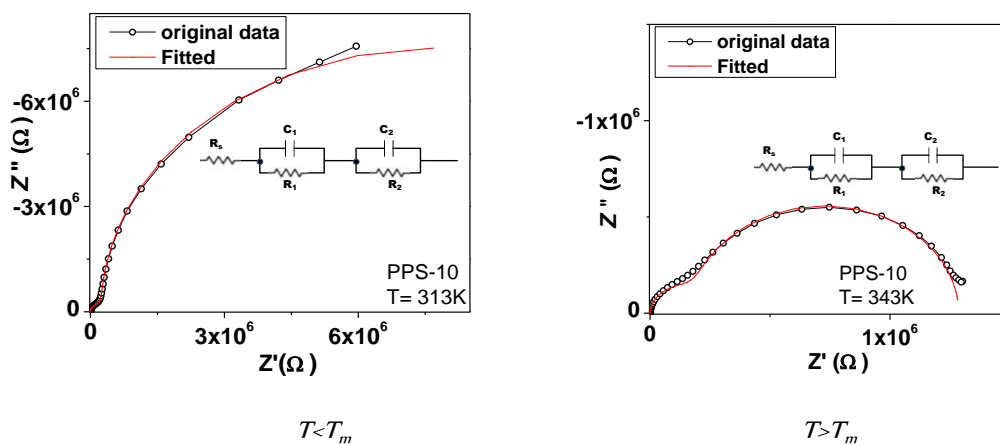
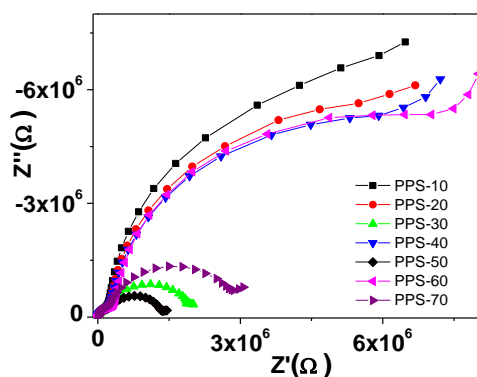
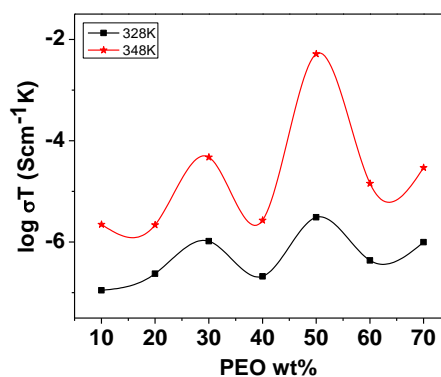


Fig. 5.6 Fitted impedance plot (equivalent circuit-inset) for PPS-10 sample at 313 and 343K.



**Fig. 5.7** Plot of  $Z'$  vs.  $Z''$  for PPS-system at 323K.



**Fig.5.8** Variation of ionic conductivity for all PEO blended polymer samples (PPS-System).

the fitted semicircle on the real axis ( $Z'$  axis) is used to obtain the bulk resistance ( $R_b$ ) of the sample [15]. The intercept of real axis shifts towards origin i.e., the bulk resistance of the sample decreases with increase of temperature in all the samples. The fitted impedance plots represent a series combination of two parallel lumped RC circuits. Fig.5.6 shows the fitted curve for PPS-10 polymer film and its inset shows its equivalent fitted circuit. The first semicircle arises due to the bulk resistance of the sample while the other semicircle ( $R_2C_2$  couple) arises due to polarization of mobile  $Ag^+$  ions at the electrode–electrolyte interface [15, 16]. The temperature dependence of the obtained impedance plots can be divided in two regions: region - I; below melting temperature  $T_m$  of PEO, and, region - II-above  $T_m$ . Below  $T_m$  (region I), a gradual decrease in the  $R_b$  values and a sudden/large decrease of  $R_b$  near  $T_m$  is observed. In region II (above  $T_m$ ), the decrease in  $R_b$  value is quite substantial compared to below  $T_m$ . Similar behavior with different quantitatively values in other samples is observed. The impedance plot for various concentrations of PEO in polymer blend system (PPS-system) in Fig. 5.7 shows that the polymer films with 30 wt% and 50wt% demonstrate the lowest bulk resistance

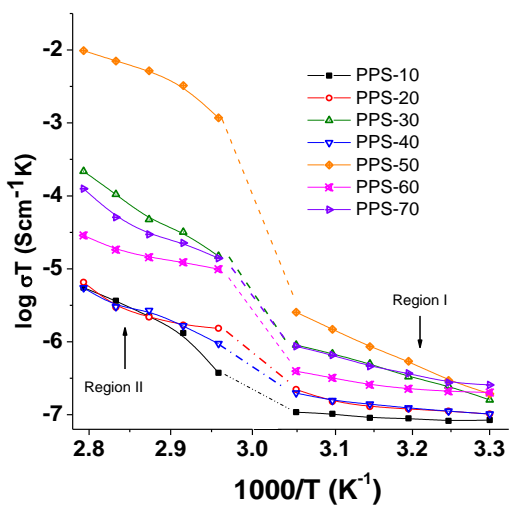


**Fig.5.9** Ionic conductivity vs.  $1000/T$  plots for all blended samples (PPS-system).

values compared to other samples.

To understand the variation of conductivity due to blending of PEO with PMMA, the plot of logarithmic of ionic conductivity versus reciprocal of temperature for various concentrations of PEO are shown in Fig.5.9. Two distinct regions of conductivity, one below  $T_m$  and other one above  $T_m$  are clearly seen. A sudden increase of slope in the curve near melting temperature  $T_m$  has been reported by many a workers [17-19]. Beyond  $T_m$ , the rise in the conductivity with temperature is larger than that below  $T_m$ .

According to Druger *et. al.* [20, 21], the increase in conductivity with temperature in solid polymer electrolyte is due to segmental (i.e. polymer chain) motion and free volume of the system. This, in turn, results in the hopping of ions from one site to another and provides a pathway for ions to move. The segmental movement of the polymer facilitates the translational ionic motion, thus, increasing the charge carrier mobility. The matrix amorphosity supports the faster internal polymer chain movement in which bond rotations produce segmental motion to favor inter and intra-chain ion hopping, and thus

the degree of conductivity becomes high [22].

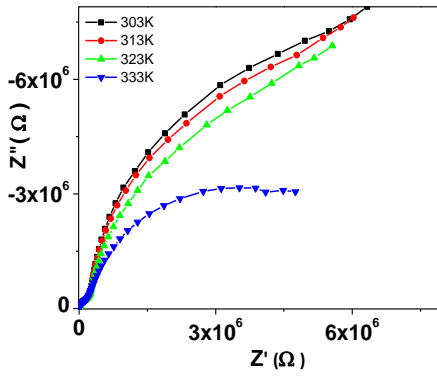
Below the transition temperature  $T_m$ , the rise in conductivity with temperature which is interpreted to be due to the hopping processes between coordination sites, local structural relaxations and segmental motion of the polymer chains, is observed to be very nominal. While above  $T_m$ , due to dominating amorphous regions in the polymer blend system, the polymer chains acquire faster internal modes in which bond rotations produce faster segmental motion resulting in the temperature assisted rise in the conductivity.

The conductivity isotherm for the first (PPS) system is plotted and shown in Fig. 5.9. Two conductivity maxima at PPS-30 and PPS-50 in 30 wt% and 50wt% of PEO in polymer blend electrolytes are observed in the conductivity isotherms. Also an enhancement in conductivity with increment in PEO concentration is observed. The observed enhancement in ionic conductivity might be occurring due to increased segmental motion and ionic mobility due to melting of PEO in the blend matrix. According to Straka *et. al.* [23], PEO crystalline regions are separated by amorphous layers of PEO and PMMA in PEO-PMMA polymer blend. The highest conductivity for PPS-50 polymer sample is obtained with a value of  $9.42 \times 10^{-9}$  S/cm at 328K. Occurrence of two conductivity maxima in ionic conductivity isotherms have been reported by several workers [24-28]. Singh *et. al.* [24] observed two maxima in conductivity plot in PEO-NH<sub>4</sub>I-ZnS polymer electrolyte system due to two different percolation threshold for two mobile species i.e., cations and anions. While Chandra *et. al.* [25] have reported two maxima in conductivity isotherms in PEO-AgNO<sub>3</sub> polymer electrolytes, where first maxima is attributed to the amorphous phase of polymer complex and second maxima is probably due to the redissociation of non-conducting pairs. Several workers [26-28]

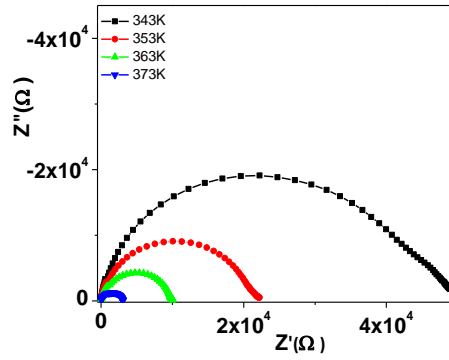
assigned the reason of two maxima in conductivity plot to percolation process in polymer electrolytes. According to Bunde *et. al.* [29], in a percolation process, percolating paths give rise to conductivities characteristic of metal salts in the polymer electrolytes. In the present case, the values of conductivity lie between the conductivity values of pure PEO and PMMA which suggests the optimization of the PPS-system with PEO: PMMA as 50:50 ratio of further study.

After, optimization of blend ratio in polymer complexes, the effect of plasticization using PEG and EC plasticizers in PEO-PMMA polymer blends has been undertaken. It is well known that a plasticizer is a low molecular weight polymer with high salt-solvating power, sufficient mobility of ionic conduction and reduction in crystalline nature of the polymer matrix as main features [30, 31]. Plasticizers are additives that increase the fluidity of the host material in which these are added. It is to be noted here that the addition of plasticizer does not supply ions to the system; but instead it dissolves enough charge carriers and provides a more mobile medium for the ions. Thus, plasticizer contributes to conductivity enhancement by opening up narrow rivulets of plasticizer-rich phases for ionic transport. In general, the addition of plasticizer enhances the conductivity of polymer electrolytes (i) by increasing the amorphousity of polymer electrolytes; (ii) by dissociation of ion aggregates and (iii) lowers the glass transition temperature  $T_g$  of the polymer electrolyte system [32]. Plasticization of polymer, on one hand, generally enhances the electrical properties however; on the other hand, it may lead to decrease in mechanical, thermal, electrical and electrochemical stabilities.

Small working voltage range, narrow electrochemical window, high vapor

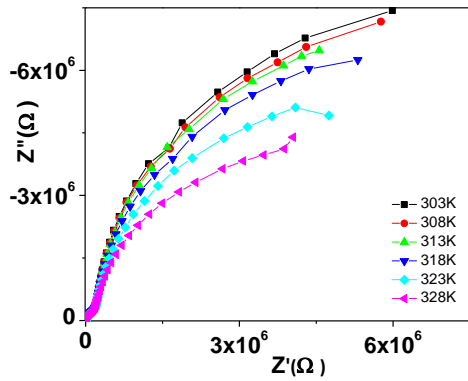


$T < T_m$

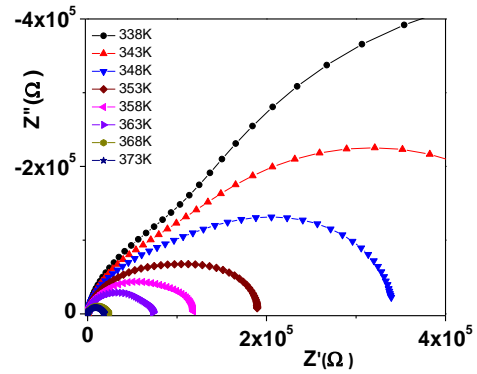


$T > T_m$

**Fig. 5.10** Impedance plot for PPSP-10 polymer film.

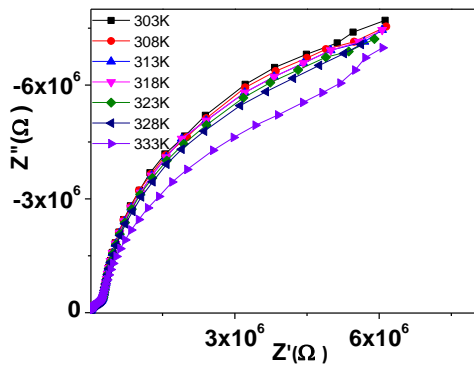


$T < T_m$

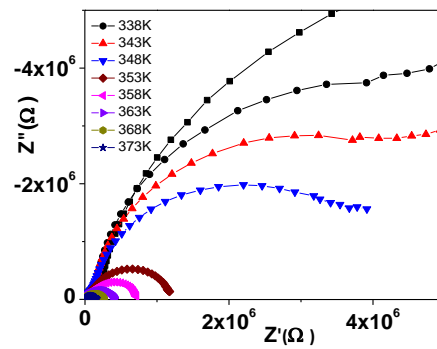


$T > T_m$

**Fig. 5.11** Impedance plot for PPSP-12 polymer film.



$T < T_m$



$T > T_m$

**Fig. 5.12** Impedance plot for PPSP-15 polymer film.

pressure and poor interfacial stability with electrodes are the disadvantages of plasticized-gel polymer electrolytes [33, 34]. The impedance plots at various temperatures for PEO-PMMA-AgNO<sub>3</sub>-PEG polymer electrolytes i.e.; PPSP system are obtained (Fig.5.10 to Fig. 5.12) and equivalent-circuit fitted (Fig. 5.13). The impedance plots in this PPSP-system are depressed semicircles which is a general feature occur in solid electrolytes. The obtained depressed semicircles indicate distribution of relaxation times [16]. With the rise of temperature, the radius of the semicircle reduces. This implies a reduction in bulk resistance values with increase in temperature. A sharp decrease in bulk resistance value near the 333K is observed which is attributed to the melting of crystalline PEO in polymer complex. Fig. 5.14 shows the impedance plot of PPSP-system for different PEG concentrations. The impedance plots do not show any systematic change with PEG concentration, though the bulk resistance value for the polymer film with PEG-5 wt% is found to be lowest.

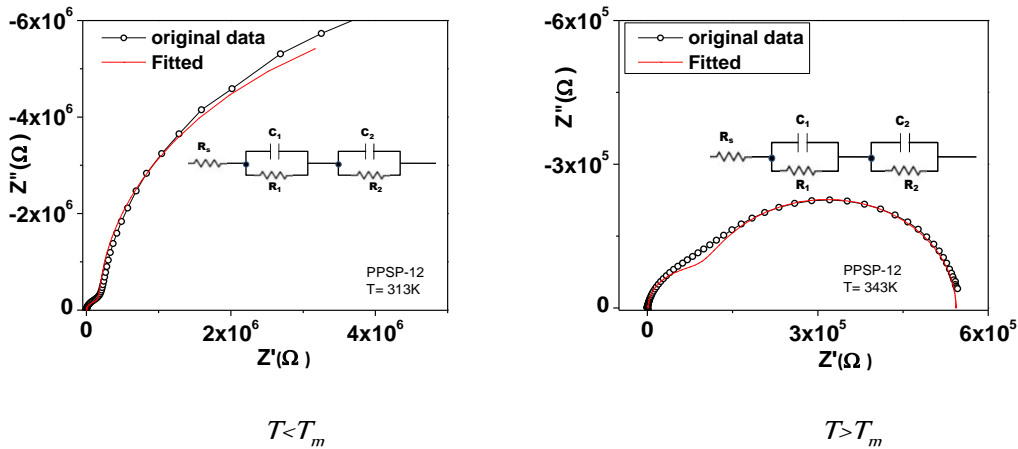


**Fig. 5.13** Equivalent-circuit fitting of impedance plot for PPSP-12 sample at 313 and 343 K .

The conductivity isotherms as a function of PEG concentration (PPSP system) are presented in Fig.5.15. In PEO-PMMA-AgNO<sub>3</sub>-PEG polymer matrix (PPSP-system), polyethylene glycol (PEG) has been varied from 5 to 15wt%. PEG is supposed to be a

soft PEO polymer with similar structure as PEO and having low molecular weight with lower dielectric constant. In PEO-PMMA-PEG polymer blend system, due to similar structure of PEO and PEG which promoted the organization of segmental units [35]. The decrease in the conductivity due to the addition of PEG in the polymer blend

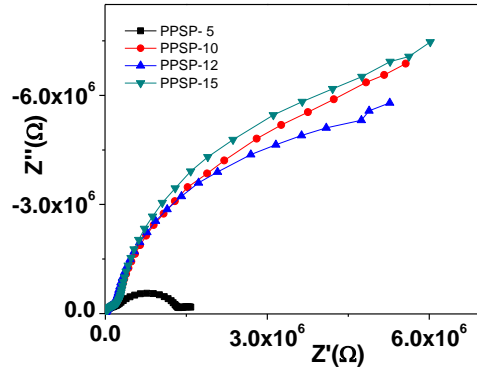


Fig.5.14 Impedance plot of PPSP (second) system.

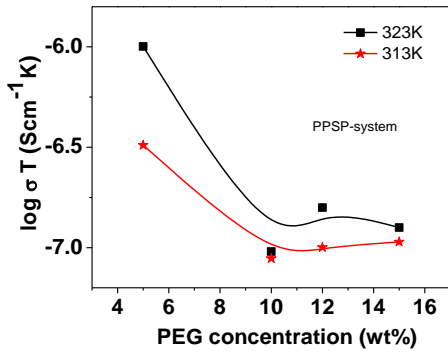


Fig.5.15 Variation of ionic conductivity with PEG concentration.

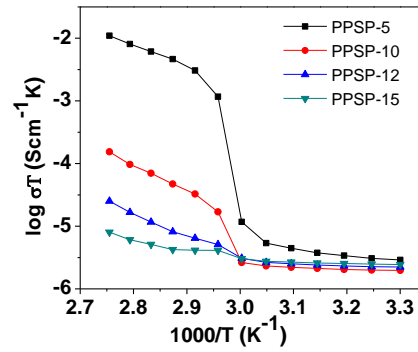


Fig.5.16 Logarithmic of ionic conductivity vs.  $1000/T$  plot.

system could be ascribed to the dielectric constant of the plasticizer, which played an important role in the modification of the conductivity of the polymer electrolytes. The differences of dielectric constant can cause the possibility of chemical interaction; thus, the chemical bonds and linkages in the polymer complex were expected to be affected by the addition of the PEG plasticizer.

The dielectric constant of PEG is smaller than that of PEO. The low dielectric

constant of PEG arises from the high ratio of alkyl segments and a strong crystallization correlated with the high organization and rigidity of segmental units in PEO. After PEG-5wt% concentration in PEO-PMMA polymer blends, the crystalline phase of the polymer blend increases and is supported by IR studies (In Chapter 4). Kumar and Sekhon [36] have suggested that polymer-polymer and/or polymer-plasticizer interactions depend on the molecular weight of plasticizer and polymer. The higher value of the dielectric constant of plasticizer helps in the dissociation of salt and ion aggregates. The ionic conductivity behavior of PEO-AgCF<sub>3</sub>SO<sub>3</sub>-PEG-SiO<sub>2</sub> system (plasticized polymer system) is reported to depend on the structure, molecular weight, viscosity and dielectric constant of plasticizer, polymer-plasticizer interaction, and ion-plasticizer coordination [35]. In general, charge carriers (Ag<sup>+</sup>-ions) migrate through less viscous system due to plasticization effect which enhances the mobility of ions. Also, plasticizer occupies inter chains and intra-chains free volume by disrupting polymer-polymer interactions. In the present case, the used polymers are of approximately same molecular weights and the plasticizer PEG possesses a low dielectric constant than as that of PEO or PMMA.

The increase in degree of crystallinity beyond 5 wt% of PEG electrolyte films are in agreement with the results obtained from the increased value of  $T_m$  from DSC and higher intensive peaks observed in FTIR.

To investigate the temperature dependence of conduction mechanism in PPSP-system, the conductivity measured from impedance plot is shown in Fig.5.16. A sudden increase/transition in the conductivity near  $T_m$  is the main feature of the conductivity plots in this system. The non-linear nature of temperature dependent conductivity is generally observed for PEO based systems [37-39]. The observed rise in conductivity with

temperature can be explained on the basis of free volume model [40, 41] which explains that the coordination sites come closer due to increase in temperature enabling the ions to hop from the occupied site to the unoccupied site requiring lesser energy. Amplitude of vibration of the polymer backbone and side chains also supports in increase of the fraction of free volume in the polymer electrolytes. This facilitates ionic translational motion and/or hopping by the dynamical segmental motion of the polymer. And liquid like phase of PEO in PEO-PMMA polymer matrix due to melting near  $T_m$  increases larger segmental motion of polymer chains.

Further, the plasticization using ethylene carbonate (EC) plasticizer has been done in PEO-PMMA-AgNO<sub>3</sub> system. The impedance plots of polymer electrolyte films plasticized with various concentrations of EC are obtained. Figs.5.17- 5.19 show the impedance plots PPSE-5, PPSE-7 and PPSE-15 at different temperatures and Fig.5.20 depicts equivalent-circuit (inset of Fig) fitted impedance curve for PPSE-15 polymer film at 313 and 323K. These curves show depressed semicircular arcs followed by a spur at low frequencies. The spur indicates the presence of the interfacial polarization. It can be observed that the size of the arcs reduces with temperature which implies that the bulk resistance decreases with increase of temperature. Fig.5.21 depicts the impedance plot obtained for different EC concentrations at 323K which shows that the bulk resistance value increases with the increase in EC concentration up to 10wt% and after that a decrease in bulk resistance is observed.

The ionic conductivity plot for the PPSE system i.e., PEO-PMMA-AgNO<sub>3</sub> system with varying amount of EC is given in Fig.5.22. It is observed from figure that conductivity initially drops at 7wt% and thereafter it increases non-linearly with addition

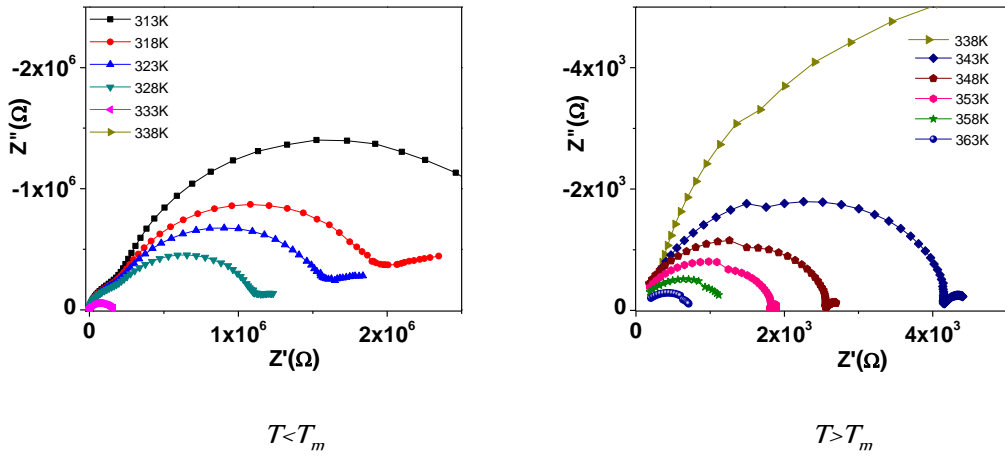


Fig..5.17  $Z'$  vs.  $Z''$  plot for PPSE-5 polymer film.

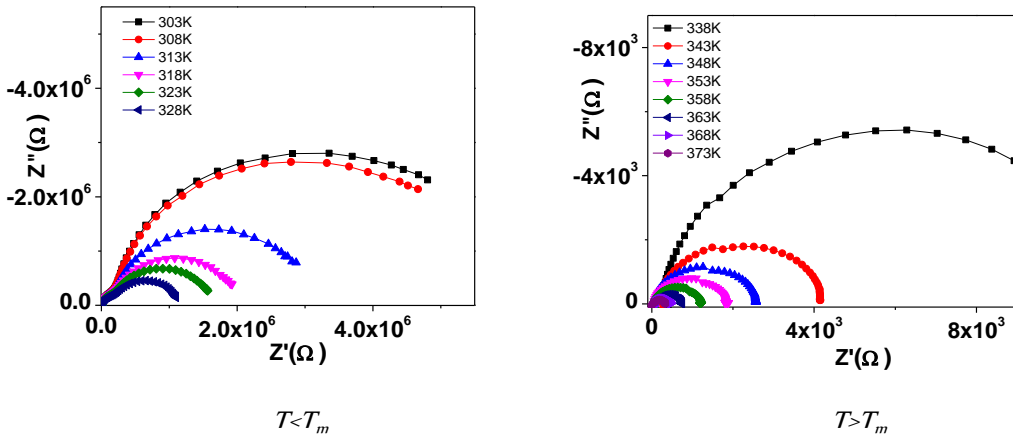


Fig..5.18  $Z'$  vs.  $Z''$  plot for PPSE-7 polymer film.

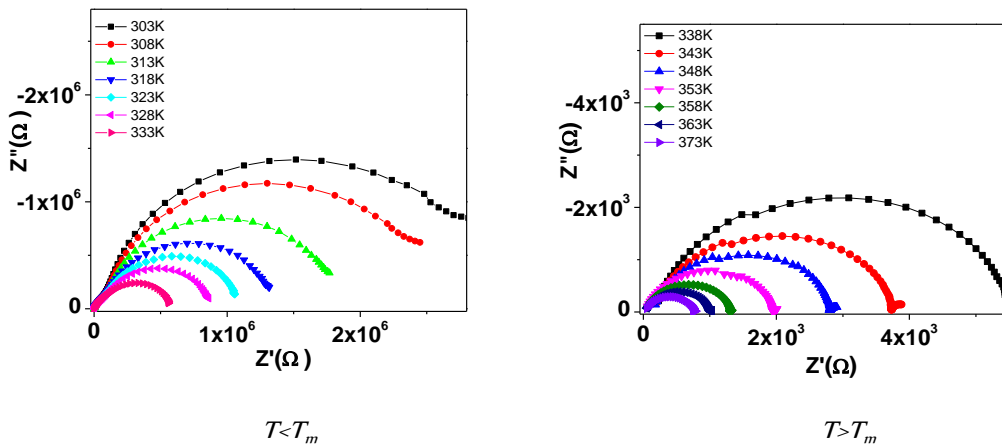


Fig..5.19  $Z'$  vs.  $Z''$  plot for PPSE-15 polymer film.

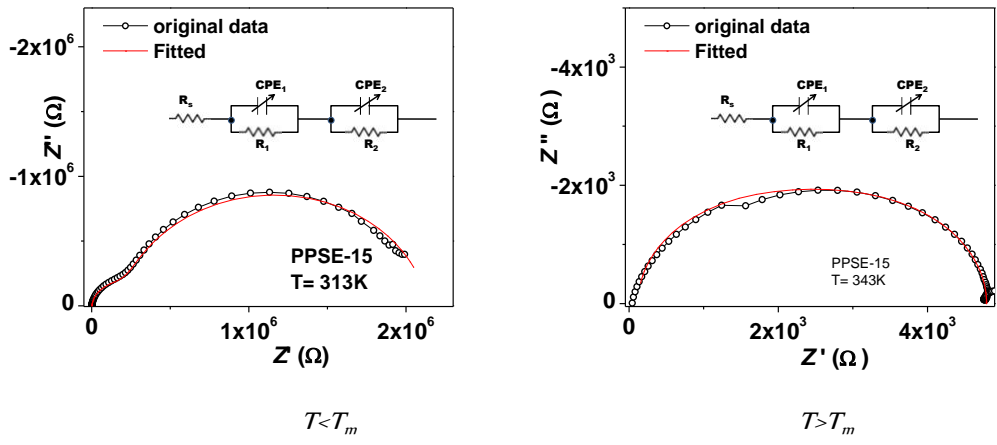


Fig. 5.20 Equivalent-circuit fitting for PPSE-15 sample at 313 and 343 K .

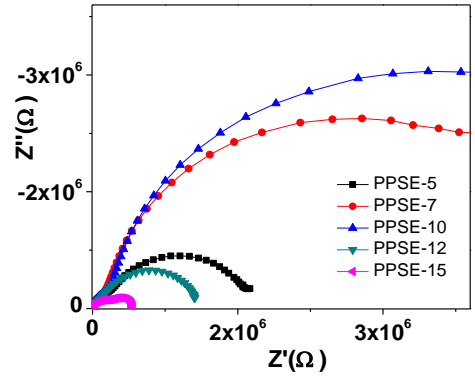


Fig. 5.21 Z' vs. Z'' plot for all samples of PPSE series and 323K.

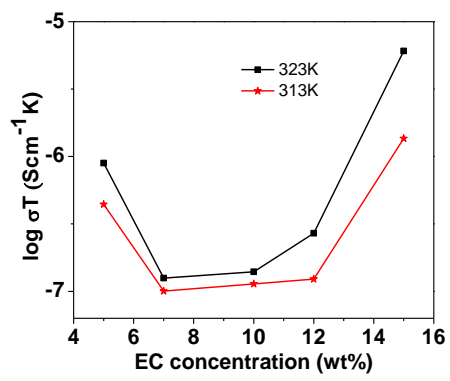


Fig.5.22 Compositional variation of ionic conductivity PPSE system.

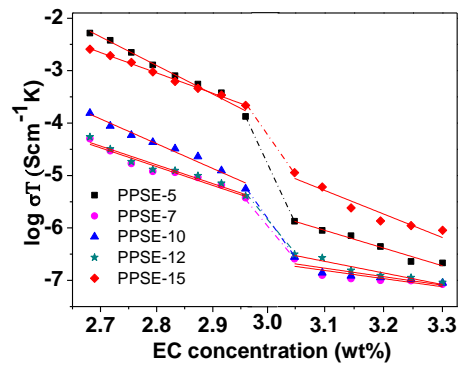
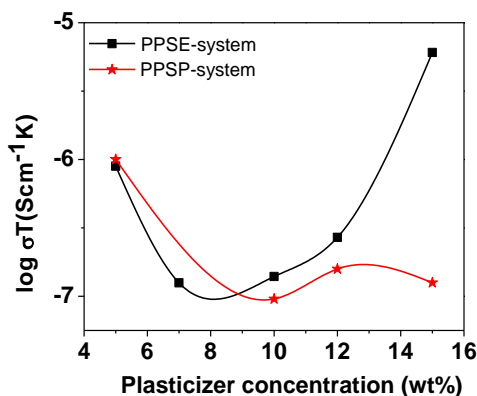


Fig.5.23 Temperature dependence of ionic conductivity.

of EC. The lowest conductivity in EC-7wt% is due to the increased degree of crystallinity as supported by its XRD and DSC studies. Generally, the plasticizer concentration in polymer complexes reduces the inter-ion Coulomb interactions and dissociates more salt content to make more number of cations available for conduction [36]. The addition of plasticizer has been found to lower the melting temperature,  $T_m$  as well as increases the amorphous level of polymer blend system.



**Fig. 5.24** Variation of ionic conductivity for plasticizer concentration in PEO-PMMA polymer blends system.

H.J. Rhoo *et. al.*[42] argued the opening of the narrow rivulets of plasticizer-rich phase and large free volume for higher conductivity. The increase in conductivity after 7 wt% of EC for PPSE-system may be ascribed to the dissociation of more salt supporting the enhancement in conductivity. Huang *et. al.*[43] described the presence of plasticizer as a lubricant in a polymer which makes the ions more mobile within the polymer system. Fig.5.23 shows the temperature dependence of ionic conductivity for PPSE system. The ionic conductivity of plasticized polymer with EC in blend complex increases with the temperature. Figure shows a sudden and/or sharp rise in conductivity near  $T_m$  which is ascribed due to the softening of PEO polymer near  $T_m$  in the polymer complexes and has been reported by several workers [17-19, 37-39]. For comparison, the variation of conductivity for both the plasticizers PEG and EC is shown in Fig.5.24 at

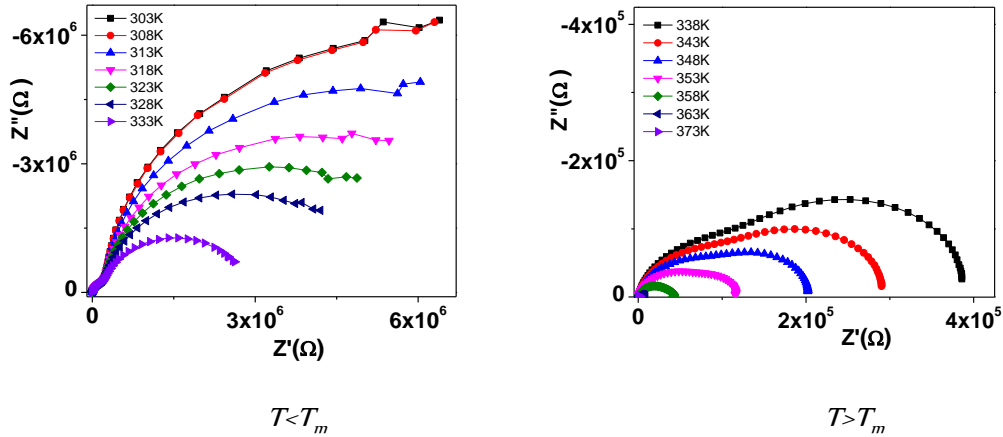


Fig. 5.25 Impedance plot for PPSPA-1 polymer electrolyte film.

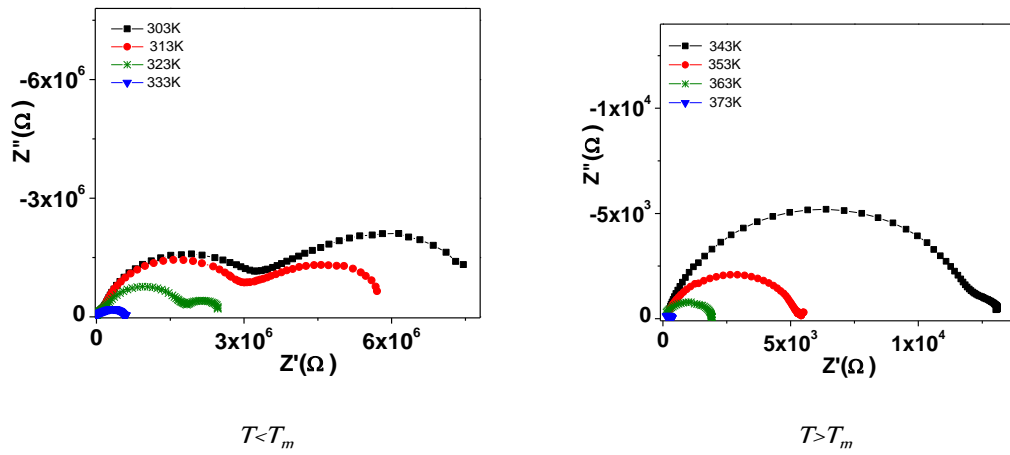


Fig. 5.26 Impedance plot for PPSPA-2 polymer electrolyte film.

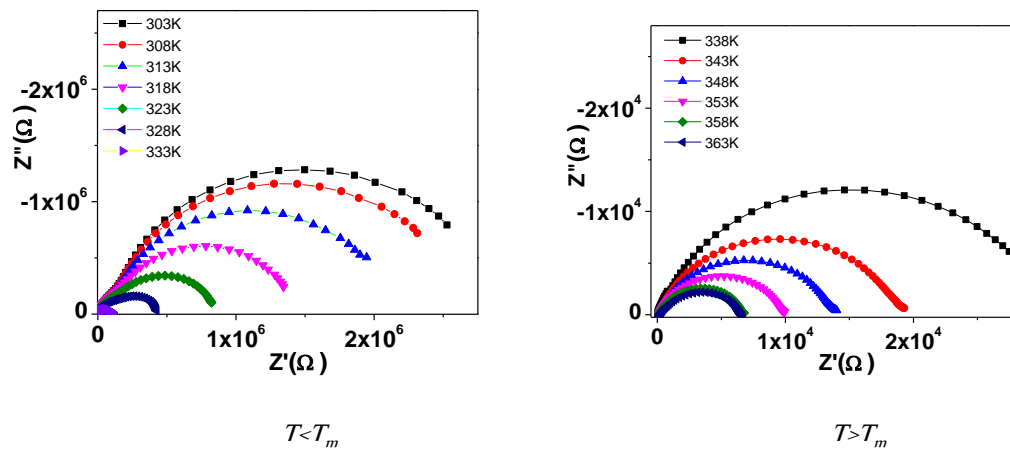


Fig. 5.27 Impedance plot for PPSPA-3 polymer electrolyte film.

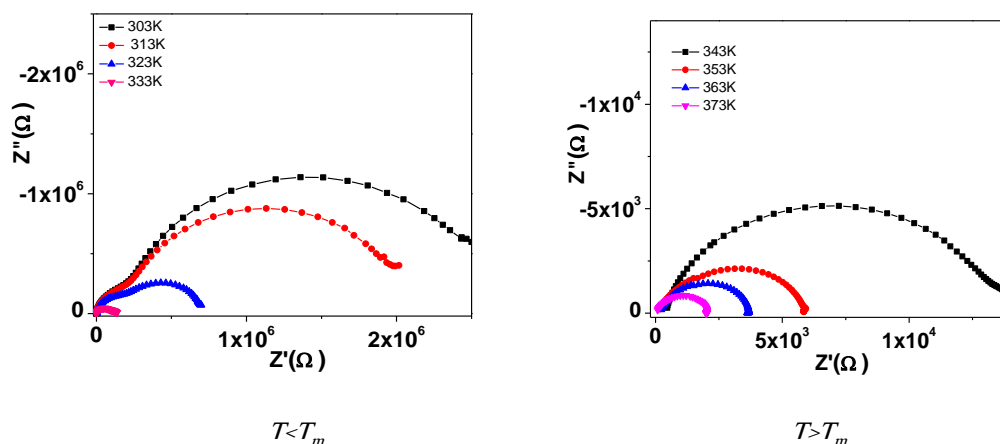


Fig. 5.28 Impedance plot for PPSPA-4 polymer electrolyte film.

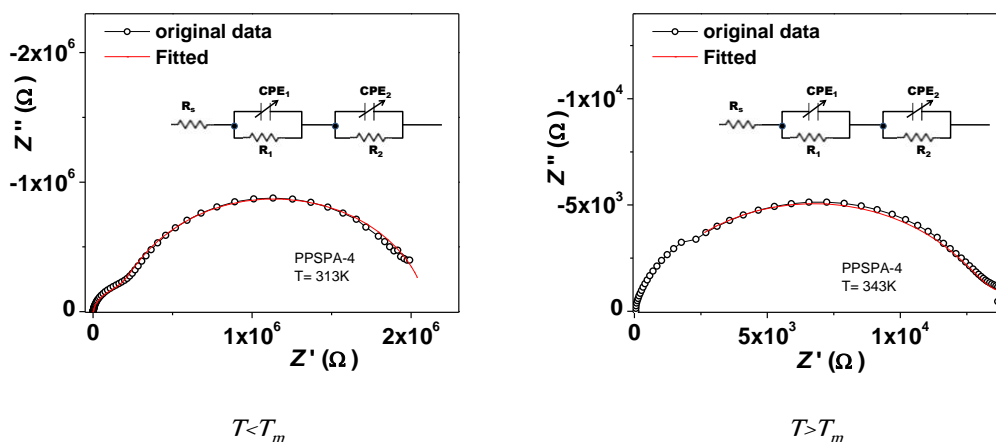


Fig. 5.29 Equivalent-circuit fitting of impedance plot for PPSPA-4 sample at 313(left) and 343 K (right).

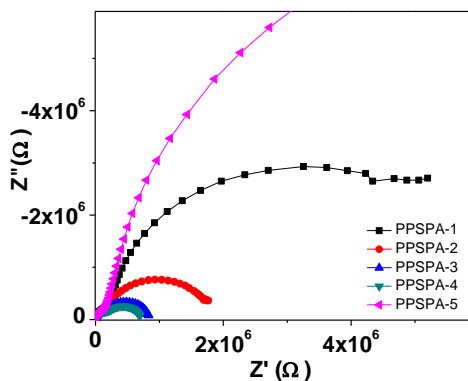


Fig. 5.30 Impedance plot for all PPSPA samples at 323K.

323K. The conductivity is nearly same at 5 wt% of both plasticizers. The minimum conductivity is observed at 7 wt% in EC system whereas at 10wt% for PEG. An increase in conductivity beyond minima is observed only in EC based electrolyte system.

The variation of conductivity with nano-filler concentration is an important feature in polymer composites. The presence of nano-filler is expected to favor additional transient sites for ion migration and also to promote amorphous phase in polymer that allows polymer chains to be more dynamic, thus providing favorable conducting pathways for charge carriers [44]. The effect of dispersion of nano-filler in the highest conducting plasticized polymer films is undertaken. The amount of nano-filler from 1 to 5wt% is varied in PPSP and PPSE systems.

The impedance plots of the polymer nano-composites plasticized with PEG (i.e.; PPSPA- polymer electrolyte system) with the nano-filler ( $\text{Al}_2\text{O}_3$ ) concentration are obtained and analyzed at different temperatures. Impedance plots of plasticized polymer electrolyte films with  $\text{Al}_2\text{O}_3$ -from 1wt% to 4wt% nano-filler concentration are shown in Figs.5.25-5.28 and fitted impedance plot is shown in Fig. 5.29. Impedance spectra in these polymer nano-composites show two semicircles namely; one at high frequency and other at low frequency region. As temperature approaches  $T_m$ , the impedance spectra shows only single semicircle and the intercept of real axis shifts towards origin, i.e.; bulk resistance value decreases in solid electrolytes. Impedance plot obtained for different amount of nano fillers at 323K is shown in Fig. 5.30. The bulk resistance decreases with the nano-filler concentration in the system as is evident from the shifting of the intercept towards origin. However, polymer electrolyte film with 5 wt% of  $\text{Al}_2\text{O}_3$  shows a reverse effect.

Fig.5.31 represents the variation of ionic conductivity with nano-filler concentration in this PPSPA system at 323K. The ionic conductivity increases with the addition of nano-filler  $\text{Al}_2\text{O}_3$  upto 4 wt%. The addition of nano-filler in the polymer system increases the flexibility with an enhanced level of amorphousness (observed from XRD and DSC studies). Ekanayake *et al.* [45] and others [46-48] reported the increased ionic conductivity due to creation of more conducting pathways for the migration of ions with the addition of nano-fillers. Johan *et al.* [49] reasoned the enhancement in conductivity due to increase in the amorphous phase with CuO nano-filler. Wieczorek *et al.* [46] suggested that migrating ionic species interact with O-OH surface groups on alumina grains of nano filler which provide transient hopping sites and conducting pathways for migrating ions.

In the present system, however, the favorable high conducting pathways for silver ions, created by alumina nano-filler grains, may be responsible for rise in ionic conductivity. The retarding effect in conductivity after 4wt% of  $\text{Al}_2\text{O}_3$  nano-filler is attributed to the conglomeration of excessive nano-filler reaching a threshold which makes the long polymer chains immobilized leading to a decrease in the conducting pathways. This maximum shows the balance between the opposing forces: increase in free volume as well as chain flexibility and decreasing polymer segmental mobility. The results from characterization are also in good agreement with the results which support the drop in conductivity at 5 wt%. Temperature dependence of ionic conductivity for PPSPA-system is shown in Fig. 5.32. Figure shows the variation of the logarithm of ionic conductivity with inverse absolute temperature for various concentrations of nano-fillers. Similar to earlier-systems, this system shows two regions in temperature dependent

conductivity. It is observed that within the investigated temperature range, ionic conductivity increases with increasing temperature as suggested by free volume theory [20]. With the increase in temperature, the polymer matrix can expand easily and produce free volume in which ions, solvated molecules or polymer segments can move. This enhances the motion of  $\text{Ag}^+$ -ion as well as polymer segmental mobility resulting in increase in ionic conductivity. The sudden rise in conductivity is attributed to the melting of PEO in host PEO-PMMA polymer matrix.

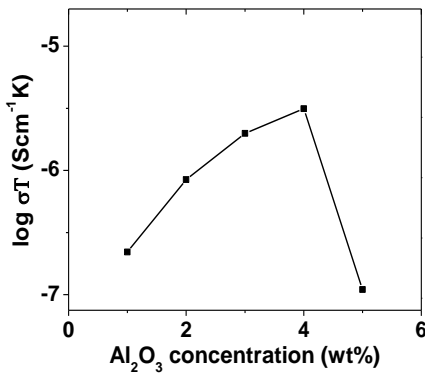


**Fig.5.31** Variation of ionic conductivity with nano-filler ( $\text{Al}_2\text{O}_3$ ) concentration in PPSPA system at 323K.

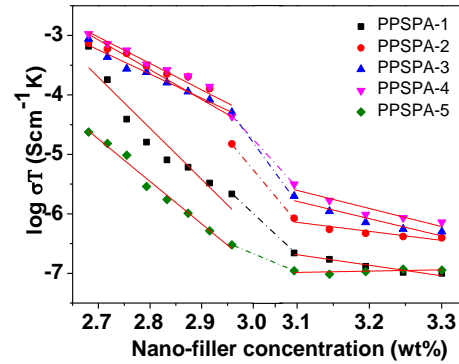


**Fig.5.32** Temperature dependent variation of ionic conductivity

To understand the effect of nano-filler concentration in polymer blend system plasticized with EC, the impedance plots of polymer electrolyte with different concentration of nano-filler  $\text{Al}_2\text{O}_3$  in PPSE-system at different temperatures is studied. Impedance spectra of PPSEA-2, PPSEA-4 and PPSEA-5 polymer electrolyte films at different temperatures are shown in Figs. 5.33-5.35, respectively and Fig. 5.36 shows the equivalent-circuit fitted curves for PPSEA-2. Impedance plots show the presence of two semicircles and as temperature approaches  $T_m$  of PEO, the second semicircle at lower frequencies gradually disappears and the bulk resistance decreases with increase of temperature with a transition near the melting temperature of PEO as observed in other

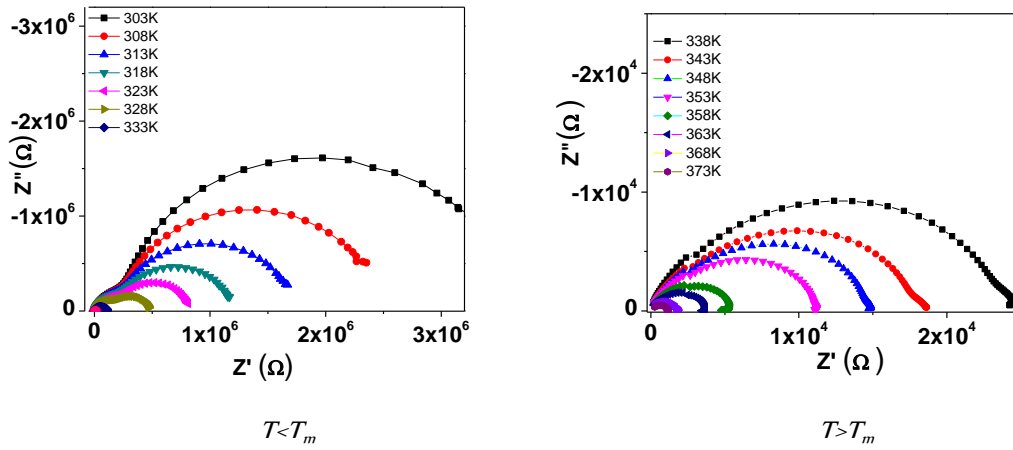


Fig. 5.33 Impedance plot for PPSEA-2 sample.

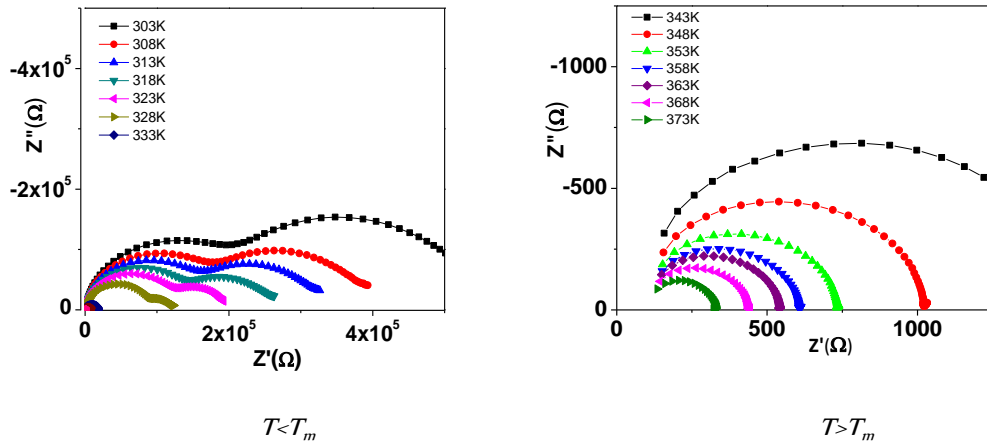


Fig. 5.34 Impedance plot for PPSEA-4 sample.

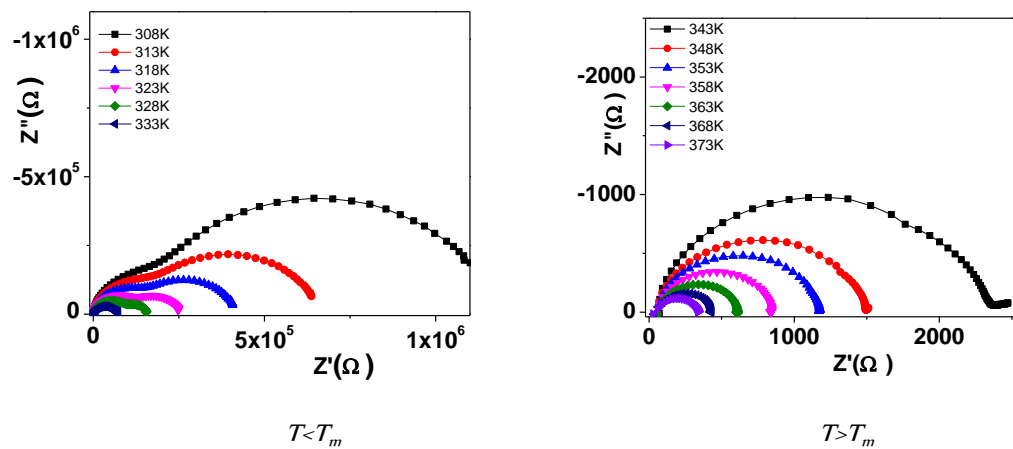


Fig. 5.35 Impedance plot for PPSEA-5 sample.

systems also. Fig.5.37 depicts the impedance plot for different nano filler amounts obtained at 323K. The bulk resistance value decreases up to 4wt% of nano-filler concentration. However, in the polymer film with 5 wt%  $\text{Al}_2\text{O}_3$ , the  $R_b$  value increases.

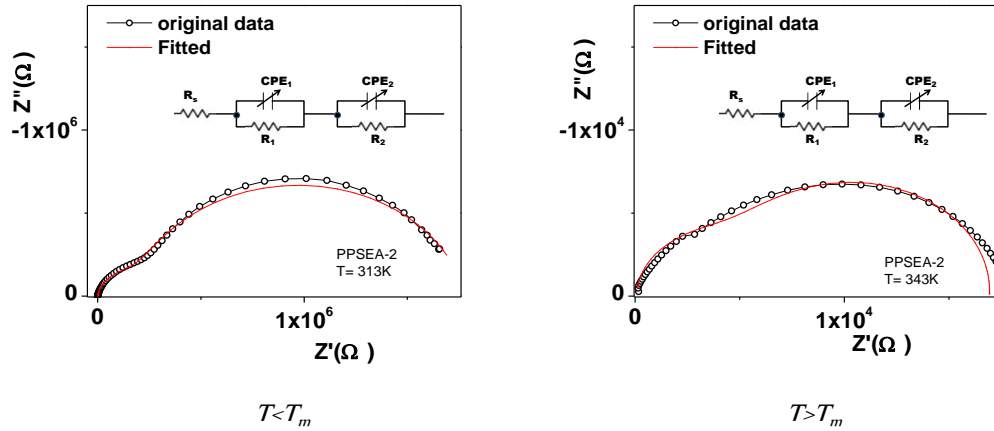


Fig. 5.36 Equivalent-circuit fitting for PPSEA-2 polymer film at 313 and 343 K .

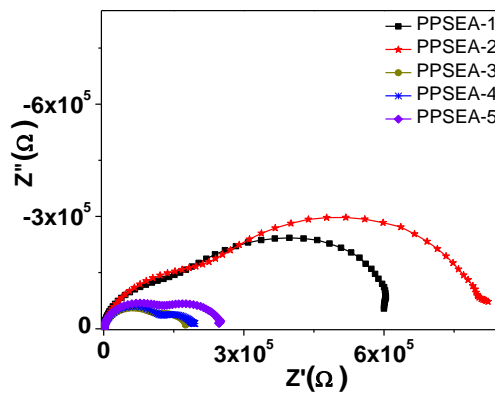
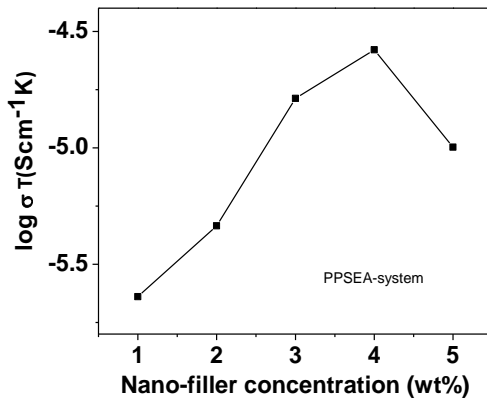


Fig. 5.37 Compositional impedance plot for PPSEA series (fifth series).

In general, the ionic conductivity increases as the degree of crystallinity decreases. The increase in ionic conductivity with nano-filler concentration is an indication of enrichment of amorphous phase as discussed above. The ionic conductivity in this system is shown in Fig.5.38. This system shows an enhancement in ionic conductivity with nano-filler concentration up to 4wt% and further addition in nano-filler

concentration results a drop in conductivity as was seen in PEG based system. The observed fall in conductivity at 5wt% of  $\text{Al}_2\text{O}_3$  concentration is attributed to the conglomeration of nano-filler which make the long polymer chains more immobilized obstructing the migration of ions and provide a threshold value for the present system. A recent work by M.R. Johan *et. al.* [52] has also reported the drop in conductivity due to the aggregation of nano-filler in the polymer. Within investigated temperature range, the enhancement in ionic conductivity with temperature shows two regions as observed in other studied systems. Polymer matrix can expand easily and produce free volume due to rise in temperature [53].



**Fig. 5.38** Compositional variation of ionic conductivity with nano-filler.

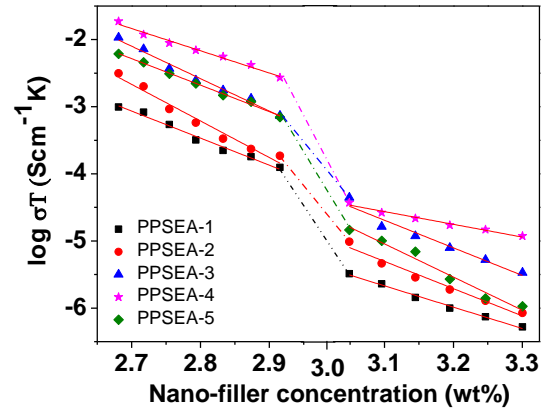


**Fig. 5.39** Temperature wise variation of ionic conductivity.

Fig.5.39 depicts the temperature dependent ionic conductivity for PPSEA-system. The conductivity of PEG and EC based nano-composites can be summarized in Fig.5.40. The conductivity of EC based plasticized polymer electrolyte system is higher (nearly more than one order of magnitude) than the conductivity of PEG based polymer nano-composite system below melting temperature  $T_m$  and 2 to 3 order higher for EC based

system above  $T_m$ .

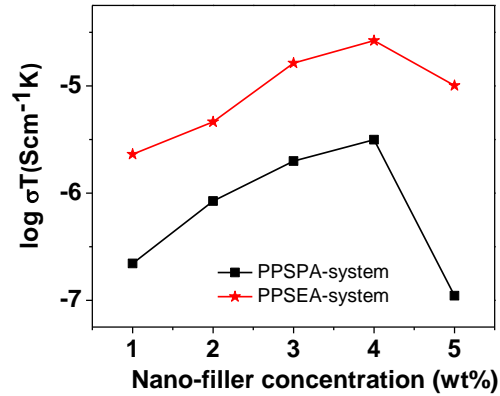


**Fig. 5.40** Conductivity as a function of nano-filler concentration for PPSPA and PPSEA systems at 323K.

### 5.3 Frequency dependent conductivity

The blending effect of PEO concentration with respect to PMMA in PEO-PMMA polymer blends in terms of frequency dependence of conductivity (or AC conductivity) at different temperatures is studied. Frequency dependent conductivity in the investigated temperature range shows two different features region-I and II (i.e.; below and above  $T_m$ ) in conductivity spectra in polymer blend electrolytes (Figs. 5.41 (a)-(d)). In region-I i.e., below  $T_m$ , the AC conductivity shows two dispersion frequencies: one at low frequencies and other at higher frequencies. In this region, with the rise in temperature, the observed low frequency dispersion gradually shifts towards high frequency side while the high frequency dispersion does not shift markedly with the increment in temperature. As temperature approaches near  $T_m$ , low frequency dispersion starts disappearing and a systematic shift of the dispersion frequency towards high frequency is observed in high frequency dispersion. The frequency dependence of conductivity is a sum of conductivity due to movement of free charges and polarization conductivity due to movement of bound charges ( $\sigma^* = \sigma_{\text{polarisation}} + \sigma_{\text{ion}}$ ) [54]. The conductivity value at low frequencies is

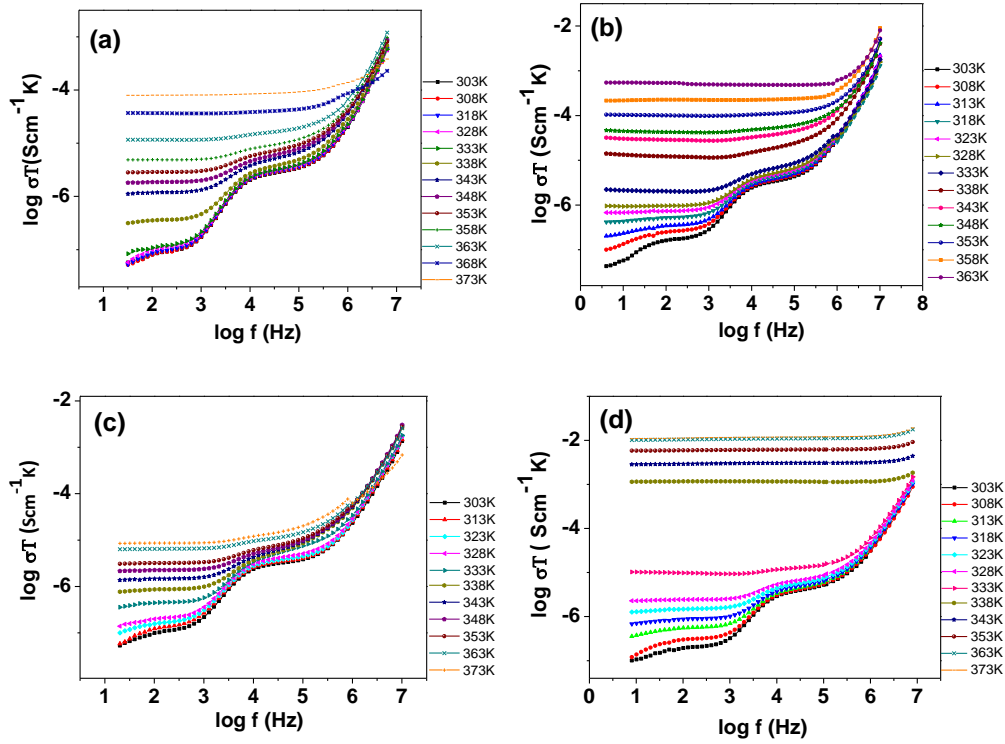


**Fig. 5.41** Conductivity spectra for (a) PPS-10, (b) PPS-30, (c) PPS-40 and (d) PPS-50 polymer samples of first series (PPS-system) at different temperatures.

related to the accumulation of ions due to the slow periodic reversal of the electric field.

In high frequency region, the conductivity sharply increases with frequency. The variation of conductivity with frequency in high frequency region is expressed by the well known power law of ac behavior [16, 54, -57] given by the following equation,

$$\sigma(\omega) = \sigma_0 + A\omega^n \quad \dots(5.1)$$

where  $\sigma(\omega)$  is the conductivity at a particular frequency,  $\sigma_0$  is the conductivity at low frequencies,  $A$  is a constant and  $n$  is the frequency exponent. The curves of best fits to Jonscher's Power law are shown in Fig. 5.42. The above expression is known as the *power law of ac behavior*. Because the power law of ac behavior is observed in wide range of materials, Jonscher called it "*Universal Behavior*" [9, 55, 56]. The frequency exponent  $n$  was calculated from the slope of the plot  $\log(\sigma' - \sigma_0)$  versus  $\log \omega$  (straight

line curve) and is a measure of degree of interaction with the environment. The exponent  $n$  values, in the range  $n < 1$ , indicates a preference on the part of ions that have hopped away to the site from where they started. It is documented that  $n$  can also hold values larger than one. Papathanassiou *et.al.* [58] suggested that there is no physical argument to restrict the value of  $n$  below one. Many researchers [59-61] have reported that  $n$  can have values  $0 < n < 2$ . The values of  $n \sim 0.5 - 1$  cover either ion conduction by translation motion or by displacive movement of caged ions while  $n \geq 1$  values may be attributed to other ion movements such as vibrational etc. The calculated values of  $n$  from eq. 5.1 for PPS-System at different temperatures are tabulated in Table.5.1. In the present case, the values of  $n$  are found to be greater than one.

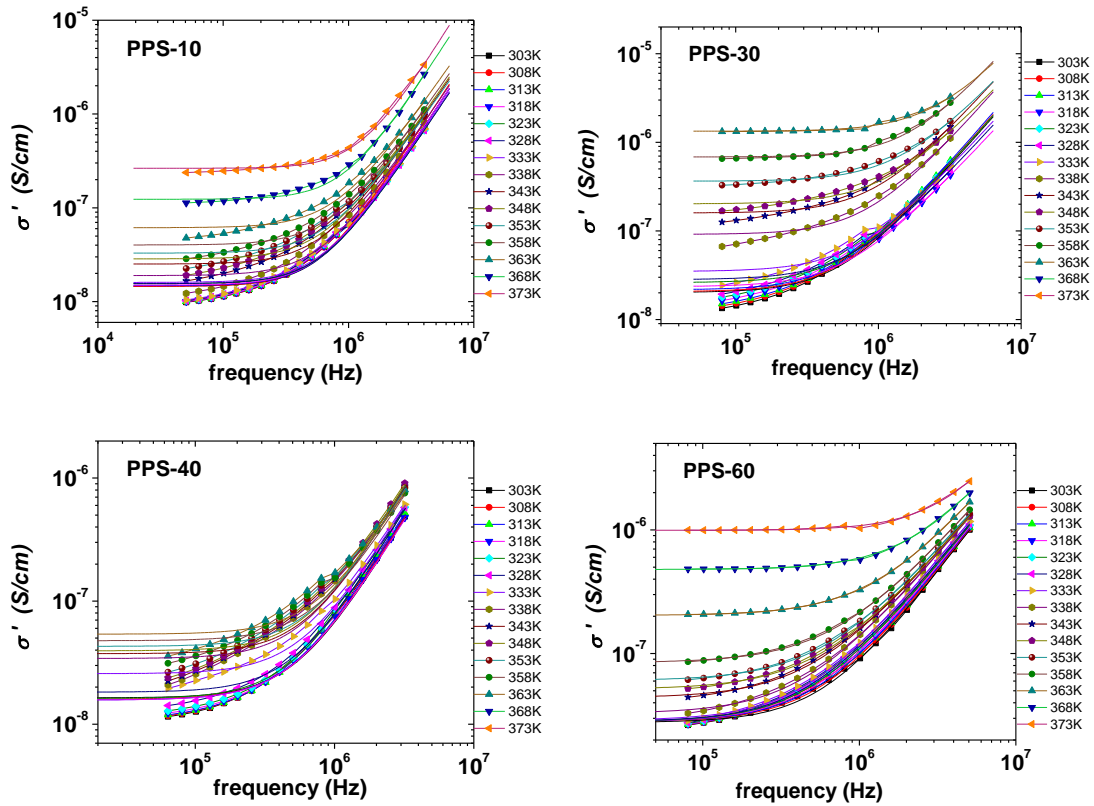


**Fig. 5.42** Fitting of conductivity spectra at different temperatures (the continuous lines are best fits to Jonscher's Power law).

All the samples show only 1-2 orders of magnitude rise in conductivity from region I to region II except for the samples with PEO- 30 and 50wt% possessing the highest conductivity, which have demonstrated the rise in conductivity of 3 and 5 orders of magnitude respectively.

The observed frequency dependence of conductivity below  $T_m$  is due to presence of semi-crystalline as well as due to the amorphous regions [62] present in PEO-PMMA host polymer matrix. As temperature approaches near  $T_m$ , the semi-crystalline region of PEO melts and the amorphous region preponderates in the PMMA matrix. Above  $T_m$ , i.e.; in region II, the melted PEO penetrates in the PMMA polymer matrix, making the overall polymer system, a gel-like system in which polymer chains acquire faster internal movement and segmental motion dominates, giving only a single dispersion in high frequency region.

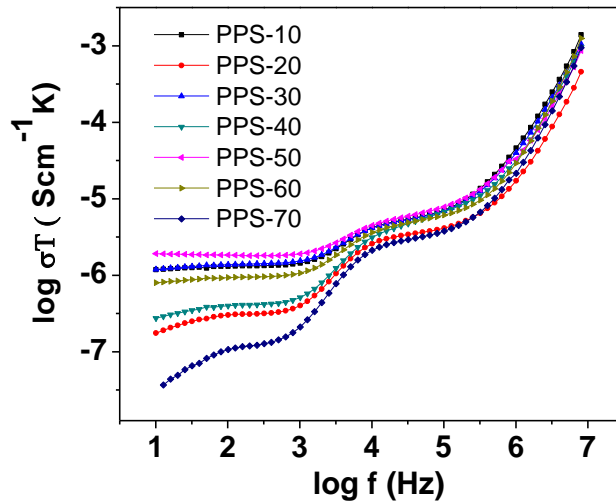


**Fig. 5.43** Conductivity spectra for all the samples of PPS system at 333K.

Such frequency dependent conductivity features are observed in all the polymer blend samples. The observed rise in conductivity with temperature can be explained on the basis of free volume theory [20] in which the system acquires more free space

allowing, in turn, easy ion transport. Low frequencies variation of conductivity is due to accumulation of charges at the electrode-electrolyte interfaces producing polarization effects [63]. The conductivity is almost independent of frequency in low frequency region. As frequency increases, the conductivity increases continuously because charge carriers get enough excitation energy from the electrical signal. At high frequencies, mobility of charge carriers,  $\text{Ag}^+$ -ions is high, the relaxation times decreases and hence conductivity rises. Frequency dependent conductivity spectra for all blended polymer electrolyte films of PPS-system at a 323K are shown in Fig.5.43.

It is clear that the ac conductivity  $\sigma_{ac}(\omega)$  for all the samples exhibit the same characteristics of the curve with increasing conductivity values with different PEO: PMMA ratios. PPS-50 composition, the highest conducting sample, is selected to investigate the effect of plasticizers PEG and EC in the blend.

Frequency dependence of conductivity at different temperatures for PEG system is studied. AC conductivity spectra for PPSP-12 and PPSP-15 samples are shown in Figs.5.44 (a) & (b), respectively. Temperature dependence of AC conductivity of polymer blends plasticized with PEG shows a frequency independent region at low frequencies below  $T_m$ . The transition from the slow change in conductivity to its abrupt increase in conductivity signifies the onset of conductivity relaxation due to dipolar motions caused by the segmental and normal-mode dynamics of the polymer host.

The conductivity value at low frequencies is related to the accumulation of ions due to the slow periodic reversal of the electric field and the ions travel much slower at lower frequency enabling ion to jump from one site to another vacant sites. With the rise in temperature, the dispersion region at low frequency below  $T_m$  gradually starts

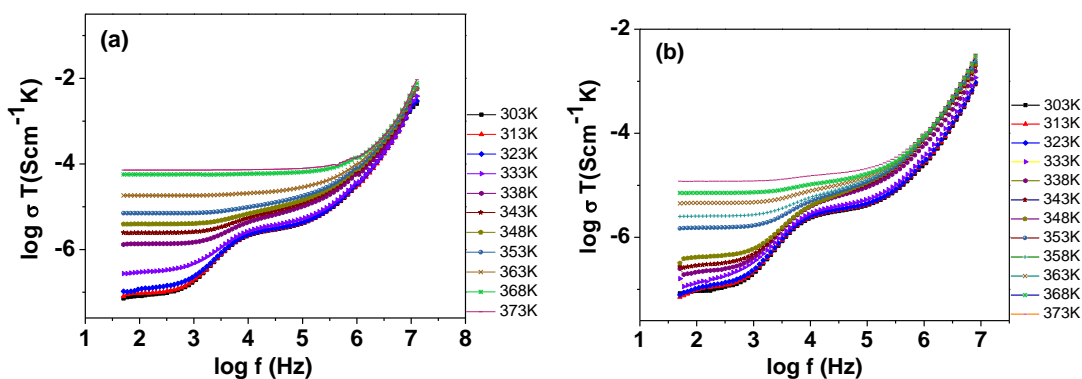


**Fig.5.44** Conductivity spectra at different temperatures for (a) PPSP-12 and (b) PPSP-15 samples of second series.

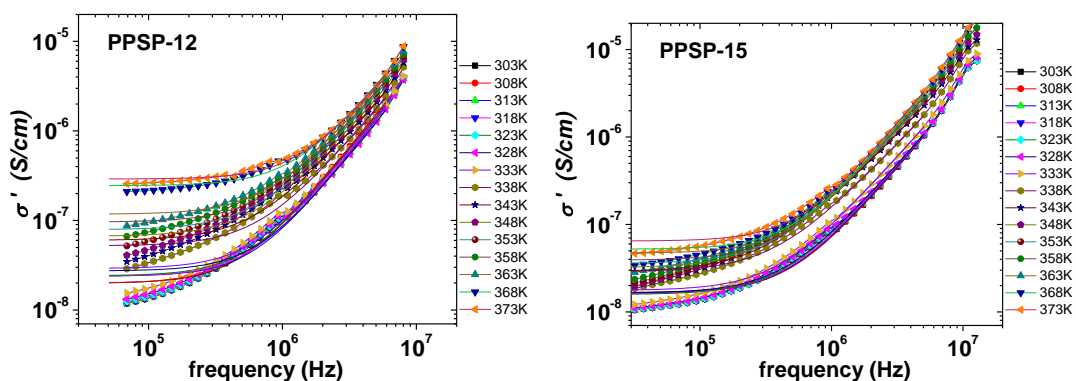


**Fig. 5.45** Fitting of conductivity spectra for PPSP-12 and PPSP-15 polymer films at different temperatures (the continuous lines are best fits to Jonscher's Power law).

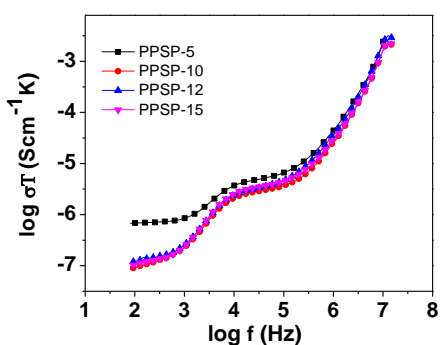


**Fig.5.46** Conductivity spectra all samples of PPSP system at 323 K.

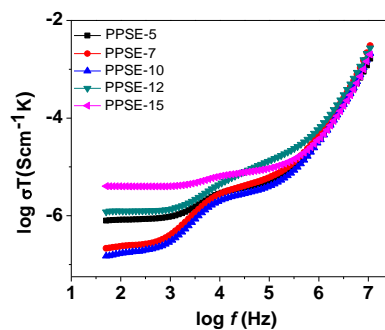


**Fig.5.47** Conductivity spectra for all samples of PPSE-system at 323 K.

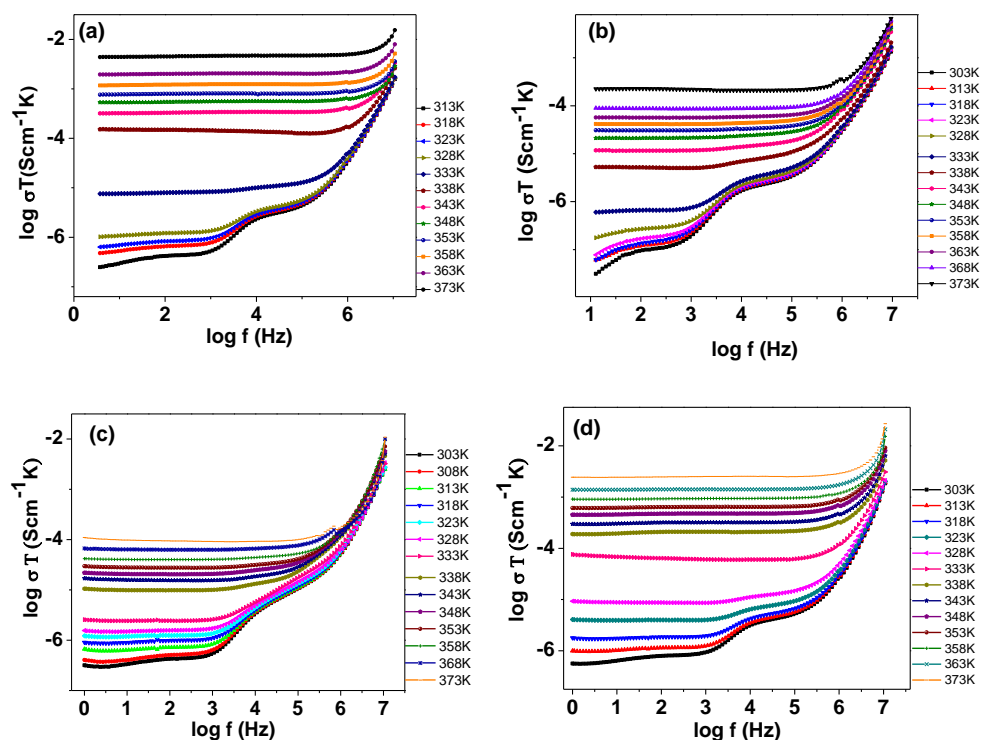


**Fig.5.48** Conductivity spectra for (a) PPSE-5, (b) PPSE-10, (c) PPSE-12 and (d) PPSE-15 polymer electrolyte films at different temperatures.

disappearing and dispersion at high frequency region shifts to higher frequency side. The curves of fitting of conductivity to *Jonscher's Power law* at high frequency for PPSP-12 and PPSP-15 samples are shown in Fig. 5.45. Here again, within the investigated temperature range, the ac conductivity is observed to increase more than two orders of magnitude in all samples while the highest conducting polymer sample (PEG 5wt %) shows rise of four orders of magnitude. AC conductivity spectra with PEG concentration at 323K is shown in Fig.5.46. The sample with 5 wt% PEG depicts the highest conductivity at all frequencies.

The variation of AC conductivity with different concentrations of EC plasticizer at 323K is depicted in Fig.5.47. AC conductivity values are higher in the polymer films

with EC-5wt% and 15 wt%. Figs.5.48 (a)-(d) represents the temperature dependence of AC conductivity spectra of different EC polymer films and Figs. 5.49 (a)-(d) show the *Jonscher's Power law* fitted curves. AC conductivity shows two dispersion regions; one in low frequency region and other in high frequency region. Dispersion in low frequency region starts disappearing near to melting temperature and only high frequency dispersion is seen in all samples. In the high frequency region, mobility of charge carriers is high near to relaxation times and hence, conductivity increases with frequency. The system with EC shows an enhancement in conductivity of nearly four orders of magnitude for highest conducting samples.

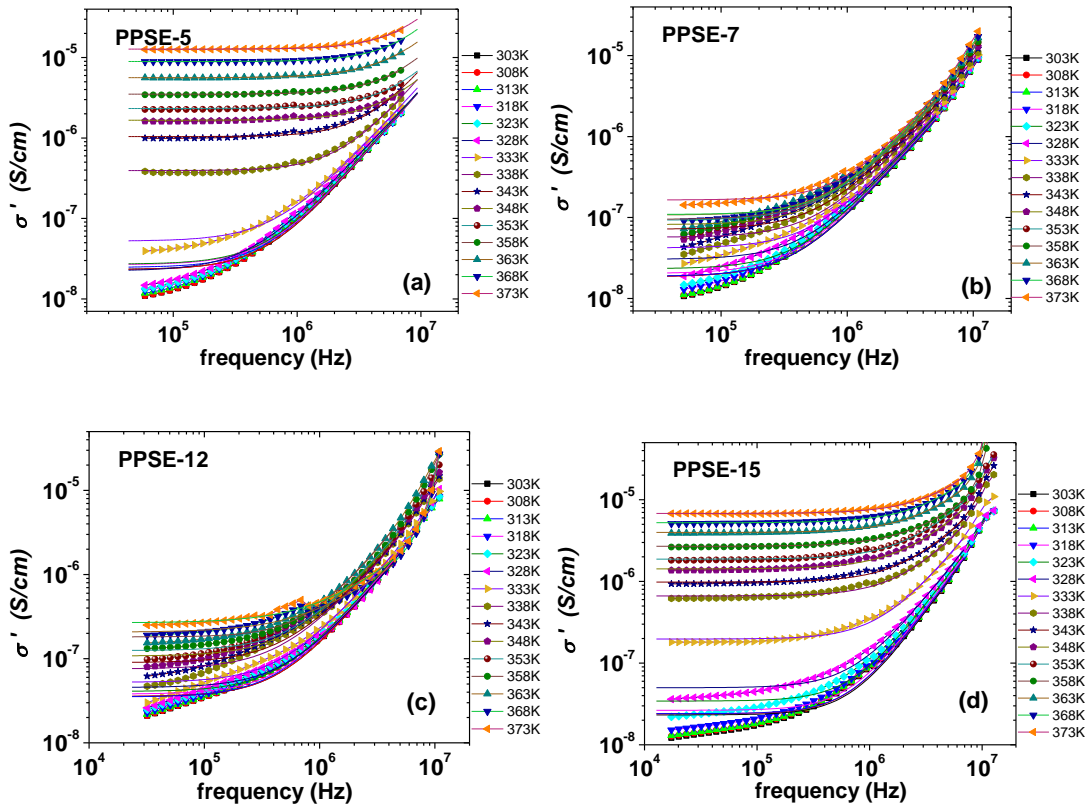


**Fig. 5.49** JPL fitting of conductivity spectra for (a) PPSE-5, (b) PPSE-7, (c) PPSE-12 and (d) PPSP-15 polymer films at different temperatures.

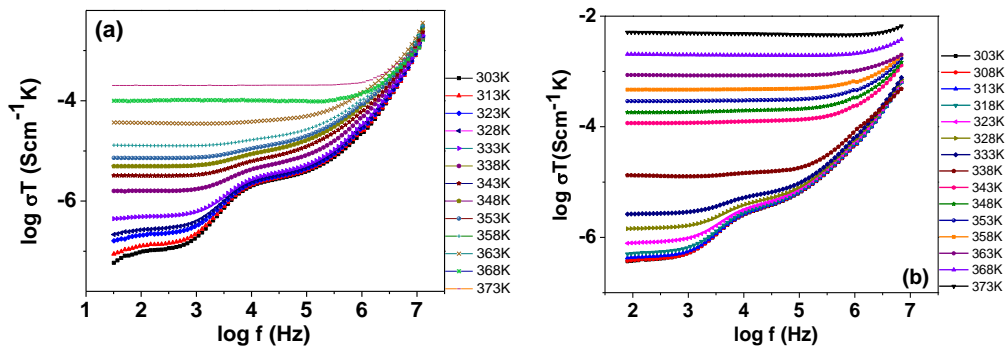


**Fig.5.50** Conductivity spectra for (a) PPSPA-1 and (b) PPSPA-2 polymer electrolyte films at different temperatures.

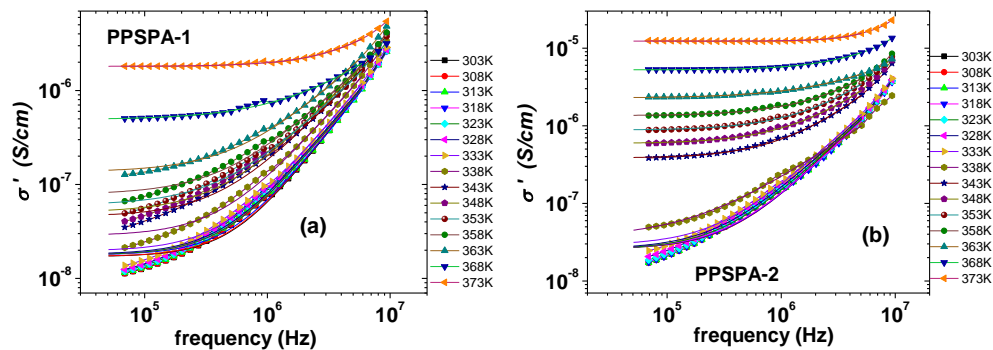


**Fig. 5.51** JPL fitting of conductivity spectra for (a) PPSPA-1 and (b) PPSPA-2 samples at different temperatures.

AC conductivity spectra of polymer nano-composite films plasticized with PEG (PPSPA systems) at different temperatures is studied and for PPSPA-1 and PPSPA-2 polymer films are represented in Figs.5.50 (a) & (b). The AC conductivity spectra for polymer electrolyte films show two regions below and above  $T_m$ . In all spectra, a frequency independent region at low frequency followed by two distinguishable dispersion regions in high frequency is observed. The observed frequency independent conductivity in low frequency region is attributed to electrode polarization which masks the ionic conduction of the bulk material. At higher frequencies, the mobility of charge carrier is high. AC conductivity increases with temperature and the relaxation frequency also shifts towards high frequency side. The observed frequency dispersion spectra are

fitted using *Jonscher's Power Law* and fitted curves are shown in Figs.5.51 (a) & (b).

The calculated values of power exponent  $n$  are tabulated in Table 5.1.

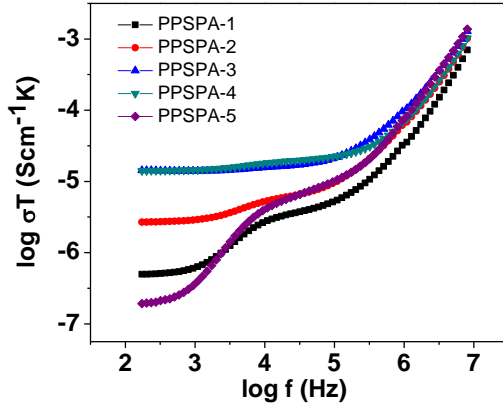


**Fig. 5.52** Conductivity spectra for all samples of PPSPA-system at 323K.

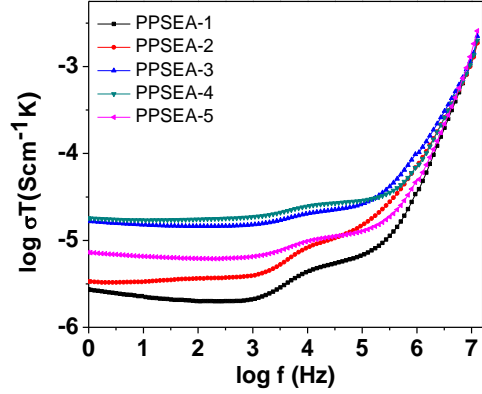


**Fig. 5.53** Conductivity spectra for PPSEA-system (fifth series) at 323K.

In nano-composite polymers with plasticizer, the increase in conductivity with temperature is discussed (Section 5.2) on the basis of free volume theory which favors the volume expansion with the rise in temperature. Near  $T_m$ , a sudden rise in ac conductivity is attributed to increase in mobility of  $\text{Ag}^+$  ions due to formation of additional amorphous regions. Conductivity enhancement in this system is of nearly three orders of magnitude within investigated temperature range. It is noticed that different concentration of nano-fillers in the present studies show similar trend with different values, however dominance of the double dispersion decreases with nano-filler concentration with a reverse effect at PPSPA-5 polymer film. Compositional variation of AC conductivity for the samples of PPSPA-system at 323K is given in Fig.5.52.

AC conductivity spectra for different compositions of  $\text{Al}_2\text{O}_3$  nano-filler in PEO-PMMA - $\text{AgNO}_3$ -EC polymer electrolyte (PPSEA-system in fifth series) at 323K is represented in Fig 5.53. The values of conductivity increase with nano-filler

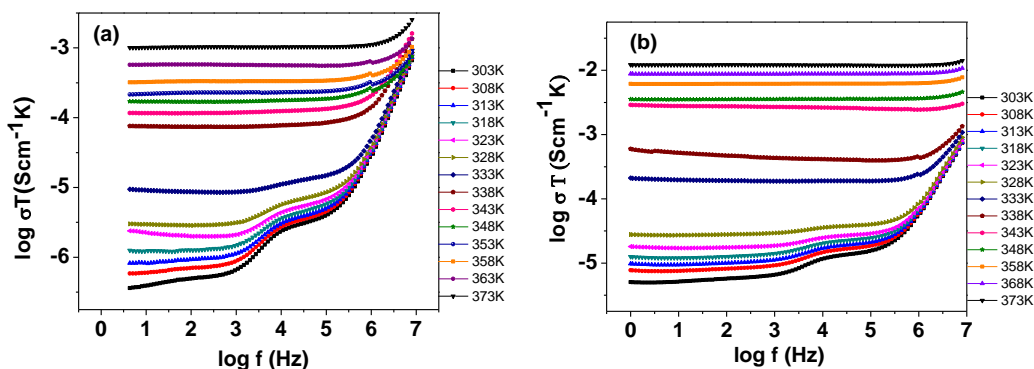


**Fig. 5.54** AC Conductivity spectra for (a) PPSEA-1 and (b) PPSEA-4 polymer electrolytes at different temperatures.

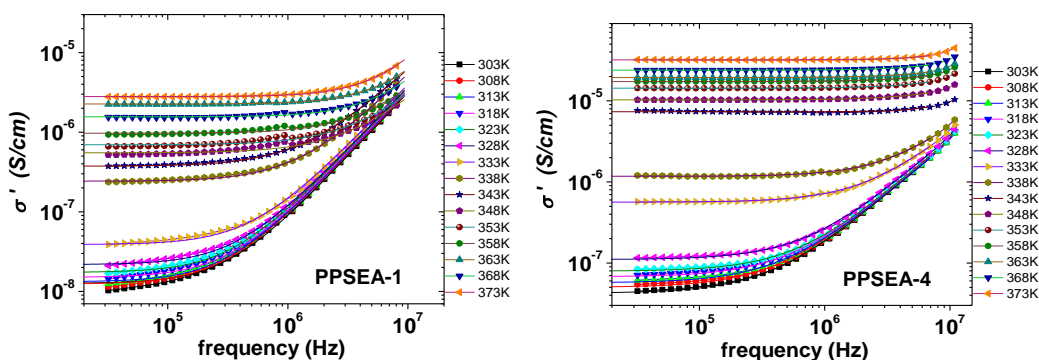


**Fig. 5.55** JPL fitting of conductivity spectra for (a) PPSEA-1 and (b) PPSEA-4 samples at different temperatures.

concentration as observed in ionic conductivity results. The lower frequency dispersion seems to disappear at a temperature which gradually decreases with the addition of  $\text{Al}_2\text{O}_3$ , indicating some structural change in the electrolyte samples. Figs. 5.54 (a) & (b) and Figs. 5.55 (a) & (b) show the frequency dependent (AC) conductivity behavior for PPSEA-1 and PPSEA-4 samples and their respective JPL fitted conductivity spectrum respectively. Double dispersions are observed in  $T < T_m$  temperature range in the ac conductivity spectra. With the increase in temperature, the dispersion frequency shifts towards high frequency side.

**Table 5.1** Frequency exponent 'n' values for PPS, PPSP, PPSE, PPSPA and PPSEA systems at 323K.

	<b>Sample name</b>	<b>n values</b>
<b>PPS-system</b>	PPS-10	1.4
	PPS-20	1.3
	PPS-30	1.1
	PPS-40	1.2
	PPS-50	1.3
	PPS-60	1.4
	PPS-70	1.3
<b>PPSP-System</b>	PPSP-5	1.3
	PPSP-10	1.3
	PPSP-12	1.5
	PPSP-15	1.4
<b>PPSE-System</b>	PPSE-5	1.2
	PPSE-7	1.2
	PPSE-10	1.4
	PPSE-12	1.1
	PPSE-15	1.2
<b>PPSPA-System</b>	PPSPA-1	1.1
	PPSPA-2	1.1
	PPSPA-3	1.1
	PPSPA-4	1.2
	PPSPA-5	1.4
<b>PPSEA-System</b>	PPSEA-1	1.5
	PPSEA-2	1.0
	PPSEA-3	1.5
	PPSEA-4	1.4
	PPSEA-5	1.3

## 5.4 Dielectric studies

Dielectric materials are understood as the materials in which electrostatic fields can persist for a long time. These materials offer a very high resistance to the passage of electric current under the action of the applied direct-current voltage. Materials are characterized by their dielectric response of either the bound or free charge. Generally, dielectric means insulator which has no free charge but produce change in electric field. Dielectrics are a class of materials that are poor conductors of electricity, in contrast to materials such as metals that are generally good electrical conductors [65].

In a dielectric substance, an electric field gives rise to no net flow of electric

charge because electrons are tightly held by individual atoms. However, when electric field is applied, nuclei are attracted to one side and the electron cloud to the other side. This process of alignment of dipoles is known as polarization. In addition to these dipoles, there may also be permanent dipoles in the crystal. The alignment of these dipoles may not give a zero dipole moment or a net dipole moment. The net dipole moment leads to certain characteristic properties to solids.

The dielectric constant is a measure of the influence of electric field on the capacitance of a condenser due to a particular dielectric material. It measures how well a material separates the plates in a capacitor and is defined as the ratio of the capacitance of a set of electrodes with the dielectric material between them to the capacitance of the same electrodes with vacuum between them.

Complex dielectric function,  $\epsilon^*$  of the materials dependent on frequency is given by  $\epsilon^* = \epsilon' - i\epsilon''$ .  $\epsilon^*$  reflects the molecular relaxation and transport processes of the material [8, 66, 67]. The real part of dielectric permittivity,  $\epsilon'$  has same significance as that of ordinary dielectric constant i.e.; it measures the elastically stored energy in the material during each cycle of applied alternating field and the energy returned to the field at the end of each cycle. The higher the value of  $\epsilon'$  the better is the electrical conductivity. When an electrical field is applied to a material, the dipoles in the material show the tendency to orient them in the direction of the applied field [67]. However, the mobilization of the dipole depends on the ductility of the materials. The imaginary part of dielectric permittivity,  $\epsilon''$  corresponds to the dielectric loss factor due to the conduction of ionic species in the material when an electrical field applied. At higher temperatures, dipoles can orient easily whereas a highly cross-linked material finds difficulty in

orientation. The delayed response to a stimulus in a system is called *relaxation*. The orientation involves a characteristic time called *relaxation time*  $\tau$  [68].

The dielectric loss of a system can be explained as the ratio of the energy dissipated per radian in the material to the energy stored at the peak of polarization. This parameter is usually described by the so called loss tangent,  $\tan \delta$  and is defined as [69]

$$\tan \delta = \varepsilon''/\varepsilon'$$

Frequency dependent dielectric behavior of prepared polymer electrolytes systems is investigated. In an ion conducting system, the dielectric constant has contribution from dipoles as well as from mobile ions to the relative permittivity of the materials. To study the dielectric properties of prepared blended, plasticized and nano-filled polymer electrolyte films, frequency dependent real and imaginary parts of dielectric permittivity are calculated and analyzed at different temperatures using formulas given in Chapter 3. At first the polymer blended system with various ratios of PEO to PMMA at different temperatures are studied. For this, real ( $\varepsilon'$ ) and imaginary ( $\varepsilon''$ ) parts of permittivity as function of frequency at different temperatures are plotted. Figs 5.56 (a)-(c) and 5.56 (d)-(f) show the variation of  $\varepsilon'$  and  $\varepsilon''$  for PPS-10, PPS-50 and PPS-70 polymer electrolyte films, respectively. Observing the data of dielectric properties, it is clear that dielectric constant decreases with increase of frequency and saturates at higher frequencies [71]. Both dielectric constant and dielectric loss rise sharply at low frequencies and this behavior have been attributed to the occurrence of electrode polarization and space charge effects [70-72]. The presence of this polarization effect indicates the non-Debye type of behavior and the periodic reversal of the electric field at high frequencies does not allow any excess ion diffusion in the direction of the field leading to decrease in

polarization resulting in a drop in dielectric constant and dielectric loss. The degree of salt dissociation of ion aggregates increases with temperature resulting in the increase in number of free ions or charge carrier density. The frequency of dispersion in the dielectric permittivity shifts towards higher frequency side implying the faster relaxation of polymer chain segments. This introduces flexibility in the polymer chain segment and

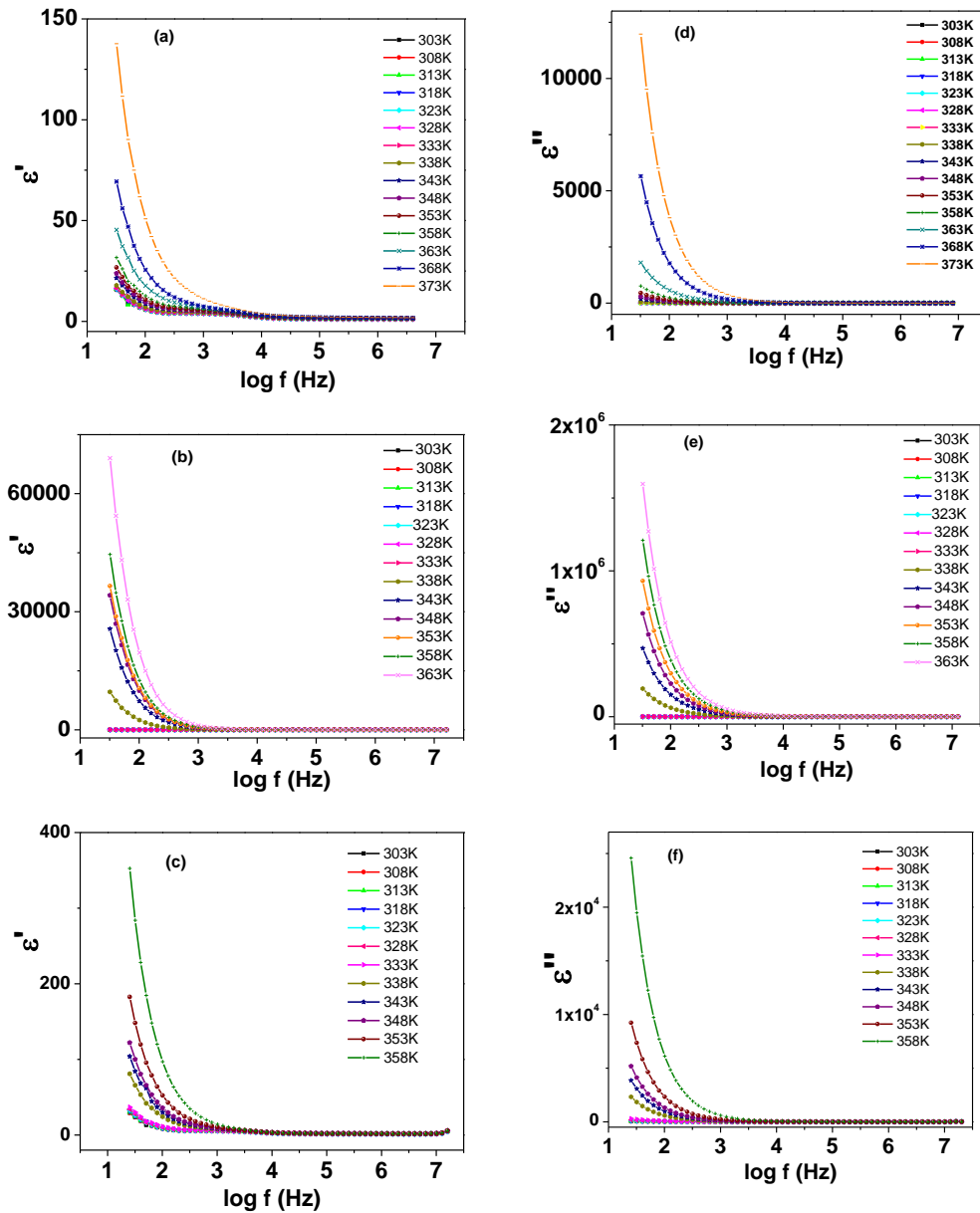


**Fig. 5.56** Frequency dependent  $\epsilon'$  plots for (a) PPS-10, (b) PPS-50 and (c) PPS-70 and  $\epsilon''$  plots for (d) PPS-10, (e) PPS-50 and (f) PPS-70 samples at different temperatures.

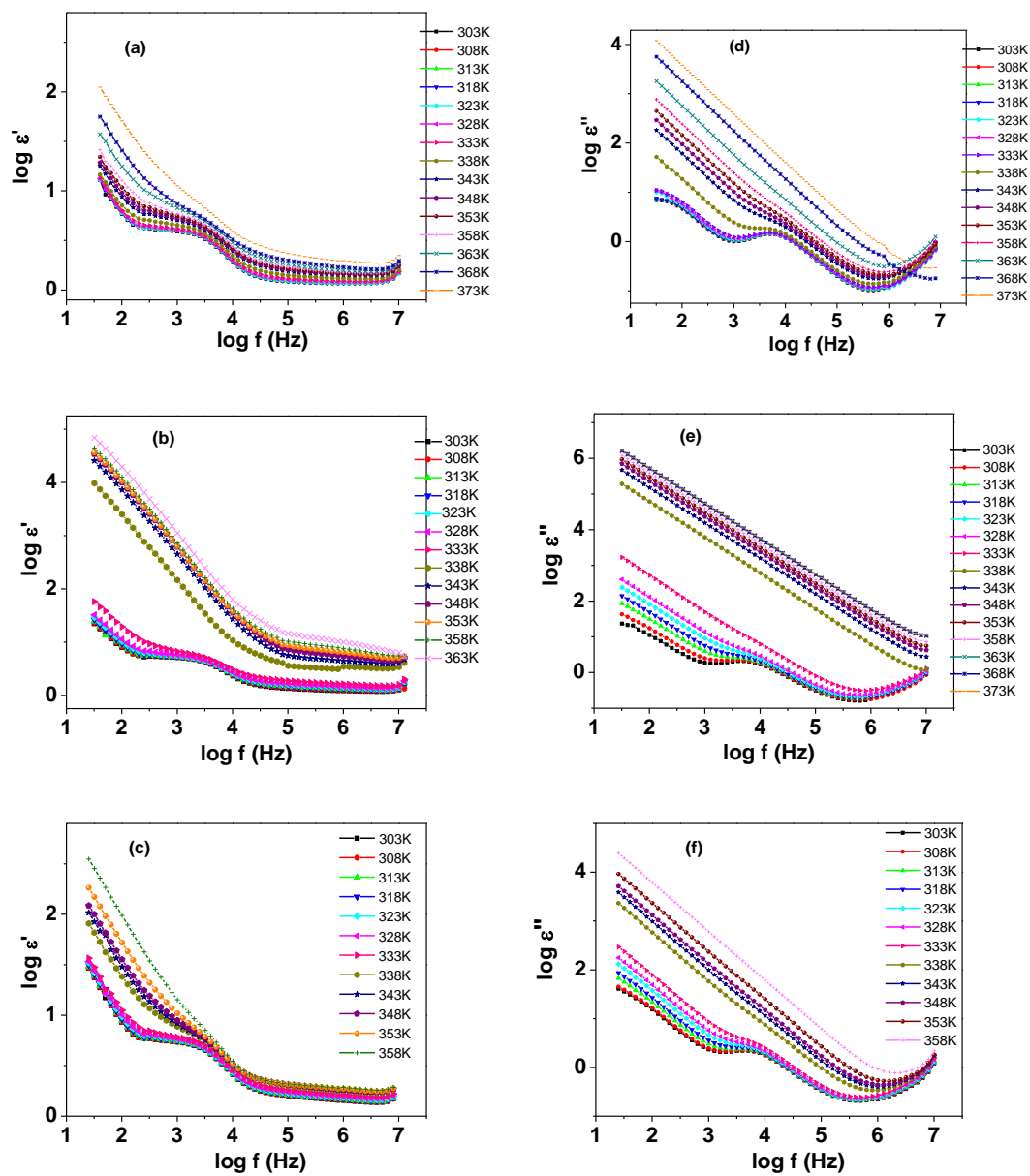


**Fig. 5.57** Frequency dependent logarithmic  $\epsilon'$  plots for (a) PPS-10, (b) PPS-50 and (c) PPS-70 and  $\epsilon''$  plots for (d) PPS-10, (e) PPS-50 and (f) PPS-70 samples at different temperatures.

thereby its mobility. In logarithmic scale, dielectric constant steadily decreases with increasing frequency and becomes almost constant at higher frequencies (Figs. 5.57 (a)-(c)). Imaginary part of dielectric permittivity show higher values at low frequencies which is due to the free charge motion in the electrolyte material [8] and is observed to

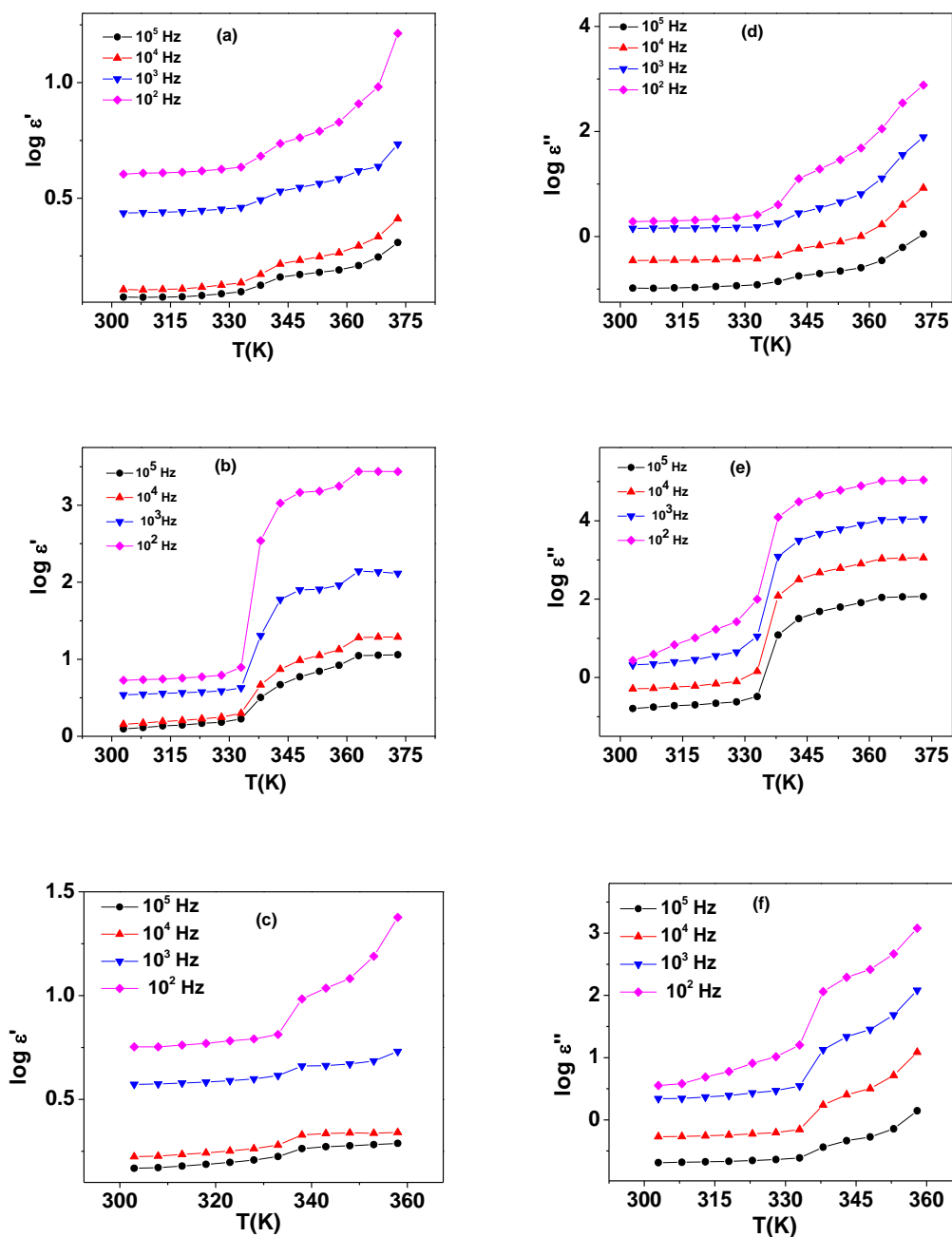


**Fig. 5.58** Temperature dependent  $\epsilon'$  plots for (a) PPS-10, (b) PPS-50 and (c) PPS-70 and  $\epsilon''$  plots for (d) PPS-10, (e) PPS-50 and (f) PPS-70 samples at different frequencies.

decrease with increasing frequency (Figs. 5.57 (d)-(f)).

Temperature dependence of permittivity and imaginary part of dielectric permittivity are seen in Figs 5.58(a)-(c) and 5.58 (d)-(f) for PPS-10, PPS-50 and PPS-70 polymer electrolyte films, respectively. However, real ( $\epsilon'$ ) and imaginary ( $\epsilon''$ ) part of

permittivity values show a sudden rise near the melting temperature of PEO as observed in conductivity spectra in section 5.2. Saroj et. al [73] suggested that with increase in temperature, the crystalline phase in semi-crystalline polymeric materials dissolves progressively into amorphous phase. This behavior influences the polymer dynamics and thus the dielectric properties increase.

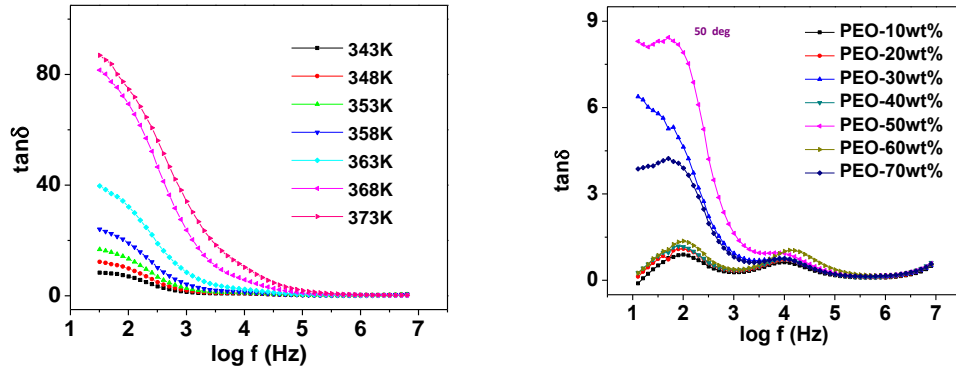


**Fig. 5.59** Variation of  $\tan \delta$  for (a) PPS-10 polymer film at different temperatures (b) PPS-System at 323K.

The variation of loss tangent with frequency for PPS-10 polymer film, shown in Fig. 5.59(a), decreases with increasing frequency and becomes constant at higher frequencies because ion migration mitigates at high frequency and a decrease in dielectric loss is observed. The loss increases with increase in temperature [73]. This high value of dielectric loss is due to the contribution of ion jump and dc conduction loss of ions in addition to the polarization loss. Similar behavior is observed in other samples. Fig. 5.59(b) shows the  $\tan \delta$  plot for different amount of PEO concentration in PPS-system. The figure clearly depicts that losses increase with PEO concentration and maximum for highest conducting samples i.e.; PPS-30 and PPS-50.

Both the values of the permittivity show a strong dispersion in frequency at the temperature above melting point. This type of dispersion in  $\epsilon'$  may be regarded as

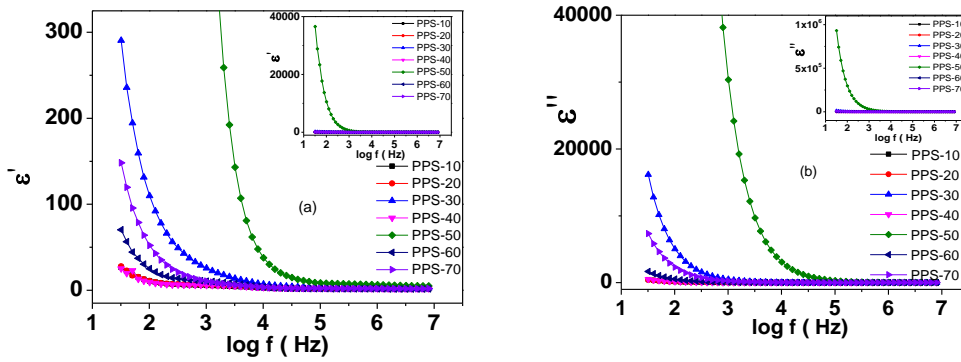


**Fig. 5.60** (a)  $\epsilon'$  and (b)  $\epsilon''$  plots for PPS-System at 353K and insets show the complete spectra.

relaxation behavior concerned with the high mobility of  $\text{Ag}^+$  -ions under the force of an external electric field. This increase in dielectric permittivity with temperature is ascribed due to the formation of molecular dipoles. These dipoles remain frozen when the temperature is low. At the melting temperature of PEO, the dipoles having more rotational freedom become more thermally activated. Such temperature dependence of dielectric permittivity has been reported in other solid electrolytes [8, 39].

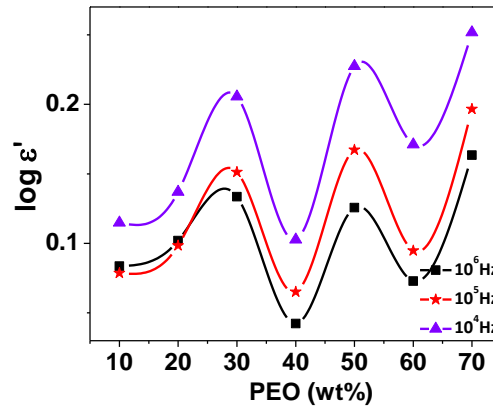


**Fig.5.61** Variation of real part of permittivity for PPS-System at different frequencies.

Figs. 5.60(a) & (b) show the compositional variation of  $\epsilon'$  and  $\epsilon''$  for PEO blended with PMMA polymer complexes as a function of frequency at 353K. The dielectric constant values are found to increase with PEO concentration (in both  $\epsilon'$  and

$\epsilon'$ 'spectra) and found to be highest for PPS-50 polymer electrolyte sample. Compositional variation of dielectric constant at different frequencies, depicted in Fig.5.61, also indicates that dielectric permittivity increases with PEO concentration and shows two maxima at PPS-30 and PPS-50 similar to the conductivity isotherm of PPS-system.

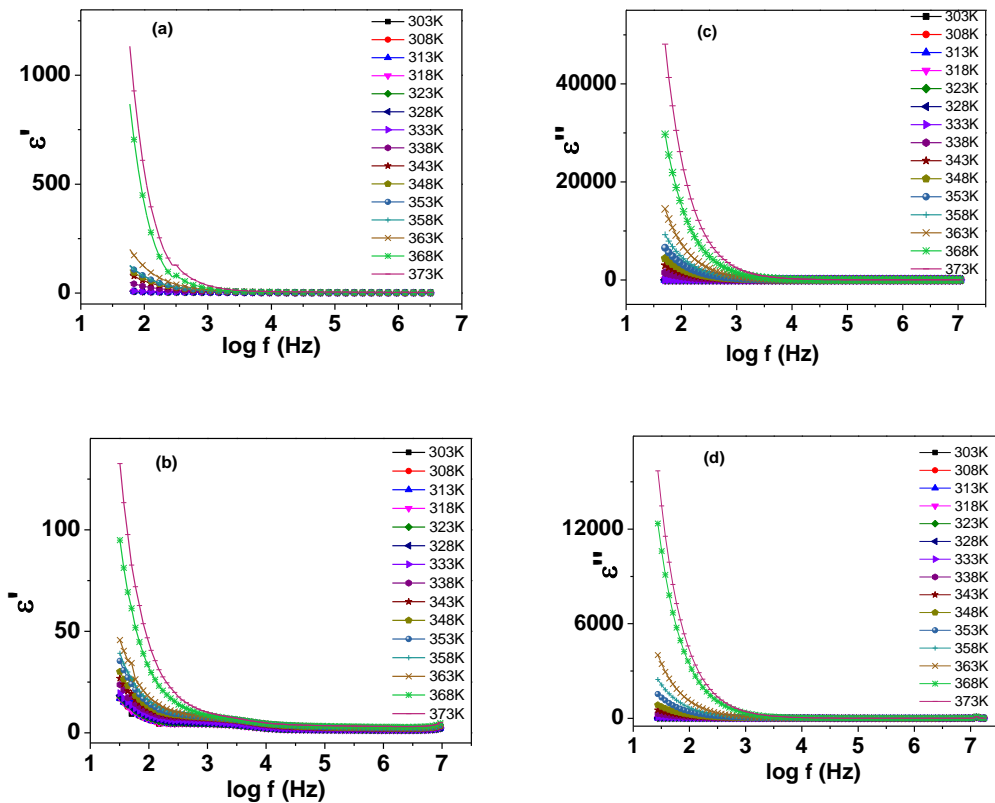


**Fig. 5.62** Frequency dependent  $\epsilon'$  plots for (a) PPSP-10 and (b) PPSP-12 and  $\epsilon''$  plots for (c) PPSP-10 and (d) PPSP-12 samples at different temperatures.

When plasticization is carried out in PEO-PMMA-AgNO<sub>3</sub> polymer electrolyte with PEG and EC, the system shows similar frequency dependent behavior of real and imaginary permittivity as observed in pure blended samples at different temperatures. Both the real and imaginary part of dielectric permittivity rise sharply near low frequencies indicating that electrode polarization and space charge effects are still there and confirm its non-Debye dependence (Figs.5.62 & 5.63). Plasticizer PEG having

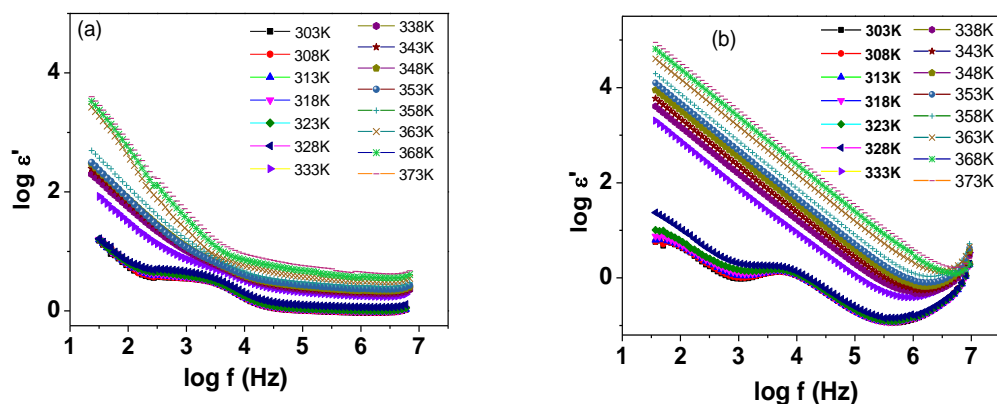


**Fig. 5.63** Frequency dependent logarithmic  $\epsilon'$  and  $\epsilon''$  plots for PPSP-10 ((a) & (b)) respectively at different temperatures.

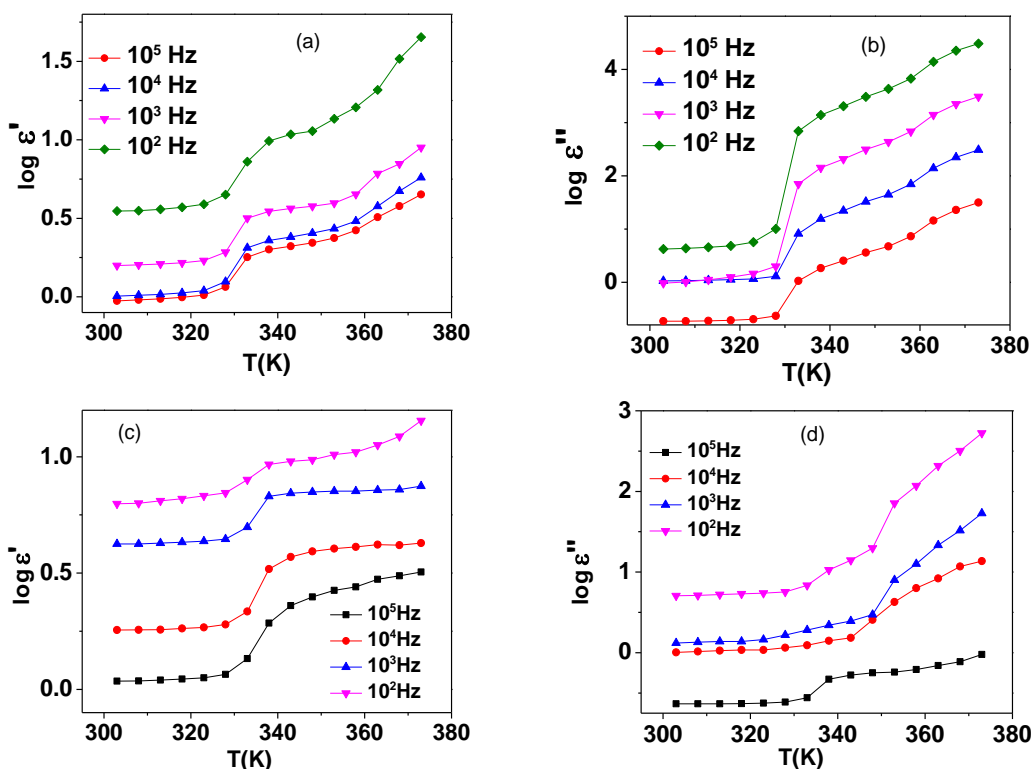


**Fig. 5.64** Temperature dependent  $\epsilon'$  and  $\epsilon''$  plots for (a & b) PPSP-10 and (c & d) PPSP-15 at different frequencies.

similar structure as PEO and low dielectric constant, promotes the organization of segmental units and in turn, modifies the blend structure. Figs.5.64 (a) - (d) show the temperature dependence of real and imaginary parts of permittivity at different frequencies for PPSP-10 and PPSP-15 samples. The steep rise above melting temperature

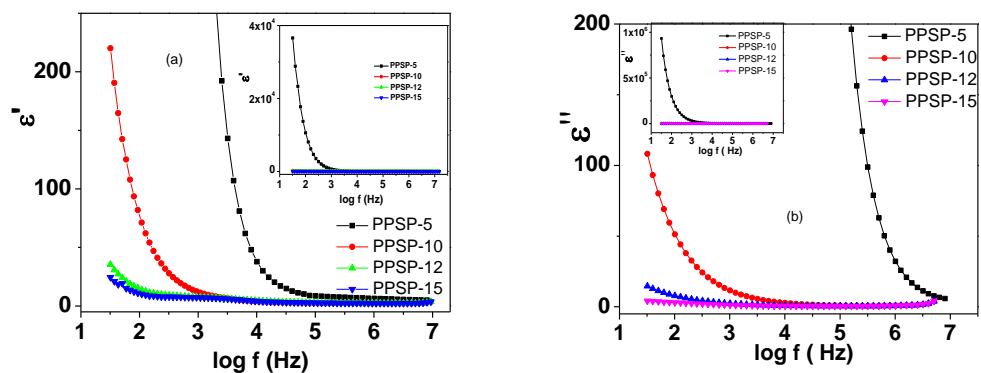


**Fig. 5.65** (a)  $\epsilon'$  and (b)  $\epsilon''$  plots for PPSP-System at 353K and insets show the complete spectra.

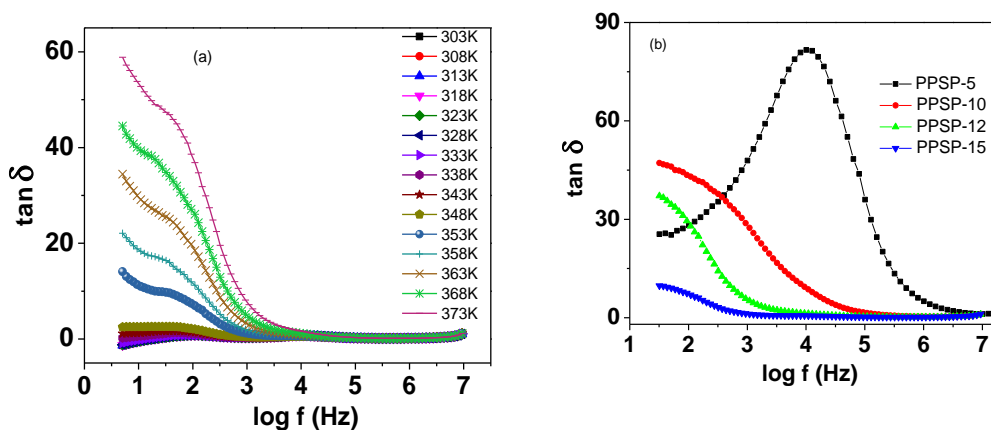


**Fig. 5.66** Variation of  $\tan\delta$  for (a) PPSP-10 polymer film at different temperatures (b) PPSP-System at 323K.

is the main feature of all the samples. Compositional dependence of dielectric permittivity (Fig. 5.65) reveals the high values for the polymer films above melting temperature than at below melting with highest values for PPSP-5 sample. The loss tangent values are slightly increased and the frequency of dispersion decreases with the addition of PEG whereas with temperature the frequency of dispersion shifts towards high frequency side in the system (Fig.5.66). Never the less, EC based polymer blended electrolyte system also shows similar behavior as observed in PEG system. Variation of dielectric constant and dielectric loss for different EC concentrations in silver-ion

conducting PEO-PMMA polymer blend is shown in Figs 5.68 and 5.69. The observed decrease in  $\varepsilon'$  and  $\varepsilon''$  values is due the fact that as the frequency increases, the polarizability contribution from ionic and orientation sources decreases and finally disappears due to their inertia [8, 39]. With the rise in temperature (Fig. 5.70), the ionic and electronic polarizability start to increase which result in enhancement in dielectric constant values. Compositional variation of  $\varepsilon'$  and  $\varepsilon''$  values initially decrease as

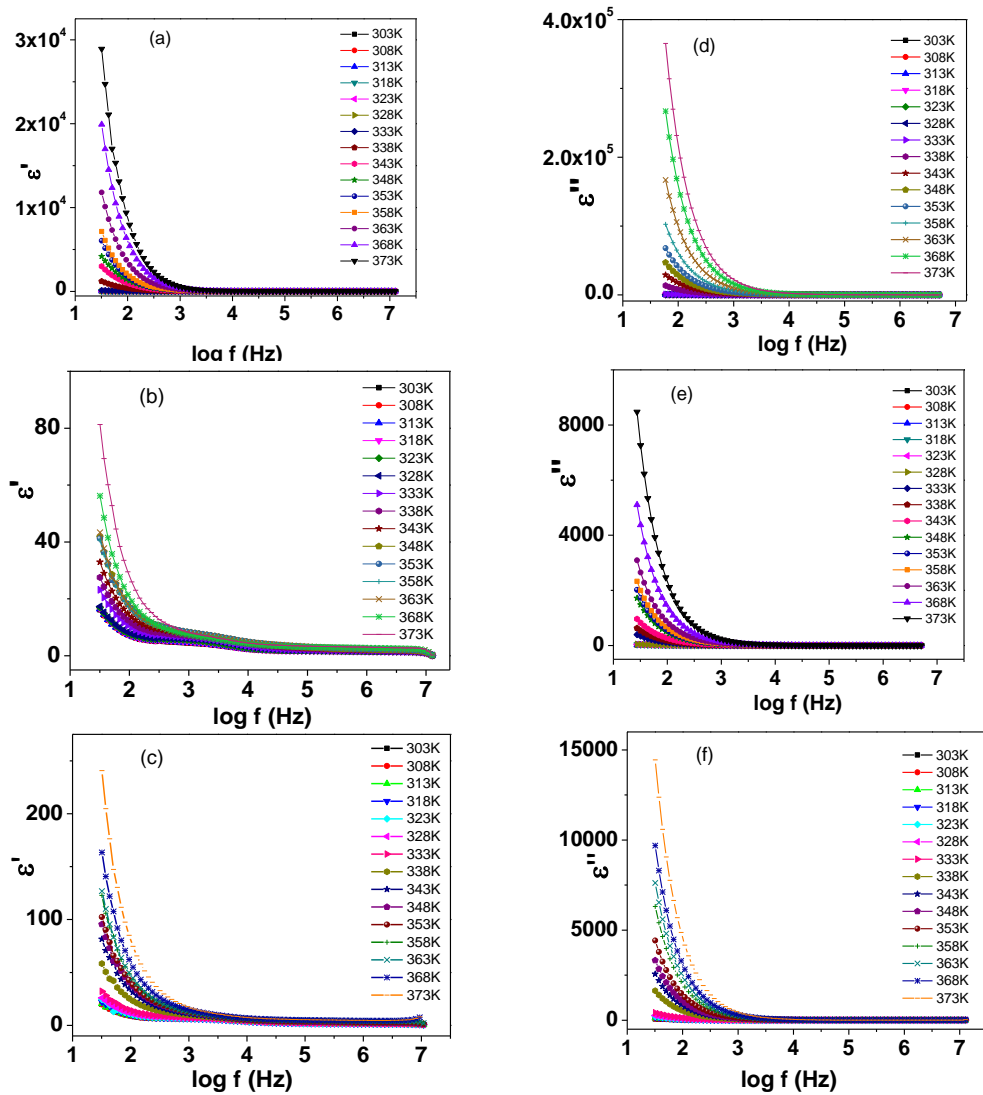


**Fig. 5.68** Frequency dependent (a)-(c)  $\varepsilon'$  and (d)-(f)  $\varepsilon''$  plots for PPSE-5, PPSE-7 and PPSE-12 at different temperatures.

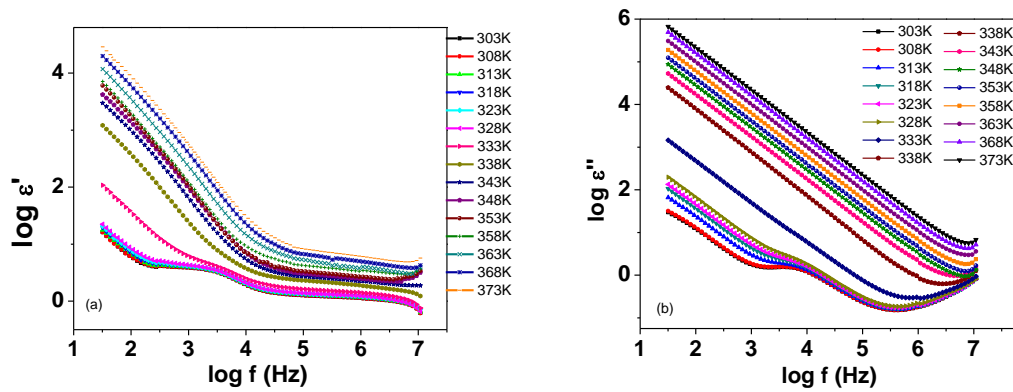


**Fig. 5.69** Frequency dependent logarithmic (a)  $\epsilon'$  and (b)  $\epsilon''$  plots for PPSE-5 sample at different temperatures.

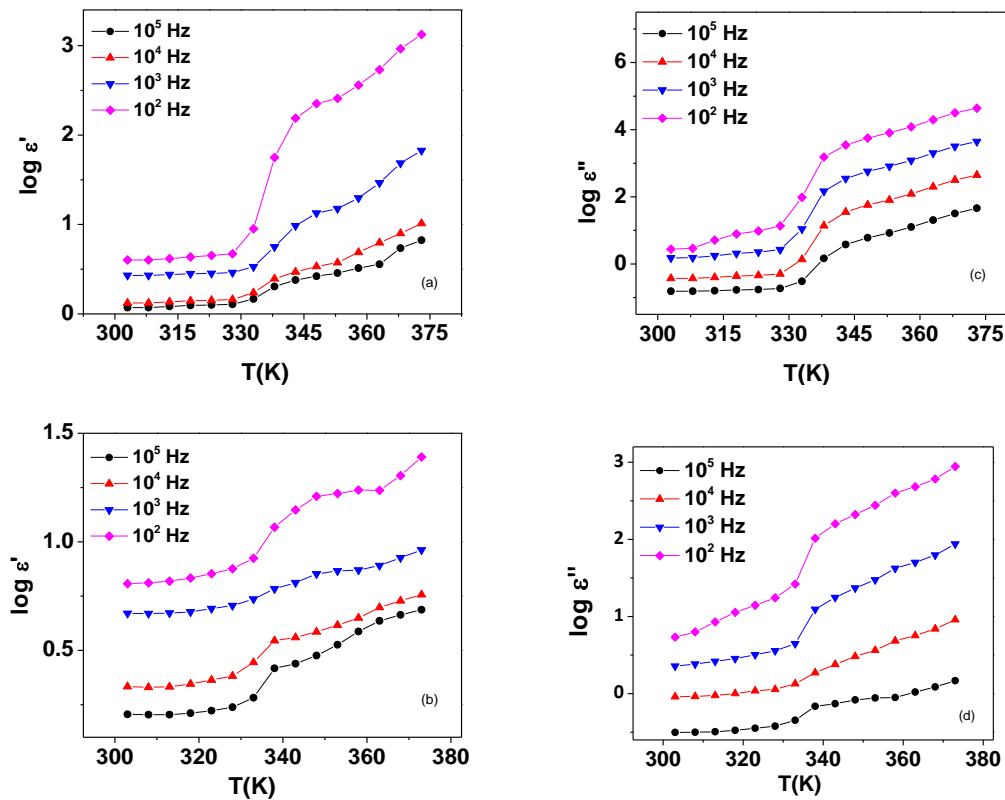


**Fig. 5.70** Temperature dependent (a)-(b)  $\epsilon'$  and (c)-(d)  $\epsilon''$  plots for (a) PPSE-5 and (b) PPSE-12 at different frequencies.

ethylene carbonate concentration increases up to 7 wt% and further addition of EC concentration leads to rise of more than one order of magnitude in the values of permittivity.

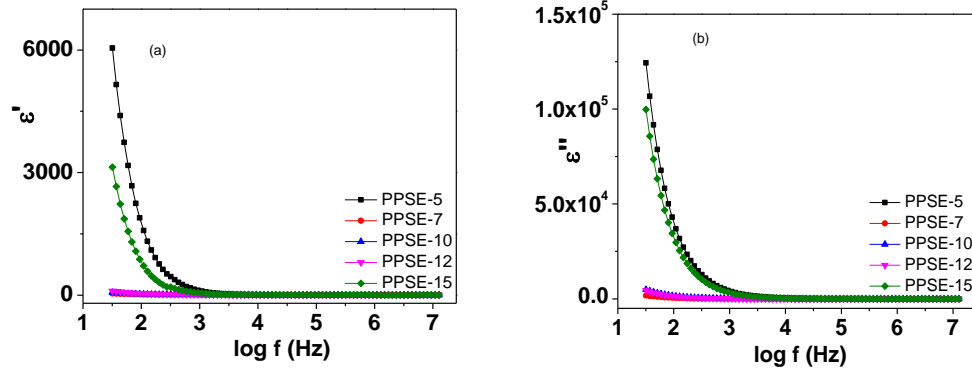


**Fig. 5.71** (a)  $\epsilon'$  and (b)  $\epsilon''$  plots for PPSE-System at 353K.

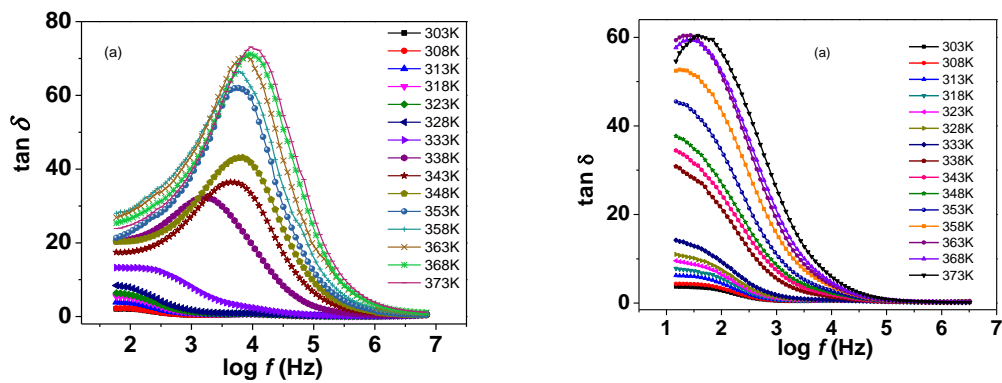


**Fig. 5.72** Variation of  $\tan\delta$  for (a) PPSE-5 and (b) PPSE-12 at different temperatures.

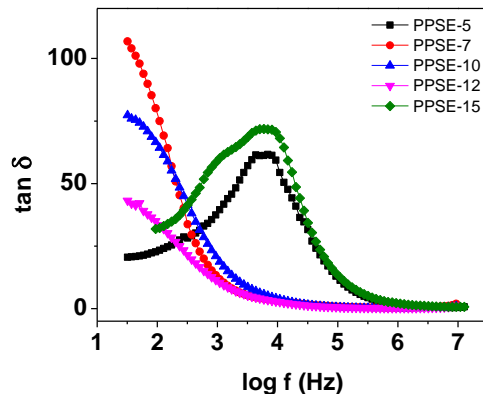


**Fig.5.73** Variation of  $\tan\delta$  for PPSE-System at 323K.

Variation of loss tangent ( $\tan \delta$ ) with temperature for PPSE-5 and PPSE-12 samples is represented in Figs. 5.72 (a) & (b) respectively. A peak maxima in  $\tan \delta$  start to appear as temperature approaches near  $T_m$ . This peak maximum in loss tangent slightly shifts towards higher frequency with rise in temperature. It is worth mentioning here that

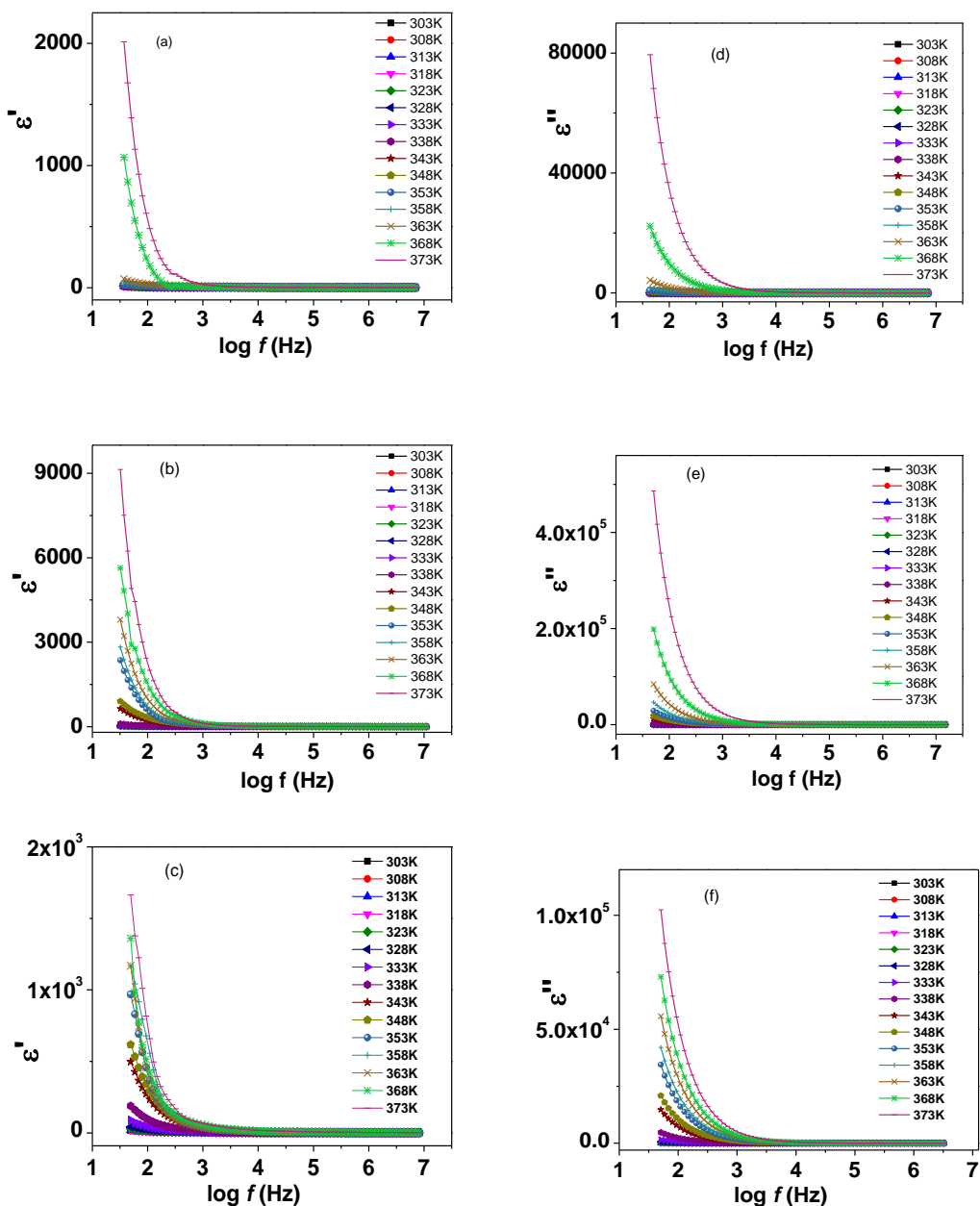


**Fig. 5.75** Frequency dependent (a)-(c)  $\epsilon'$  and (d)-(f)  $\epsilon''$  plots for PPSA-1, PPSA-2 and PPSA-4 at different temperatures.

$\tan \delta$  is situated at low frequency region, where dc conductivity dominates. In addition to this, dielectric losses at lower frequencies are significantly higher than those occurring at higher frequency. This kind of dependence of  $\tan \delta$  on frequency is associated with losses by conduction. Consequently, the dielectric loss for samples with high conductivity

(PPSE-5 & PPSE-15) is higher than the samples with lower conductivity. The main advantages of the composite electrolyte are the enhancement of room temperature ionic conductivity and an improved stability at the electrode- electrolyte interface. The inert fillers, due to its large surface area, prevent the local chain reorganization with the result of locking in a high degree of disorder characteristic of the amorphous phase, which favors the high ionic transport. Therefore, the effect of nano- filler  $\text{Al}_2\text{O}_3$  concentration on dielectric properties of polymer electrolytes plasticized with PEG behavior is observed.

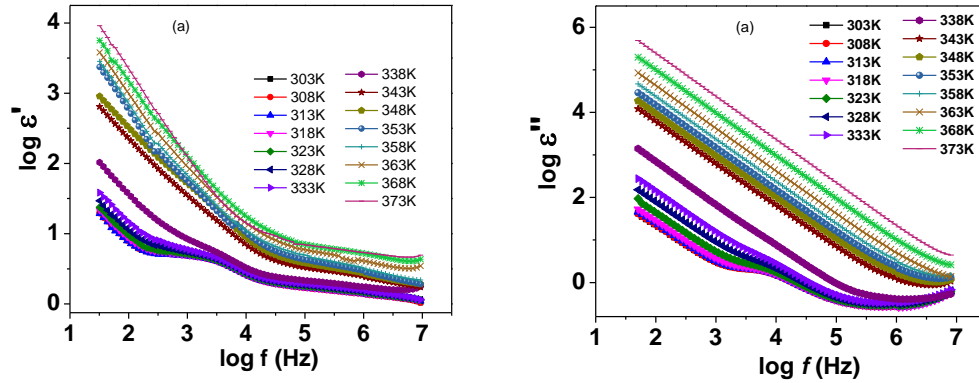


**Fig. 5.76** Frequency dependent logarithmic (a)  $\epsilon'$  and (b)  $\epsilon''$  plots for PPSPA-4 and at different temperatures.

Fig.5.75 shows the frequency dependence of real and imaginary parts of dielectric constant at different temperatures for 1, 2 and 4 wt% of  $\text{Al}_2\text{O}_3$  in PPSP sample. It is clear from the figure that permittivity decreases monotonically with increasing frequency and after a cross-over frequency, shows a saturation plateau in the higher frequency region. The accumulation of charge at the interface of electrode-PPSPA nano-composites at low frequency ascribes the polarization and the fast periodic reversal of electric field at higher frequencies charge accumulation decreases which is responsible for a fall in dielectric constant. At  $T < T_m$  temperatures, in Fig. 5.76,  $\epsilon'$  plot reveals a step-like behavior or two

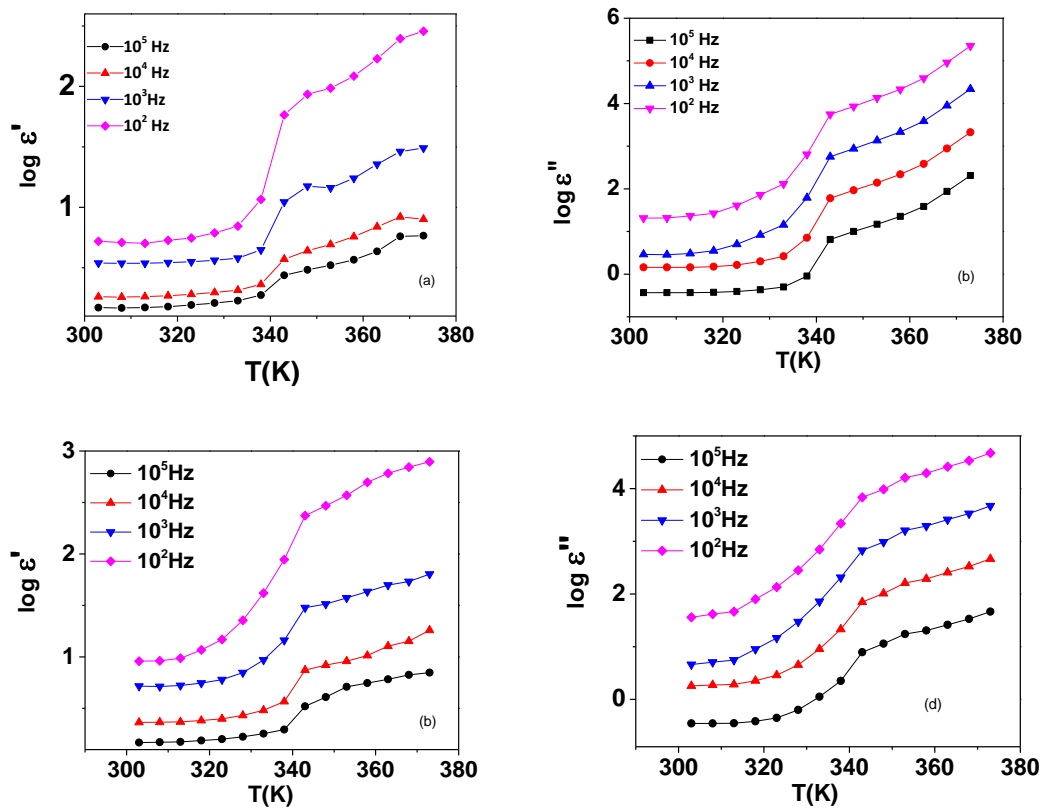


**Fig. 5.77** Temperature dependent (a) & (b)  $\epsilon'$  and (c) & (d)  $\epsilon''$  plots for PPSA-2 and PPSA-4 samples respectively, at different frequencies.

plateaus of dielectric which shifts to higher frequency side with the increase in temperature, and above  $T_m$ , double plateau region gradually converts into a single dispersion with the increase in temperature. Similar behavior is observed in other samples. A sudden increase in dielectric constant also features beyond the melting temperature and this increase is more pronounced at lower frequencies as is evident from Fig.5.77. It can be clearly made out from the Fig.5.78 that the values of the dielectric constant, both above and below the melting temperature of PEO, increase with the addition of nano-filler in the blend electrolyte samples except at 5wt%.

Figs.5.79 (a) & (b) show the frequency dependent loss tangent of the investigated polymer nano-composite system at various temperatures for PPSA-4 and PPSA-5

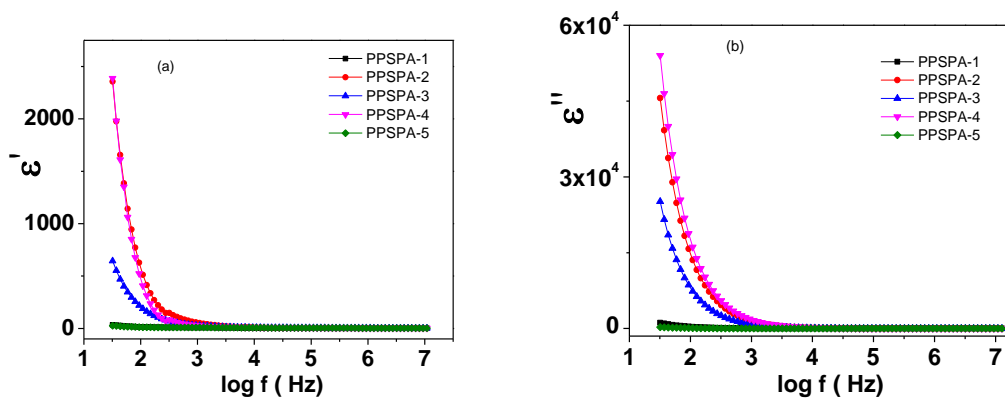


Fig. 5.78 (a)  $\epsilon'$  and (b)  $\epsilon''$  plots for PPSPA-System at 353K.

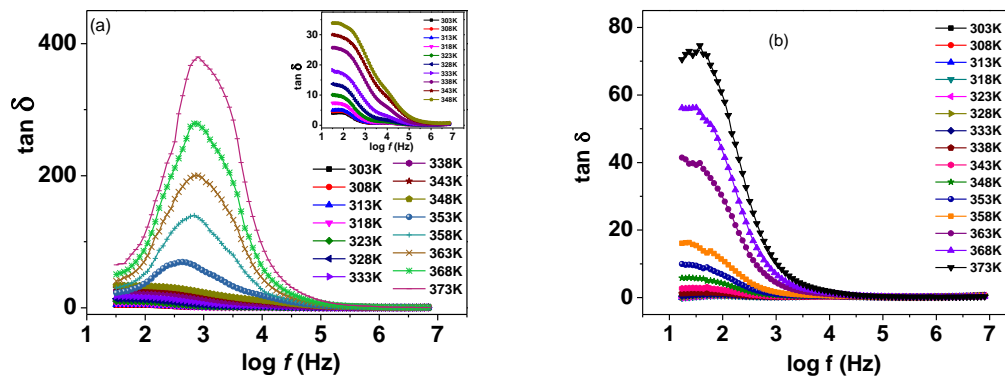


Fig. 5.79 Variation of  $\tan \delta$  for (a) PPSPA-4 and its inset shows  $T < T_m$  temperature range and (b) PPSPA-5 at different temperatures.

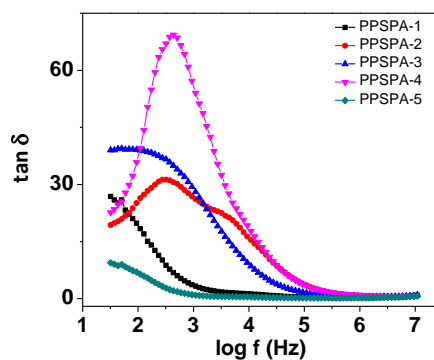
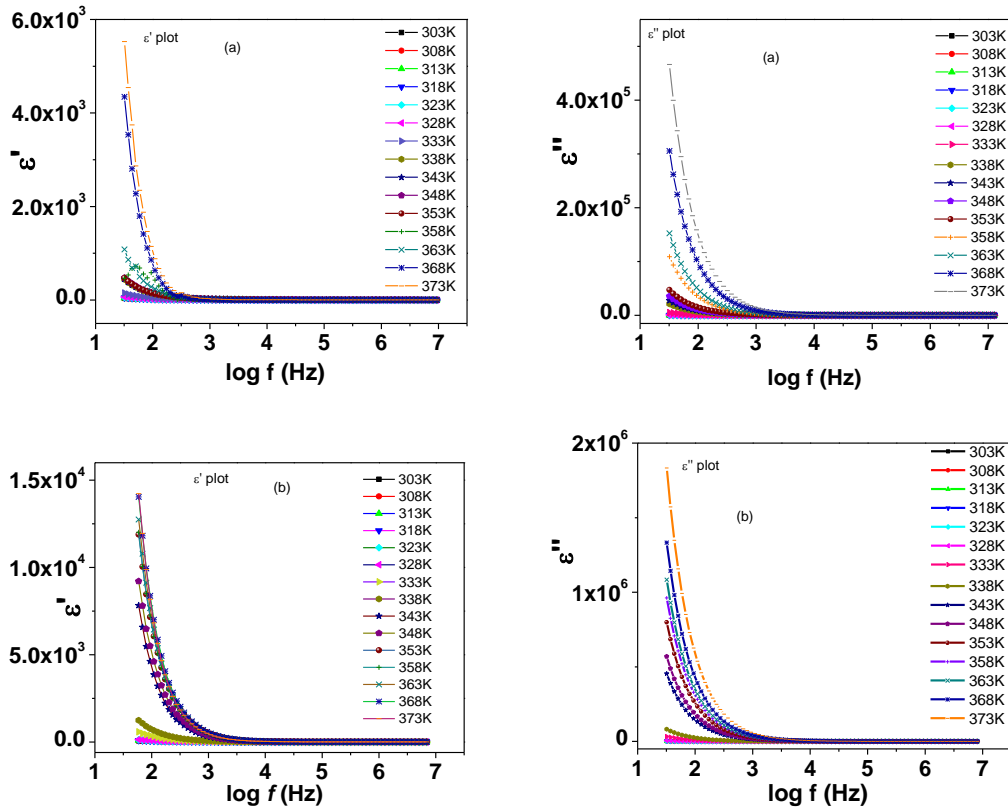


Fig. 5.80 Variation of  $\tan \delta$  for PPSPA-system at 353K.

samples. Observed from figure, it is apparent that the losses increase with temperature. At  $T < T_m$ , loss peak in  $\tan \delta$  spectra is very feeble with no shifting with the rise in temperature. The peak values at lower frequencies are high and its values decrease with

frequency. Loss peak at  $T > T_m$  shifts towards high frequency side with rise in temperature. The loss peaks and their shifts with temperature indicate a dielectric relaxation process. The dielectric losses also increase with the filler concentration up to 4 wt% and decreases at higher amount of  $\text{Al}_2\text{O}_3$  (Fig.5.80).



**Fig. 5.81** Frequency dependent  $\epsilon'$  and  $\epsilon''$  plots for (a) PPSEA-2 and (b) PPSEA-4 at different temperatures.

Similar observations in EC based polymer nano-composites are observed. The variations of real and imaginary parts of dielectric constant, as a function of frequency, are shown in Fig.5.81 (for PPSEA-2 and PPSEA-4 samples) and Fig.5.82 (for PPSEA-4 polymer film). The dielectric permittivity rises sharply towards low frequency due to electrode polarization effects [74]. A sudden increase in  $\epsilon'$  and  $\epsilon''$  values near  $T_m$  (Fig. 5.83) is one of the main features in this system too. The highest values of  $\epsilon'$  and  $\epsilon''$

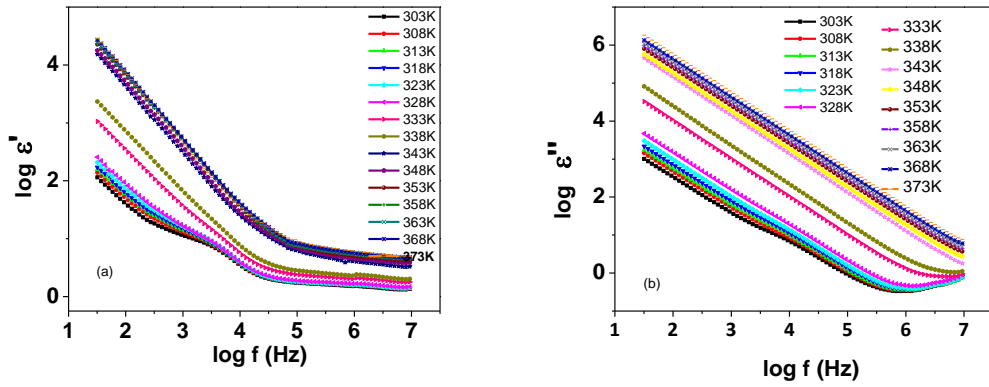


**Fig. 5.82** Frequency dependent logarithmic (a)  $\epsilon'$  and (b)  $\epsilon''$  plots for PPSEA-4 at different temperatures.

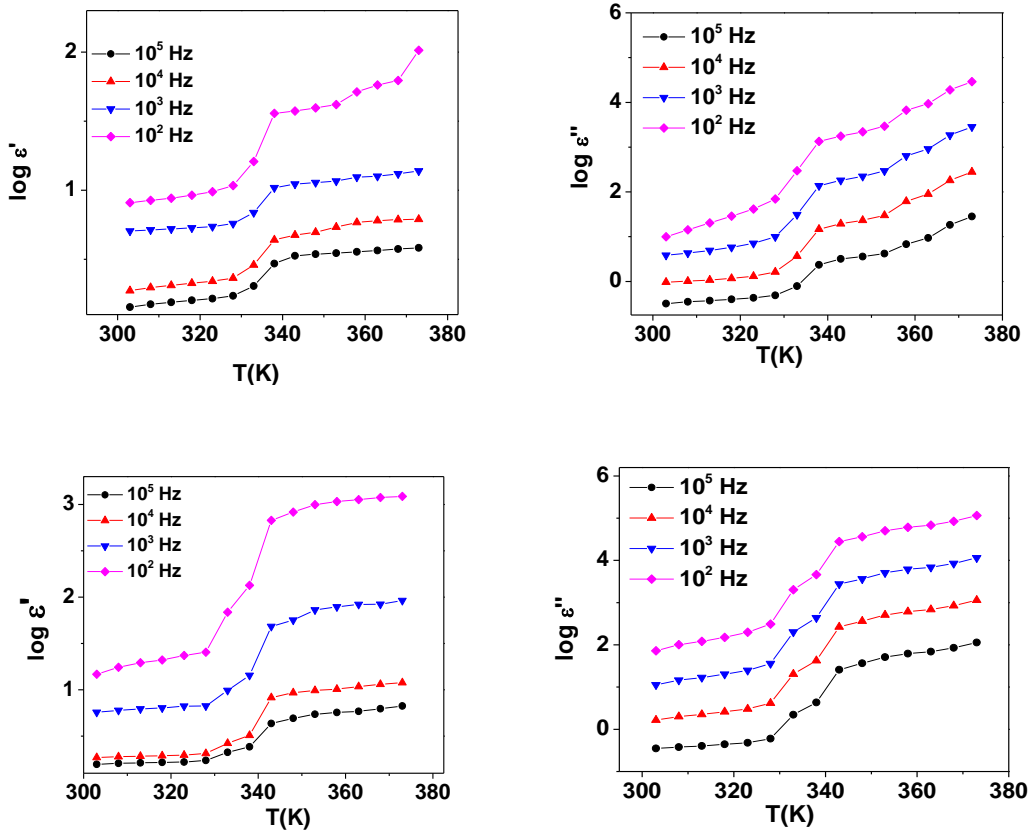


**Fig. 5.83** Temperature dependent  $\epsilon'$  and  $\epsilon''$  plots for (a) PPSEA-2 and (b) PPSEA-4 at different frequencies.

for PPSEA-4 sample indicates the enhanced charge carrier density at the space charge accumulation region, resulting in an increase in the equivalent capacitance.

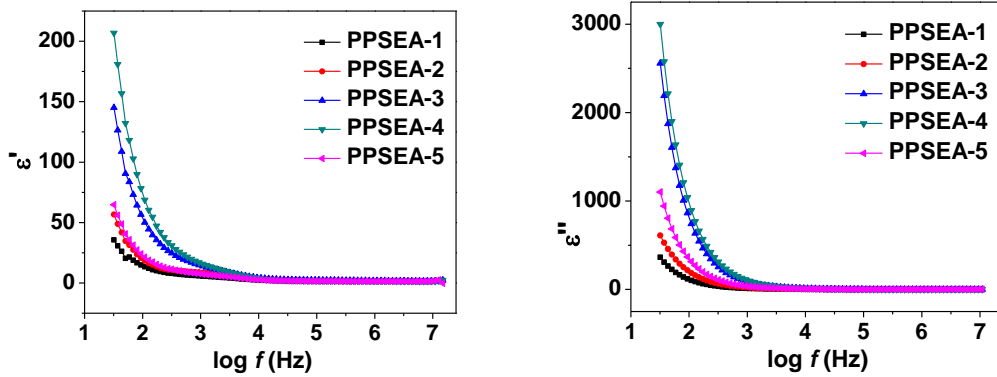


**Fig. 5.84**  $\epsilon'$  and  $\epsilon''$  plots for PPSEA-System at 353K.

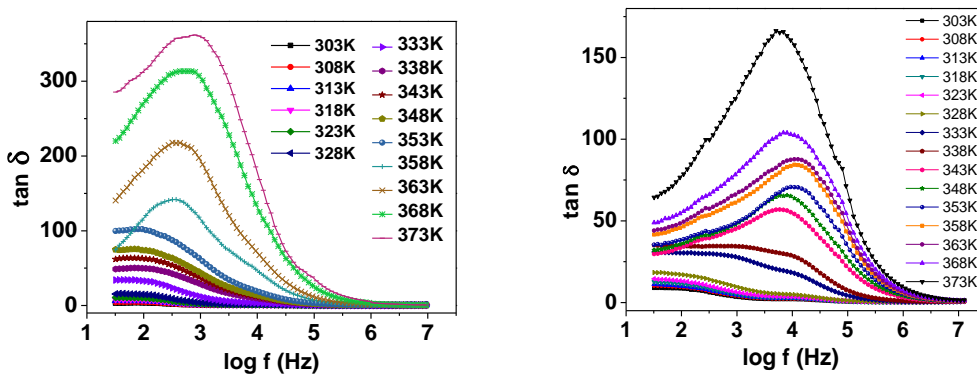


**Fig.5.85** Variation of  $\tan \delta$  for (a) PPSEA-2 and (b) PPSEA-4 at different temperatures.

Loss tangent of polymer nano-composite system plasticized with EC for PPSEA-2 and PPSEA-4 samples, shown in Fig.5.84 at various temperatures increase with the rise in temperature. Losses rise with the filler concentration up to 4 wt% but decrease at higher amount of  $\text{Al}_2\text{O}_3$  (Fig.5.85). Dielectric constant values as a function of nano-filler concentration is given in Fig.5.86. It can be concluded from figure that the values are quite higher (more than one order of magnitude) in EC based nano-composites. This is found in good agreement with conductivity results shown in Fig.5.39.

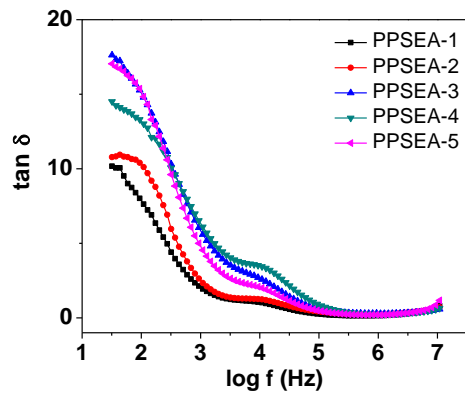


**Fig.5.86** Variation of  $\tan\delta$  for PPSEA-system at 323K.

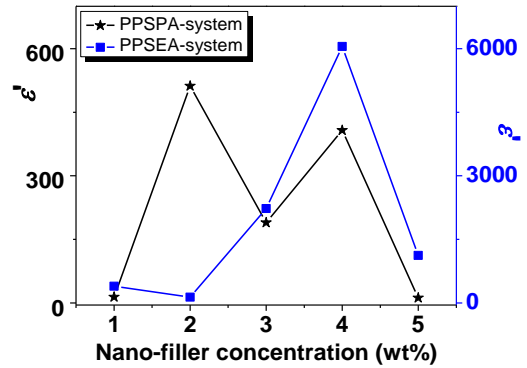


**Fig.5.87** Variation of  $\epsilon'$  in polymer nano-composites plasticized with PEG and EC at 353K.

## 5.4 Modulus Analysis

The electrode-electrolyte interface polarization due to accumulation of charges at low frequency is so much prominent that it is difficult to separate other relaxation effects apart from polarization. Hence, further analysis of the dielectric behavior, using the formulation of electric modulus, pioneered by Macedo *et. al.* [13] is used to overcome this [75, 76]. Electric modulus is an electrical analog to the mechanical shear modulus.

Electrical modulus formalism is useful to study the relaxation process in a wide variety of materials [76-78]. The electrical relaxation process is due to distribution of relaxation times which may be due to inhomogeneity, conducting domain and mixture of phases etc. The modulus formalism transforms a monotonically increasing function of frequency (the real part of ac conductivity  $\sigma'(\omega)$ ) into one exhibiting a peak in  $M''(\omega)$  representation. The electric modulus data can be obtained from the complex impedance data [77] according to the relation given in Chapter 3.

The variation of  $M'$  and  $M''$  at low and high frequencies can be predicted by the following model proposed by Macedo *et. al.* [13]

$$\begin{array}{ll}
\lim_{\omega\tau_{\sigma}\ll 1} M' = 0 & \lim_{\omega\tau_{\sigma}\gg 1} M' = M_s \\
\lim_{\omega\tau_{\sigma}\ll 1} M'' = 0 & \lim_{\omega\tau_{\sigma}\gg 1} M'' = 0
\end{array}$$

and  $M''$  passes through a maximum. At first, the effect of blending of different ratios of PEO with PMMA concentration on modulus spectra at different temperatures is studied. The modulus spectra of various concentrations of PEO in PEO-PMMA blended system at different temperatures are studied. The frequency dependent real and imaginary parts of modulus,  $M'(\omega)$  and  $M''(\omega)$  spectra for polymer blend PPS-10, PPS-20, PPS-30, PPS-50, PPS-60 and PPS-70 polymer electrolytes at various temperatures are shown in Figs. 5.88(a)- (f) and Figs. 5.89(a)- (f). It shows an increase in  $M'(\omega)$  values with frequency and attain a constant value at higher frequency. The observed small value of  $M'(\omega)$  in low frequency region facilitates the migration of ion conduction [76].

However, the frequency dependent values of  $M'(\omega)$  at high frequencies decreases with the increase in temperature and the relaxation frequency shifts towards the higher frequency side with temperature. The reduction in the value of  $M'(\omega)$  with increase in temperature is due to the increase in the mobility of the polymer segment and charge carriers with the temperature. Below  $T_m$ ,  $M'$  plot shows two dispersion regions (similar to regions observed in PPS and PPSP-systems) which turn into single one as temperature approaches  $T_m$ . The frequency dependent  $M'(\omega)$  and  $M''(\omega)$  spectra (Fig. 5.88 and Fig. 5.89.) are divided in two regions; region I and region II which are in the temperature range  $T < T_m$  and  $T > T_m$  respectively. In region I,  $M'(\omega)$  and  $M''(\omega)$  spectra show two dispersions and two relaxation peaks, respectively. Low frequency dispersion and/or first

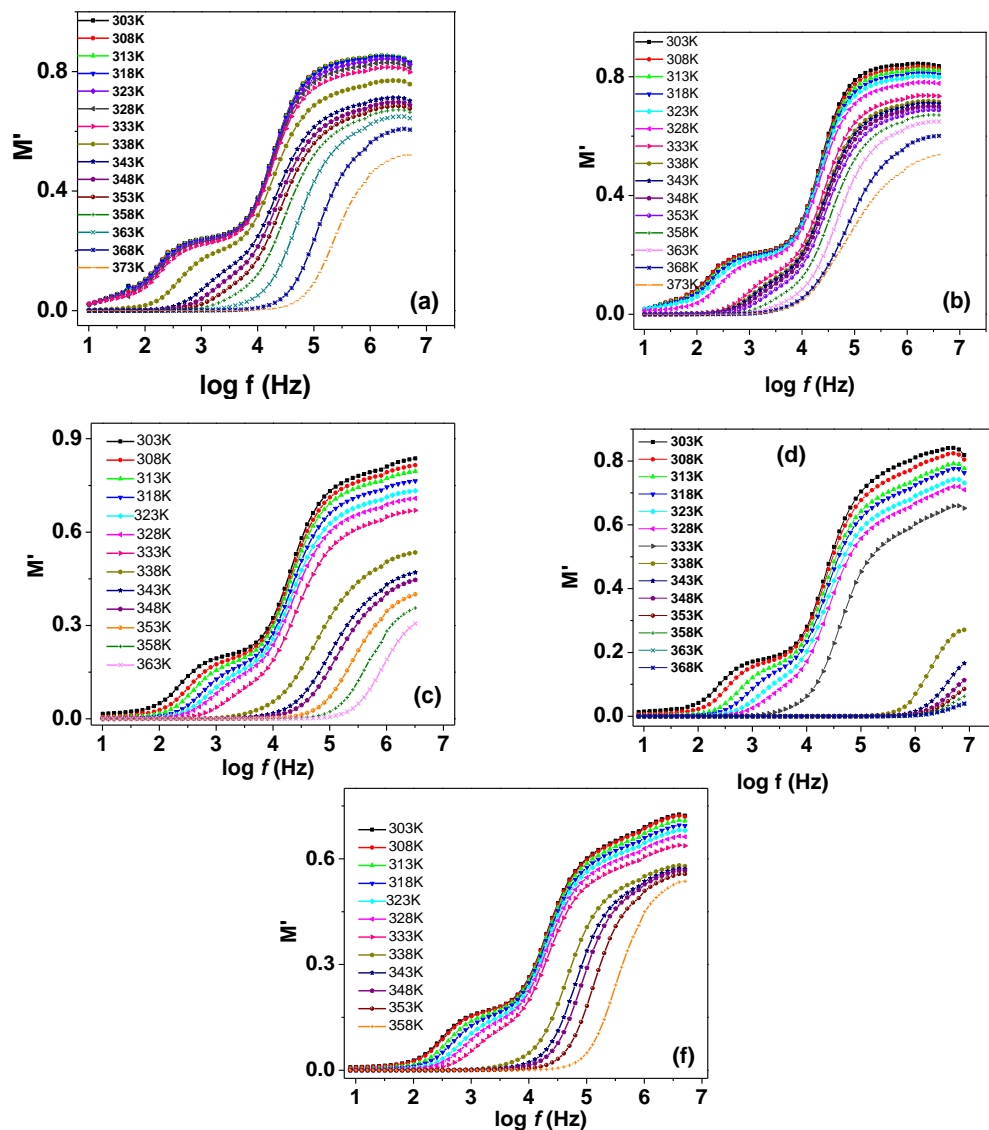


**Fig. 5.88** Frequency dependent real part of modulus,  $M'$  plots for (a) PPS-10 (b) PPS- 20 (c) PPS- 30 (d) PPS-50 (e) PPS-60 and (f) PPS-70 polymer films at different temperatures.

relaxation peak gradually shift towards high frequency side with temperature and finally disappear as temperature approaches near  $T_m$ . The second dispersion frequency observed in higher frequency region, does not shift but a reduction in the value peak height of  $M''$  is observed. The low frequency relaxation peak of  $M''(\omega)$  is observed to be centered at the first dispersion region of  $M'(\omega)$ . This peak is assigned to the transition region from long

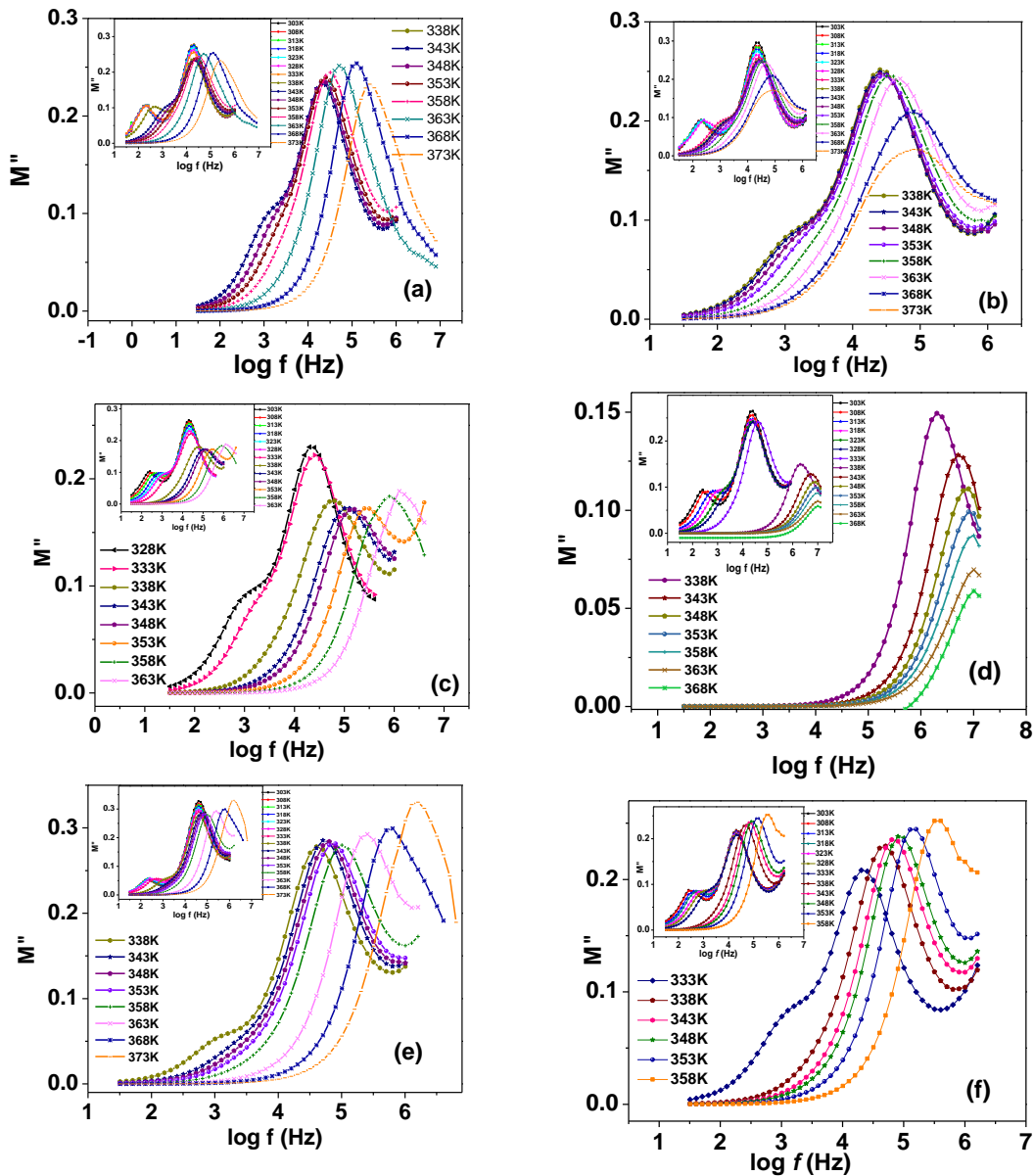


**Fig. 5.89** Frequency dependent imaginary part of modulus,  $M''$  plots for (a) PPS-10 (b) PPS- 20 (c) PPS- 30 (d) PPS-50 (e) PPS-60 and (f) PPS-70 polymer films at different temperatures.

range ionic mobility to dipole mobility (rotation). The double relaxation peaks in  $M''(\omega)$  spectra is expected one due to the presence of semi-crystalline regions and other due to amorphous regions in the present polymer blends. As the temperature approaches near  $T_m$ , semi-crystalline region of PEO melts and amorphous region preponderates in the PMMA matrix. In region II, the melted PEO penetrates in PMMA polymer making the

polymer system as gel like system in which polymer chains acquire faster internal movement and segmental motion dominates giving rise to only a single relaxation peak in

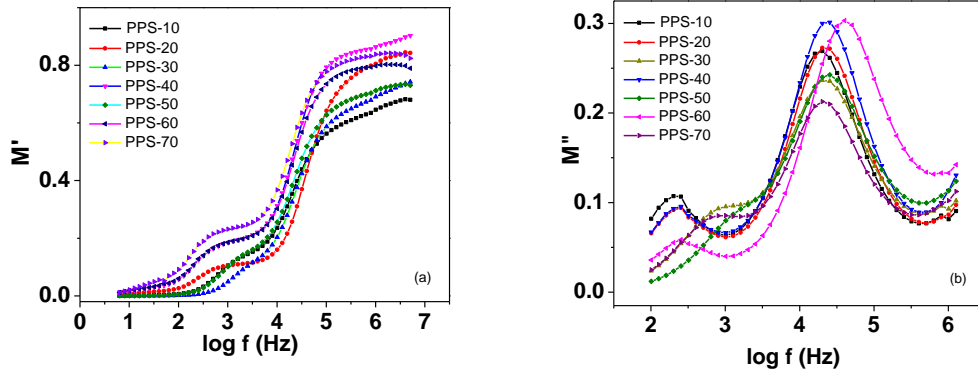


**Fig.5.90** Compositional frequency dependent (a)  $M'$  and (b)  $M''$  plots at 323K.

high frequency region. In this region, the frequency of  $M''_{max}$  is found to shift systematically towards higher frequency side with the increase in temperature. Similar behavior is observed in other samples too. The observed shift in  $M''_{max}$  either in low frequency region or in high frequency region with increase in temperature suggests that the increased movement of the charge carriers leading to decrease the relaxation time in their respective regions. This behavior suggests that the relaxation is a thermally activated process and occurrence of hopping of charge carriers. Effect of blending of PEO with PMMA on imaginary modulus spectra can be seen from Figs.5.90 (a) & (b).

$M'(\omega)$  and  $M''(\omega)$  spectra show a long tail at the low frequency region. This long tail provides evidence of the large capacitance associated with the electrodes. This is due to accumulation of a large amount of charge carriers at the electrode-solid polymer electrolyte interface. Frequency dependent  $M''$  plot shows asymmetric relaxation peak in the dispersion region of  $M'$  and the occurrence of relaxation peak indicate long range to the short range mobility with increase in frequency [77]. The charge carriers are mobile

over long distances in the left side region of the peak and they are spatially confined to their potential wells region in the right side of peak [76].

In optimized polymer blending ratio as 50:50 of PEO and PMMA polymers, effect of increasing plasticizer (PEG and EC) concentrations is studied. Figs. 5.91(a)-(d) and Figs. 5.92(a)-(d) show the frequency dependent  $M'$  &  $M''$  spectra for PPSP-5, PPSP-10, PPSP-12 and PPSP-15 polymer electrolyte films respectively at different temperatures. The occurrence of long tail at lower frequencies in  $M'$  and  $M''$  plots indicate the negligible contribution of electrode polarization.  $M'$  shows increasing trend with frequency and level off at higher frequencies. Similar to PPS-system,  $M''(\omega)$  spectra is divided in two regions in  $T < T_m$  and  $T > T_m$  temperature regions and shows two peaks.

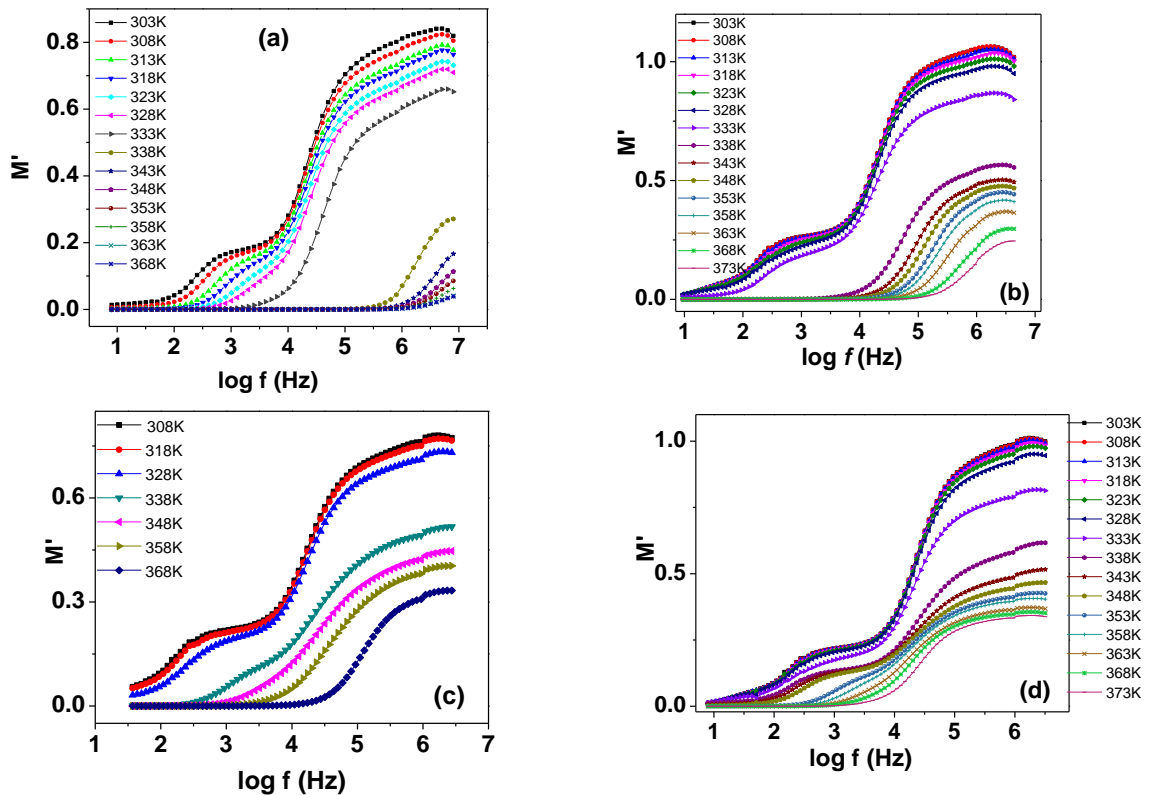


**Fig. 5.91** Frequency dependent real part of modulus plots for (a) PPSP-5 (b) PPSP-10 (c) PPSP-12 and (d) PPSP-15 polymer films at different temperatures.

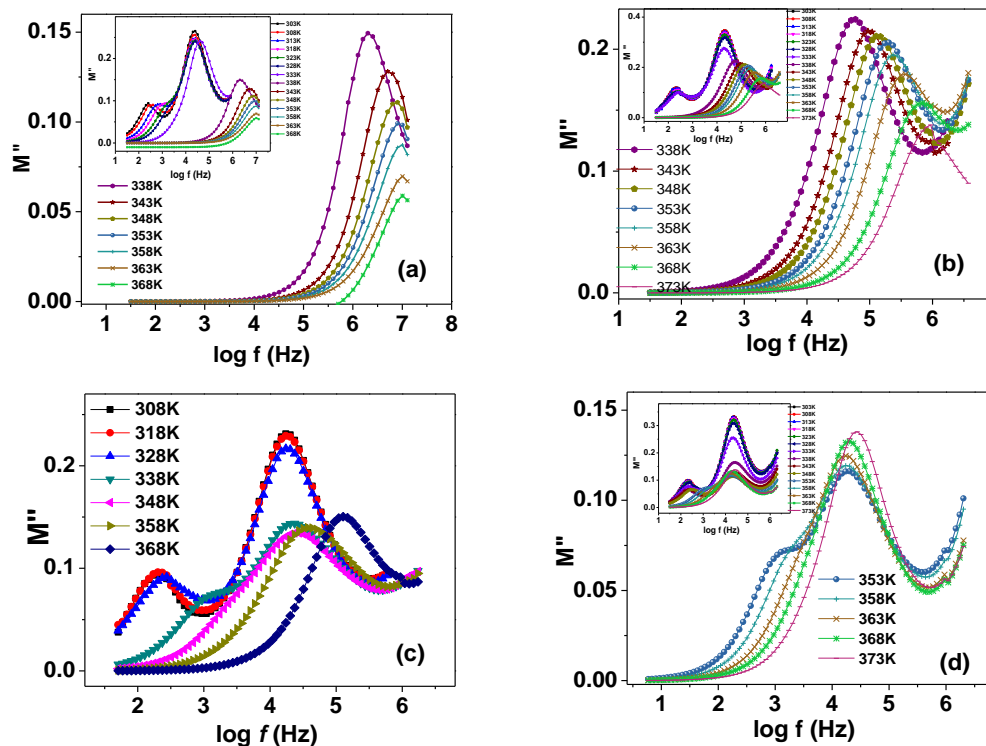


**Fig. 5.92** Frequency dependent real part of modulus plots for (a) PPSP-5 (b) PPSP-10 (c) PPSP-12 and (d) PPSP-15 polymer films at  $T > T_m$  and inset shows the  $T < T_m$  temperatures.

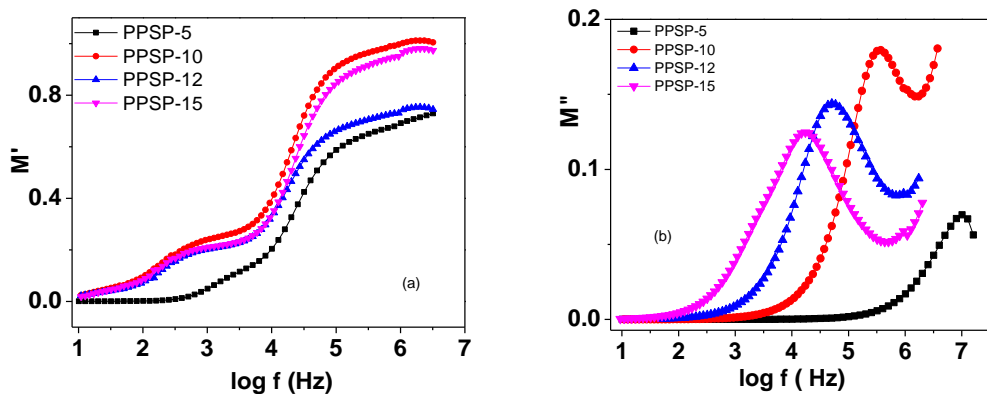


**Fig. 5.93** Frequency dependent (a) real,  $M'$  and (b) imaginary,  $M''$  parts of modulus plots for PPSP-system at 323K and 353K respectively.

With the increase in temperature the peak in low frequency region becomes feeble and disappears near  $T_m$ . The shifting of  $M''$  peak towards higher frequencies side, with the increase in temperature is due to faster movement of the charge carriers ( $\text{Ag}^+$ -ion), leading to decreased relaxation time. The presence of asymmetric relaxation peak

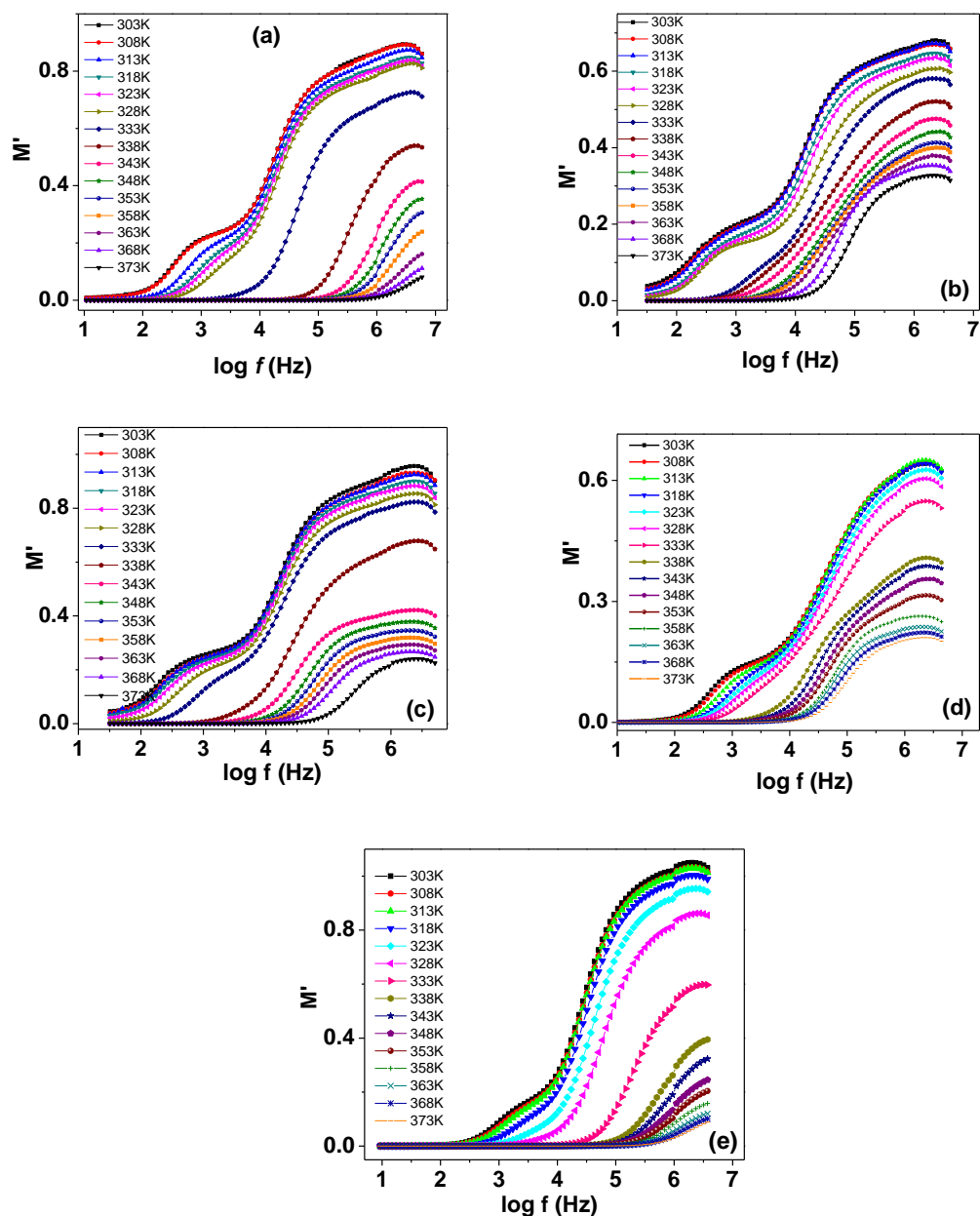


**Fig. 5.94** Frequency dependent real part of modulus plots for (a) PPSE-5 (b) PPSE-7, (c) PPSE-10, (d) PPSE-12 and (e) PPSP-15 polymer films at different temperatures.

indicates non-Debye nature i.e., distribution of relaxation times. Figs.5.93 (a) & (b) depict the  $M'$  and  $M''$  plots for various compositions of PEG plasticizer in silver ion conducting PEO-PMMA polymer blend. Polymer film with highest conductivity shows dispersion at higher frequency and lowest maxima values in their respective plots as

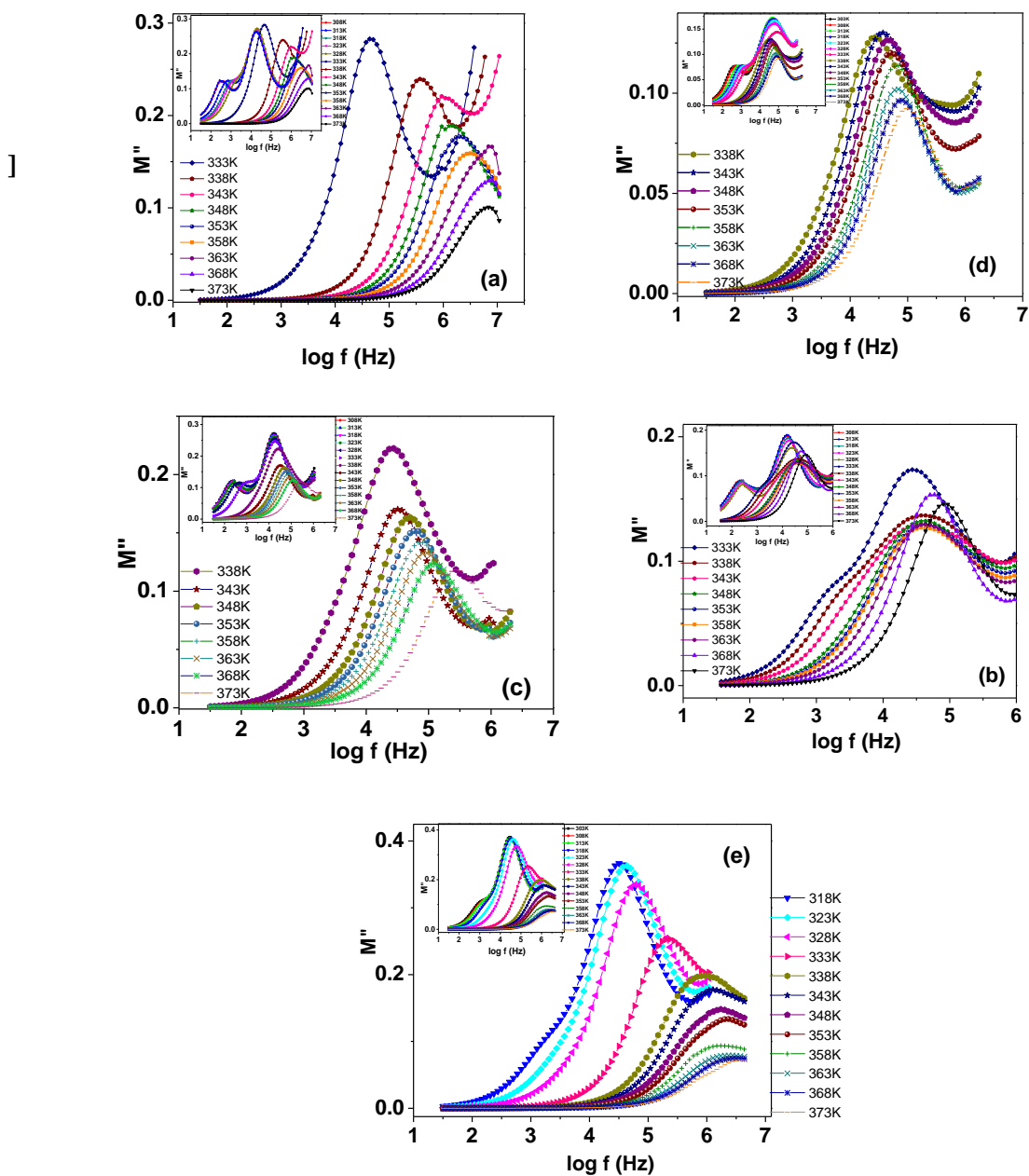


**Fig.5.95** Frequency dependent imaginary part of modulus plots for (a) PPSE-5 (b) PPSE-7, (c) PPSE-10, (d) PPSE-12 and (e) PPSP-15 polymer films at  $T > T_m$ , and inset shows the  $T < T_m$  temperatures.

compared to other samples.

Frequency dependent  $M'$  and  $M''$  spectra of various concentrations of EC in PEO-PMMA-AgNO<sub>3</sub> polymer films are shown in Figs.5.94 and 5.95, respectively.  $M'$  and  $M''$  spectra show an increasing trend with frequency at a particular temperature indicating the

bulk effect. The significantly lower or negligible values of  $M'$  and  $M''$  at lower frequencies indicates that the electrode polarization phenomena makes small contribution to electrical modulus. Below  $T_m$ ,  $M'$  plot shows two dispersion regions (similar to regions observed in PPS and PPSP-systems) which turn into single one as temperature approaches  $T_m$ . Similarly below  $T_m$ , frequency dependent  $M''$  spectra (Fig.5.95) show two peak maxima and as temperature approaches  $T_m$ , first peak in low frequency region disappears and single relaxation peak in mid frequency region remains.

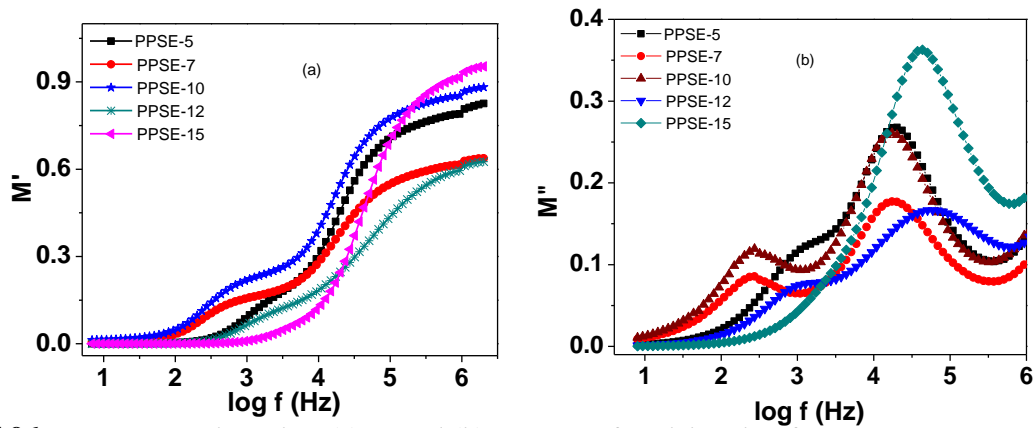


**Fig. 5.96** Frequency dependent (a)  $M'$  and (b)  $M''$  parts of modulus plots for PPSE- system at 323K.

These double relaxation features at temperatures  $T < T_m$  are also in agreement with ac conductivity behavior. This behavior can be explained as at higher temperatures i.e.,  $T > T_m$ , the semi-crystalline regions of PEO melts, in other words, the system becomes amorphous which results in single dispersion in conductivity or single relaxation in modulus plots. At  $T > T_m$ , the frequency corresponding to  $M''_{max}$  is found to shift systematically towards higher frequency side with the increase in temperature. Similar features in modulus spectra at below and above melting temperature  $T_m$  of PEO in mixed electrolytes of MEEP-PEO doped with NaSCN are reported by Subramony *et. al.*[79]. The results obtained in the present system are in good agreement with the Macedo's model [13].

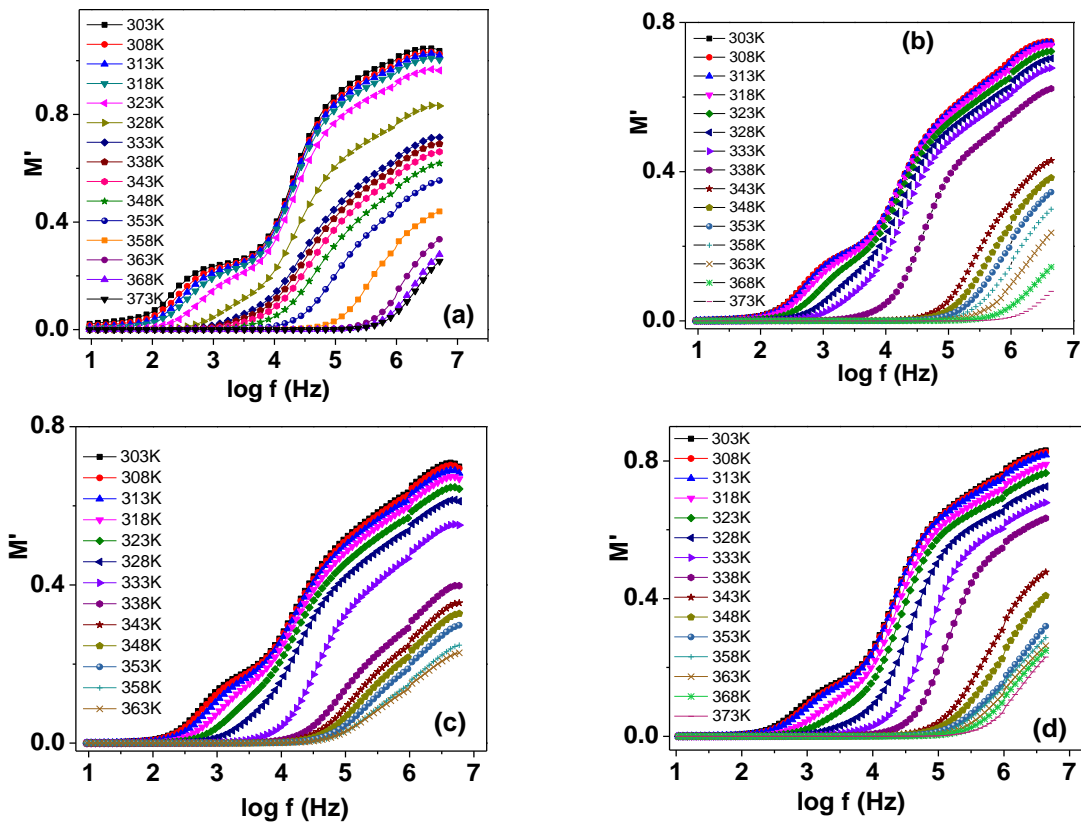


**Fig. 5.96** Frequency dependent  $M'$  plots for (a) PPSA-1 (b) PPSA-2 (c) PPSA-3 and (d) PPSA-4 polymer films at different temperatures.

Further in the present work, the effect of incorporation of nano-fillers on both plasticized (PEG and EC) polymer electrolytes in terms of electrical modulus spectra has been undertaken. Figs.5.96 and 5.97 show the  $M'$  and  $M''$  plots at various temperatures for different concentrations of nano-filler  $\text{Al}_2\text{O}_3$  in PPSA-system, respectively. Similar to blended and plasticized systems,  $M'$  and  $M''$  variation as a function of frequency at different temperatures show two dispersion or relaxation regions, namely one prior to melting and other above melting temperature.  $M'$  and  $M''$  have S-shaped dispersion and a peak respectively in high frequency region. The electrode polarization effects are seems to vanish in this (modulus) formalism in contrast to dielectric formulation (Fig. 5.76 and 5.76).

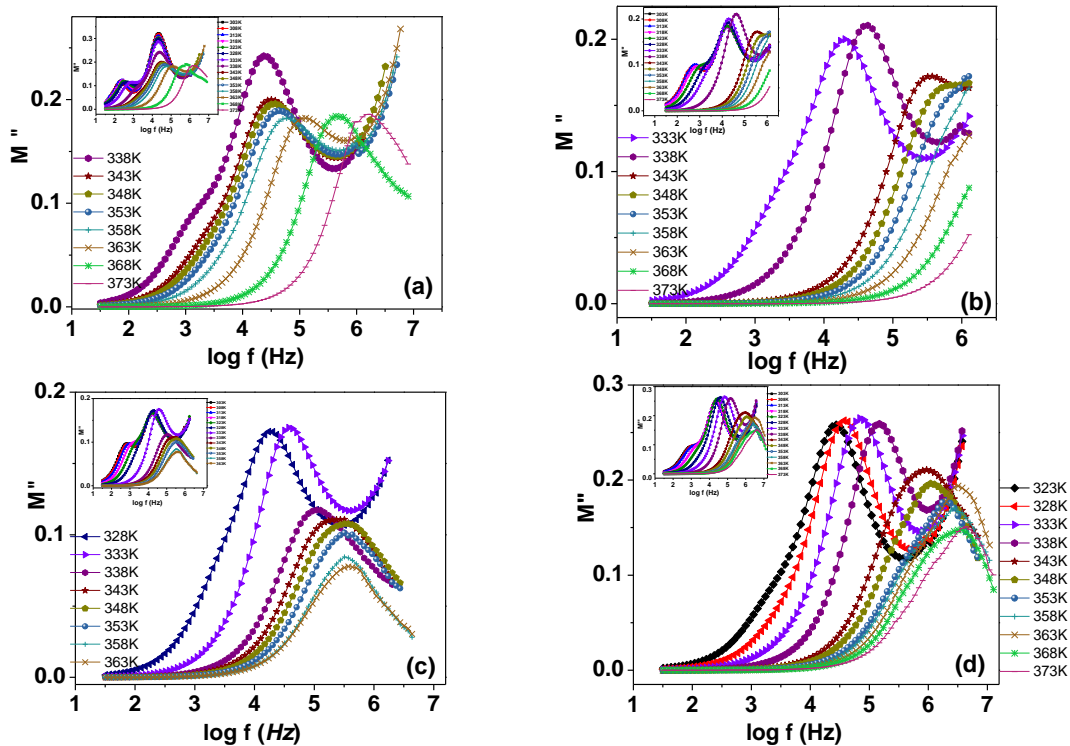


**Fig. 5.97** Frequency dependent  $M''$  plots for (a) PPSPA-1 (b) PPSPA-2 (c) PPSPA-3 and (d) PPSPA-4 polymer films at  $T > T_m$  and inset shows the  $T < T_m$  temperatures.

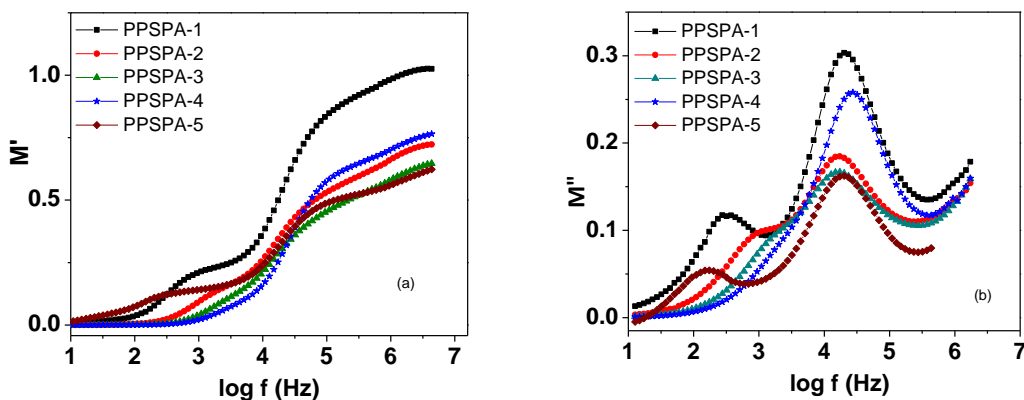


**Fig. 5.98** Frequency dependent (a)  $M'$  and (b)  $M''$  parts of modulus plots for PPSPA-system at 323K.

The observed peaks in  $M''$  spectra are assumed to be related to the translational ion dynamics and mirror the conductivity relaxation of mobile ions. The observed frequency dependent  $M''$  spectra for different compositions indicate a shifting of peak towards high frequency side with the increase in nano-filler concentration. However, a

shift towards lower frequency side is observed for the polymer film with 5 wt% of  $\text{Al}_2\text{O}_3$  (Fig.5.98). This result is found to be in consistent with the characterization as well as conductivity results.

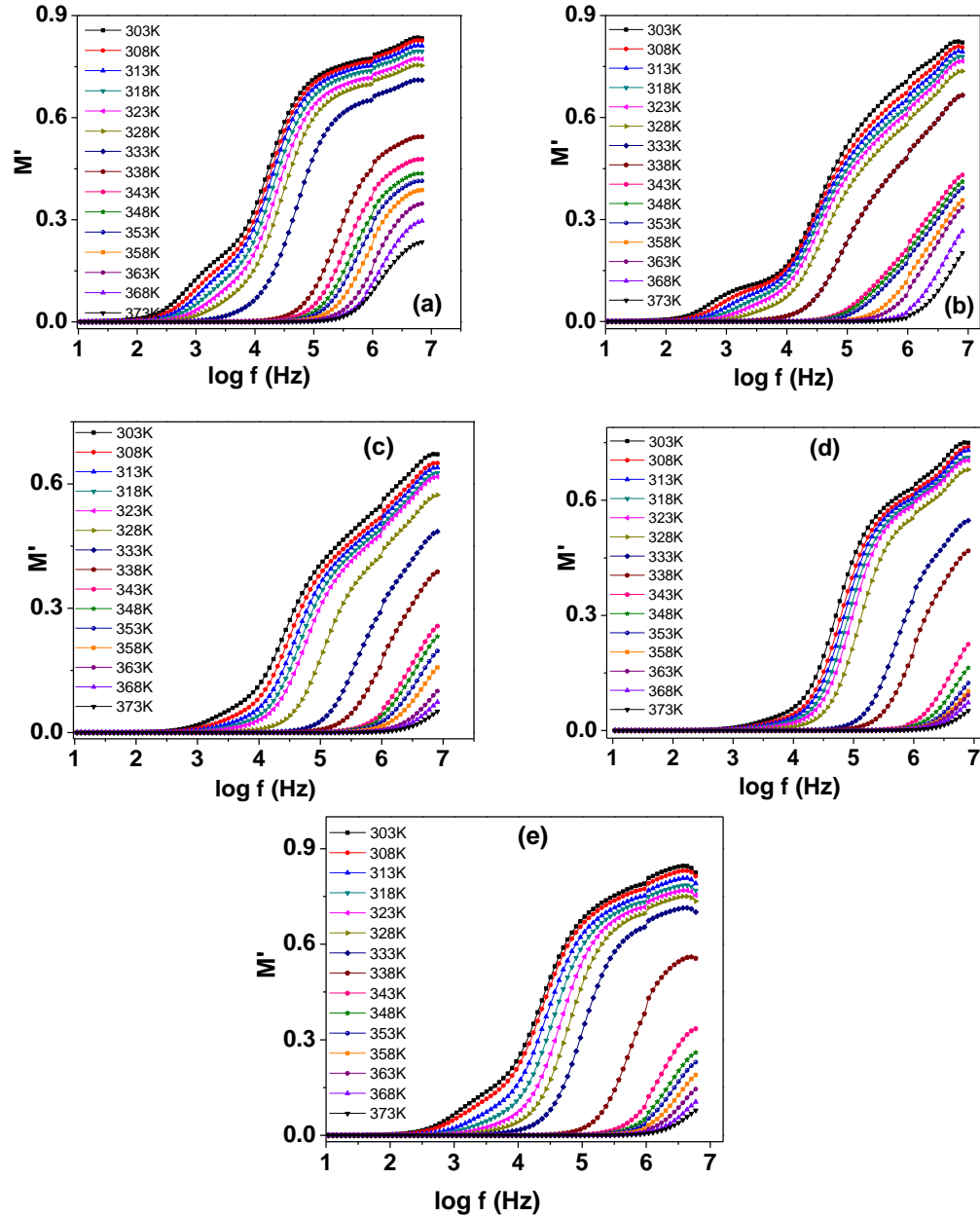


**Fig.5.99** Frequency dependent  $M'$  plots for (a) PPSEA-1 (b) PPSEA-2 (c) PPSEA-3, (d) PPSEA-4 and (d) PPSEA-5 polymer films at different temperatures.

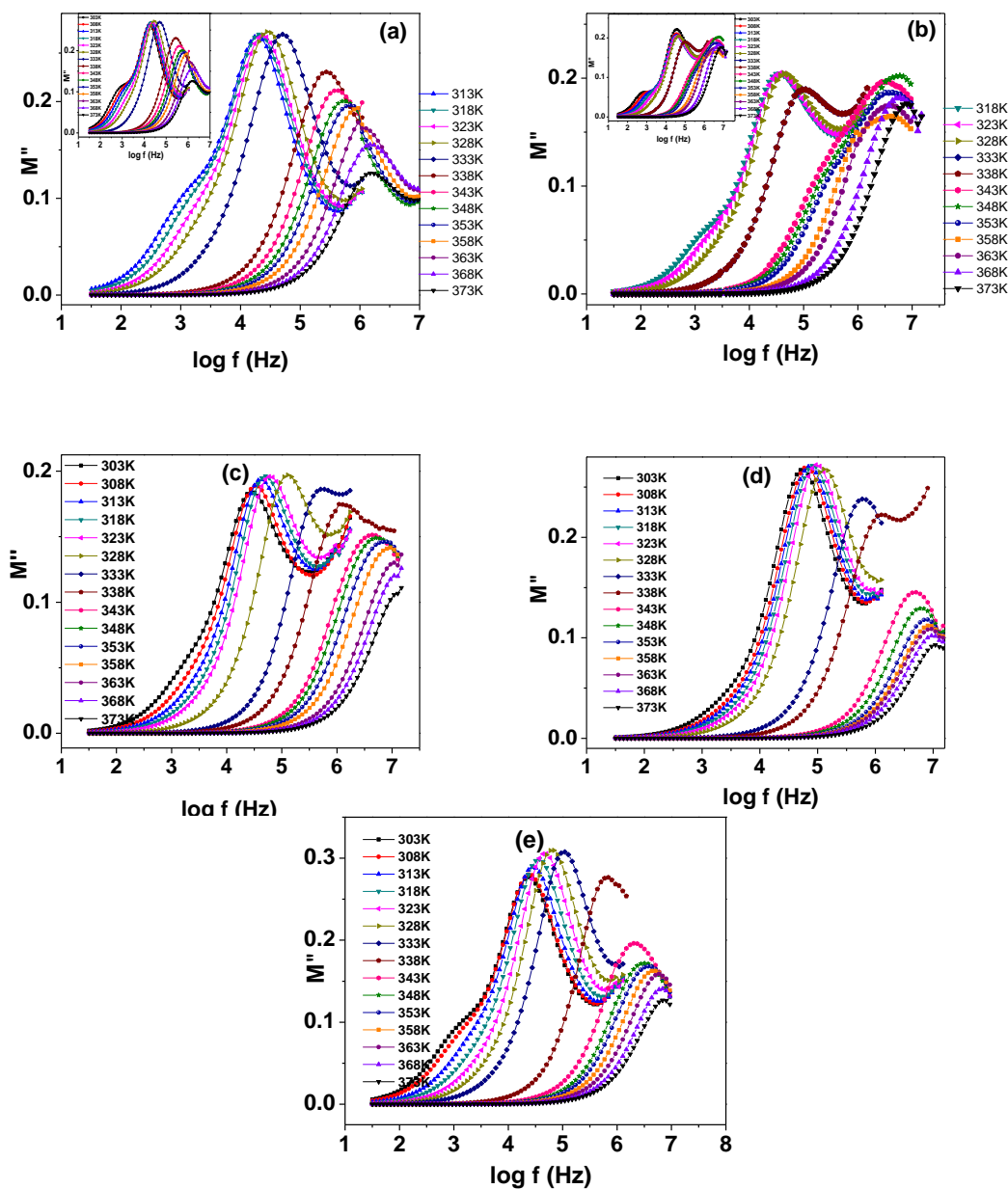


**Fig.5.100** Frequency dependent  $M''$  plots for (a) PPSEA-1 (b) PPSEA-2 (c) PPSEA-3, (d) PPSEA-4 and (e) PPSEA-5 polymer films at different temperatures.

Figs.5.99 and 5.100 show  $M'$  and  $M''$  spectra as a function of frequency in the investigated temperature range for different concentrations of nano-filler  $Al_2O_3$  in polymer blended electrolyte plasticized with EC system (PPSEA-system). In the low frequency region, both  $M'$  and  $M''$  values tend to zero indicating the fact that the electrode polarization make a negligible contribution. The long tail at lower frequencies is due to

the large capacitance associated with the electrodes.  $M'$  and  $M''$  variation as a function of frequency show an increasing trend towards high frequencies. The observed peak in  $M''$  spectra for all polymer films imply that the polymer electrolyte films are ionic conductors. As discussed in previous sections,  $M'$  and  $M''$  variation as a function of frequency at different temperatures of these polymer electrolyte films also show two dispersion or relaxation regions which turns into single one as temperature approaches melting of PEO.  $M'$  and  $M''$  spectra for PPSEA-system at 323K is shown in Fig.5.101. Similar to PPSPA-system, this system also depicts that with increasing the nano-filler concentration, dispersion in  $M'$  spectra and peak maxima in  $M''$  spectra shift towards high frequency side with a reverse behavior in PPSEA-5 sample. This result is in good agreement with the characterization and conductivity results.

The modulus plots are non-symmetric which is in agreement with the non-exponential behavior of the electrical function and it is well described by the Kohlrausch-William-Watts (KWW) exponential function [80-82] as given in eq.2.33 and is known to provide satisfactory fit for the asymmetrical  $M''$  peaks. The *stretched exponent*  $\beta$  values can be evaluated by knowing the full width at half maximum (FWHM) of the  $M''_{max}$  plot, where  $\beta = \frac{1.14}{FWHM}$  value.  $\beta$  is a measure of the degree of deviation from the Debye behavior of single relaxation.  $\beta \sim 0$  indicates the maximum interaction between ions and other factors which give rise to effects for ion transportation. The exponent  $\beta$  is widely used to describe different kinds of relaxation processes in amorphous materials. The calculated values of  $\beta$  for PPS, PPSP, PPSE, PPSPA and PPSEA systems are tabulated in Table 5.2. The  $\beta$  values are found to be greater than 1 for all except for PPSEA system.

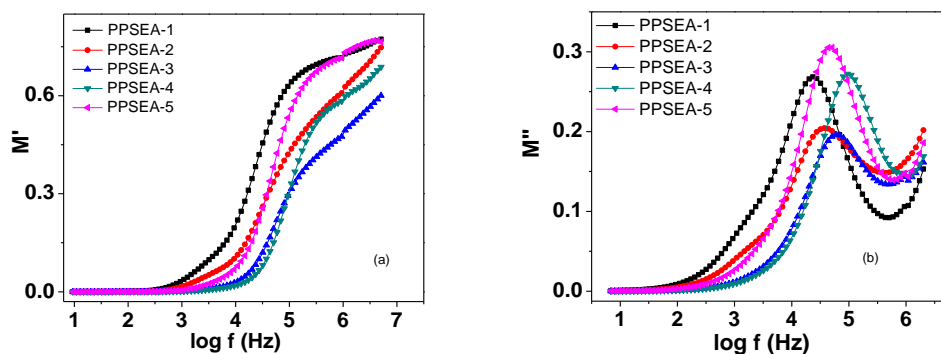


**Fig.5.101** Frequency dependent (a) real,  $M'$  and (b) imaginary,  $M''$  parts of modulus plots for PPSEA-system at 323K.

**Table 5.2** KWW exponential function  $\beta$  values for PPS, PPSP, PPSE, PPSPA and PPSEA systems at different temperatures.

**PPS-system**

T(K)	PPS-10	PPS - 20	PPS - 30	PPS - 40	PPS - 50	PPS - 60	PPS - 70
303	1.33	1.23	1.23	1.21	1.15	1.25	1.02
308	1.37	1.27	1.26	1.28	1.17	1.10	1.02
313	1.32	1.24	1.29	1.25	1.25	1.06	1.07
318	1.29	1.23	1.30	1.24	1.33	1.12	1.11
323	1.31	1.25	1.32	1.22	1.32	1.13	1.14
328	1.26	1.04	1.26	1.23	1.29	1.09	1.22
333	1.23	1.29	1.22	1.20	1.05	1.14	1.20
338	1.26	1.29	0.82	0.99	1.00	1.16	0.84
343	1.26	1.24	0.82	1.27	1.01	1.12	0.87
348	1.32	1.24	0.85	1.12	0.97	1.14	0.85
353	1.25	1.22	0.88	1.43	0.92	1.09	0.88
358	1.20	1.21	0.76	1.10	0.89	1.00	0.91
363	1.20	1.12	0.76	1.24	1.00	0.96	

**PPSP-system**

T(K)	PPSP-5	PPSP-10	PPSP-12	PPSP-15
303	1.06	1.01	0.74	0.98
308	1.06	1.01	0.77	0.98
313	1.11	1.03	0.75	0.73
318	1.12	1.04	0.76	1.00
323	1.13	1.05	0.80	1.01
328	0.95	1.06	0.81	0.98
333	0.83	1.05	0.84	1.00
338	0.87	0.82	0.67	0.77
343	0.85	0.85	0.40	0.70
348	0.85	0.84	0.43	0.69
353	0.88	0.84	0.51	1.05
358	0.78	0.84	0.52	0.92
363	0.87	0.83	0.64	0.68
368	0.74	0.78	0.76	0.76
373	0.77	0.76	0.82	0.84

**PPSE-system**

<b>T(K)</b>	<b>PPSE-5</b>	<b>PPSE-7</b>	<b>PPSE-10</b>	<b>PPSE-12</b>	<b>PPSE-15</b>
303	1.10	1.12	1.04	0.67	0.66
308	1.15	1.132	1.12	0.54	0.64
313	1.18	1.03	1.07	0.66	0.68
318	1.23	1.09	1.07	0.69	0.64
323	1.21	1.05	1.13	0.67	0.58
328	1.15	0.74	1.11	0.59	0.55
333	0.83	0.89	1.16	0.58	0.54
338	0.84	0.40	0.74	0.70	0.71
343	0.79	0.43	0.86	0.77	0.77
348	0.76	0.58	0.87	0.78	0.75
353	0.77	0.56	0.88	0.79	0.81
358	0.75	0.55	0.90	0.84	0.87
363	0.70	0.68	0.86	0.81	0.88
368	0.73	0.88	0.88	0.84	0.85
373	0.78	0.90	0.90	0.86	0.87

**PPSPA-system**

<b>T(K)</b>	<b>PPSPA-1</b>	<b>PPSPA-2</b>	<b>PPSPA-3</b>	<b>PPSPA-4</b>	<b>PPSPA-5</b>
303	0.68	0.99	0.97	1.05	1.05
308	0.65	0.95	0.92	1.11	1.11
313	0.66	0.97	1.04	1.09	1.09
318	0.74	1.02	1.25	1.15	1.15
323	0.76	1.19	1.13	1.12	1.12
328	0.78	1.2	0.63	0.85	0.85
333	0.74	0.73	0.79	0.81	0.81
338	0.71	0.87	0.69	0.85	0.85
343	0.50	0.76	0.61	0.61	0.61
348	0.48	0.68	0.62	0.60	0.61
353	0.53	0.63	0.65	0.61	0.61
358	0.53	0.61	0.73	0.56	0.56
363	0.58	0.62	0.70	0.59	0.59
368	0.68	0.50	--	0.63	0.63
373	0.64	0.30	--	0.59	0.60

**PPSEA-system**

<b>T(K)</b>	<b>PPSEA-1</b>	<b>PPSEA-2</b>	<b>PPSEA-3</b>	<b>PPSEA-4</b>	<b>PPSEA-5</b>
303	0.89	0.45	0.56	0.76	0.82
308	0.95	0.39	0.69	0.77	0.81
313	0.92	0.49	0.67	0.80	0.71
318	0.84	0.37	0.56	0.76	0.75
323	0.82	0.37	0.54	0.74	0.80
328	0.68	0.35	0.70	0.77	0.79
333	0.66	0.36	0.94	0.74	0.84
338	0.62	0.41	0.77	0.56	0.79
343	0.73	0.40	0.53	0.75	0.56
348	0.66	0.30	0.56	0.81	0.60
353	0.64	0.37	0.54	0.85	0.67
358	0.67	0.24	0.63	0.85	0.73
363	0.65	0.29	0.86	0.88	0.82

368	0.61	0.51	0.52	0.88	0.85
373	0.65	0.70	0.66	0.89	0.93

In solid electrolytes, conduction of ionic carriers and dipoles gives the relaxation phenomenon and  $M''$  peak position is a measure for the conductivity relaxation time,  $\tau$ , which is assumed to represent a characteristic time scale of the ionic motion. The observed peak in  $M''(\omega)$  spectrum indicates the conductivity relaxation time of  $\text{Ag}^+$ -ion,

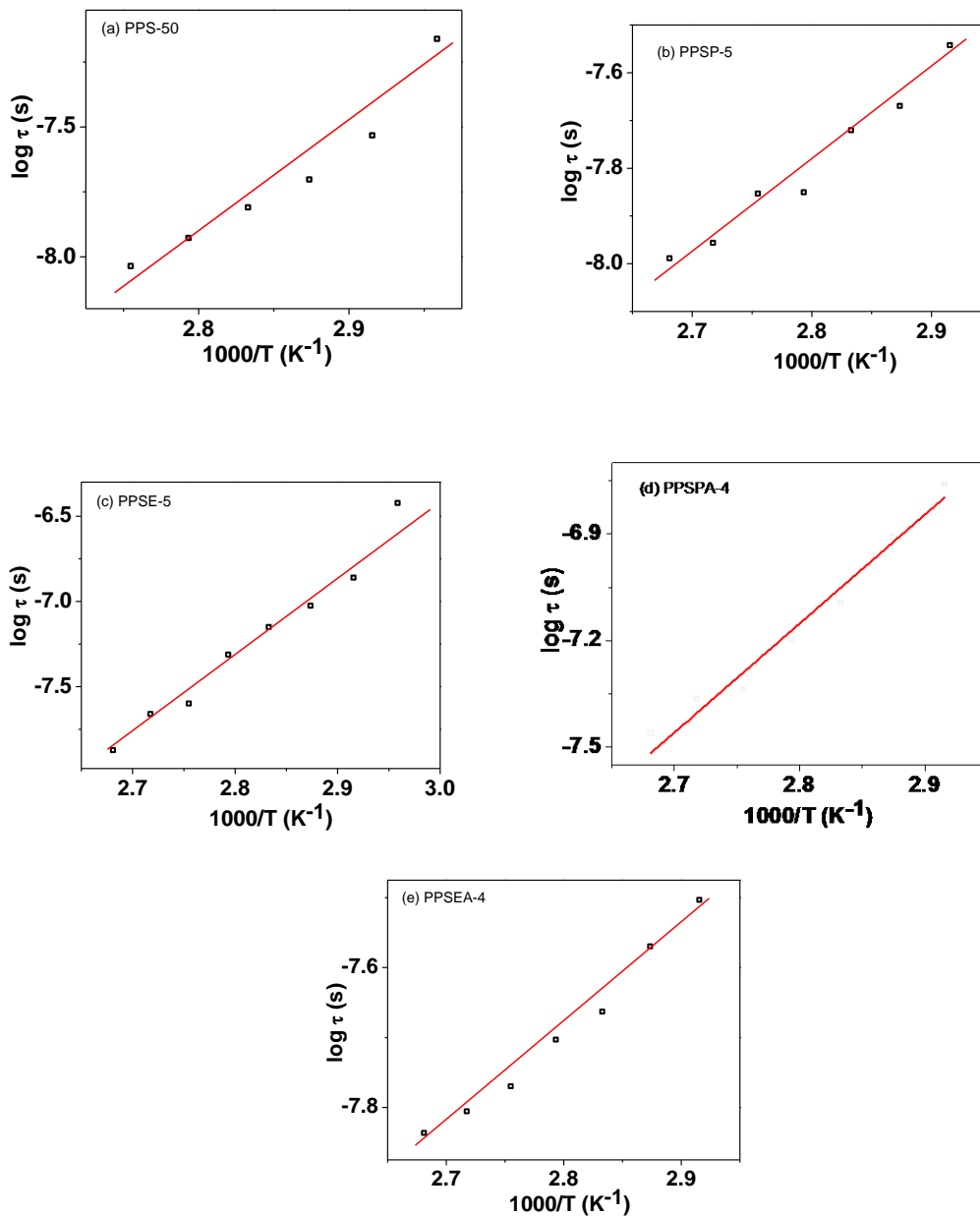


Fig. 5.102 Arrhenius plots of relaxation time in  $T > T_m$  temperature range.

by  $2\pi f_{max} \tau = 1$  [83] where  $f_{max}$  is the peak frequency and  $\tau$  is the relaxation time [84]. Values of the relaxation time are found to decrease with the increase of temperature. Above the melting temperature of PEO in polymer complexes, the variation of relaxation time follows a systematic Arrhenius type behavior (Fig. 5.102). The activation energy for PPS-50 is 0.77 eV which is a slightly lower when compared with the activation energy calculated from conductivity plot (0.80 eV). In the same manner, for other plasticized and nano-composites systems, the variation of relaxation time is found to be Arrhenius in region II (above  $T_m$ ) and the activation energies are found to be in the range of 0.6-0.9 eV. The difference in the values of activation energy indicates that the ions have to overcome different potential barriers in conduction and relaxation processes.

In case of an ideal circuit, the impedance and modulus spectroscopic plots i.e.,  $Z''$ ,  $M''$  versus  $\log f$  plots are completely super imposable and is given below:

$$Z'' = R \frac{\omega RC}{1 + (\omega RC)^2} \quad \text{and} \quad M'' = \frac{C_0}{C} \frac{\omega RC}{1 + (\omega RC)^2} \quad \dots \quad (5.2)$$

The Debye like peak shapes in the spectroscopic plots is given by the term,  $\frac{\omega RC}{1 + (\omega RC)^2}$  in the imaginary parts of both  $Z''$  and  $M''$ . It can be seen that the  $Z''$  peaks are scaled by  $R$  where as the  $M''$  peaks are scaled by  $C_0/C$ . But in practice, for solid electrolytes, they need to be represented by a series array of  $RC$  elements in order to account for various layers within the material, as observed in Section 5.2 [85]. As a result, there occurs usually a distribution of relaxation times, in which case the maxima in the impedance and modulus spectra no longer coincide [85].

To understand the non-Debye behavior of the present system, impedance and modulus spectrum at 343K have been plotted and shown in Fig. 5.103 for PPS-10, PPS-

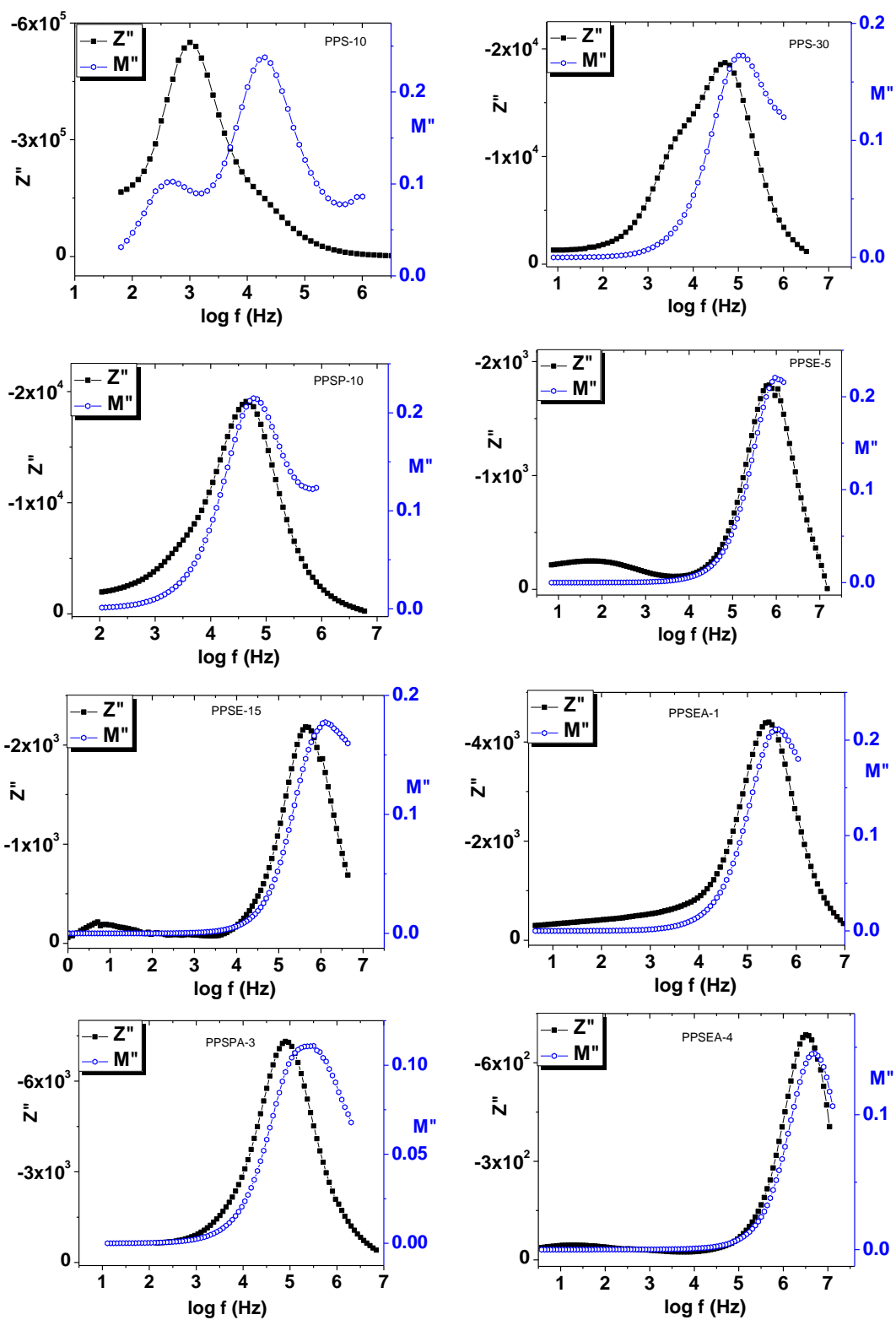


**Fig. 5.103** Frequency dependent  $Z''$  and  $M''$  plots for PPS, PPSP, PPSE polymer electrolyte films at 343K.

30, PPSP-10, PPSE-5, PPSE-15, PPSPA-1, PPSPA-3 and PPSEA-4 polymer electrolyte samples. It can be seen from the figure that  $Z''_{max}$  and  $M''_{max}$  in all spectra do not coincide at the same frequency.  $Z''$  spectrum broadened on the low frequency side while  $M''$  spectrum broadened on the high frequency side indicating distribution of relaxation times, i.e., non-Debye nature of polymer films. Similar impedance and modulus with log frequency behavior are also observed for other samples.

## 5.5 Scaling

Scaling and universality are important concepts that arise in many situations in our physical world [86]. Often one encounters processes in the laboratory that at first appear to behave differently for differing materials, but which when appropriately scaled, display an underlying common behavior among all materials. In these instances, scaling and universality provide to reduce the procedure to simpler parts so that a clear understanding might be achieved. Universality of conductivity and dielectric relaxation processes in an ion conducting materials can be established using scaling of respective spectra to show whether the processes are independent of charge concentration and/or are thermally activated. Scaling is an important property for any dynamic process to possess as it implies that one may separate the thermodynamics, entering only through the scales themselves, from the inherent physics involved in the dynamical process which is completely described by a single scaling function [87]. The ability to scale different data sets so as to collapse all to one common curve indicates the process can be separated into a common physical mechanism modified only by thermodynamic scales [88]. The conductivity, dielectric and modulus spectra are scaled using the different scaling laws given by different workers.

In general, the master curve of AC conductivity spectra can be obtained using the relation [89]:

$$\tilde{\sigma} = F\left(\frac{C}{\sigma_{dc}} \omega\right)$$

where  $F$  is the function describing the master scaling,  $C$  may depend on variables like charge carrier concentration  $n$  and temperature  $T$  etc.

Different scaling approaches to scale AC conductivity and modulus spectra by many workers have been reported in past to establish time-temperature superposition principle (TTSP) of conduction or relaxation processes. In these scaling approaches, dc conductivity ( $\sigma_{dc}$ ) is used to scale AC conductivity i.e.;  $\frac{\sigma'}{\sigma_{dc}}$  and frequency axis is scaled by different factors as  $\frac{\omega}{\omega_p}$  [90],  $\frac{f}{\sigma_{dc}T}$  [91],  $\frac{f}{\sigma_{dc}T} x$  and  $\frac{f \varepsilon_0 \Delta \varepsilon}{\sigma_{dc}}$  [88] etc. where  $\omega_p$ ,  $x$ ,  $\varepsilon_0$  and  $\Delta \varepsilon$  are hopping frequency, number density of mobile ions, the permittivity of free space (constant) and permittivity change respectively. Usually, the frequency- and temperature-dependent conductivity spectra obey the time-temperature superposition principle. This means that, for a given material, the conductivity isotherms can be collapsed to a master curve upon appropriate scaling of the conductivity and frequency axes. The master curves of different solids may have very similar shapes.

In the present studies, Ghosh scaling's approach [90] is used to scale conductivity and modulus spectra, since it takes into account the dependence of the conductivity spectra on structure and the possible changes of the hopping distance experienced by the mobile ions. Ghosh's scaling approach is given by the relation:

$$\frac{\sigma'(\omega)}{\sigma_{dc}} = F\left(\frac{\omega}{\omega_p}\right)$$

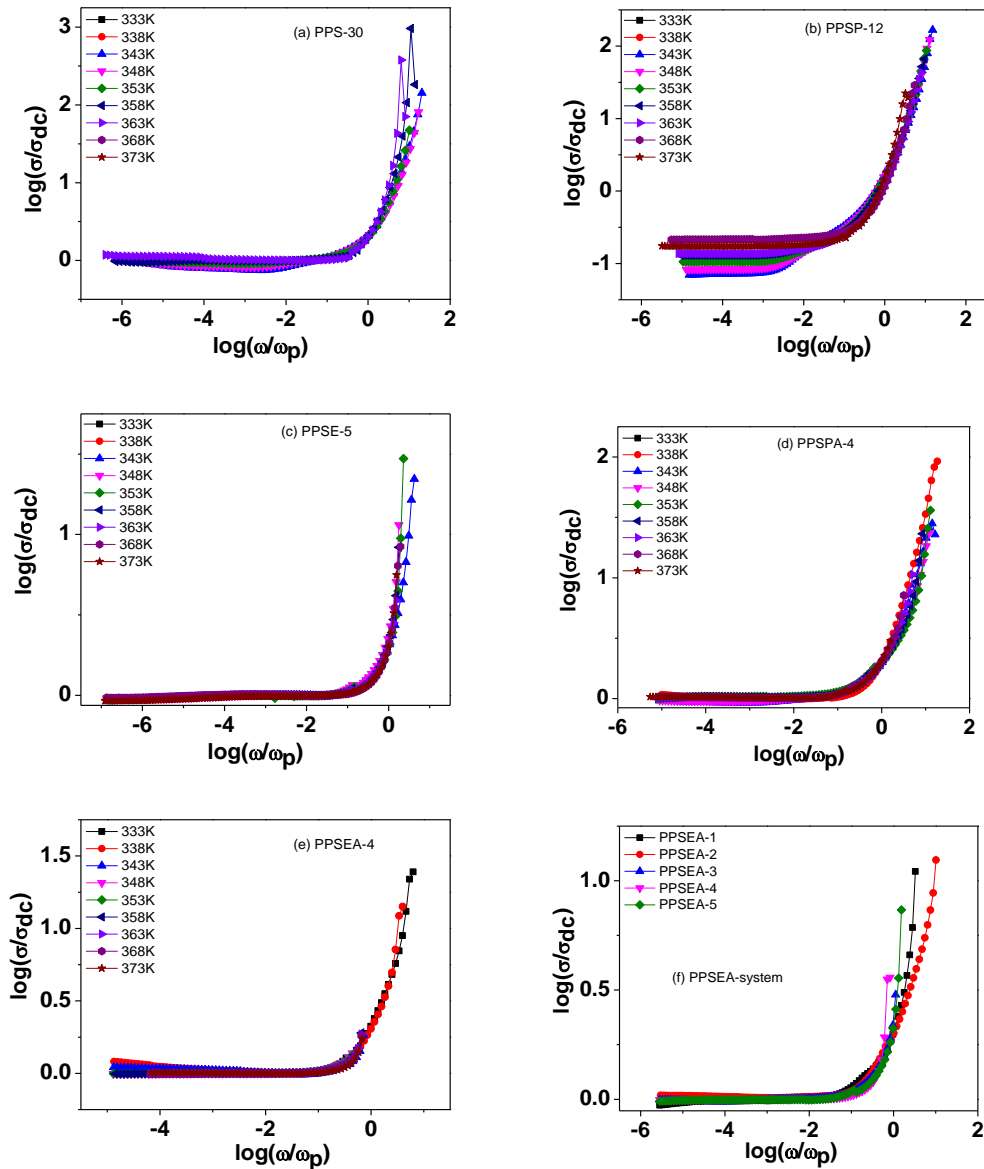


**Fig. 5.104** Scaled AC conductivity spectra for (a) PPS-30 (b) PPSP-12, (c) PPSE-5, (d) PPSPA-4, (e) PPSEA-4 at different temperatures and (f) PPSEA-system at 343K.

Figs.5.104 (a)-(e) show the scaled spectra of AC conductivity, using Ghosh's scaling law, for PPS-30, PPSP-12, PPSE-5, PPSPA-4 and PPSEA-4 polymer electrolyte films, respectively at different temperatures ( $T > T_m$  temperature range). It is observed from figures that all AC conductivity spectra merge near perfectly onto a single master

curve giving a TTSP spectra. Compositional AC conductivity spectra for all PPS, PPSP, PPSE, PPSPA and PPSPE polymer system at a particular temperature are plotted individually and analyzed. Scaled conductivity spectra for all the samples for PPSEA-system gives a nearly same curve only at a particular temperature (Fig.5.104(f)) while other systems revealed merging at higher frequencies with deviation at lower frequencies, which might be occurring due to dominance of polarization at electrodes at these frequencies.

The scaling behavior of the imaginary part of modulus spectra provides an insight into temperature and composition dependence of the relaxation dynamics. Imaginary part of modulus spectra is generally scaled using Ghosh's scaling law in which the modulus axis (y-axis) is scaled by peak maximum value of modulus ( $M''_{max}$  value) and frequency axis (x-axis) is scaled by frequency corresponding to maximum value of modulus. In other words, scaling function can be defined as:

$$\frac{M''}{M''_{max}} = F\left(\frac{f}{f_{max}}\right)$$

A remarkable characteristic of this type of data representation is that a direct comparative analysis can be performed for each branch of curves  $M''/M''_{max}$  versus  $\log(f/f_{max})$ . In the same way, any type of dispersion phenomenon can be easily detected. The scaling of the frequency by  $f_{max}$  parameter gives a distribution of  $M''/M''_{max}$  values considering logarithmic representation at around  $(f/f_{max})=1$ . At frequency above this value, some degree of dispersion can be observed depending on the composition formulation and temperature of measurement.

Figs.5.105 (a)-(b) show the normalized spectra of imaginary part of modulus,  $M''$  at different temperatures for PPS-30, PPS-50 and PPS-70. Fig.5.105 (c) represents the

normalized modulus spectra at 353K for different concentration of PEO. The normalized plot of imaginary part of modulus shows a single normalized peak i.e., merging of  $M''$  plot at different temperatures and as well as for different concentrations of PEO at a particular temperature confirming the temperature and as well as compositional independence of relaxation in PEO: PMMA polymer blend electrolyte system. Similar behavior is observed for other samples as well. This time-temperature superposition attributes a temperature independent relaxation behavior or the dynamical processes occurring at different temperatures are independent of temperature. The asymmetrical shape of the plots attributes the existence of distribution of relaxation times.

Scaling approach in  $M''$  spectra for PEG and EC containing systems are also

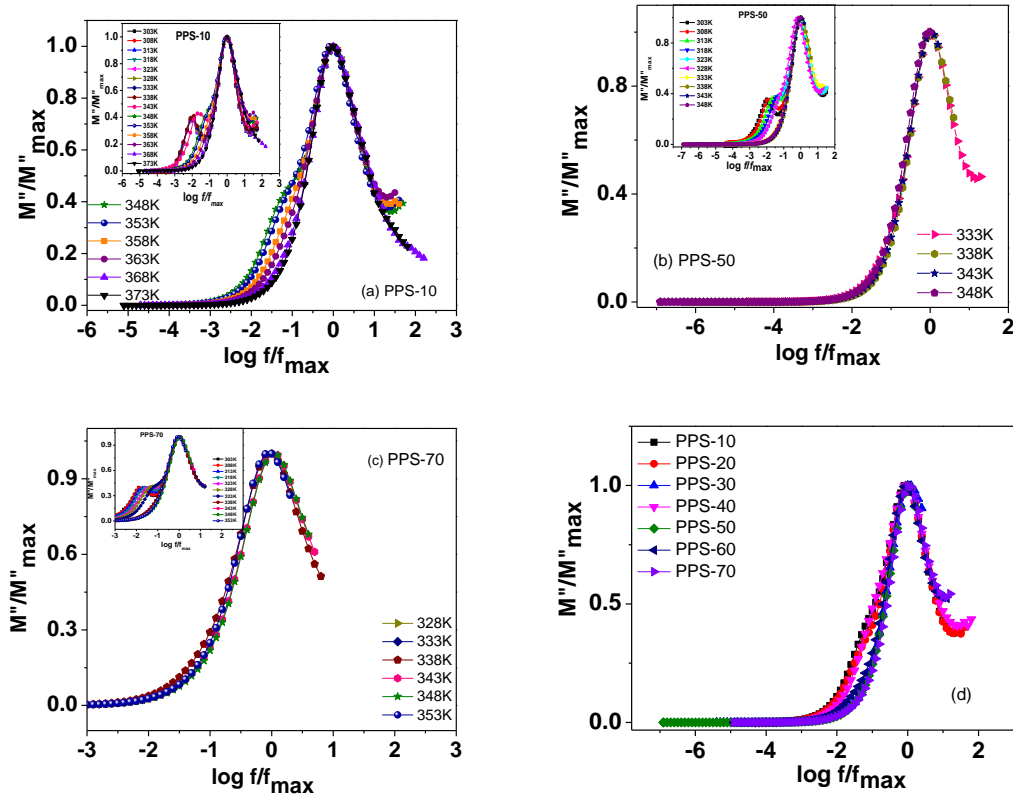


**Fig. 5.105** Scaled  $M''$  spectra for (a) PPS-30 (b) PPS-50, (c) PPS-70 at  $T > T_m$  temperatures (inset shows the complete temperature range) and (d) PPS-system at 353K.

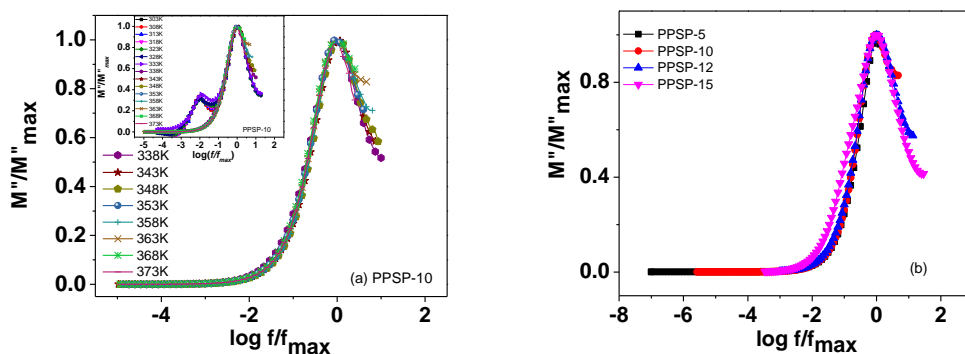


**Fig. 5.106** Scaled  $M''$  spectra for (a) PPSP-10 sample at  $T > T_m$  temperatures (inset shows the complete temperature range)(b) PPSP-system at 358K.

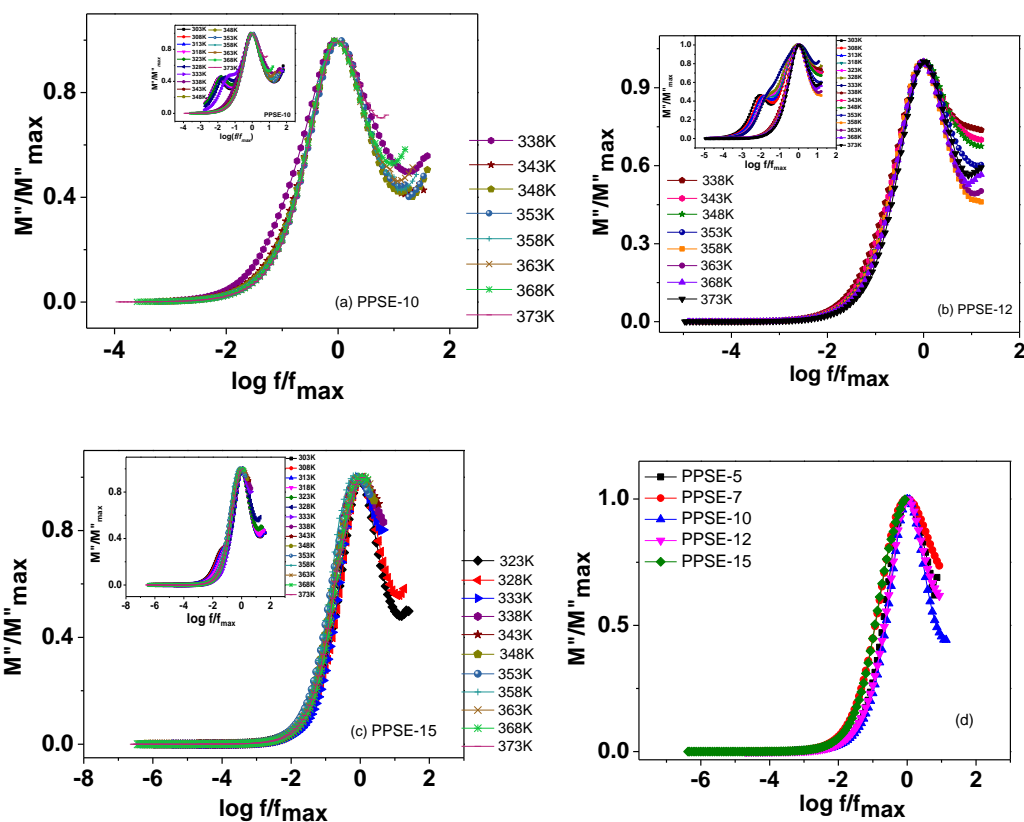


**Fig. 5.107** Scaled  $M''$  spectra for (a) PPSE-10, (b) PPSE-12, (c) PPSE-15 samples at  $T > T_m$  temperatures (inset shows the complete temperature range)(d) PPSE-system at 358K.

applied. The perfect merging of scaled  $M''$  versus normalized frequency plot at  $T > T_m$  temperatures is observed and shown in Fig. 5.106(a) for PPSP-10. Other concentrations of this series also showed the similar behavior. A master plot of the

modulus isotherms for the PPSP system at 358K is shown in Fig. 5.106(b). The near perfect overlap of the data at different temperatures on a single master curve indicates that all the dynamic processes occurring at different time scales exhibit the relaxation mechanism involved is temperature independent or merely thermally activated. Similarly the normalized imaginary part of the modulus versus normalized frequency  $\log (f/f_{max})$  plots for PPSE-10, PPSE-12 and PPSE-15 polymer electrolyte films are shown in Fig. 5.107(a)-(c), respectively. It can be seen from figures that the plots are clearly super imposable and the data points are found to collapse very well for all the temperatures ( $T > T_m$  temperatures) studied. The super imposition of the plots indicates that the dynamical processes of ion transport are same throughout the investigated temperature and frequency window. The scaled spectra of  $M''$  for different compositions of PPSE-system at 358K is shown in Fig. 5.107(d). The curves present nearly superimposition leading to the same master curve behavior at different compositions. This development suggests a common relaxation mechanism in these polymer electrolytes for the studied composition range.

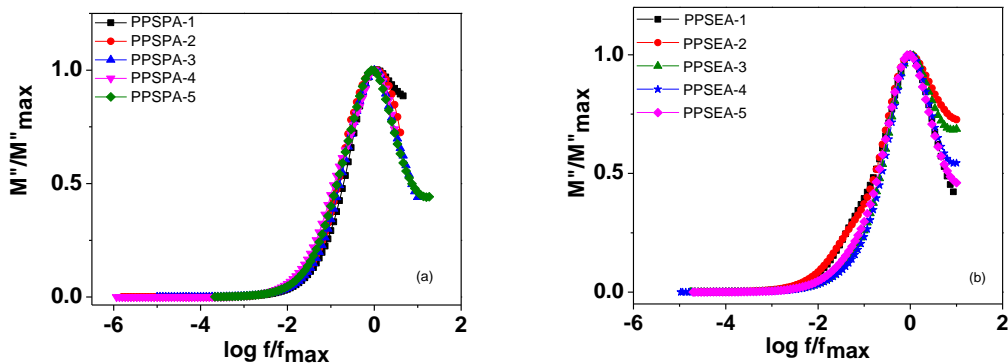


**Fig. 5.108** Scaled  $M''$  spectra for (a) PPSPA and (b) PPSEA-systems at 363K.

Next to plasticized polymer electrolyte systems, scaling in nano-composites plasticized with PEG and EC is carried out. Fig. 5.108 (a) & (b) depict the scaling of

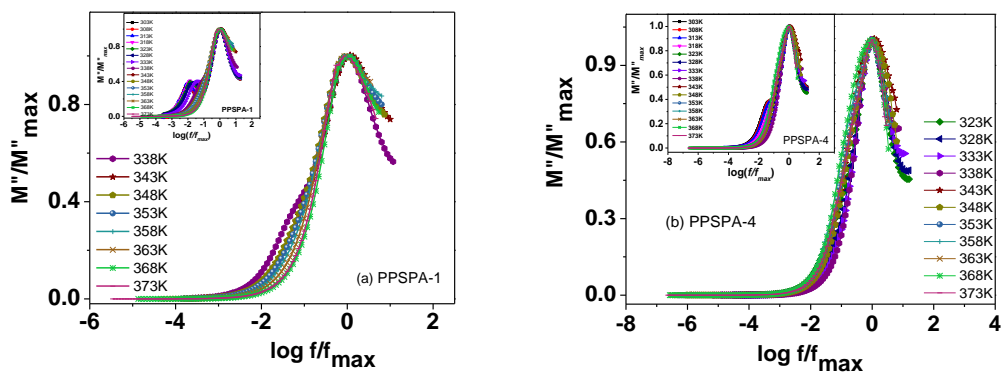


Fig. 5.109 Scaled  $M''$  spectra for (a) PPSPA-1 and (b) PPSPA-4 at  $T > T_m$  temperatures (inset shows the complete temperature range).

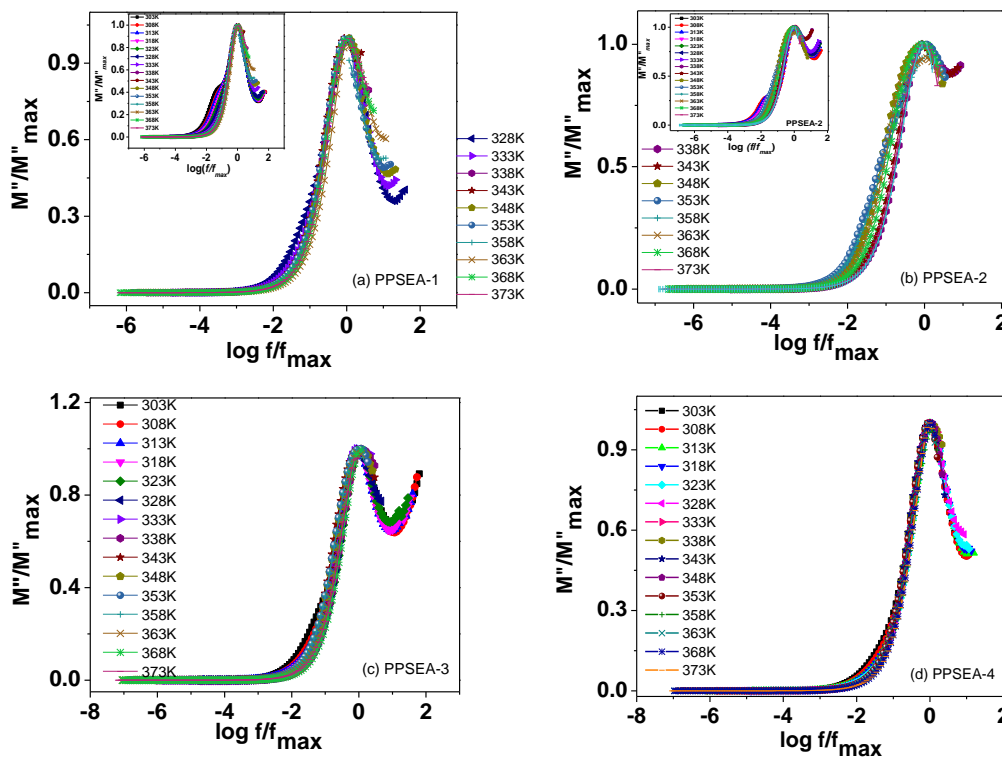


Fig. 5.110 Scaled  $M''$  spectra for (a) PPSEA-1 (inset shows the complete temperature range), (b) PPSEA-2, (c) PPSEA-3 and (d) PPSEA-4 samples at different temperatures.

modulus of PPSPA and PPSEA-systems at 363K, respectively. Perfect overlapping of  $M''$  spectra for all compositions in their respective systems is observed indicating that the relaxation processes of conducting  $Ag^+$ -ions in PEG and EC containing polymer nano-composites are independent of composition. The temperature wise scaled  $M''$  plots for

PPSPA-1 and PPSPA-2 samples are depicted in Fig. 5.109(a) & (b). The same plots for PPSEA-1, PPSEA-2, PPSEA-3 and PPSEA-4 samples are shown in Fig.5.110 (a) - (d). Temperature wise as well compositional perfect merging of modulus spectra giving single master curve is the beauty of polymer nano-composite system plasticized with PEG and EC.

## References:

1. J.R. Macdonald, *Impedance Spectroscopy Emphasizing Solid Materials and Systems*, Wiley, New York, 1987.
2. J.R. Macdonald, *Annals Biomed. Engg.* 20(1992) 289-305.
3. E. Barsoukov, J.R. Macdonald, *Impedance Spectroscopy: Theory, experiment, and applications*, Wiley, New York, 2005.
4. U. Retter, H. Lohse *Chapter II.5, Electrochemical Impedance Spectroscopy*, F. Scholz (ed.), *Electroanalytical Methods*, 2nd ed., Springer-Verlag Berlin Heidelberg 2010.
5. S. Nakamura, H. Nishikawa, T. Aoki, Y. Ogami, *J. Power Sources* 186 (2009) 278–285
6. F. M. Gray, *Solid Polymer Electrolytes* (VCH, New York, 1991).
7. C.S. Sunandana, P.S. Kumar, *Bull. Mater. Sci.* 27(2004)1–17.
8. D. K. Pradhan, R. N. P. Choudhary, B. K. Samantaray, *Int. J. Electrochem. Sci.* 3 (2008) 597 - 608.
9. A.K. Jonscher, *Dielectric relaxation in Solids*, Chalsea Dielectric press, London, 1983.
10. W. Cao and R. Gerhardt, *Solid State Ionics* 42 (1990) 213-221
11. Y. Feldman, A. Puzenko, Y. Ryabov, *Fractals, Diffusion, and Relaxation in Disordered Complex Systems: A Special Volume of Advances in Chemical Physics, Volume 133, Part A*, W. T. Coffey and Y. P. Kalmykov. (Ed.), 2006 John Wiley & Sons, pp. 1-125.
12. W. Graham, D.K. Thomas. "Phenomenological and molecular theories of dielectric and electrical relaxation of materials." Novocontrol Applications Note—Dielectrics (1998).
13. P.B. Macedo, C.T. Moynihan, R. Bose, *Phys. Chem. Glasses* 13 (1972) 171.
14. C. Chanmal, J. Jog, *Characterization Techniques for Polymer Nanocomposites V. Mittal*. (Ed.), 2012 Wiley VCH Verlag & Co., pp. 167-181.
15. J.R. Macdonald, W. B. Johnson. *Impedance Spectroscopy: Theory, Experiment, and Applications*, Second Edition 2005 John Wiley & Sons.
16. M.S. Jayswal, D.K. Kanchan, P. Sharma, M. Pant, *Solid State Ionics* 186 (2011)7–13.
17. G.P. Pandey, Y. Kumar, S.A. Hashmi, *Solid State Ionics* 190(2011) 93–98. 16.
18. S.K. Chaurasia, S.K. Singh, S. Chandra, *Solid State Ionics* 183(2011) 32–39.
19. B.K. Money, K. Hariharan, *Appl. Phys. A* 88(2007) 647-652.
20. S.D. Druger, M.A. Ratner, A. Nitzam *Phys. Rev. B*, 31 (1985), 3939.
21. S.D. Druger, A. Nitzam, M.A. Ratner, *J. Chem. Phys.* 79 (1983) 3133–3143.
22. V. Raja, A.K. Sharma, V.V.R.N. Rao, *Mater. Lett.* 58 (2004) 3242–3247.]
23. J. Straka, P. Schmidt, J. Dybal, B. Schneider, J. Spevacek, *Polymer* 36 (1995) 1147-1155.
24. P.K. Singh, R. Pratap, A. Chandra, *Prog. Cryst. Growth Character. Mater.* 44 (2002) 175-182.
25. S. Chandra, S.A. Hashmi, M. Saleem, R.C. Agrawal, *Solid State Ionics* 67 (1993)1-7.
26. R.C. Agarwal, S.A. Hashmi, G.P. Pandey, *Ionics* 13(2007) 295-298.
27. Th. J. Singh, T. Mimani, K.C. Patil, S.V. Bhatt, *Solid State Ionics* 154–155(2002) 21– 27.
28. M. Stainer, H. L. Charles, D.H. Whitmore, D.F. Shriver, *J. Electrochem. Soc.* 131 (1984) 784–790.
29. A. Bunde, W. Dietrich, E. Roman, *Phys. Rev. Lett.* 55(1985)5.
30. S. Rajendran, M. Sivakumar, R. Subadevi, *Mater. Lett.* 58(2004) 641-649.
31. S.A. Suthanthiraraj, D.J. Sheeba, B.J.Paul, *Mater. Res. Bull.* 44 (2009)1534-1539.
32. M. Kumar, S.S. Sekhon, *Euro. Polymer J.* 38 (2002) 1297–1304.
33. G.P. Pandey, S.A. Hashmi, *J. Power Sources* 187 (2009) 627–634.
34. K.S. Kim, S.Y.Park, S.Choi, H.Lee *J. Power Sources* 155(2006) 385–390.
35. N. Gondaliya, D.K. Kanchan, P. Sharma, P. Joge, *J. Appl. Polymer Sci.* 125(2012)1513–1520.
36. M. Kumar, S.S. Sekhon, *Ionics* 8 (2002) 223-233.
37. G.P. Pandey, Y. Kumar, S.A. Hashmi *Solid State Ionics* 190(2011)93–98.

38. Y. Kumar, S.A. Hashmi, G.P. Pandey, *Electrochim. Acta* 56(2011)3864–3873.
39. A. Bhide, K. Hariharan, *Euro. Poly. J.*, 43 (2007) 4253-4270.
40. T. David, M.H. Cohen, *J. Chem. Phys.* 34 (1961) 120.
41. H. Fujita, *Adv. Polymer Sci.* 3 (1961) 1-47.
42. H.J. Rhoo, H.T. Kim, J.K. Park, T.S. Hwang, *Electrochim. Acta* 42(1997) 1571-1579.
43. B. Huang, Z. Wang, G. Li, H. Huang, R. Xue, L. Chen, F. Wang, *Solid State Ionics* 85(1996) 79-84.
44. C.W. Nan, L. Fan, Y. Lin, Q. Cai, *Phys. Rev. Lett.* 91(2003)266104.
45. P. Ekanayake, M.A.K.L. Dissanayake, *J. Solid State Electrochem.* 13 (2009) 1825.
46. W. Wiexzorek, K. Such, Z. Florjanczyk, J.R. Stevens, *Electrochim. Acta* 40 (1995) 2417.
47. S. Rajendran, O. Mahendran, R. Kannan, *Phys. Chem. Solids* 63 (2002) 303.
48. M.R. Johan, O.H. Shy, S. Ibrahim, S. M. M. Yassin, T. Y. Hui, *Solid state Ionics* 196 (2011) 41.
49. M.R. Johan, L.B. Fen *Ionics* 16(2010)335–338.
50. M. Watanabe, T. Endo, A. Nishimoto, K. Miura, M. Yanagida *J. Power Sources* 81–82 (1999)786–789
51. K.K. Maurya, N. Srivastava, S. A. Hashmi, S. Chandra, *J. Mater. Sci.* 27 (1992) 6357-6364.
52. M.R. Johan, O. H. Shy, S. Ibrahim, S.M. M. Yassin, T.Y. Hui, *Solid State Ionics* 196(2011)41-47.
53. M.R. Johan, L.M. Ting, *Int. J. Electrochem. Sci.* 6 (2011) 4737 – 4748.
54. M. Pant, *Ph.D. Thesis*, submitted to M.S. University of Baroda, Gujarat, 2011.
55. A.K. Jonscher, *Nature* 267(1977)673.
56. A.K. Jonscher, *J. Phys. D: Appl. Phys.* 32 (1999) R57–R70.
57. R. Belin, G. Taillades, A. Pradel, M. Ribes, *Solid State Ionics* 136–137 (2000) 1025–1029.
58. A.N. Papathanassiou, I. Sakellis, J. Grammatikakis, *Appl. Phys. Lett.* 91 (2007) 122911.
59. J.P. Tiwari, K. Shahi, *Philosophical Magazine* 87(2007) 4475-4500.
60. K. Funke, R. D. Banhatti, S. Bruckner, C. Cramer, C. Krieger, A. Mandanici, C. Martiny, I. Ross, *Phys. Chem. Chem. Phys.* 2002,4, 3155-3167
61. M. Kumar, T. Tiwari, N. Srivastava, *Cabohydrate Polymers* 88 (2012)54-60.
62. M. Marzantowicz, J.R. Dygaa, F. Krok, *Electrochim. Acta* 53 (2008) 7417–7425.
63. S. Ramesh, T. F. Yuen, C. J. Shen, *Spectrochim. Acta A* 69 (2008) 670-675.
64. S.O. Nelson, *J. Microwave Power Electromag. Energy* 44(2010) 98-113.
65. F. Kremer, A. Schonhals, eds., *Broadband Dielectric Spectroscopy*, Springer-Verlag, Berlin, 2003.
66. A.K. Jonscher, K. L. Deori, J.M. Reau, J. Moali, *J. Mater. Sci.* 14(1979) 1308-1320.
67. J. Soumen, W. H. Zhong, *J. Mater. Sci.* 43(2008) 4607-4617.
68. M.G. McLin, C.A. Angell, *Solid State Ionics* 53-56 (1992) 1027-1036
69. A.L. Saroj, R.K.Singh, *J. Phys. Chem. Solids* 73(2012)162–168.
70. E. Sheha, M.K. El-Mansy, *J. Power Sources* 185 (2008) 1509–1513.
71. A. Sawada, *J. Chem. Phys.* 129(2008) 064701.
72. G.J. Papaioannou, M. Exarchos, V. Theonas, J. Psychias, G. Konstantinidis, D. Vasilache, A. Muller, D. Neculoiu, *Appl. Phys. Lett.* 89(2006)103512.
73. M.M. Elkholy, L.M. S. El-Deen, *Mater. Chem. Phys.* 65(2000)192–196.
74. S. Ibrahim, S.M.M. Yasin, N. M. Nee, R. Ahmad, M.R. Johan, *Solid State Commun.* 152 (2012) 426–434
75. A.D. Hollingsworth, *Current Opinion in Colloid Interface Science* 18 (2013) 157–159.
76. A. Karnakar, A. Ghosh, *Current Appl. Phys.* 12(2012) 539-543.
77. R.J. Grant, M.D. Ingram, A. R. West, *Electrochim. Acta* 22(1977)729-734.
78. D.P. Almond, A.R. West, *Nature* 306 (1983) 456-457.
79. J.A. Subramony, A.R. Kulkarni *Solid state Ionics* 67(1994)235-239.
80. R. Kohlrausch, *Prog. Ann. Phys. Chem.* 91 (1854) 179.

81. G. Williams, D.C. Watts, *Trans. Faraday Soc.* 66 (1970) 80.
82. G. Williams, D.C. Watts, S.B. Dev and A.M. North, *Trans. Faraday Soc.* 67 (1971) 1323.
83. M. Pant, D.K. Kanchan, N. Gondaliya, *Mater. Chem. Phys.* 115(2009) 98-104.
84. B. K. Money, K. Hariharan, J. Swenson, *Solid State Ionics* 225 (2012) 346–349.
85. I. M. Hodge, M.D. Ingram, A.R. West, *J. Electroanal. Chem.* 74 (1976) 125-143.
86. D.L. Sidebottom, J. Zhang, *Phys. Rev. B* 62(2000) 5503-5507.
87. D.L. Sidebottom, P.F. Green and R. K. Brow, *Phys. Rev. B* 56(1997)170-177.
88. D. L. Sidebottom, *Phys. Rev. Lett.* 82 (1999) 3653-3656.
89. T.B. Schroder, J.C. Dyre, *Phys. Rev. Lett.* 84(2000)310-313.
90. A. Ghosh, A. Pan, *Phy. Rev. Lett.* 84 (2000) 2188.
91. B. Roling, A. Happe, K. Funke, M.D. Ingram, *Phys. Rev. Lett.* 78 (1997) 2160.

## **CHAPTER 6-Conclusions**

---

In this chapter, conclusions emerged out from the characterization analysis, AC conductivity, dielectric and modulus studies and their dependence on the temperature and compositions are summarized.

---

This chapter summarizes all the experimental results observed in the present investigation of silver based fast ion conducting polymer nano-composite electrolytes. It also gives the scope of further research work and the possible electrochemical applications of the polymer blend nano-composite electrolyte materials.

In the present investigation, a systematic study on PEO-PMMA polymer blend nano-composite electrolytes with silver salt has been undertaken. For this, firstly, the ratio of PEO to PMMA is optimized to find the effect of blending and then plasticization of optimized ratio of polymer blend with different plasticizers is carried out. Finally, incorporation of nano-fillers in plasticized polymer blend electrolytes is done to investigate the effect on transport mechanism. After the preparation of samples, characterization is performed using XRD, SEM, DSC, FTIR and transport number measurement. To understand the effect of blending, plasticizer and nano-filler on conduction and relaxation mechanism impedance spectroscopy technique is adopted.

XRD results indicate that the PEO-PMMA makes a good blend system. The absence of any X-ray peak of the silver nitrate salt in systems attributes to the complete dissolution of salt in the polymer matrix. The highest conducting sample with PEO: PMMA ratio as 50:50 (PPS-50) shows the lowest crystallinity. However, the addition of plasticizer PEG and EC in the (50PEO-50PMMA)-5wt% AgNO<sub>3</sub> system predominantly supports the formation of an amorphous matrix which in turn, enhances chain flexibility and the segmental motion. X-ray confirms the highest amorphousity for the polymer films with 5wt% of PEG (PPSP-5) and EC-5wt% (PPSE-5). Further enhancement in the level of amorphousity of the blend is observed on the addition of nano-fillers in the plasticized electrolyte samples. The maximum level of amorphousity content at 4wt % of Al<sub>2</sub>O<sub>3</sub> in the polymer electrolyte matrix

with both PEG and EC systems is observed. The samples with the lowest peak intensity in their respective X-ray spectra demonstrate the highest conductivity.

SEM micrographs indicate the presence of spherulitic structure in highest conducting films (PPS-30 and PPS-50). Addition of plasticizer beyond 5 wt% PEG in PPS-50 sample, an increment in surface roughness and clear spherulites structures is observed in EC based plasticized system. However, dispersion of nano-fillers in both plasticized systems improves the uniformity, smoothness and homogeneity of the surface up to 4wt% of nano-filler content.

DSC thermograms of all prepared polymer films show a sharp endothermic peak of melting temperature ( $T_m$ ) which is attributed to the transition from semi-crystalline to amorphous phase. In the plasticized systems as well as plasticized polymer nano-composites i.e.; PPSP, PPSE, PPSPA and PPSEA systems, the samples with highest amorphousity show the lowest  $T_m$  values in their respective systems. The decrease in melting temperature is attributed to the reduced degree of crystallinity.

The molecular vibrational spectra due to the interaction of polymer blend with salt, plasticizer and nanofiller in the system were analyzed by FTIR. The features including the characteristic vibrational peaks of PEO at 524, 1457, 1596  $\text{cm}^{-1}$ , a broad band in the wave number range 2700 - 2950  $\text{cm}^{-1}$  and an intense peak at 1721  $\text{cm}^{-1}$  due to C=O stretching vibration of ether oxygen of PMMA, are present in all prepared PEO-PMMA polymer blend host. In addition to this, the absence of characteristic absorption band corresponding to  $\text{NO}_3^-$  ion of pure  $\text{AgNO}_3$  confirms the complexation of salt in host polymer. Addition of plasticizer results in the broadening of the IR spectra (PPSP and PPSE systems). Further, dispersion of nano-fillers results in the disappearance of stretching vibration and wagging mode of  $\text{CH}_2$  of pure PMMA and PEO respectively. The IR bands become gradually feeble due to reduction in their

intensity. Additionally, these bands get broadened with nano-filler concentration up to Al<sub>2</sub>O<sub>3</sub>-4wt% in both nano-composite systems (PPSPA and PPSEA). At higher concentration of nano-filler the reappearance of more intensified IR bands indicate the retardation of process of amorphousity.

To study the ionicity, ionic transference number ( $t_i$ ) of polymer films was measured. The ionic transference number ( $t_i$ ) of polymer films shows that the conduction mechanism is principally due to the transport of ions and the highest conducting samples (PPS-50, PPSP-5, PPSE-5, PPSPA-4 and PPSEA-4) represent the highest transference number  $\sim 0.9$ .

PEO-PMMA polymer blend is a semi-crystalline polymer host that exhibits different conduction and relaxation processes, below and above the melting temperature of PEO. From the results presented in this thesis, it is proposed that the temperature dependence of electrical response can be explained in terms of two regions namely; (1) in the temperature range of  $T < T_m$ , (2) a sudden jump/ transition near the melting of PEO at  $T > T_m$  in polymer blend electrolyte systems. AC conductivity, dielectric permittivity and electrical modulus are determined over a range of composition and temperature using impedance data. All the samples with the highest transport number show the highest ionic conductivity in PPS-50, in both plasticized systems with 5wt% plasticizer content and at 4wt% of Al<sub>2</sub>O<sub>3</sub> in both plasticized nano-composite systems.

The frequency dependent conductivity shows a power law variation at high frequencies. Dispersion in ac conductivity spectra has been fitted by Jonscher's power law to determine the frequency exponent  $n$  where from, the values of frequency exponent ' $n$ ' are found to be higher than 1.

The real part of dielectric permittivity,  $\epsilon'$  decreases with the increase in

frequency and saturates at higher frequencies whereas the dielectric loss,  $\epsilon''$  also varies inversely with frequency. The frequency and temperature dependent dielectric studies confirm the ion migration and polarization. Dielectric behavior also shows the sudden rise near  $T_m$  in all samples. The dielectric loss i.e.,  $\tan \delta$  increases with the increase of temperature at low frequencies and dispersion in  $\tan \delta$  shifts towards high frequency with increase in temperature.

The conductivity relaxation of the mobile ion has been examined using electrical modulus formalism. The modulus plot shows the non-Debye behavior and is asymmetric with respect to the peak maximum, which confirms the distribution of relaxation time in the conduction process. Non exponential decay function from modulus spectra provides  $\beta$  values and is found to be  $> 1$  and independent of temperature and composition. The relaxation time ( $\tau$ ) calculated from the modulus peak ( $f_{max}$ ) is thermally activated and follows the variation in conductivity plots in the  $T > T_m$  region confirming that the ionic species are responsible for conductivity and relaxation effect in the present systems.

Scaling of AC conductivity for all PPS, PPSP, PPSE, PPSPA and PPSEA- systems at different temperatures (in  $T > T_m$  region) follow time-temperature superposition principle. Only PPSEA-system shows the compositional scaling of AC conductivity at a particular temperature while other systems reveal the merging at higher frequencies with the deviation at lower frequencies. Modulus spectra for each sample from each system showed scaling behavior as a function of temperature. Moreover; in each system, scaling of modulus spectra is observed as a function of composition also at any particular temperature (in  $T > T_m$  temperature range). Therefore, the relaxation mechanism involved in presently investigated systems is confirmed to be temperature and composition independent.

In summary, PEO-PMMA polymers make a good polymer blend. All prepared polymer blends show a sudden rise in conduction process near  $T_m$  which is due to the melted PEO in host polymer system. Plasticization in PEO-PMMA using PEG plasticizer does not support conductivity due to the similar structures of PEO and PEG. However, EC plasticizer supports the enhancement in the conduction mechanism at higher concentrations. Addition of nano-filler in plasticized polymer electrolytes (PPSP and PPSEA systems) enhances the electrical properties. The polymer nano-composites with EC plasticizer are found to be better polymer electrolyte system than the same with PEG. Hence, PPSEA system i.e.; PEO-PMMA- $\text{AgNO}_3$ -EC- $\text{Al}_2\text{O}_3$  system can be used as a good electrolyte at higher temperatures.

\*\*\*\*\*

## LIST OF PUBLICATIONS BASED ON THE PRESENT RESEARCH WORK

- 1) Effect of Nano-Filler on Structural and Ionic Transport Properties of Plasticized Polymer Electrolyte  
**Poonam Sharma, D.K.Kanchan, N. Gondaliya** (2012)  
*Open Journal of Organic Polymer Materials*, 2:38-44.
- 2) Characterization studies of plasticized PEO-PMMA nano-composite polymer electrolyte system,  
**Poonam Sharma, D.K.Kanchan, N. Gondaliya, M. Pant, M.S. Jayswal, P. Joge** (2012)  
*AIP Conference Proceedings* 1447:241-242.
- 3) Structural and electrical properties of plasticized polymer electrolytes  
**Poonam Sharma, D.K.Kanchan, M.S. Jayswal** (2012)  
*National Journal of Applied Sciences and Engineering* 1:32-40.
- 4) Effect of ethylene carbonate concentration on structural and electrical properties of PEO-PMMA polymer blends  
**Poonam Sharma, D.K.Kanchan, N. Gondaliya**  
*Ionics* 19 (2013) 777-785.
- 5) Conductivity relaxation in Ag<sup>+</sup> ion conducting PEO-PMMA-PEG polymer blends  
**Poonam Sharma, D.K.Kanchan, N. Gondaliya, M. Pant, M.S. Jayswal**  
*Ionics* 19 (2013) 301-307.
- 6) Influence of nano filler on conductivity in PEO-PMMA-AgNO<sub>3</sub> polymer blend  
**Poonam Sharma, D.K. Kanchan, N. Gondaliya, M. S. Jayswal, P. Joge**  
*Indian Journal of Pure and Applied Physics* 51 (2013) 346-349.
- 7) A comparison of effect of PEG and EC plasticizers on relaxation dynamics of PEO-PMMA-AgNO<sub>3</sub> polymer blends  
**Poonam Sharma, D.K.Kanchan** (2013)  
*Ionics* DOI 10.1007/s11581-013-0851-z.
- 8) Effect of nanofiller concentration on conductivity and dielectric properties of poly(ethylene oxide)-poly(methylmethacrylate) polymer electrolytes  
**Poonam Sharma and D. K. Kanchan** (2013)  
*Polymer International* DOI 10.1002/pi.4504.
- 9) Structural and Dielectric Properties of Blend PEO-PMMA-AgNO<sub>3</sub> Solid Polymer Electrolytes Plasticized with PEG  
**Poonam Sharma, D.K. Kanchan, N. Gondaliya** (2013)  
Submitted to *Journal of Macromolecular Science B*

## PAPERS IN CONFERENCE/PROCEEDINGS

- 1) Conductivity Studies in PEO-PMMA-AgNO<sub>3</sub> Plasticized Polymer Blends  
**Poonam Sharma, D.K.Kanchan, N. Gondaliya, M. Pant, M.S. Jayswal, P. Joge**  
*National Conference on Recent Trend in Material Science, JUIT, Solan, H.P.* 8-10 October, 2011
- 2) Conductivity studies on Plasticized Blend of PEO-PMMA Nano-Composite Electrolyte System  
**Poonam Sharma, D.K.Kanchan, N. Gondaliya, M. Pant, M.S. Jayswal, P. Joge**  
*17<sup>th</sup> National Symposium on Solid State track Detectors and their Applications, MSU Baroda, Gujarat* 17-19 Oct 2011.
- 3) Electrical Conductivity Studies In PEO-PMMA-AgNO<sub>3</sub> Polymer Blend With Nano Filler Al<sub>2</sub>O<sub>3</sub>  
**Poonam Sharma, D.K.Kanchan, N. Gondaliya, M. Pant, M.S. Jayswal, P. Joge**  
*National Conference on Solid State Ionics, JIIT, Noida, India, 15-17 Dec. 2011.*

- 4) Characterization studies of plasticized PEO-PMMA nano-composite polymer electrolyte system  
**Poonam Sharma**, D.K.Kanchan, N. Gondaliya, M. Pant, M.S. Jayswal, P. Joge  
*Proceeding of 56<sup>th</sup> DAE Solid State Physics Symposium*, SRM University, Kattankulathur, India, 19-23 Dec. 2011
- 5) AC conductivity studies of plasticized polymer blend nano-composite  
**Poonam Sharma**, D.K.Kanchan, N. Gondaliya, M. Pant, M.S. Jayswal, P. Joge  
*14<sup>th</sup> International Conference of International Academy of Physical Sciences (CONIAPS XIV)*, SVNIT, Gujarat 22-24 Dec. 2011
- 6) Structural and Dielectric properties of Ag<sup>+</sup>-ion Conducting PEO-PMMA Plasticized Polymer Blends  
**Poonam Sharma**, D.K.Kanchan, N. Gondaliya  
*Seminar on Preparation and characterization of crystalline and non-crystalline*, MSU Baroda, Gujarat 2<sup>nd</sup> Nov 2012.

### LIST OF PUBLICATIONS IN GLASSES

#### REFEREED JOURNALS

- 1) The conductivity studies of super ionic Silver Iodide Vanado-tellurite Glass system  
**Poonam Sharma**, D. K. Kanchan, M. Pant, M. S. Jayswal, A. M. Awasthi and S. Bharadwaj, 11<sup>th</sup>  
*Asian conference in Solid State Ionics 2008*, Coimbatore, pp. 371-378.
- 2) Transport properties of super ionic AgI-Ag<sub>2</sub>O-V<sub>2</sub>O<sub>5</sub>-TeO<sub>2</sub> glasses  
**Poonam Sharma**, D. K. Kanchan, M. Pant, K. P. Padmasree  
*Indian Journal of Pure and Applied Physics*, 48 (2010) 39-46.
- 3) Conductivity studies in proton irradiated AgI-Ag<sub>2</sub>O-V<sub>2</sub>O<sub>5</sub>-TeO<sub>2</sub> super-ionic glass system  
**Poonam Sharma**, D. K. Kanchan, Meenakshi Pant, K. P. Singh  
*Materials Sciences and Applications*, 1(2010) 59-65.
- 4) Effect of AgI on Conduction Mechanism in Silver–Vanadate Superionic Glasses  
**Poonam Sharma**, D. K. Kanchan, M. Pant, M. S. Jayswal, N. Gondaliya  
*New Journal of Glass and Ceramics* 1(2011) 112-118.
- 5) The effect of Mixed Iodide salts on the Conductivity Behavior in Ag<sub>2</sub>O-V<sub>2</sub>O<sub>5</sub>-B<sub>2</sub>O<sub>3</sub> Superionic Glass System  
**Poonam Sharma**, D. K. Kanchan, N. Gondaliya, M. Pant, M. S. Jayswal  
*New Journal of Glass and Ceramics* 1(2011) 125-129.
- 6) Effect of Plasticizer Concentration on the Conductivity in PAAM:AgNO<sub>3</sub> Solid Polymer,  
**Poonam Sharma**, D.K. Kanchan, M. Pant, N. Gondaliya, M.S.Jayswal,  
*AIP Conf. Proc.* 1349, (2011) pp. 933-934.
- 7) Study of Relaxation Dynamics in Mixed Iodide Doped Silver-Vanado-Borate Superionic Glass System,  
**Poonam Sharma**, D.K. Kanchan, M. Pant, N. Gondaliya, M.S.Jayswal,  
*AIP Conf. Proc.* 1349 (2011) pp. 551-552.

#### PAPERS IN CONFERENCE/PROCEEDINGS

- 1) Conductivity studies in irradiated and unirradiated AgI-Ag<sub>2</sub>O-V<sub>2</sub>O<sub>5</sub>-TeO<sub>2</sub> super ionic glass system: a comparative study  
**Poonam Sharma**, D. K. Kanchan, M. Pant, N. Gondaliya and K. P. Singh,  
*18<sup>th</sup> National Symposium on Radiation Physics*, 2009, MLSU, Udaipur, pp. 204-206.
- 2) Conductivity studies in AgNO<sub>3</sub> doped poly (Acrylamide) polymer electrolyte films

- Poonam Sharma**, D. K. Kanchan, M. Pant, N. Gondaliya,  
*8<sup>th</sup> National conference on solid State Ionics*, 2009, H. S. G. U., Sagar, pp. 45.
- 3) Conductivity studies in PVA-AgNO<sub>3</sub> polymer electrolyte  
**Poonam Sharma**, D. K. Kanchan, P. Joge N. Gondaliya, M. Pant,  
*54<sup>th</sup> DAE Solid State Physics Symposium*, 2009, M.S.U., Vadodara, pp.903-904.
- 4) Characterization of Silver ion conducting (AgI-Ag<sub>2</sub>O-V<sub>2</sub>O<sub>5</sub>-TeO<sub>2</sub>) glass system  
**Poonam Sharma**  
*School on Glass Formers and Glasses JNCASR*, Bengaluru, India, 4-20 January 2010.
- 5) Relaxation Dynamics in PAAM: AgNO<sub>3</sub>: EC Solid Polymer Electrolytes  
**Poonam Sharma**, D.K. Kanchan, M. Pant, N. Gondaliya, M.S. Jayswal  
*3<sup>rd</sup> International Symposium on Materials Chemistry*, BARC, Mumbai, 7-11 Dec. 2010
- 6) Electrical conduction studies on a newly plasticized PAAM:AgNO<sub>3</sub> nano-composite polymer electrolyte system  
**Poonam Sharma**, D.K. Kanchan, M. Pant, N. Gondaliya, M. S. Jayswal,  
*National conference on Physics for Tomorrow, St.Xavier's college, Gujarat* 3-4 March 2011.